



PREPARATION AND OPERATIONS OF THE MISSION PERFORMANCE
CENTRE (MPC) FOR THE COPERNICUS SENTINEL-3 MISSION

S3MPC STM Annual Performance Report - Year 1



*Mission
Performance
Centre*



Ref.: S3MPC.CLS.APR.002
Issue: 1.1
Date: 23/05/2018
Contract: 4000111836/14/I-LG

Customer: ESA	Document Ref.: S3MPC.CLS.APR.002
Contract No.: 4000111836/14/I-LG	Date: 23/05/2018
	Issue: 1.1

Project:	PREPARATION AND OPERATIONS OF THE MISSION PERFORMANCE CENTRE (MPC) FOR THE COPERNICUS SENTINEL-3 MISSION		
Title:	S3MPC STM Annual Performance Report - Year 1		
Author(s):	STM ESLs		
Approved by:	S. Labroue	Authorized by	J. Bruniquel, Service Manager
Distribution:	ESA, S3MPC		
Accepted by ESA	P. Féménias, ESA TO		
Filename	S3MPC.CLS.APR.002 - i1r1 - STM Annual Performance Report - Year 1.docx		

Copyright ©2018 – CLS, ECMWF, isardSAT, LEGOS, MSSSL, NOVELTIS, PML

All rights reserved.

No part of this work may be disclosed to any third party translated, reproduced, copied or disseminated in any form or by any means except as defined in the contract or with the written permission of ACRI-ST

Disclaimer

The work performed in the frame of this contract is carried out with funding by the European Union. The views expressed herein can in no way be taken to reflect the official opinion of either the European Union or the European Space Agency.





Sentinel-3 MPC
S3MPC STM Annual Performance
Report - Year 1

Ref.: S3MPC.CLS.APR.002
Issue: 1.1
Date: 23/05/2018
Page: iii

Changes Log

Version	Date	Changes
1.0	23/02/2018	First version
1.1	23/05/2018	Second version following ESA and EUMETSAT review

List of Changes

Version	Section	Answers to RID	Changes



Table of content

CHANGES LOG	III
LIST OF CHANGES	III
TABLE OF CONTENT	IV
LIST OF FIGURES	VII
LIST OF TABLES	XV
1 INTRODUCTION	1
1.1 Scope of the document	1
1.2 Applicable documents	1
1.3 Reference documents	1
1.4 Acronyms and abbreviations	1
2 EXECUTIVE SUMMARY	2
2.1 Sentinel-3 Surface Topography Mission	2
2.2 SRAL and MWR sensors	2
2.3 Sea Level	3
2.4 Winds and Waves	4
2.5 Land and Sea Ice	5
2.6 Inland waters	6
3 SRAL AND MWR MISSION EVENTS	8
4 PROCESSING BASELINE STATUS	12
4.1 Land and Marine Products	12
4.2 Processing Baseline History	13
4.2.1 Summary of Processing Baseline Content	13
4.2.2 Model and standard history	14
4.3 Status of the current Processing Baseline	15
4.4 List of anomalies in the Processing Baseline	16
5 SENSORS STATUS	17
5.1 SRAL	17
5.2 MWR	19
5.2.1 MWR processing	19
5.2.2 MWR Calibration timeline	20
5.2.3 MWR Calibration parameters	20
5.2.4 MWR Brightness Temperatures monitoring	21
6 SRAL TRACKING PERFORMANCES	24



Sentinel-3 MPC
S3MPC STM Annual Performance
Report - Year 1

Ref.: S3MPC.CLS.APR.002
Issue: 1.1
Date: 23/05/2018
Page: v

6.1	Over Ocean	24
6.2	Over Land	25
7	PERFORMANCE MISSION OVER OCEAN	30
7.1	Outliers detection.....	30
7.1.1	Ice detection.....	30
7.1.2	Outliers detection over ocean.....	32
7.2	Monitoring of SRAL parameters.....	35
7.2.1	Significant Wave Height	35
7.2.2	Backscatter coefficient	38
7.2.3	Dual-Frequency ionospheric correction.....	41
7.2.4	Off-Nadir angle waveform.....	45
7.3	Wet tropospheric correction.....	47
7.3.1	Along-track analyses.....	47
7.3.2	Crossover analyses	50
7.4	Sea Level Performances	52
7.4.1	Along-track analyses.....	53
7.4.2	Crossovers	55
7.5	Global Mean Sea Level	60
7.6	Wind/Wave Performance.....	61
7.6.1	Backscatter coefficient	62
7.6.2	Altimeter Wind Speed	65
7.6.3	Significant Wave Height	77
7.7	Investigation: SARM Sensitivity to the tracker command.....	89
7.8	Investigation : Quality assessment of SAMOSA 2.5 ocean retracker	91
7.9	Investigation: SRAL Sensitivity to the Swell Waves.....	93
7.10	Performance over Coastal areas	96
8	PERFORMANCE MISSION OVER SEA ICE	99
8.1	SRAL Instrument Mode over Sea Ice	99
8.2	20Hz Ku Band Surface Classification (surf_class_20_ku)	101
8.3	20Hz Ku Band Altimeter Derived Surface Type (surf_type_class_20_ku).....	103
8.4	20Hz Ku band Freeboard (freeboard_20_ku).....	105
8.5	Sea Surface Height Anomaly (sea_ice_ssha_20_ku).....	106
8.6	20Hz Ku Band Interpolated Sea Surface Height Anomaly (int_sea_ice_ssha_20_ku)	108
8.7	20Hz Ku band Sea Ice Concentration (sea_ice_concentration_20_ku)	110
8.8	Availability of Geophysical Corrections over Sea Ice	112
8.9	Availability of Snow Density, Snow Depth and Sea Ice Concentration over Sea Ice.....	114



Sentinel-3 MPC
S3MPC STM Annual Performance
Report - Year 1

Ref.: S3MPC.CLS.APR.002
Issue: 1.1
Date: 23/05/2018
Page: vi

9	PERFORMANCE MISSION OVER LAND ICE	115
9.1	SRAL Instrument Mode over Land Ice	115
9.2	20Hz Ku-band Ice Sheet Elevation.....	119
9.3	20Hz Ku-band OCOG Elevation.....	124
9.4	20Hz Ku-band Waveform Quality Flag for Ice Sheets	125
9.5	Slope Correction Assessment	127
9.6	20Hz Ku-band Ice Sheet Range (range_ice_sheet_20_ku).....	128
9.7	20Hz Ku Band Ice Sheet Sigma0 (sig0_ice_sheet_20_ku)	130
9.8	20Hz Ku Band OCOG (Ice-1) Sigma0 (sig0_ocog_20_ku)	133
9.9	20Hz Ku Band PLRM Ice Range (range_ice_20_plrm_ku)	135
9.10	20Hz Ku Band PLRM Sigma0 (sig0_ice_20_plrm_ku).....	137
9.11	20Hz Ku Band Surface Class (surf_class_20_ku)	139
9.12	Availability of Geophysical Corrections over Ice Sheets (NTC Products)	141
9.13	Availability of Geophysical Corrections over Ice Shelves (NTC Products).....	143
10	PERFORMANCE MISSION OVER INLAND WATERS	144
10.1	Products used for the analysis	144
10.2	Validation over Issykkul lake	144
10.3	Behaviour of the OLTC (open loop Tracking Command).....	147
11	RANGE AND SEA LEVEL ABSOLUTE CALIBRATION.....	148
11.1	Calibration with Crete transponder	148
11.2	Calibration over Corsica sites	153
12	BIAS ASSESSMENT OF THE DIFFERENT RETRACKERS	158
12.1	Ocean retracker.....	158
12.2	OCOG retracker	158
12.3	Sea Ice retracker.....	160
12.4	Ice margin retracker	161
12.5	Summary	165
13	ANNEX - PROCESSING BASELINE DETAILS.....	166
13.1	Processing Baseline 2.12	166
13.1.1	Ground processors versions (Instrument Processor Facility).....	166
13.1.2	Evolutions	166
13.1.3	Fix of anomalies.....	166
13.2	Processing Baseline 2.24	167
13.2.1	Ground processors versions (Instrument Processor Facility).....	167
13.2.2	Evolutions	167



13.2.3	Fix of anomalies.....	167
13.3	Processing Baseline 2.27	170
13.3.1	Ground processors versions (Instrument Processor Facility).....	170
13.3.2	Evolutions	170
13.3.3	Fix of anomalies.....	170
13.3.4	Anomalies not solved	171
14	ANNEX REFERENCES.....	179

List of Figures

Figure 1	Geographical mask for L2 Land and Marine products coverage: blue is Marine products only, white is Land products only, brown is for regions available in both products.....	12
Figure 2:	Ku band CAL1 SAR Time Delay series.	17
Figure 3:	Ku band CAL1 SAR Integrated and Peak Power series.	18
Figure 4:	Ku band CAL1 SAR PTR width series.	18
Figure 5:	Ku band CAL2 SAR waveforms series.	19
Figure 6:	Geolocation of MWR measurements in DNB mode	20
Figure 7:	Number of measurements in DNB mode along the year	20
Figure 8:	Monitoring of MWR calibration parameters: Receiver gain (top line), Noise injection temperature (bottom line) for both channels: 23.8GHz (left) and 36.5GHz (right)	21
Figure 9:	Coldest temperature over ocean for Sentinel-3A, SARAL/AltiKa, Metop02/AMSU-A, Jason3/AMR for two channels 23.8GHz (left) and 36.5GHz (right).....	22
Figure 10:	Hottest temperatures over the Amazon forest for Sentinel-3A, SARAL/AltiKa, Metop02/AMSU-A, Jason3/AMR for two channels 23.8GHz (left) and 36.5GHz (right)	23
Figure 11:	Monitoring of the daily percentage of available measurements for Sentinel-3A over Ocean and coastal area (green curve), Sentinel-3A over open Ocean (red curve) and Jason-3 over open Ocean (blue curve). This metric is computed with respect to the theoretical track and the theoretical number of measurements expected.....	24
Figure 12:	Map of the gridded percentage of missing measurements over Ocean computed from December 2016 to December 2017. The analysis is based on the NTC Level-2 Marine products delivered on the fly.	25
Figure 13:	Map of the SRAL tracking mode plotted for cycle 26 (from 20 th of December2017 to 16 th of January 2018). Orange color corresponds to Open-Loop acquisition mode. Black color corresponds to Close-Loop acquisition mode.	26

	Sentinel-3 MPC S3MPC STM Annual Performance Report - Year 1	Ref.: S3MPC.CLS.APR.002 Issue: 1.1 Date: 23/05/2018 Page: viii
---	--	---

Figure 14: Global map (top panel) of the Sentinel-3A missing measurements for cycle 25 (from 11th of November 2017 to 20th of December 2017). Zoom (bottom panel) over Central and South America of the missing Sentinel-3A measurements (plotted in white) superimposed on a bathymetry grid.-----27

Figure 15: left panels show the Sentinel-3A missing measurements for cycle 25 (from 11th of November 2017 to 20th of December 2017) over Antarctica (left panel) and over the Arctic (right panel) areas. Bottom left panel shows the ocog backscatter coefficient over Antarctica for cycle 25. This variable is derived from both S3A L2 LAND and WATER products. The bottom right panel shows the ocog backscatter coefficient for one pass that cross the Antarctica continent. The along-track profile is derived from both S3A L2 LAND and WATER products.-----28

Figure 16: Gridded map of the range ocog Default Value percentage with respect to the available measurements. It is plotted over cycle 25 (from 11th of November 2017 to 20th of December 2017)/----29

Figure 17: left panel shows the Sentinel-3A sea ice flag derived from both L2 LAND and WATER products over cycle 25 (from 11th of November 2017 to 20th of December 2017). Presence of sea ice corresponds to the value 1, open ocean water is represented by the value of 0. Middle panel shows the sea ice concentration percentage derived from OSISAF model over the month of December. Right panel shows the sea concentration percentage derived from NSIDC model over the month of December. -----31

Figure 18: left panel shows the gridded of map of the outliers percentage detected by the Sentinel-3A sea ice flag over the year 2016 (from December 2016 to December 2017). Right panels shows the gridded of map of the outliers percentage detected by the SARAL/AltiKa ice flag over the whole mission period.-----31

Figure 19: Monitoring of the daily averaged percentages of outliers detected by Sentinel-3A sea ice flag (green curve) and AltiKa ice flag (blue curve) over Ocean. -----32

Figure 20: left panel shows the Sentinel-3A (green curve) and SARAL/AltiKa (blue curve) total percentage of outliers over ocean. Right panel shows the gridded map of Sentinel-3A percentage of total outliers over the year 2017. -----33

Figure 21: left panel shows the Sentinel-3A (green curve) and Jason-3 (blue curve) percentage of outlier detected by the dynamical atmospheric thresholds. Right panel shows the percentage of Sentinel-3A (red curve), Jason-3 (blue curve) and AltiKa (green curve) percentage of outliers detected by the MWR WTC thresholds.-----34

Figure 22: Gridded maps of Sentinel-3A SARM (top left panel) P-LRM (right left panel) and Jason-3 (bottom panel) SWH computed over the year 2017. -----36

Figure 23: Daily monitoring of the Sentinel-3A SARM (green curve) P-LRM (red curve) and Jason-3 (blue curve) SWH. -----37

Figure 24: left panel shows the SWH differences computed at crossovers over the year 2017 between Sentinel-3A SARM and Jason-3 (blue curve) and between Sentinel-3A P-LRM and Jason-3 (green curve) as a function of the Jason-3 SWH. Due to the high temporal variability of the SWH parameters a selection was applied to select crossover time lags below 3hours. Right panel shows the gridded map of collocated SWH differences between Sentinel-3A SARM and P-LRM over the year 2017.-----38

	Sentinel-3 MPC S3MPC STM Annual Performance Report - Year 1	Ref.: S3MPC.CLS.APR.002 Issue: 1.1 Date: 23/05/2018 Page: ix
---	--	---

Figure 25: Gridded maps of Sentinel-3A SARM (top left panel) P-LRM (right left panel) and Jason-3 (bottom panel) backscatter coefficient computed over the year 2017. -----39

Figure 26: Daily monitoring of the Sentinel-3A SARM (green curve) P-LRM (red curve) and Jason-3 (blue curve) backscatter coefficient. -----40

Figure 27: Gridded maps of the collocated backscatter differences between Sentinel-3A SARM and P-LRM over the year 2017 (left panel) and of the Sentinel-3A altitude computed over cycle 25 (right panel).40

Figure 28: Gridded maps of Sentinel-3A SARM (top left panel) P-LRM (right left panel) and Jason-3 (bottom panel) dual frequency ionospheric correction computed over the year 2017. -----41

Figure 29: Top panels shows the gridded maps of the collocated differences between Sentinel-3A SARM dual frequency ionosphere correction and GIM model for ascending (left panel) and descending (right panel) passes. Bottom panels show the gridded maps of the collocated differences between Jason-3 dual frequency ionosphere correction and GIM model for ascending (left panel) and descending (right panel) passes. The ionosphere corrections derived from altimeter were filtered at 300km. -----43

Figure 30: Along-track maps of the Sentinel-3A local hours for ascending (left panel) and descending (right panel) passes computed over cycle 25. -----43

Figure 31: Top panel shows the daily monitoring of the collocated differences between Sentinel-3A SARM dual-frequency ionosphere correction and the GIM model. The Sentinel-3A local hours were split by four hours bins and plotted separately. Bottom panel shows the daily monitoring of the Sentinel-3A SARM, P-LRM dual-frequency ionosphere correction and the collocated GIM model. Ascending and Descending passes were plotted separately. -----44

Figure 32: Top panels show the gridded maps of Sentinel-3A off-nadir angle derived from waveforms (left panel) and derived from Star-Trackers (right panel) over the year 2017. Bottom panels show the off-nadir angle derived from waveforms for Jason-3 (left panel) and SARAL/AltiKa (right panel) over their respective whole mission lifetime. -----46

Figure 33: Daily monitoring of the Sentinel-3A P-LRM (green curve), Jason-3 (blue curve) and SARAL/AltiKa (red curve) off-nadir angle derived from waveforms.-----46

Figure 34: Monitoring of MWR (3P) - ECMWF wet tropospheric correction for Sentinel-3A, SARAL/AltiKa, Jason3/AMR: mean (left), standard deviation (right)-----48

Figure 35: Difference of SAR/P-LRM wet tropospheric correction for Sentinel-3A, SARAL/AltiKa, Jason3/AMR-----48

Figure 36: Monitoring of 3P and 5P MWR - ECMWF wet tropospheric correction for Sentinel-3A -----49

Figure 37: Map of the difference 5P - 3P wet tropospheric correction for Sentinel-3A (using NTC data) -49

Figure 38: Difference of variance of Δ SSH at crossover points for Sentinel-3A, SARAL, Jason3 : var(SSH with WTC 3P MWR)-var(SSH with WTC ECMWF) global ocean (top) and low oceanic variability (bottom)50

Figure 39: Difference of variance of SSH at crossover points SAR (left) / P-LRM (right) -----51

Figure 40: Difference of variance of SSH at crossover points for Sentinel-3A, SARAL/AltiKa, Jason3/AMR: var(SSH with WTC 5P MWR)-var(SSH with WTC ECMWF)-----51



Sentinel-3 MPC
S3MPC STM Annual Performance
Report - Year 1

Ref.: S3MPC.CLS.APR.002
 Issue: 1.1
 Date: 23/05/2018
 Page: x

Figure 41: Difference of variance of SSH at crossover points SAR (left) / P-LRM (right) -----52

Figure 42: Gridded maps of Sentinel-3A SARM (top left panel) P-LRM (right left panel) and Jason-3 (bottom panel) SLA computed over the year 2017.-----53

Figure 43: Daily monitoring of the Sentinel-3A SARM (green curve) P-LRM (red curve) and Jason-3 (blue curve) mean SLA (left panel) and its standard deviation (right panel).-----55

Figure 44: Cycle per cycle monitoring of the SSH differences computed at mono-mission crossovers for Sentinel-3A SARM (blue curve) and Jason-3 (green curve).-----56

Figure 45: Gridded maps of Sentinel-3A SSH differences computed at mono-mission crossovers in SARM (left panel) and in P-LRM (right panel) over the year 2017.-----57

Figure 46: Cycle per cycle monitoring of the system error computed at mono-mission crossovers for Sentinel-3A (blue curve) and Jason-3 (green curve). The system error is computed through the cyclic SSH differences standard deviation at crossovers and divided by 2 because of the cumulation of the ascending and descending errors. The red curve shows the Sentinel-3A SARM system error when the mean time lag at crossovers is consistent with the Jason-3 one.-----57

Figure 47: Gridded maps of SSH differences computed at Sentinel-3A and Jason-3 crossovers in SARM (left panel) and in P-LRM (right panel) over the year 2017.-----58

Figure 48: Cycle per cycle monitoring of the SSH differences computed at Sentinel-3A and Jason-3 crossovers in SARM (blue filled curve) and in P-LRM (red curve). The dashed blue curve shows the evolution of the bias when the Jason-3 SSH is computed using an updated SSB (SSB Tran et al. 2012 instead of GDR-D SSB). -----59

Figure 49: Cycle per cycle monitoring of the pseudo time tag bias for Sentinel-3A (green curve), Jason-3 (blue curve) and SARAL/AltiKa (red curve). The pseudo time tag biases are computed at mono-mission crossovers.-----60

Figure 50: Evolution of the Global Mean Sea Level computed with Jason-3 (top panel) and Sentinel-3A SARM (bottom panel) SLA. -----61

Figure 51: Sentinel-3A SRAL surface wind speed PDF over the whole global ocean for one year from 13 December 2016 to 12 December 2017. -----63

Figure 52: Comparison between backscatter PDF's of various altimeters over the year from 13 December 2016 to 12 December 2017 is shown in the upper panel. Better comparison can be carried out when PDF's are shifted to have their peak estimates coincide with that of Sentinel-3A (lower panel). The amount of shift is given in the legend of the lower panel. -----64

Figure 53: Time series of global mean (top) and standard deviation (bottom) of backscatter coefficient of SRAL Ku-band after quality control. Mean and SD are computed over a moving time window of 7 days. Vertical dashed lines show events which may have impact on the comparison. This includes Sentinel-3 STM Instrument Processing Facility (IPF) and Processing Baseline (PB) changes. -----65

Figure 54: Sentinel-3A SRAL surface wind speed PDF over the whole global ocean for the year running between 13 December 2016 and 12 December 2017. The corresponding ECMWF (collocated with Sentinel-3) PDF is also shown for the same period for comparison purposes.-----66

	Sentinel-3 MPC S3MPC STM Annual Performance Report - Year 1	Ref.: S3MPC.CLS.APR.002 Issue: 1.1 Date: 23/05/2018 Page: xi
---	--	---

Figure 55: Comparison between wind speed PDF's of various altimeters over the year from 13 December 2016 to 12 December 2017 is shown in the upper panel. The corresponding model PDF's as collocated with the measurements used for the upper panel are shown in lower panel. The abbreviations are as follows: .S3A: Sentinel-3A, J3: Jason-3, CS: CryoSat-2, SA: SARAL/AltiKa and J2: Jason-2 -----67

Figure 56: Time series of global mean (top) and standard deviation, SD, (bottom) of SAR wind speed from SRAL after quality control. The collocated model wind speed mean and SD are also shown. Mean and SD are computed over a moving time window of 7 days. Vertical dashed lines show events which may have impact on the comparison. This includes Sentinel-3 STM Instrument Processing Facility (IPF) and Processing Baseline (PB) changes as well as ECMWF IFS model changes like CY43R3. -----68

Figure 57: Global comparison between Sentinel-3A SRAL and ECMWF model analysis surface wind speed values over one-year period from 13 December 2016 to 12 December 2017. The number of collocations in each 0.5 m/s x 0.5 m/s 2D bin is color-coded as in the legend. The crosses are the means of the bins for given x-axis values (model) while the circles are the means for given y-axis values (Sentinel-3). -----69

Figure 58: Same as Figure 57 but the comparison is done against in-situ observations (mainly in the NH).70

Figure 59: Time series of weekly wind speed bias defined as altimeter - model (top) and standard deviation of the difference (bottom) between SRAL Ku-band and ECMWF model analysis. -----71

Figure 60: Time series of weekly wind speed bias defined as altimeter - buoy (top) and standard deviation of the difference (bottom) between SRAL Ku-band and in-situ (buoy) measurements. -----71

Figure 61: Time series of weekly global wind speed bias defined as altimeter - model (top) and standard deviation of the difference (bottom) between various altimeters (including SRAL) and ECMWF model analysis. SRAL curves are same as the global curves in Figure 59. -----72

Figure 62: Geographical distribution of mean Sentinel-3 wind speed (a) as well as the bias (b); the SDD (c) and the SI (d) between Sentinel-3 and ECMWF model AN during the period from 13 December 2016 to 12 December 2017. Bias is defined as altimeter - model. -----73

Figure 63: Global comparison between Sentinel-3A PLRM and ECMWF model analysis wind speed values over the one-year period from 13 December 2016 to 12 December 2017. Refer to Figure 57 for the meaning of the crosses and the circles as well as the colour coding. -----76

Figure 64: Time series of weekly PLRM wind speed bias defined as altimeter - model (top) and standard deviation of the difference (bottom) between SRAL PLRM and ECMWF model analysis. -----77

Figure 65: Sentinel-3A SRAL SWH PDF over the whole global ocean for the one-year period from 13 December 2016 to 12 December 2017. The corresponding ECMWF (collocated with Sentinel-3A) PDF is also shown for comparison. -----78

Figure 66: Global SWH PDF's from 5 altimeters for the one-year period from 13 December 2016 to 12 December 2017 (upper panel). The corresponding ECMWF (collocated with Sentinel-3) PDF's are shown in the lower panel for comparison. -----80

Figure 67: Same as in Figure 66 but for the global ocean region extending from 65° N to 65° S which is common for all altimeters considered here. -----81



Sentinel-3 MPC
S3MPC STM Annual Performance
Report - Year 1

Ref.: S3MPC.CLS.APR.002
Issue: 1.1
Date: 23/05/2018
Page: xii

Figure 68: Time series of global mean (top) and standard deviation (bottom) of significant wave height from SRAL Ku-band after quality control. The collocated ECMWF model SWH mean and SD are also shown. The mean and SD are computed over a moving time window of 7 days. -----82

Figure 69: Global comparison between Sentinel-3A and ECMWF model first-guess SWH values over the one-year period from 13 December 2016 to 12 December 2017. The number of collocations in each 0.25 m x 0.25 m 2D bin is coded as in the legend. Refer to Figure 57 for the crosses and the circles. -----83

Figure 70: Same as Figure 69 but the comparison is done against in-situ observations (mainly in the NH).83

Figure 71: Time series of weekly global significant wave height bias defined as altimeter - model (top) and standard deviation of the difference (bottom) between SRAL and ECMWF model first-guess.-----84

Figure 72: Time series of monthly global significant wave height bias defined as altimeter - buoy (top) and standard deviation of the difference (bottom) between SRAL and in-situ measurements.-----85

Figure 73: Time series of weekly global significant wave height bias defined as altimeter - model (top) and standard deviation of the difference (bottom) between 5 altimeters including Sentinel-3A SRAL (same as the global curves in Figure 71) and the ECMWF model first-guess. -----86

Figure 74: Geographical distribution of mean Sentinel-3A SWH (a) as well as the bias (b); the SDD (c) and the SI (d) between Sentinel-3A and ECMWF model FG during the one-year period from 13 December 2016 to 12 December 2017. Bias is defined as altimeter - model. -----86

Figure 75: top panels shows the Gridded map of the Sentinel-3A collocated backscatter coefficient differences between SARM and P-LRM for ascending (left panel) and descending (right panel) passes. These maps were computed using L2 measurements derived from SAMOSA DPM2.3. Bottom panels shows the corresponding variation of the epoch for ascending (left panel) and descending (right panel) passes.-----90

Figure 76: Differences between Sentinel-3A SARM and P-LRM backscatter coefficients (left panel, in dB), ranges (middle panel, in meters) and SWH (right panel, in meters) as a function of the epoch variations (in meters).-----90

Figure 77 Difference between SARM Ku band and PLRM Ku band range wrt SWH for previous processing baseline (blue curve) and Processing Baseline 2.24 (green curve). The curve obtained for the CNES S3 prototype (red curve) is also represented to provide an external reference. -----92

Figure 78 Difference between SARM Ku band and PLRM Ku band SWH wrt SWH for previous processing baseline (blue curve) and Processing Baseline 2.24 (green curve). The curve obtained for the CNES S3 prototype (red curve) is also represented to provide an external reference. -----92

Figure 79 Difference between SARM Ku band and PLRM Ku band backscatter coefficient for previous processing baseline (right map) and Processing Baseline 2.24 (left map). The maps display only the ascending tracks to better highlight the finer details of the difference in the maps.-----93

Figure 80: Polar plot of the SARM (left panel) and P-LRM (right panel) range noises as a function of the mean swell period and as a function of the azimuth angle between swell and track directions. The wave height was fixed between 2 and 3 m.-----94

	Sentinel-3 MPC S3MPC STM Annual Performance Report - Year 1	Ref.: S3MPC.CLS.APR.002 Issue: 1.1 Date: 23/05/2018 Page: xiii
---	--	---

Figure 81: Polar plot of the SWH differences as a function of the mean swell period and the azimuth angle between swell and track direction.-----95

Figure 82 Pattern of Sentinel-3 ground tracks over the southwest UK for the interleaved phase. E1 is the location (4°22.5'W, 50°2.6'N) of a meteorological buoy and a long-term sampling station as part of the Western Channel Observatory, implying that many ancillary data are available. The green circle indicates the rough coverage of the HF radar system, with transmitters at Pendeen and Perrenporth (marked by the black dots).-----96

Figure 83 Comparison of data from S-3A (x-axis) with meteorological buoy. (left) Orbit 128, (track 256) which passes 36 km to west of buoy (Right) Orbit 208 (track 415), which passes 15 km to the east of the buoy. Altimeter data are the 20 Hz records within 45 km of the buoy, and buoy data are the 5 nearest hourly values to the time of the overpass, with mean SWH in blue and maximum wave height in red. --97

Figure 84 Mean values of SAR mode σ_{HS} (in metres) for repeat cycles of Sentinel-3A over the southwest UK.-----98

Figure 85 Measures of uncertainty in wave height (σ_{H_s}) and range (σ_h) as a function of H_s . The top row shows 2-D histograms for open ocean conditions, with the population density shown by grey shading (using a logarithmic scale) and the magenta lines indicating the 5th, 50th and 95th percentiles in each narrow H_s bin. The bottom row shows how the median values increase as the coast is approached, with the different coloured solid lines for >25 km; 11-13 km, 7-9 km and 3-5 km being indistinguishable). This indicates that the median performance in SAR mode is as good at 3-5 km from coast as in open ocean. However, there are differences at the higher percentiles, because a small proportion of the coasts are high enough to have an effect within the SAR footprint. For comparison, the uncertainty estimates obtained from the Pseudo-LRM (PLRM) processing for >25 km from the coast are shown by the blue dashed lines.-----98

Figure 86: Map of SRAL mode over the Antarctic sea ice for cycle 25 NTC----- 100

Figure 87: Map of SRAL mode over the Arctic sea ice for cycle 25 NTC----- 101

Figure 88: Maps of 20Hz Ku Band Surface Classification (surf_class_20_ku) ----- 102

Figure 89: Maps of 20Hz Ku Band Altimeter Derived Surface Type (surf_type_class_20_ku) ----- 104

Figure 90: Maps of 20Hz Ku band Freeboard (freeboard_20_ku)----- 106

Figure 91: Maps of 20Hz Ku band Sea Ice SSHA (m)----- 108

Figure 92: Maps of 20Hz Ku band Interpolated Sea Ice SSHA (m) ----- 110

Figure 93: Maps of 20Hz Ku band Sea Ice Concentration (sea_ice_concentration_20_ku) ----- 112

Figure 94: Maps of SRAL Instrument Mode, Antarctica and Greenland (Cycle 25, Nov/Dec 2017) ----- 117

Figure 95: Maps of SRAL Instrument Mode, Antarctica and Greenland (Cycle 10, Oct/Nov 2016)----- 119

Figure 96: Failure rate of ice sheet elevation over different ice surfaces since start of mission ----- 120

Figure 97: Maps of Ku band Ice Sheet Elevation, Antarctica and Greenland (Cycle 25, Nov/Dec 2017) 122

Figure 98: Maps of Ku band Ice Sheet Elevation, Dome-C, Antarctica (Cycle 25, Nov/Dec 2017)----- 123



Sentinel-3 MPC
S3MPC STM Annual Performance
Report - Year 1

Ref.: S3MPC.CLS.APR.002
 Issue: 1.1
 Date: 23/05/2018
 Page: xiv

Figure 99: Maps of Ku band Ice Sheet Elevation, SPIRIT Zone, Antarctica (Cycle 25, Nov/Dec 2017)----- 123

Figure 100: Maps of Ku band OCOG range, Antarctica, Greenland (Cycle 25, Nov/Dec 2017) ----- 125

Figure 101: Maps of % 20Hz Ku Waveform Quality Flag Test Failure Densities (in 10 km² grid) for cycle 25, Antarctica and Greenland Ice Sheets ----- 127

Figure 102: Maps of % Slope Correction Failure Density in a 10km grid ----- 128

Figure 103: Maps of 20Hz Ku Band Ice Sheet Sigma0 (sig0_ice_sheet_20_ku) ----- 132

Figure 104: Maps of 20Hz Ku Band OCOG (Ice-1) Sigma0 (sig0_ocog_20_ku)----- 134

Figure 105: Maps of 20Hz Ku Band PLRM Ice Range (range_ice_20_plrm_ku)----- 136

Figure 106: Maps of 20Hz Ku Band PLRM Sigma0 (sig0_ice_20_plrm_ku) ----- 138

Figure 107: Maps of 20Hz Ku Band Surface Class (surf_class_20_ku) ----- 140

Figure 108: Percentage of Geophysical Correction Non-availability over Antarctic Ice Sheets ----- 141

Figure 109: Percentage of Geophysical Correction Non-availability over the Greenland Ice Sheet----- 142

Figure 110: Availability of Geophysical Corrections over Antarctic Ice Shelves ----- 143

Figure 111 Campaign done in 2016 (October). Track 666 and 707 were followed by the boat carrying the GPS receiver.----- 145

Figure 112 Accuracy of Jason2, Jason-3 and Sentinel-3A determined over the period from January 2016 to July 2017 using satellite water height of the lake at each pass and the in situ measurements of the permanent gauge.----- 145

Figure 113 Absolute bias of Sentinel-3A with the tracker ocean over the cycle 9 (October 2016) for the two tracks (666 and 707) where the boat has measured the water height above ellipsoid at the date of pass of the satellite. The absolute bias observed was -14 +/-20 mm)----- 146

Figure 114 Range Bias Results and Datation Bias Results----- 151

Figure 115 Alignment Results and Stack Noise Results----- 152

Figure 116: Absolute CALVAL configuration in Corsica. The regions in colours show the two high-resolution mean sea surfaces that were specifically measured to link the calibration sites to the altimetry data----- 153

Figure 117: Impact of the change in the method for the selection of the altimetry points on the high-resolution mean sea surfaces at the Corsica calibration sites – Sentinel-3A track 741 – Cycles 5 to 19. 155

Figure 118: Sentinel-3A absolute bias estimates in Senetosa (upper plot) and Ajaccio (lower plot) on track 741----- 157

Figure 119 Range difference: OCOG-Ocean over Arctic in L2 Land products STC Cycle 26----- 159

Figure 120 Backscatter coefficient difference: OCOG-Ocean over Arctic in L2 Land products STC Cycle 26160

Figure 121 Range difference: Ocean-Ice margin over Arctic in L2 Land products STC Cycle 26----- 162

Figure 122 Range difference: OCOG-Ice margin over Antarctica in L2 Land products STC Cycle 26 ----- 163

	Sentinel-3 MPC S3MPC STM Annual Performance Report - Year 1	Ref.: S3MPC.CLS.APR.002 Issue: 1.1 Date: 23/05/2018 Page: xv
---	--	---

Figure 123 Backscatter coefficient difference: Ocean-Ice margin over Arctic in L2 Land products STC Cycle 26 ----- 164

Figure 124 Backscatter coefficient difference: OCOG-Ice margin over Antarctica in L2 Land products STC Cycle 26 ----- 165

List of Tables

Table 1 History of SRAL and MWR mode changes----- 8

Table 2: Main Sentinel-3A SRAL and Platform events since the SRAL switch on. The shaded lines correspond to a data gap impact on Level-2 products. -----11

Table 3 Model and standard history in L2 products-----15

Table 4: Characteristics of missions with microwave radiometer -----21

Table 5: Outliers detection thresholds and corresponding percentages computed over the year 2017. -34

Table 6: Detail of the standard used to compute Sentinel-3A and Jason-3 SLA and SSH. For Sentinel-3A over the year 2017 some of these standards have been updated, thus they are detailed as a function of the IPF-SM2 versions.-----52

Table 7: Detail of the standard used to compute Sentinel-3A and Jason-3 SLA and SSH. For Sentinel-3A over the year 2017 some of these standards have been updated, thus they are detailed as a function of the IPF-SM2 versions.-----53

Table 8: List of the main parameters (involved in the SLA computation) impacted by the IPF-SM2 upgrade from version 06.07 to 06.10 and the corresponding impact on SARM parameters and P-LRM parameters. -----55

Table 9: % Non Availability of Geophysical Corrections over Sea Ice (NTC)----- 113

Table 10: % Availability of Snow Density, Snow Depth, Sea Ice Concentration over Sea Ice----- 114

Table 11: Results of TRP passes processing ----- 149

Table 12: Geophysical Corrections of TRP passes processing----- 150

Table 13 : Sentinel-3A products and parameters used to compute the absolute bias estimates----- 154

Table 14 : Statistics on the Sentinel-3A SAR and PLRM SSH absolute bias estimates in Corsica on track 741, before and after change in the method. The colours refer to the plots on Figure 118. ----- 155



1 Introduction

This document is the Year 1 Annual Performance Report version of the MPC Altimetry report prepared by the ACRI-ST consortium for the realisation of the “Preparation and Operations of the Mission Performance Centre (MPC) for the Copernicus Sentinel-3 Mission”, ESA contract 4000111836/14/I-LG.

1.1 Scope of the document

This document provides a summary of the end-to-end mission performance since the start of the mission and of main activities carried out by the S3 Mission Performance Centre during the first year of the routine operations phase, started on the 1st of February, 2017.

It addresses more specifically activities related to the Surface Topography Mission (an equivalent report – S3MPC.ACR.APR.001 – is issued to address OPT and general activities).

1.2 Applicable documents

The full Applicable Documents (AD) ID correspondence is provided in the Configuration Item Data List (S3MPC.ACR.LST.002).

1.3 Reference documents

The full Reference Documents (RD) ID correspondence is provided in Configuration Item Data List (S3MPC.ACR.LST.002).

1.4 Acronyms and abbreviations

The definition of the acronyms and abbreviations used in this document is provided in the List of Acronyms and Definitions (S3MPC.ACR.LST.003).



2 Executive Summary

2.1 Sentinel-3 Surface Topography Mission

The series of Sentinel satellites mark a major step forward in the collection of Earth Observation data with the commitment to a series of spacecraft and sensors to construct long time series of data suitable for both climate applications and widespread operational use. Each Sentinel mission is based on a constellation of two satellites to fulfil revisit and coverage requirements, providing robust datasets for Copernicus Services.

Sentinel-3A is a multi-instrument mission to measure sea-surface topography, sea- and land-surface temperature, ocean colour and land colour with high-end accuracy and reliability. The mission will support ocean forecasting systems, as well as environmental and climate monitoring.

Sentinel-3A was launched on 16 February 2016 and the SRAL and MWR sensors were switched-on 1 March and 29 February 2016 respectively. After 5 months of commissioning, the Routine operations started in July 2016.

After 6 first weeks of acquisition in LRM mode, Sentinel-3A was switched to SAR mode on 12 April 2016 and since then it has operated in SAR mode continuously and over all surfaces, being the first altimetry mission to use this mode at global scale.

When SRAL altimeter operates in SAR mode, an LRM-like processing can be performed to derive waveforms that are close to the standard altimetry (Low Resolution Mode) waveforms but with a higher speckle compared to LRM echoes. This is the so-called Pseudo Low Resolution Mode (P-LRM) and this mode is used as a reference to assess the quality of the SARM measurements.

2.2 SRAL and MWR sensors

All the SRAL instrumental parameters are indicating a good instrument performance. The instrumental drifts are taken into account in the ground processing and thus are not affecting science data. The drift magnitudes are generally bigger than the ones in other ESA altimetry missions such as EnviSat and CryoSat-2. Anyhow, all the parameters are meeting the mission requirements. The CAL1 SAR Ku BAND total power is the only calibration having a decay outside of the expected range at the beginning of the mission, but it does not degrade measurement quality and the drift is becoming more stable.

All the MWR instrumental parameters are indicating a good instrument performance. The estimated calibration parameters are slightly drifting but other indicators, such as the vicarious calibrations show a good stability of the brightness temperatures. All the parameters are meeting the mission requirements.



2.3 Sea Level

Since almost 2 years in orbit, Sentinel-3A has been providing high quality sea surface height observations over ocean. This report summarizes a variety of results, including comparisons with Jason-3 and SARAL/AltiKa data to highlight and quantify the mission performance over ocean. The main points of this performance assessment are summarized below:

- ❖ Sentinel-3A provides an excellent coverage of the ocean, with more than 99.9% of measurements available over ocean. There is still some lost data due to the MWR calibration performed over ocean surface. A new calibration scheme was uploaded on 1 March 2018 to solve this issue.
- ❖ Data quality and stability is excellent, with only 4.1 % of outliers detected on the ocean measurements (after removal of sea ice contaminated data). Considering that we are rejecting 1% of sea level observations due to the MWR calibrations, this means that the rejected measurements will be close to 3.1 % after change of the MWR calibration timeline, which is fully consistent with the same metric observed for Jason-3 (3.4%) and SARAL/AltiKa missions (2.6%). Note that this low percentage for Sentinel-3A is excellent considering the larger coverage of the mission at high latitudes compared to Jason-3 mission when sea ice is not present.
- ❖ Sea level statistics show no long-term drifts, even if the analysed period is not long enough to have yet good confidence in the capability to detect very small drift
- ❖ Sentinel-3 and Jason-3 observe very similar SLA features when considering temporal evolution of global averages but also geographical patterns. Data quality is excellent in P-LRM mode while there is still some room for improvement in SARM. Since the version 2.24 of the Processing Baseline, quality of the SARM data has been dramatically improved by reducing the geographic errors and thus getting closer to the Jason-3 sea level quality.
- ❖ Absolute bias of sea level in SARM is estimated to be below 2 cm, based on absolute calibration sites and range transponder calibration. Global cross calibration with Jason-3 altimeter also confirm this low value of absolute bias, especially after the implementation of SAMOSA 2.5 retracker.
- ❖ At crossovers Sentinel-3A shows a performance similar to Jason-3 mission with a system error of 3.5 cm.
- ❖ Orbit quality is excellent for all product latencies (NRT, STC and NTC), even if crossovers analysis with NTC products suggests that the consistency between ascending and descending tracks can be further improved at basin scale.
- ❖ The time tag bias observed on Sentinel-3A is low with a mean value below 150 microseconds which is meeting the requirements.
- ❖ MWR Wet tropospheric correction shows a good performance with a standard deviation of 1.4cm for the difference with the model correction (Δwtc), and a variance reduction of -1.5cm^2 for the diagnosis at crossover points with respect to the model correction.



2.4 Winds and Waves

Sentinel-3A SRAL altimeter has been providing excellent wind speed and SWH observations over ocean. This report summarizes a variety of results, including comparisons with Jason-3, model and in-situ data to highlight and quantify the mission performance for Wind and Waves. The following conclusions are observed:

- ❖ Global statistics against the model are excellent. The agreement between Sentinel-3 winds and their model counterpart is very good with virtually no bias (except for slight bias at high wind speed values). The standard deviation of the difference (SDD) with respect to the model, which can be used as a proxy to the random error, is about 1.1 m/s. The correlation coefficient is higher than 0.95. These values are similar to those of the other altimeters.
- ❖ Global statistics against the buoys are excellent. The bias against in-situ observation for this period is rather small (about 0.1 m/s). The SDD is about 1.4 m/s which is about 17% of the mean. The correlation coefficient is higher than 0.92. These figures are comparable to same statistics emerging from the comparison of wind speeds from other altimeters against in-situ observations.
- ❖ While the SARM altimeter mean wind speed, the SDD and SI distributions wrt the model all look similar to their counterparts from other altimeters, the bias between altimeter and model wind speed is rather low almost everywhere.
- ❖ The PLRM wind speed is now globally unbiased. The SDD with respect to the model improved considerably since Cycle 012. However, it is slightly higher than that of SAR winds (and other altimeters). There is a tendency of PLRM wind speed to degrade slightly in the Northern Hemisphere during the summer months (June to August). This can be only confirmed during the coming years.

Keeping in mind that Jason-3, CryoSat-2, SARAL/AltiKa and Jason-2 are all conventional altimeters, it is possible to conclude that Sentinel-3A SARM wind speed is as good as (if not slightly better than) its counterpart from the conventional altimeters.

The SRAL Processing baselines introduced so far (especially Processing Baseline 2.24) improved the already good SARM SWH. By the end of 2017, the SWH bias with respect to the model and the in-situ measurements is almost zero. However, some fine tuning of the SAR SWH product is still needed to make it one of the best altimeter SWH products.

With previous processing Baseline, we observe the following conclusions:

- ❖ The agreement between Sentinel-3 SARM SWH and its model counterpart is very good except for a slight underestimation at SWH values below ~ 2 m and an overestimation at moderate to high SWH's (above ~ 4 m). The underestimation at lower wave heights, although less noticeable, is not noticed in the case of other altimeters. In general, compared to ECMWF model, Sentinel-3A overestimates SWH by about 0.14 m. The SDD between the pair is about 0.27 m (or 11% of the mean value). The correlation coefficient is 0.983 which is quite high.



These figures indicate that Sentinel-3A SARM SWH products are what is expected from radar altimeter SWH.

- ❖ Sentinel-3A SARM SWH is 0.16 m higher than the in-situ observations. The SDD (a proxy to the random error) is 0.30 m which is ~13% of the mean. The correlation coefficient is 0.978. These numbers indicate that Sentinel-3A SARM SWH products are now very close their counterparts from other altimeters.
- ❖ The bias in Sentinel-3A SAR SWH was one of the highest among the 5 operational altimeters between December 2016 (PB 2.09) and December 2017 (PB 2.24). PB 2.24 reduced SRAL SWH bias to almost zero. However, the SDD between Sentinel-3A SAR and the model is the highest among all altimeters irrespective of the various processing changes.

2.5 Land and Sea Ice

Sentinel-3A SRAL altimeter operates in SAR mode over areas of land ice and sea ice and shares a common heritage with Cryosat, the first altimetry mission to operate predominantly in this mode over sea ice. Sentinel-3A is however the first mission to operate in SAR mode over all land ice surfaces and hence the full commissioning of Sentinel-3A over land ice requires new methods, algorithm tuning, and validation. In comparison, Cryosat operates in LRM mode over the ice sheets, and in SARin interferometric mode over the ice sheet margins.

Sentinel-3A STM is an operational mission with a single ground segment shared between all surface types (ocean, sea ice, land ice, ice shelves, inland waters, coastal zones) which all have very different properties and processing requirements at each ground processor level. The initial optimization of the Sentinel-3 L1 ground processing was for ocean surfaces (whereas Cryosat was for ice surfaces) and hence the commissioning and tuning of the Sentinel-3 L2 processors for land and sea ice has been a more complex task than a simple retuning of the Cryosat derived sea ice and land ice L2 algorithms.

Tuning of sea ice algorithms for a new altimetry mission is a multi-stage process, which requires stable cycles of data acquired over one or more full Arctic winter seasons (Oct-May). Since Sentinel-3A was launched in February 2016, it was not possible to start all the sea ice commissioning tasks until reprocessed data from the winter of Oct 2016 - May 2017 became available during the summer of 2017. Since then good progress has been made in the key stages of sea ice surface type discriminator tuning and sea ice retracker validation and testing. Following analysis of Sentinel-3A sea ice data in autumn 2017, and an in-depth comparison with contemporaneous results and upgraded algorithm methods from Cryosat, a number of essential sea ice processor upgrades (from the forthcoming Cryosat baseline-D) and tasks have been identified as a requirement in order to complete Sentinel-3A sea ice commissioning. These include replacement of the diffuse echo retracker, optimised waveform filtering and outlier removal, an upgrade of the MSS to DTU15 (already completed in PB2.24 deployed on 13 December 2017) and retracker bias calibration. These tasks have been scheduled for the first half of 2018, after which it should be possible to produce a high-quality Sentinel-3A sea ice Arctic winter freeboard in the L2 product equivalent to the excellent results available from the Cryosat mission.



Due to sea ice conditions in Antarctica, where thin sea ice and snow loading are an issue, producing accurate freeboard measurements from either Sentinel-3A or Cryosat is still an area of active research. It is currently not possible to measure freeboard from SAR altimetry during the polar summer months (June-Sept in the Arctic) as summer melt creates pooling in the sea ice which makes discrimination between sea ice leads and floe echoes impossible.

For land ice processing, good progress was made during 2017 identifying key performance issues, tuning land ice algorithms, introducing new L2 land ice product parameters requested by users such as elevation derived from the OCOG retracker, and specifying requirements for evolutions of the low-level ground processing, which should result in reaching a good level of performance over land ice surfaces in 2018. Studies using prototype processors have tested many of these improvements and shown performance comparable with or exceeding previous missions over ice sheets.

The elevation derived from the OCOG retracker will provide a greater measurement density, but in some areas a lower accuracy. Nevertheless, elevation from the Ice-1 OCOG retracker is available from all previous radar altimetry missions providing a continuity of measurement technique that makes long term multi-mission studies of ice sheet surface elevation change and mass balance possible.

Due to the complexity of the multi-surface type Sentinel-3A ground segment, some evolutions to land ice processing identified during 2017 are still to be phased in to future product baseline releases in 2018, and users should take note of current issues with product quality detailed in the Land Ice Performance section and available in the Product Notices.

2.6 Inland waters

The data quality over inland waters was analysed over the Issykkul Lake which is a calibration site for altimetry. It showed that Sentinel-3A topography observations are very good, with no bias and an improved precision compared to Jason-3 mission.

The data acquisition over inland waters has been very much improved thanks to the Open Loop (OL) mode.

During the commissioning of Sentinel-3A early 2016, a database of hydrology targets over Europe was refined and uploaded to improve SRAL data acquisition in Open Loop mode. With more than one year of data in OL mode, the percentage of acquired targets is close to 83% (France) and 98% (Europe, larger rivers). This is much better than with the classic Closed Loop mode and it is expected that the improvement will be much higher when the density of the target database will be improved (defining more small targets).

It has to be noted that narrow rivers (between 100 and 200 meters wide) which were never observed when the Sentinel3 altimeter were operated in Closed Loop mode (during the very first cycles of the commissioning phase) are now observed when the Open Loop mode was activated. And since then, they have been observed for all the overpasses.

3 SRAL and MWR Mission events

The Table below gathers the changes related to sensors mode.

Start time	Stop Time	Event
6 Dec 2016	onward	Switch from Open Loop mode to Closed Loop mode over Antarctica and Greenland margins
19 Dec 2017	onward	Switch from Open Loop mode to Closed Loop mode over Greenwich meridian
1 March 2018	onward	Change of MWR calibration timeline

Table 1 History of SRAL and MWR mode changes

The Table below gathers the major events that occurred on the STM payload.

Event type	start time	stop time	description
Platform	2017-12-13 07:58:00	2017-12-13 08:31:00	out-of-plane-manoevre
Platform	2017-11-29 09:13:00	2017-11-29 09:27:00	in-plane-manoevre
Platform	2017-09-27 08:01:00	2017-09-27 08:15:00	in-plane-manoevre
Platform	2017-09-06 10:15:00	2017-09-06 10:50:00	out-of-plane-manoevre
Platform	2017-07-12 09:38:00	2017-07-12 09:50:00	in-plane-manoevre
SRAL	2017-06-26 13:20:00	2017-06-26 13:20:00	SRAL OLTC update
Platform	2017-05-23 14:28:00	2017-05-23 14:42:00	in-plane-manoevre
Platform	2017-04-27 10:51:00	2017-04-27 11:05:00	in-plane-manoevre
Platform	2017-03-15 07:32:00	2017-03-15 08:07:00	out-of-plane-manoevre
Platform	2017-02-23 09:33:00	2017-02-23 09:46:00	in-plane-manoevre
Platform	2016-12-14 08:36:00	2016-12-14 09:10:00	out-of-plane-manoevre



Sentinel-3 MPC
S3MPC STM Annual Performance
Report - Year 1

Ref.: S3MPC.CLS.APR.002
 Issue: 1.1
 Date: 23/05/2018
 Page: 8

Event type	start time	stop time	description
Platform	2016-12-01 07:53:00	2016-12-01 08:06:00	in-plane-manoevre
Platform	2016-11-01 11:58:00	2016-11-01 12:11:00	in-plane-manoevre
Platform	2016-08-31 07:25:17	2016-08-31 07:33:56	out-of-plane-manoevre
Platform	2016-07-21 12:44:58	2016-07-21 12:45:01	in-plane-manoevre
SRAL	2016-06-23 08:23:35	2016-06-23 09:32:44	software patch (ASW v2.5)
Platform	2016-06-02 11:13:39	2016-06-02 11:13:52	in-plane-manoevre
SRAL	2016-05-29 15:35:13	2016-05-29 15:38:36	SRAL SpW ASIC Anomaly
SRAL	2016-05-25 12:26:15	2016-05-25 14:30:05	Anomaly GS3_SC-23
SRAL	2016-05-24 12:30:00	–	OLTC v4.1 uploaded.
SRAL	2016-05-23 09:32:25	2016-05-24 12:22:25	SAR CL Mode with DEM EEPROM read enabled
SRAL	2016-05-23 08:00:00	2016-05-23 09:32:00	patch of SRAL ASW v2.4
Platform	2016-05-18 08:59:17	–	MHSTR MI patch for pointing issue
SRAL	2016-05-17 15:24:00	2016-05-17 15:28:00	SRAL SpW TRM anomaly
SRAL	2016-05-15 09:28:00	2016-05-15 09:40:00	SRAL SpW TRM anomaly
SRAL	2016-05-15 03:43:00	2016-05-15 04:12:00	SRAL SpW TRM anomaly
SRAL	2016-05-09 10:42:00	2016-05-09 10:43:00	SRAL SpW TRM anomaly
SRAL	2016-05-04 21:44:00	2016-05-04 21:54:00	SRAL SpW TRM anomaly
SRAL	2016-04-29 20:30:00	2016-04-29 21:10:00	SRAL SpW TRM anomaly
SRAL	2016-04-27 12:56:27	2016-04-27 12:57:02	SRAL SpW TRM anomaly



Sentinel-3 MPC
S3MPC STM Annual Performance
Report - Year 1

Ref.: S3MPC.CLS.APR.002
 Issue: 1.1
 Date: 23/05/2018
 Page: 9

Event type	start time	stop time	description
SRAL	2016-04-27 10:57:52	2016-04-27 10:59:20	SRAL SpW TRM anomaly
SRAL	2016-04-20 10:32:30	2016-04-20 10:42:23	SRAL SpW ASIC anomal
SRAL	2016-04-19 18:53:14	2016-04-19 18:56:02	SRAL SpW ASIC anomaly
Platform	2016-04-19 12:03:00	2016-04-19 12:09:44	out-of-plane-manoevre
SRAL	2016-04-18 03:43:43	2016-04-18 06:07:14	Altimeter anomaly: bursts #1&4 are missing
SRAL	2016-04-16 19:04:00	2016-04-16 20:34:19	Altimeter anomaly: bursts #1&4 are missing
SRAL	2016-04-15 11:03:03	-	SRAL operating in CL/OL according to the ZDB
Platform	2016-04-13 09:10:56	2016-04-13 10:52:00	in-plane-manoevre
SRAL	2016-04-12 09:30:06	2016-04-15 11:03:00	SRAL operating in SAR CL
SRAL	2016-04-11 08:30:00	2016-04-11 09:07:00	Cross cal maneuver
SRAL	2016-04-08 00:00:00	2016-04-08 23:59:00	Activate SRAL SAR_OL Mode for 24 hours
SRAL	2016-04-07 00:00:00	2016-04-07 23:59:00	Activate SRAL SAR_CL and SAR_OL Mode changes
SRAL	2016-04-06 00:00:00	2016-04-06 23:59:00	SRAL SAR_CL Mode for 24 hours.
SRAL	2016-03-30 08:51:14	2016-03-30 08:51:50	SRAL Standby Mode followed by SAR Open Loop
SRAL	2016-03-29 23:56:01	2016-03-29 23:56:37	SRAL Standby Mode followed by SAR Open Loop
SRAL	2016-03-29 17:15:02	2016-03-29 17:15:38	SRAL Standby Mode followed by SAR Open Loop
SRAL	2016-03-29 12:42:26	2016-03-29 12:43:02	SRAL Standby Mode followed by SAR Open Loop

Event type	start time	stop time	description
SRAL	2016-03-24 08:06:21	2016-03-24 08:06:57	SRAL Standby Mode followed by SAR Open Loop
SRAL	2016-03-24 00:52:00	2016-03-24 00:52:36	SRAL Standby Mode followed by SAR Open Loop
SRAL	2016-03-23 16:30:09	2016-03-23 16:30:45	SRAL Standby Mode followed by SAR Open Loop
SRAL	2016-03-23 13:38:40	2016-03-23 13:39:16	SRAL Standby Mode followed by SAR Open Loop
Platform	2016-03-23 13:26:28	–	in-plane-manoevre
Platform	2016-03-21 11:17:47	2016-03-21 11:22:47	out-of-plane-manoevre
SRAL	2016-03-18 11:36:00	2016-03-18 12:03:00	SRAL Cross-Calibration Manoeuvre
Platform	2016-03-13 10:51:55	2016-03-13 10:55:00	in-plane-manoevre
SRAL	2016-03-08 10:42:00	2016-03-08 15:36:50	SRAL calibration sequence
Platform	2016-03-07 12:21:24	–	out-of-plane-manoevre
Platform	2016-03-02 15:32:56	–	in-plane-manoevre
Platform	2016-03-02 12:59:00	–	in-plane-manoevre
SRAL	2016-03-01 07:38:00	–	SRAL switch on

Table 2: Main Sentinel-3A SRAL and Platform events since the SRAL switch on. The shaded lines correspond to a data gap impact on Level-2 products.

4 Processing Baseline Status

4.1 Land and Marine Products

- ❖ Land products that cover all land areas and part of the ocean up to 300 km off the shore (white and brown on the map). This result in gathering all coastal areas, including basins such as the Mediterranean Sea, land ice regions, inland waters and part of the sea ice regions.
- ❖ Marine products that cover all ocean and land areas up to 10 km from the shore (blue and brown on the map).

Note that the brown regions on the map stand for regions that are available in both products. Since Processing Baseline 2.24, the Caspian Sea, Great Lakes and Victoria Lake are available in both Marine and Land products.

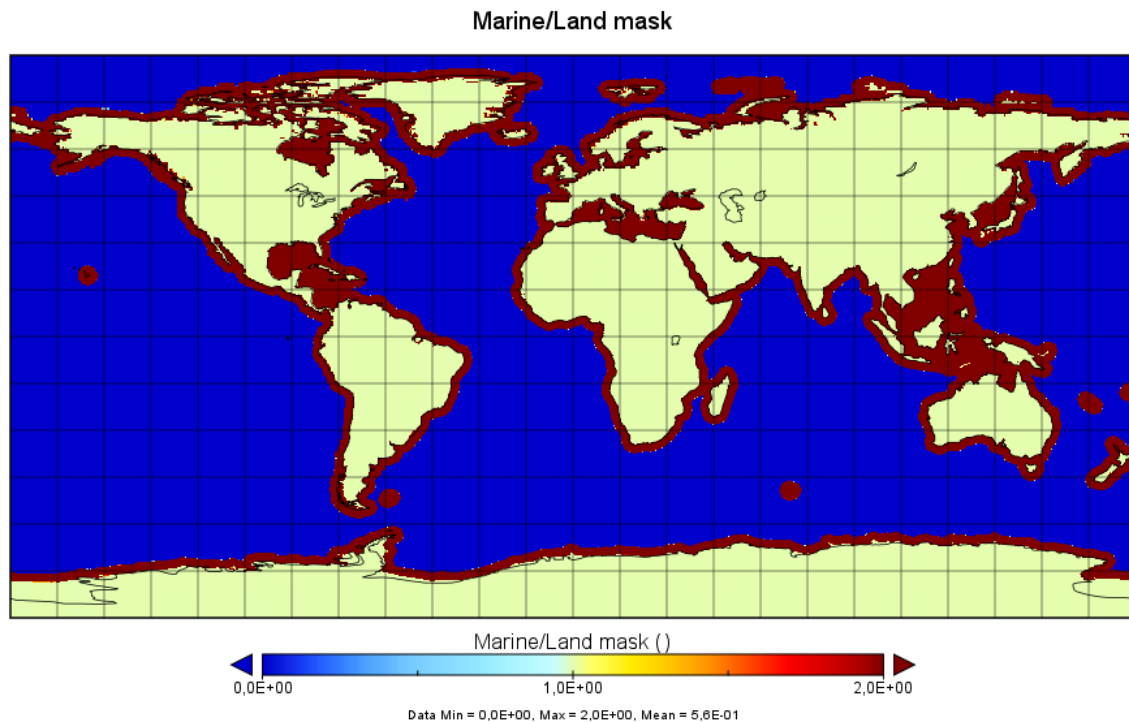


Figure 1 Geographical mask for L2 Land and Marine products coverage: blue is Marine products only, white is Land products only, brown is for regions available in both products

4.2 Processing Baseline History

The history of the processing baseline deployed in the Sentinel-3 processing centres is summarized below. All the deployment dates impact NRT and STC products while **the NTC production started on 13 December 2016 with Processing Baseline 2.9.**

Installation Date	IPF Version	Processing Baseline
2016-07-21	SM2 06.02	2.0
2016-08-03	SM2 06.03	2.1
2016-10-26	SM2 06.05	2.5
2016-11-08	SM2 06.05	2.8
2016-12-13	SM2 06.05	2.9
2017-02-28	SM2 06.06	2.10
2017-04-12	SM2 06.07	2.12
2017-12-13	SM2 06.10	2.24
2018-02-14	SM2 06.12	2.27
2018-04-04	SM2 06.14 (current)	2.33

The NTC products have been reprocessed twice:

❖ Reprocessing 1 with Processing Baseline 2.12

The products span from 16 June 2016 till 15 April 2017. Both Marine and Land L2 products were reprocessed.

❖ Reprocessing 2 with Processing Baseline 2.27

The products start since the beginning of the mission and span from 1 March 2016 till 20 January 2018. Both Marine and Land L2 products were reprocessed.

4.2.1 Summary of Processing Baseline Content

Processing Baseline 2.12 was the processor version used for deriving most of the results presented in this document. There is no evolution of algorithm nor model coming from Processing Baseline 2.12. The content is completely described by the list of the anomaly fixes detailed in Annex. The main impact is for inland waters parameters quality that have been dramatically improved thanks to fixes on OCOG retracker.



Sentinel-3 MPC
S3MPC STM Annual Performance
Report - Year 1

Ref.: S3MPC.CLS.APR.002
 Issue: 1.1
 Date: 23/05/2018
 Page: 13

Processing Baseline 2.24 represents major achievements and improvements for ocean and coastal areas, sea ice and land ice parameters quality. In addition to the resolution of the anomalies listed in Annex, Processing Baseline 2.24 brings major evolutions of product quality over ocean, coastal sea ice and land ice surfaces. These improvements are detailed in:

<https://earth.esa.int/documents/247904/3147059/Sentinel-3-STM-Product-Evolution-Processing-Baseline-2.24>

Processing Baseline 2.27 is the version used in operation and for the Reprocessing 2. In addition to some minor anomaly fixes, it brings important improvement to the land ice quality with the inclusion of ice elevation derived from the OCOG retracker and the fix of the SARM slope correction.

Processing Baseline 2.33 is the latest version used in operation. In addition to the resolution of some minor anomalies in LRM mode and for the dry tropospheric correction, the evolution deals with the inclusion of the SRAL acquisitions measurements in the SRAL Level 1 products and the evolution needed in the Level 2 ground processor to manage the new MWR calibration timeline.

4.2.2 Model and standard history

Table below summarizes the different models and standards used in the STM Processing baseline. Note that the models and standard are aligned between L2 Land and Marine products.

Correction model and standard	Processor Version			
	IPF-SM2 06.05	IPF-SM2 06.07	IPF-SM2 06.10	IPF-SM2 06.12/06.14
Orbit solution	ESA/POD solution for NRT (GPS solution) CNES/SALP solution with POE-E standards for STC (Doris solution) CNES/SALP solution with POE-E standards for NTC (Doris + GPS solution)			
SARM Ocean retracker	SAMOSA 2.3 retracker		SAMOSA 2.5 retracker	
Dry troposphere correction	ECMWF model			
Dynamical atmospheric correction	SALP/CNES Mog2D high resolution ocean model			
Radiometer wet troposphere correction	3 parameters correction		3 parameters and 5 parameters corrections	
Model wet troposphere correction	ECMWF model			
Ionospheric correction	SALP/CNES maps based on Global Ionosphere TEC Maps from JPL			
Wind Speed model	Abdalla model			
Sea State Bias	Jason-2 Sea State Bias from Tran model (2012)			

Correction model and standard	Processor Version			
	IPF-SM2 06.05	IPF-SM2 06.07	IPF-SM2 06.10	IPF-SM2 06.12/06.14
Ocean tide correction Solution 1 (including loading tide)	GOT 4.10			
Ocean tide correction Solution 2 (including loading tide)	FES 2004		FES 2014	
Solid Earth tide correction	Cartwright and Taylor			
Pole tide correction	Wahr			
Mean Sea Surface Solution 1	CNES_CLS_2011 (Referenced to 7 years mean)		CNES-CLS 2015 (Referenced to 20 years mean)	
Mean Sea Surface Solution 2	DTU13 (Referenced to 7 years mean)		DTU15 (Referenced to 20 years mean)	
SSHA for Ocean	CNES_CLS_2011		DTU15	
SSHA for Sea Ice	CNES_CLS_2011		DTU15	
Mean Dynamic Topography	CNES-CLS13 MDT			
Geoid	EGM 2008			
Bathymetry	ACE2 model with 30 second resolution			
Surface Slope Model for Land Ice	Derived from RAMP v2 DEM over Antarctica and Bamber 2001 DEM over Greenland			
Rain Flag	Envisat model (Tran et al 2008)			
Ice flag	Envisat model (Tran et al 2009)			
ice-sheet snow facies type flag	Envisat model (Tran et al 2008)			

Table 3 Model and standard history in L2 products

4.3 Status of the current Processing Baseline

The operational processing baseline is 2.33, deployed on 4 April 2018, in Land and Marine Centres.

	<p style="text-align: center;">Sentinel-3 MPC</p> <p style="text-align: center;">S3MPC STM Annual Performance</p> <p style="text-align: center;">Report - Year 1</p>	<p>Ref.: S3MPC.CLS.APR.002</p> <p>Issue: 1.1</p> <p>Date: 23/05/2018</p> <p>Page: 15</p>
---	---	--

4.4 List of anomalies in the Processing Baseline

Since June 2016, the details of the anomalies that have been closed through the different Processing Baseline versions are detailed in the different Product Notice documents issued for the SRAL L1 products, L2 Land products. These documents are published for each Processing Baseline and can be found on:

<https://sentinel.esa.int/documents/247904/2753172/Sentinel-3-Product-Notice-STM-Level-1>

<https://sentinel.esa.int/documents/247904/2753172/Sentinel-3-Product-Notice-STM-Level-2-Land>

5 Sensors status

5.1 SRAL

The SRAL Internal Calibration parameters are regularly measured on-board and have been gathered in order to monitor the performance of the instrument. Here below we have a summary, from the beginning of the mission up to the end of 2017, of the main calibration variables that impact the quality of the final geophysical retrievals.

The internal delay is measured on-board, to be then subtracted from the final range in the L1b processing. Hence, it has an additive impact in the SSH. The Ku band CAL1 SAR mode (main operational band and mode) internal delay behaviour along the mission is shown Figure 2. It has a drift of -0.9 mm/year, which is a nominal behaviour.

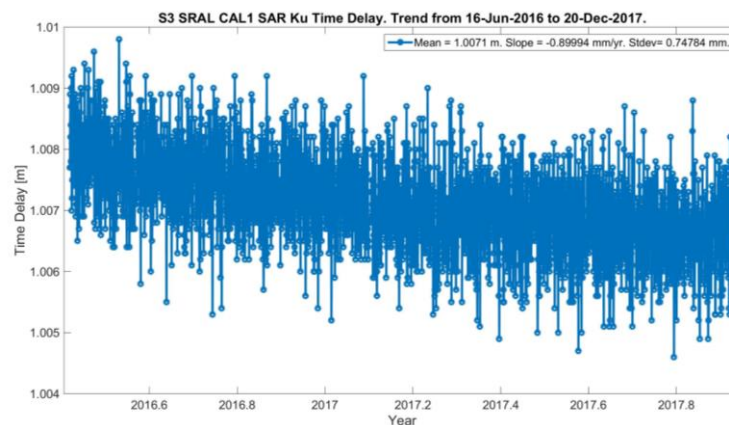


Figure 2: Ku band CAL1 SAR Time Delay series.

The calibration signal power variations with respect to ground measurements are used to compensate the science signal σ_0 in the L1b processing. It has mainly an impact in the winds retrievals. The Ku band CAL1 SAR mode total (blue line) and maximum (red line) power behaviour along the mission are plotted in Figure 3. The total power, the one used in the L1b processing, has a drift of close to -0.5 dB/year, a more stable behaviour than the one at the beginning of the mission that was close to -1 dB/year.

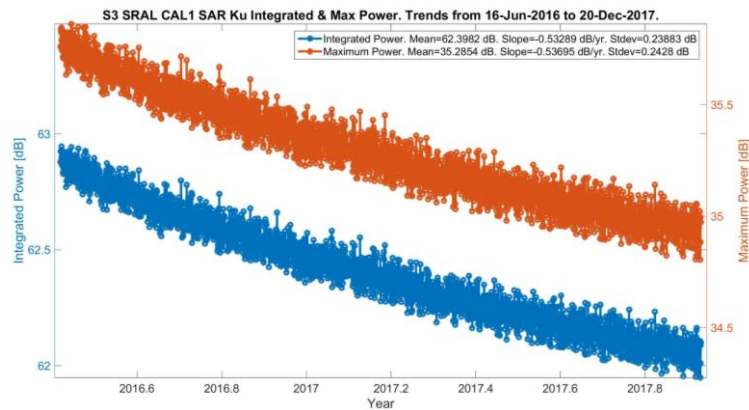


Figure 3: Ku band CAL1 SAR Integrated and Peak Power series.

The CAL1 PTR width, which impacts the SWH estimations, has a nominal drift of about -0.5mm/year, close to the standard deviation of the mission series, and three orders of magnitude below its absolute value. Its series is depicted in Figure 4.

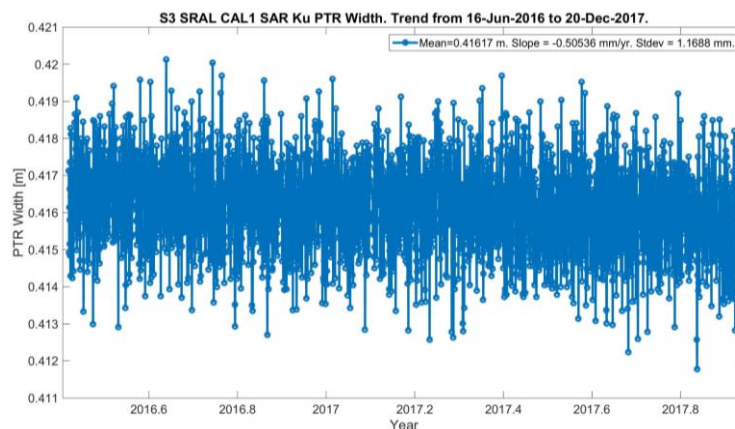


Figure 4: Ku band CAL1 SAR PTR width series.

Finally, a mesh of the mission Ku band SAR CAL2 waveforms (the system transfer function), used to correct the science waveform shape for the spectra distortions, is shown in Figure 5. The CAL2 signal presents the expected behaviour, with stable slopes and standard deviations along the mission.

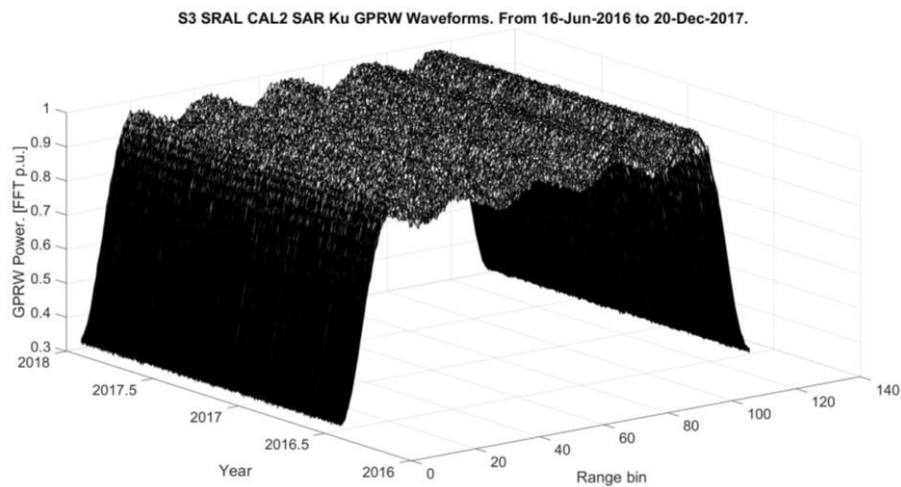


Figure 5: Ku band CAL2 SAR waveforms series.

Summarising, all the parameters are indicating a good instrument performance. The drifts are generally bigger than the ones in other ESA altimetry missions such as EnviSat and CryoSat-2. Anyhow, all the parameters are meeting the mission requirements. The CAL1 SAR Ku band total power was the only having a decay out of the expected at the beginning of the mission, but it is becoming more stable, as depicted in Figure 2 of this section (now the drift is half the one at BOM).

5.2 MWR

The MWR on-board Sentinel-3 is a noise injection radiometer operating at two frequencies (23.8GHz and 36.5GHz) with a bandwidth of 200MHz for both channels. The MWR operates as a balanced Dicke radiometer for brightness temperatures lower than the reference load. The balance is achieved by the injection of noise with a noise diode (NIR). For brightness temperatures higher than the reference, the MWR operates in a conventional Dicke mode (**Dicke Non-Balanced**).

5.2.1 MWR processing

The transition from one processing to the other will occur depending on the internal temperature of the MWR and the observed temperature. For the 23.8GHz channel, all measurements use the NIR processing. For the 36.5GHz, only a small percentage of measurements over land requires a DNB processing. The measured brightness temperatures depend of the emissivity of the surface, of its temperature, thus a seasonal dependancy in the geolocation of these measurements is observed.

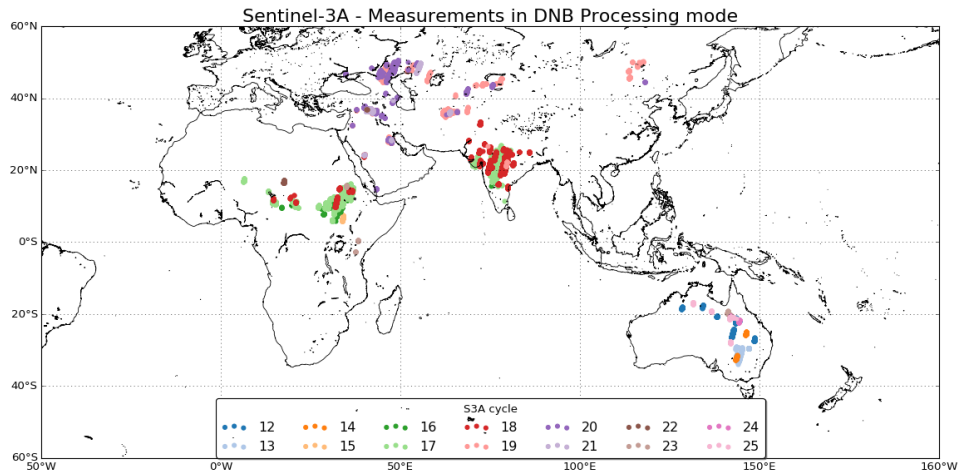


Figure 6: Geolocation of MWR measurements in DNB mode

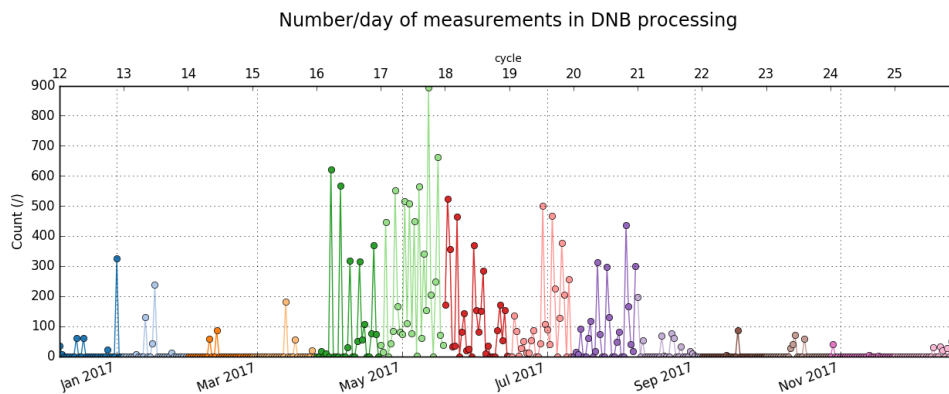


Figure 7: Number of measurements in DNB mode along the year

5.2.2 MWR Calibration timeline

The MWR is calibrated 3 times per orbit with the current settings of the calibration timeline. Each calibration sequence is about 9s long with two modes of calibration: one for the noise injection temperature, one for the receiver gain. After coregistration of MWR pixels in Level2 processing, calibration sequences cause data gaps of brightness temperatures of about 17s. A new calibration timeline has been proposed by MPC in order to reduce the length of the calibration sequences and guarantee a full coverage of brightness temperatures at Level2 processing.

5.2.3 MWR Calibration parameters

Each calibration parameter is carefully monitored. Figure 8 shows the receiver gain and the noise injection temperature monitoring since march 2016 until end of year 2017, each year being piled on top of the other. The receiver gain for channel 23.8GHz has increased since the switch-on. It has decreased for the channel 36.5 GHz eventhough it shows a period in the year with a small increase. The noise injection temperature for channel 23.8 GHz is very slowly decreasing (less than 0.2K over 2017). For

channel 36.5 GHz, the noise injection temperature is showing a global increase with a period of slow decrease during the year.

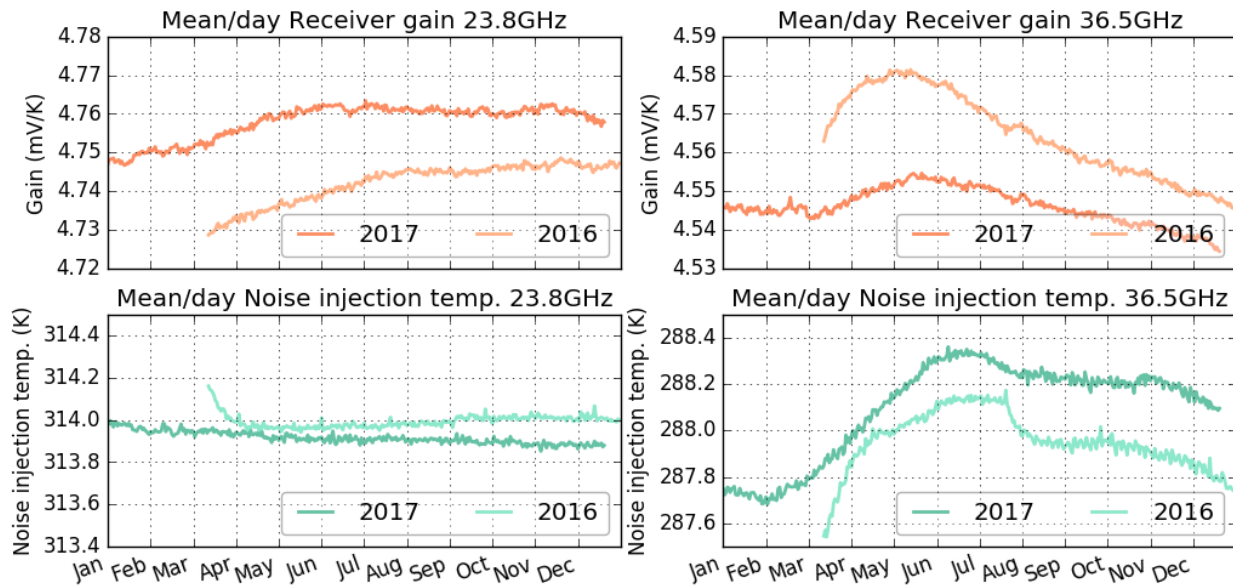


Figure 8: Monitoring of MWR calibration parameters: Receiver gain (top line), Noise injection temperature (bottom line) for both channels: 23.8GHz (left) and 36.5GHz (right)

5.2.4 MWR Brightness Temperatures monitoring

The main difficulty in microwave radiometry is the lack of reference natural target well-known or homogeneous enough that can be used for calibration or monitoring. Thus the assessment of the MWR brightness temperatures stability is performed using statistical selection over two specific regions of Earth: the coldest temperatures over ocean, the hottest temperature over the Amazon forest. Moreover these methods are applied to several missions for intercomparison: SARAL/AltiKa, Jason3/AMR and Metop02/AMSU-A. The characteristics of these missions is given in Table 4.

Table 4: Characteristics of missions with microwave radiometer

Mission	Frequencies	Inclination	Local time at A/D node
Metop02/AMSUA	23.8GHz 31.4GHz	98.7°	A 21:30
Jason-3/AMR	23.8GHz 34GHz	66°	
Sentinel-3A	18.7GHz 23.8GHz 36.5GHz	98.65°	D 10:00
SARAL/AltiKa	23.8GHz 37GHz	98.55°	A 06:00

Following the method proposed by Ruf [RD 1], updated by Eymar [RD 3] and implemented in [RD 7], the coldest ocean temperature is computed by statistic selection over clear sky condition. Ruf has demonstrated how a statistical selection of the coldest BT over ocean allows detecting and monitoring drifts. It is also commonly used for long-term monitoring or cross-calibration as in [RD 4], [RD 5] or [RD 6].

The Amazon forest is the natural body the closest to a black body for microwave radiometry. Thus it is commonly used to assess the calibration of microwave radiometers [RD 2] [RD 3]. The method proposed in these papers have been used as a baseline to propose a new method implemented in [RD 7]. In this new approach, a mask is derived from the evergreen forest class of GlobCover classification over Amazon. The average temperature is computed here over a period of one month for all missions. The same method is applied here.

5.2.4.1 Coldest ocean temperatures

Figure 9 shows the monitoring of the coldest ocean points for both channels, each year of data being piled on top of the other. For the 23.8GHz channel (frequency common to all cited missions), the average coldest ocean temperature is around 140K for AltiKa, AMSU-A and S3A, while for Jason3 it is around 134.5K due to calibration choices. For the second channel, each mission has a different frequency as shown in Table 4, thus a different average coldest ocean temperature. We retrieve a very similar level for Sentinel-3A and AltiKa due to their very close frequency. One can notice the very good consistency of the 2017 results with respect to 2016 results for all missions showing no clear sign of drifts or abnormal events along the period.

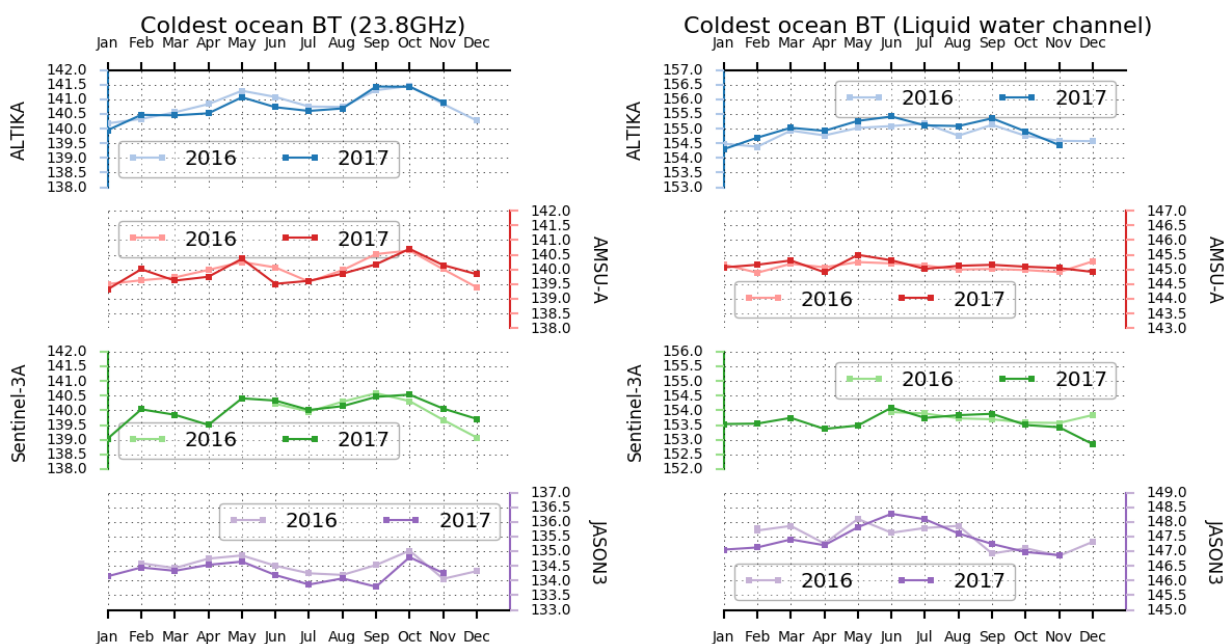


Figure 9: Coldest temperature over ocean for Sentinel-3A, SARAL/AltiKa, Metop02/AMSU-A, Jason3/AMR for two channels 23.8GHz (left) and 36.5GHz (right)

5.2.4.2 Amazon hottest temperatures

Figure 10 shows the monitoring of the hottest temperatures over the Amazon forest for both channels, each year of data being piled on top of the other. The average hottest temperature is very similar for all four missions for channel 23.8 GHz with a difference of less than 2K. The difference is a little larger for the liquid water channel due to the difference of frequency. One can notice the very good consistency of the 2017 results from may to december with respect to 2016 results over the same period for all missions. A difference between the two years is observable for the period January-April for all missions. This difference between 2016 and 2017 can be explained by the strong El Nino event of 2015 which slowly decreased until beginning of 2016 and affected water vapor content over the Amazon forest. From these results, there is no sign of drifts or abnormal events.

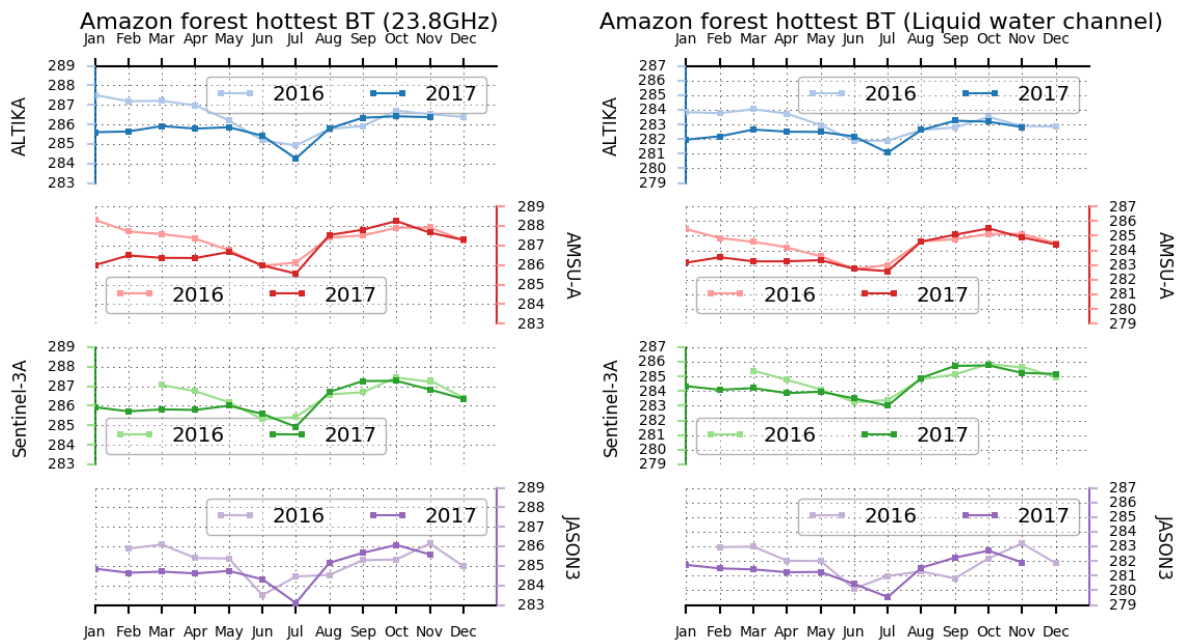


Figure 10: Hottest temperatures over the Amazon forest for Sentinel-3A, SARAL/AltiKa, Metop02/AMSU-A, Jason3/AMR for two channels 23.8GHz (left) and 36.5GHz (right)

6 SRAL Tracking performances

The analysis of the percentage of available and missing measurements gives a relevant information about the altimeter performances. It also allows to point out several kinds of events that have an impact on the satellite platform and on the data circulation.

6.1 Over Ocean

Figure 11 shows the monitoring of the daily percentage of available measurements from end of December 2016 to end of the year 2017. This diagnosis was performed using the water Non-Time-Critical (NTC) Level-2 products provided on the fly. Over one full year, it shows that 99.88% of the Sentinel-3A measurements are available. We also notice several occurrences with a lower percentage. These data gaps are related to ground segment anomalies (Marine products not available) since over this period, only one SRAL anomaly occurred on 1 September 2017. Reprocessing task allows to recover these missing measurements and thus to complete the Sentinel-3A dataset. Applying a selection to remove the land surfaces (water products include a band of 30km within land surfaces), both Sentinel-3A and Jason-3 percentage of available measurements are very close (respectively 99.97 % and 99.98%). This metric confirms that the percentage of SRAL acquisitions over ocean is excellent and we are observing 100% of acquisitions when the ground processing works nominally

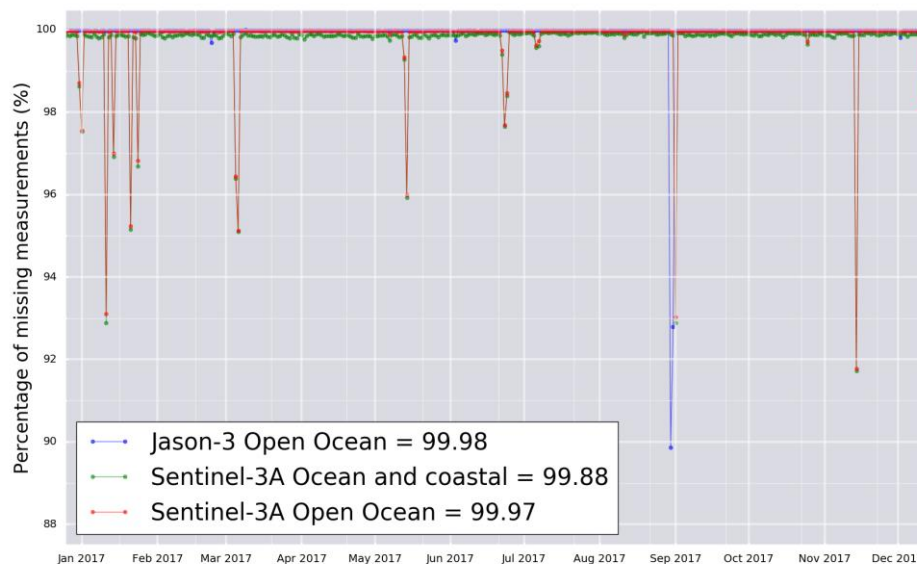


Figure 11: Monitoring of the daily percentage of available measurements for Sentinel-3A over Ocean and coastal area (green curve), Sentinel-3A over open Ocean (red curve) and Jason-3 over open Ocean (blue curve). This metric is computed with respect to the theoretical track and the theoretical number of measurements expected.

The map displayed in Figure 12 shows the geographical location of the missing measurements over Ocean surfaces only. Large along-track patterns related to period with reduced data availability are observed. These periods correspond to ground segment anomaly as mentioned previously. In any case, the Sentinel-3A data availability is within the requirements.

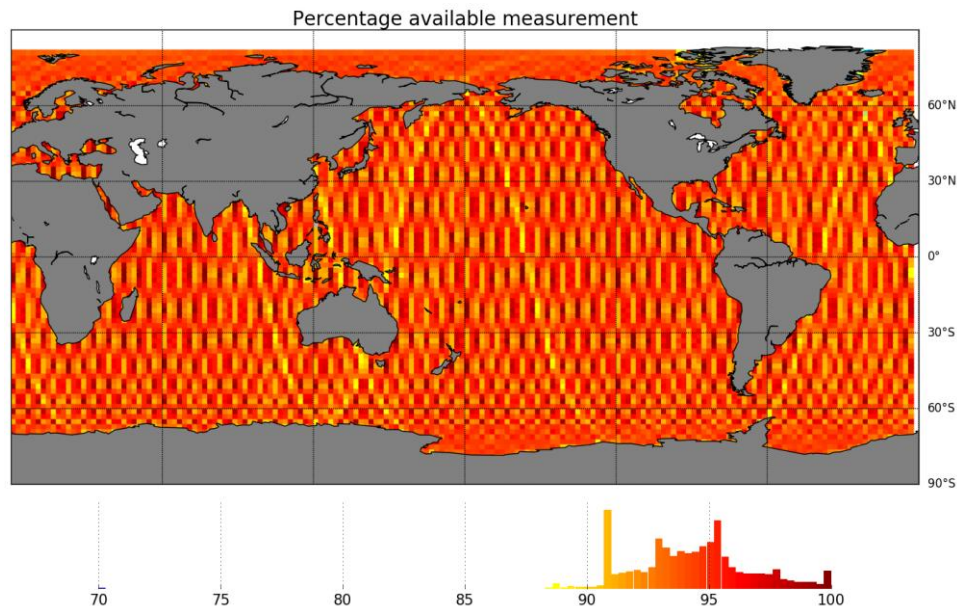


Figure 12: Map of the gridded percentage of missing measurements over Ocean computed from December 2016 to December 2017. The analysis is based on the NTC Level-2 Marine products delivered on the fly.

6.2 Over Land

While the detection of missing measurements is done at 1 Hz over ocean, the detection needs to be computed using High Rate frequency (20Hz) dataset over land. The location of the missing measurements gives a relevant information about the SRAL altimeter tracking performances. Indeed, if over open Ocean, the delay of the returned signal is easily predictable and quite constant, the surface type and topography variations over land surfaces make the measurement more complicated and challenging.

Over land, there are two different modes for SRAL acquisition: The Open-Loop (OL) and the Closed-Loop (CL) acquisitions. The SRAL acquisition mode is geographically pre-defined following the mask plotted in Figure 13. Over OL areas, the tracking command is derived from an elevation model whereas, over CL areas the tracking window is automatically adjusted as a function of the returned signal. Figure 14 top panel shows the geographical distribution of missing measurements within the land level-2 products for the cycle 25 (from 11th of November 2017 to 20th of December 2017). When the altimeter operates in OL mode, the number of missing measurements is much lower. In CL mode, the acquisition of the returned

signal mainly depends on the surface topography as illustrated by the zoom over Central America, bottom panel Figure 14. Note also that the global map highlights five areas with two parallel bands of missing measurements (South of Africa, Australia, Gobi desert, Sahara desert, Arabian Peninsula). These locations correspond to the SRAL calibration sites that are performed over the same regions for all the cycles. The three portions of track in the Sahara desert are due to the SRAL AutoCal calibrations. Finally some isolated points are observed in the Ocean, close to the coasts, they are located at the border of the Sentinel-3A water and land products mask. They could be considered as a false alarm since the position of the theoretical first measurement cannot be known precisely.

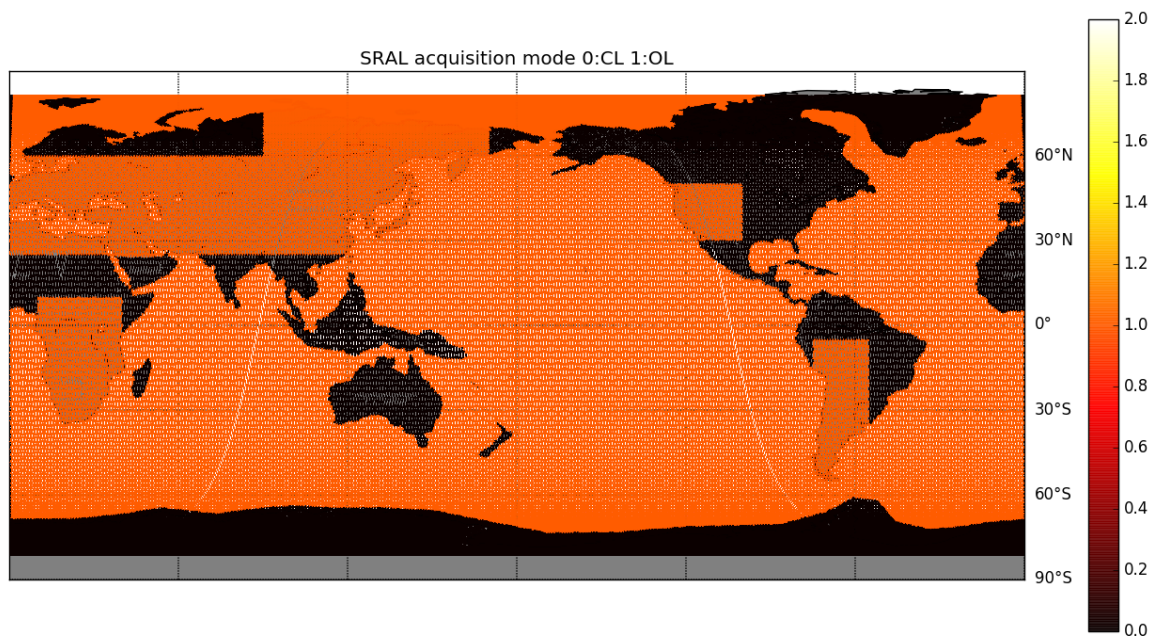


Figure 13: Map of the SRAL tracking mode plotted for cycle 26 (from 20th of December 2017 to 16th of January 2018). Orange color corresponds to Open-Loop acquisition mode. Black color corresponds to Close-Loop acquisition mode.

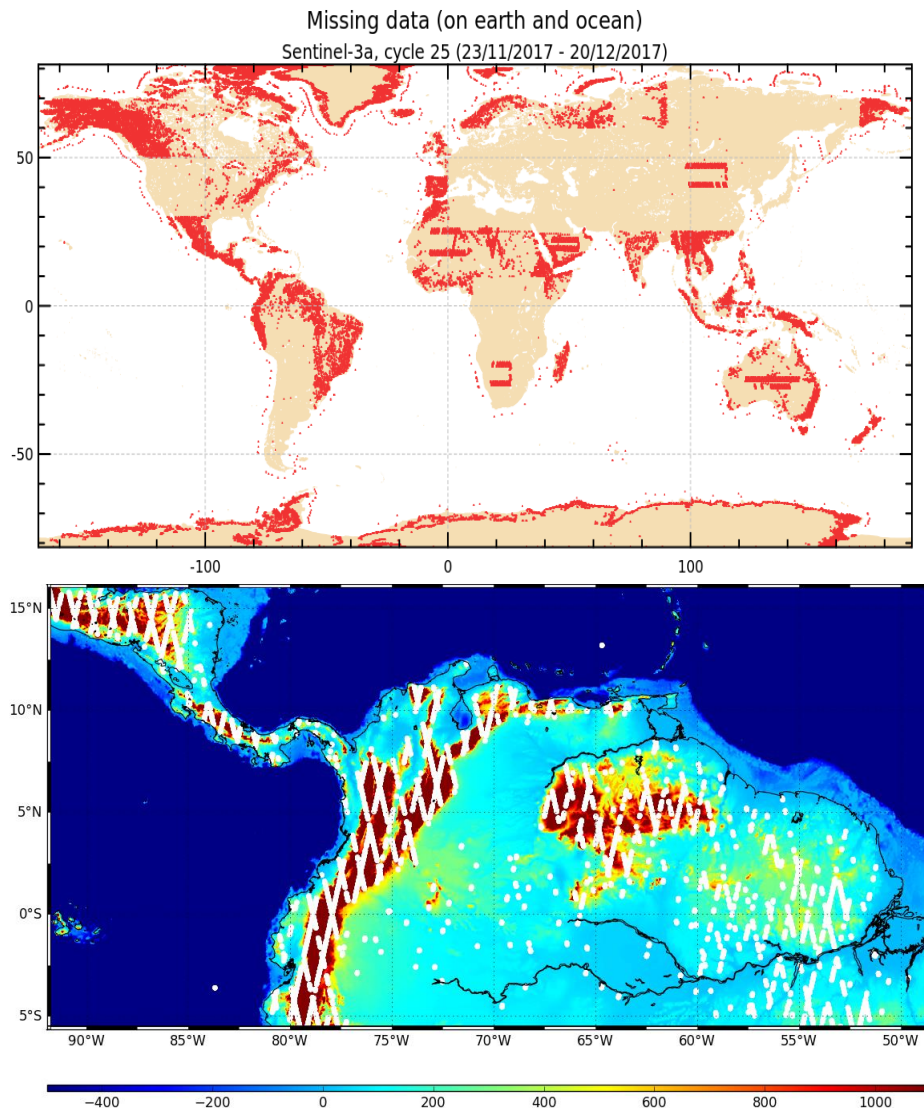


Figure 14: Global map (top panel) of the Sentinel-3A missing measurements for cycle 25 (from 11th of November 2017 to 20th of December 2017). Zoom (bottom panel) over Central and South America of the missing Sentinel-3A measurements (plotted in white) superimposed on a bathymetry grid.

A focus on the Arctic and Antarctic regions also gives interesting results. It clearly appears that when the altimeter operates in Closed-Loop mode (over Antarctica and Greenland for example) the missing measurements are mainly located over the margins. The map and the along-track plot of the backscatter coefficient over the Antarctica illustrate the surface type sampled by Sentinel-3A and helps to understand the behaviour of the tracker. The sigma0 plotted is derived from the OCOG retracker which is quite robust to retrieve a signal compared to other retracker, even if less accurate. As this is not a physical retracker the absolute value of the backscatter coefficient differs from the one obtained over Ocean with the SAMOSA ocean retracker. We applied here a -34 dB bias on the OCOG sigma0 to align it on the level of signal usually observed over ocean. The following behaviour is observed:

- ❖ Over ocean, the backscatter coefficient (sigma0) is centred on 11 dB.

- ❖ Approaching the Antarctica continent, over sea ice surfaces the backscattering energy increased and the sigma0 reaches values higher than 30 dB.
- ❖ At the borders of the Antarctica continent, over the margins, the amplitude of the measured signal is very low. This region corresponds to the location of most of the missing measurements: SRAL altimeter either lost the signal or acquired a very low signal. This behaviour was expected since SRAL sensor was not designed to acquire signal over the margins.
- ❖ Finally, over the Antarctica interior, the OCOG backscatter coefficient varies from 5 to 20 dB depending on the type of surface.

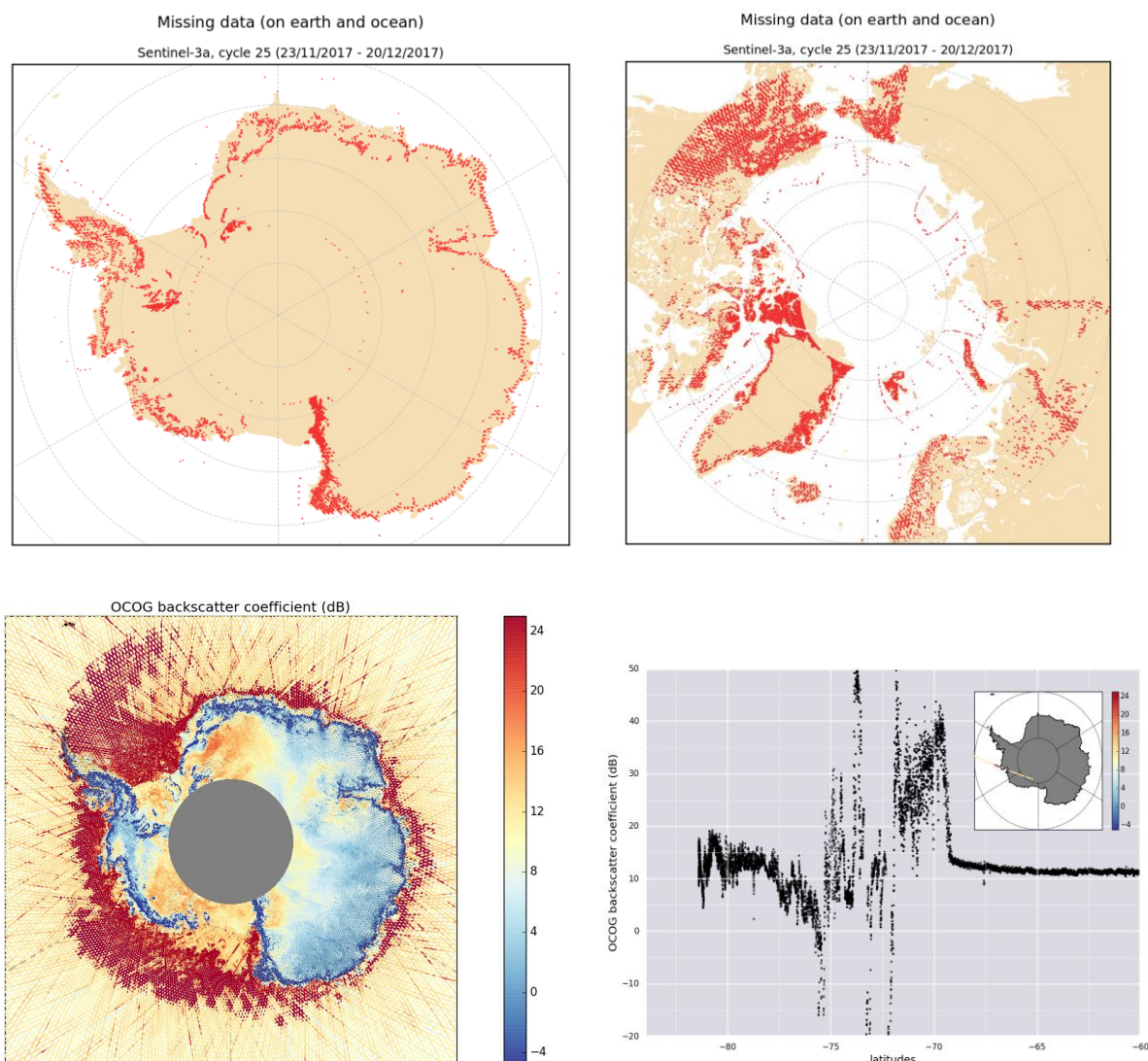


Figure 15: left panels show the Sentinel-3A missing measurements for cycle 25 (from 11th of November 2017 to 20th of December 2017) over Antarctica (left panel) and over the Arctic (right panel) areas. Bottom left panel shows the ocog backscatter coefficient over Antarctica for cycle 25. This variable is derived from both S3A L2 LAND and WATER products. The bottom right panel shows the ocog backscatter coefficient for one pass that cross the Antarctica continent. The along-track profile is derived from both S3A L2 LAND and WATER products.

Although the Open-Loop mode allows to record a larger number of measurements over land surfaces, it does not mean that these measurements are all relevant. Indeed, the plot in Figure 16 shows that many SRAL measurements acquired over Open-Loop areas have an OCOG range set to Default Value. It occurs when the corresponding waveforms are not meaningful and cannot be properly retracked. As expected, the percentage varies as a function of the surface topography. Over Closed-Loop areas this percentage is artificially lower (above 20%) since there are less acquisitions with this mode.

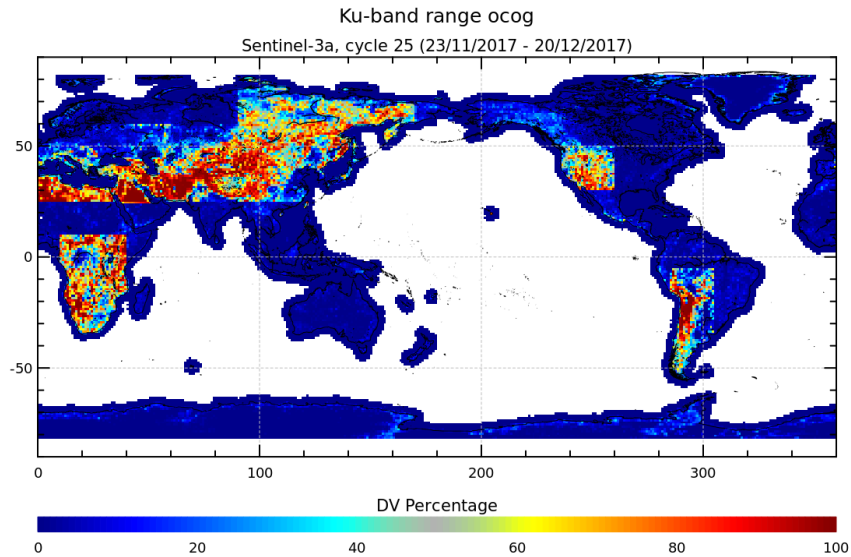


Figure 16: Gridded map of the range ocog Default Value percentage with respect to the available measurements. It is plotted over cycle 25 (from 11th of November 2017 to 20th of December 2017)/

	Sentinel-3 MPC S3MPC STM Annual Performance Report - Year 1	Ref.: S3MPC.CLS.APR.002 Issue: 1.1 Date: 23/05/2018 Page: 29
--	--	---

7 Performance Mission over Ocean

7.1 Outliers detection

The outliers detection or editing step of the Cal/Val process intends to remove any measurement that is considered as erroneous, helping to refine the different metrics that are provided in the other sections dedicated to the performance over ocean. The definition of an erroneous measurement, and of the accepted error level on the final sea level anomaly is of course a tradeoff between accuracy and data coverage. The monitoring of the percentage of valid and edited measurements also gives relevant information about the mission performances.

Editing criteria are used to detect outliers over ocean. This process is divided into 3 main parts:

- ❖ removal of all measurements affected by sea-ice.
- ❖ removal of all measurements which exceed defined thresholds on different parameters.
- ❖ further checks on along-track sla consistency.

For each step of the process, the number of outliers, per track, per day and per cycle is routinely monitored at Cal/Val level. This allows the detection of anomalies through the number of removed data, which could come from instrumental, geophysical or algorithmic changes. The process performed here is dedicated to ocean applications. Data over land are removed using a land/water mask prior to the analysis described in this section.

7.1.1 Ice detection

The ice flag (based on the `open_sea_ice_flag` field within the products) is used to remove measurements affected by sea ice in the altimeter footprint. This flag is derived from the Tran et al. algorithm developed in 2008 for Envisat mission. This algorithm combines brightness temperatures and backscatter information respectively derived from microwave radiometer and altimeter. Left panel of Figure 17 shows the location of the SRAL outliers detected in the South hemisphere in December 2017. The middle and right panels of Figure 17 are derived from external sources. They show the percentage of ice concentration derived from OSISAF (middle panel) and from NSIDC (right panel) models over the same period. The location of Sentinel-3A measurements considered as corrupted by sea ice is consistent with the results derived from the two sea ice concentration models. It confirms the relevance of this metric to remove Sentinel-3A outliers at high latitudes. Moreover, the accuracy of the Sentinel-3A sea ice detection will be improved since, today, the Tran et al. algorithm is still based on Envisat parameters tuning. A Sentinel-3A dedicated parametrization is scheduled for the coming months and cross comparisons will be made with the sea ice concentration provided at 20 Hz and displayed in section 8.7.

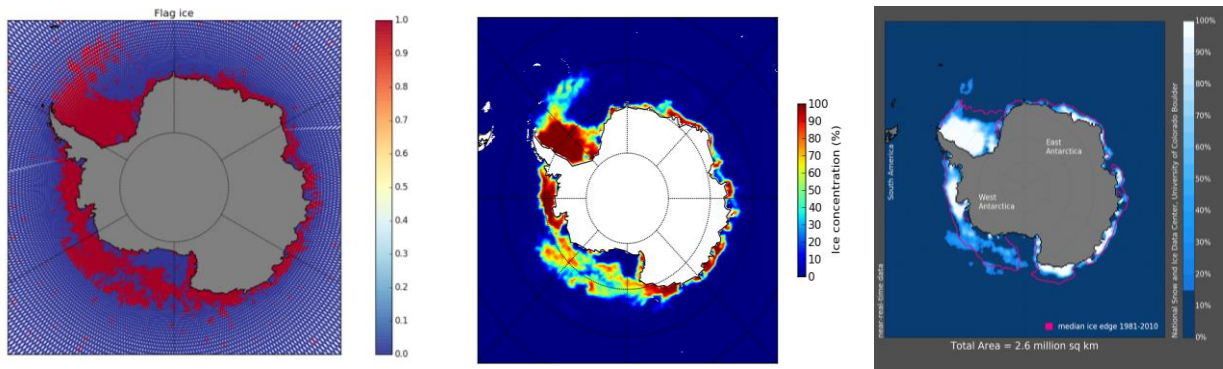


Figure 17: left panel shows the Sentinel-3A sea ice flag derived from both L2 LAND and WATER products over cycle 25 (from 11th of November 2017 to 20th of December 2017). Presence of sea ice corresponds to the value 1, open ocean water is represented by the value of 0. Middle panel shows the sea ice concentration percentage derived from OSISAF model over the month of December. Right panel shows the sea concentration percentage derived from NSIDC model over the month of December.

The percentage of measurements corrupted by sea ice is plotted Figure 18 for Sentinel-3A over the year 2016 (left panel) and for SARAL/AltiKa over the whole mission lifetime (right panel). The SARAL/AltiKa is used for these comparisons because both missions have similar high latitude coverage. Once again, there is a good agreement between the sea ice areas detected by both missions. The corresponding global temporal monitoring is plotted in Figure 19. Same temporal variations are observed with maximums in June-July (South hemisphere winter) and in November (North hemisphere winter). The percentage of outliers detected by SARAL/AltiKa sea ice flag is slightly higher (2%) than for Sentinel-3A. This could be explained by the algorithm differences, the fact that the Sentinel-3A sea ice detection parametrization is not yet definitely tuned and the difference of sensitivity of the two altimeters to the sea ice impact.

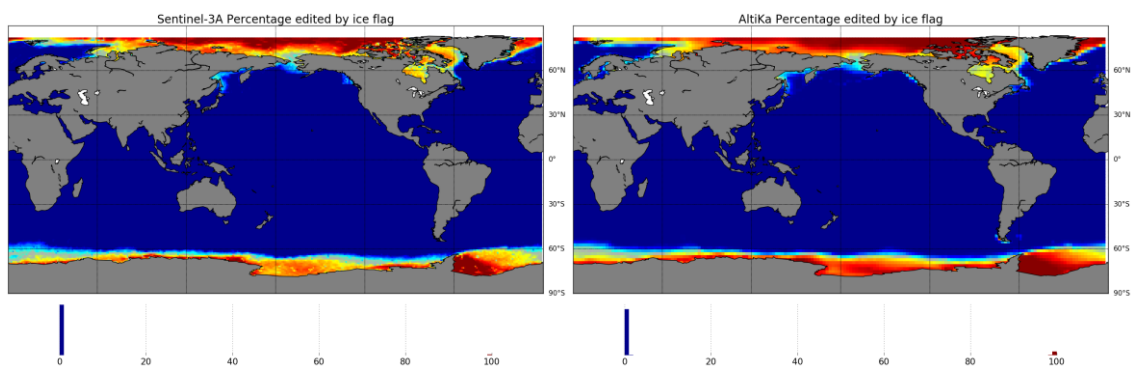


Figure 18: left panel shows the gridded of map of the outliers percentage detected by the Sentinel-3A sea ice flag over the year 2016 (from December 2016 to December 2017). Right panels shows the gridded of map of the outliers percentage detected by the SARAL/AltiKa ice flag over the whole mission period.

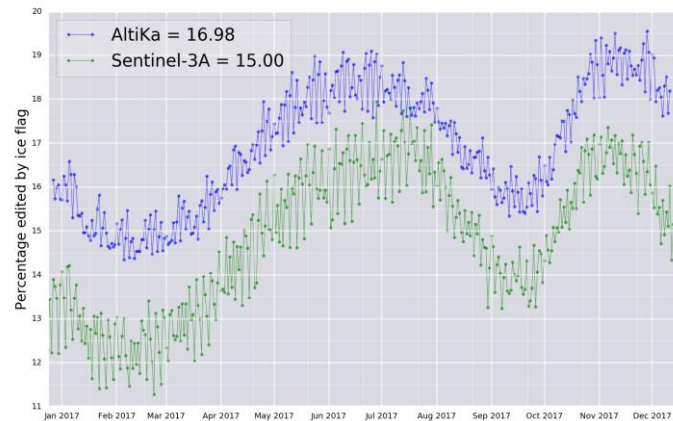


Figure 19: Monitoring of the daily averaged percentages of outliers detected by Sentinel-3A sea ice flag (green curve) and AltiKa ice flag (blue curve) over Ocean.

7.1.2 Outliers detection over ocean

Once the measurements corrupted by land and sea ice surfaces are identified, the quality of the altimeter retrieved parameters and the geophysical corrections is checked with respect to thresholds. These thresholds and the corresponding percentage of corrupted measurements are detailed in Table 5. For each of the listed parameters, the percentage of outliers detected is closely monitored cycle by cycle, day per day and pass per pass by CLS Cal/Val routines.

Figure 20 presents the monitoring of the total percentage of corrupted measurements detected over Ocean and sea ice (left panel) and the corresponding map (right panel). The temporal variations of the percentage of corrupted measurements detected for Sentinel-3A and SARAL/AltiKa are consistent. The averaged percentages are also very close: 18.5 % for Sentinel-3A against 19.7% for SARAL/AltiKa. This monitoring also highlights some peaky values for Sentinel-3A. For these days, the percentage of corrupted measurements increase because of the unavailability of some of the geophysical correction. Indeed, Figure 21 shows the monitoring of the percentage of measurements edited on the dynamical atmospheric correction criteria (left panel) and on the microwave radiometer Wet Tropospheric Correction criteria (MWR WTC) (right panel). The dynamical atmospheric correction is derived from the MOG2D model, the thresholds defined allows to detect when this correction is not defined. This was partially the case on the 13th February and on the 5th and 6th of December. These anomalies are due to ground processing errors in the Marine Centre. Note that in the reprocessed products, this dynamical atmospheric correction is correctly provided. Regarding the measurements edited on the radiometer WTC criteria, Figure 21 right panel shows:

- ❖ Peaky values for tens of days. These high percentage of edited measurement are not related to radiometer instrumental anomalies but to ground processing errors. The microwave radiometer WTC is set to Default Value. In the reprocessed products, it is correctly provided.
- ❖ A higher percentage of edited measurement compared to Jason-3 and SARAL/AltiKa: 1 % for Sentinel-3A against 0.06% and 0.07% for SARAL/AltiKa and Jason-3. This higher percentage is explained by the Sentinel-3A MWR calibration pattern (see section 5.2.2 for more details). During MWR calibrations, approximately 17 seconds 3 times per orbit, the MWR WTC is set to Default Value. This explains both the higher percentage for Sentinel-3A, and regular pixels of 25% of edited measurements over the open ocean observed in the map right panel (Figure 20). Note that this calibration scheme will be changed in February 2018 to improve Sentinel-3A coverage over ocean.

The percentage of rejected data over ocean (removing ice) is good, with only 4.1 % of outliers. Considering that we are rejecting 1% of sea level observations due to the MWR calibrations, this means that the rejected measurements will be close to 3.1 % after change of the MWR calibration timeline, which is fully consistent with the same metric observed for Jason-3 (3.4%) and SARAL/AltiKa missions (2.6%).

Regarding the map of the percentage of total outliers (Figure 20 right panel), except the along-track patterns and the isolated pixels described previously, the result at medium and low latitudes mainly highlights the rainiest areas, as usually observed for the altimeters.

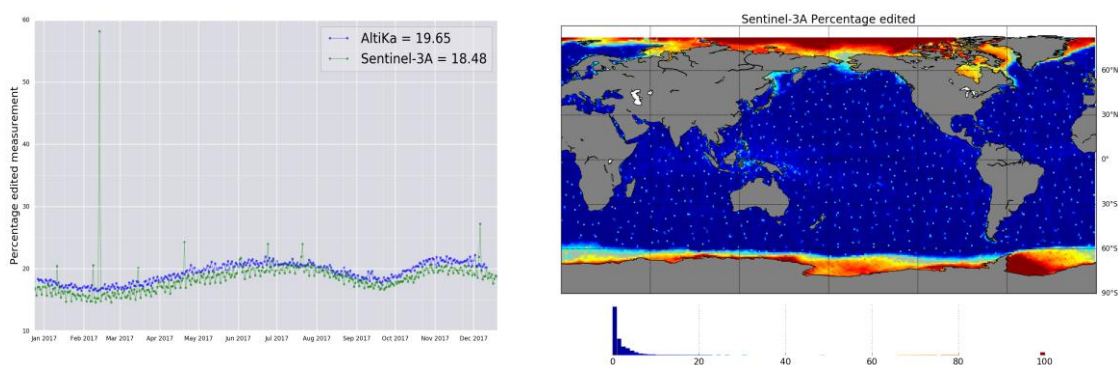


Figure 20: left panel shows the Sentinel-3A (green curve) and SARAL/AltiKa (blue curve) total percentage of outliers over ocean. Right panel shows the gridded map of Sentinel-3A percentage of total outliers over the year 2017.

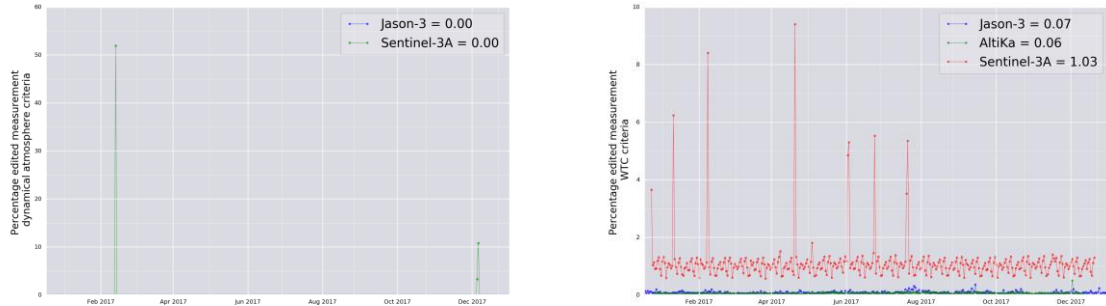


Figure 21: left panel shows the Sentinel-3A (green curve) and Jason-3 (blue curve) percentage of outlier detected by the dynamical atmospheric thresholds. Right panel shows the percentage of Sentinel-3A (red curve), Jason-3 (blue curve) and AltiKa (green curve) percentage of outliers detected by the MWR WTC thresholds.

Parameter	Min thresholds	Max thresholds	Mean edited
Sea Level Anomaly	-2	2	1.78 %
Number of range measurement	10	<i>Not applicable</i>	0.08%
Standard deviation of range	0	$0.12 + 0.02 * SWH$	1.46 %
Dry tropospheric correction	-2.5	-1.9	0.00 %
Dynamical atmospheric correction	-2	2	0.14 %
MWR Wet Tropospheric Correction	-0.5	-0.001	1.04 %
Sigma0 Standard deviation	0	0.7	3.03 %
Altimeter Wind Speed	0	30	0.06 %
Dual Frequency ionosphere correction	-0.4	-0.04	1.59 %
Sea State Bias	-0.5	0	0.06 %
Ocean Tide	-5	5	0.01 %
Earth Tide	-1	1	0.00 %
Pole Tide	-15	15	0.00 %
All Together			4.09 %

Table 5: Outliers detection thresholds and corresponding percentages computed over the year 2017.

	Sentinel-3 MPC S3MPC STM Annual Performance Report - Year 1	Ref.: S3MPC.CLS.APR.002 Issue: 1.1 Date: 23/05/2018 Page: 34
---	--	---

7.2 Monitoring of SRAL parameters

7.2.1 Significant Wave Height

The Significant Wave Height (SWH) is a parameter derived from ocean retracking. It corresponds to the average wave height of the highest third of the wave distribution in a given sample period. Moreover, at climatic scales, the study of ocean waves is of great importance to understand the interaction between ocean and atmosphere. The Copernicus Marine Environment Monitoring Service (CMEMS) collects and processes the Sentinel-3A SWH estimations (among others) every day to provide researchers with a long term and homogenous SWH dataset. This section aims at describing the global quality of Sentinel-3A SWH estimations.

Figure 22 shows the maps of Sentinel-3A SARM and P-LRM SWH and the one derived from Jason-3 over the same period. Same geographical structures are observed by both Sentinel-3A modes and both satellites: low SWH around Indonesia, in the Mediterranean Sea and in the Gulf of Mexico; high SWH in the band of latitudes around 50°S. The corresponding histograms show an important population of very low SWH in SARM (close to 0m). This is explained by the fact that the SARM processing set to 0 m all the SWH negative estimations. This artefact is more frequent in SARM, because the SWH are usually underestimated in SARM with respect to P-LRM. Negative estimations over flat sea state are possible due to the level of noise of this parameter.

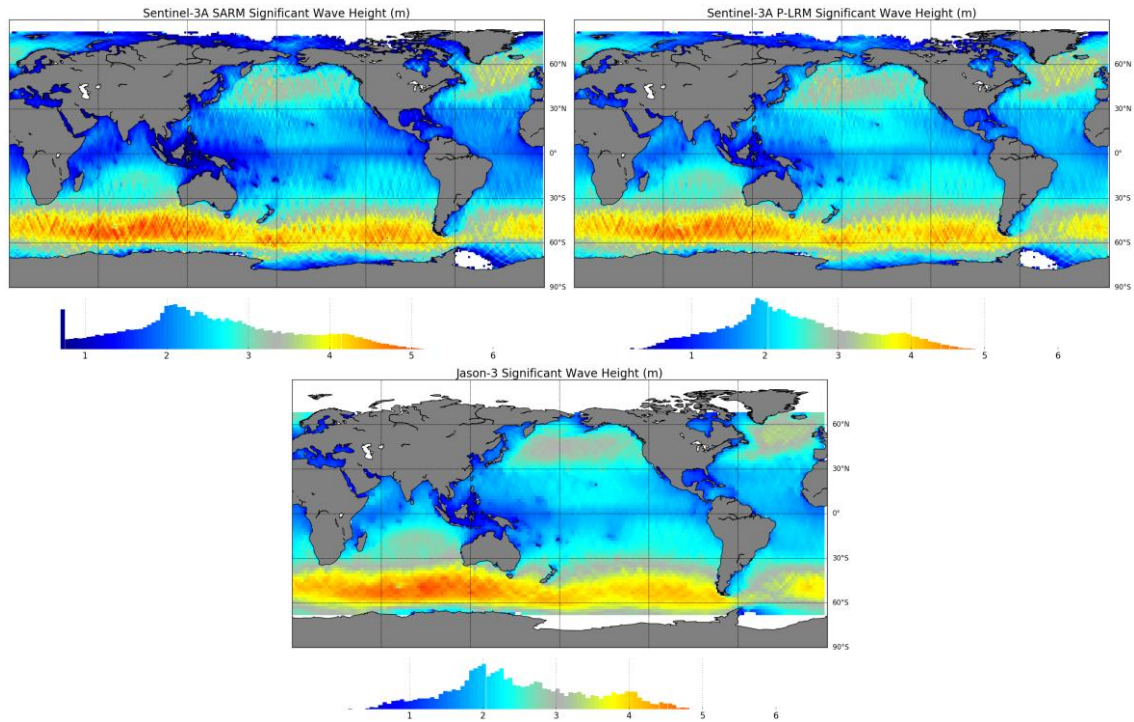


Figure 22: Gridded maps of Sentinel-3A SARM (top left panel) P-LRM (right left panel) and Jason-3 (bottom panel) SWH computed over the year 2017.

The monitoring of the daily averaged SWH (plotted in Figure 23) allows to detect abnormal events and potential significant drifts. In order to be consistent with Jason-3 global coverage, the Sentinel-3A data have been selected below 66° of latitude. The trend and the variations observed are the same for both Sentinel-3A modes and for both satellites. Although different mean values are computed, it traduces the Sentinel-3A capabilities to measure the SWH at global spatial scales. The analysis of these biases is detailed in the next paragraph. After the last Instrument Processing Facility (IPF) update (installation of the version 06.10), the SARM SWH mean value is reduced and come very close to the P-LRM and Jason-3 mean values. This is an improvement coming from the implementation of the SAMOSA 2.5 retracker for SARM observations (see section 7.8).

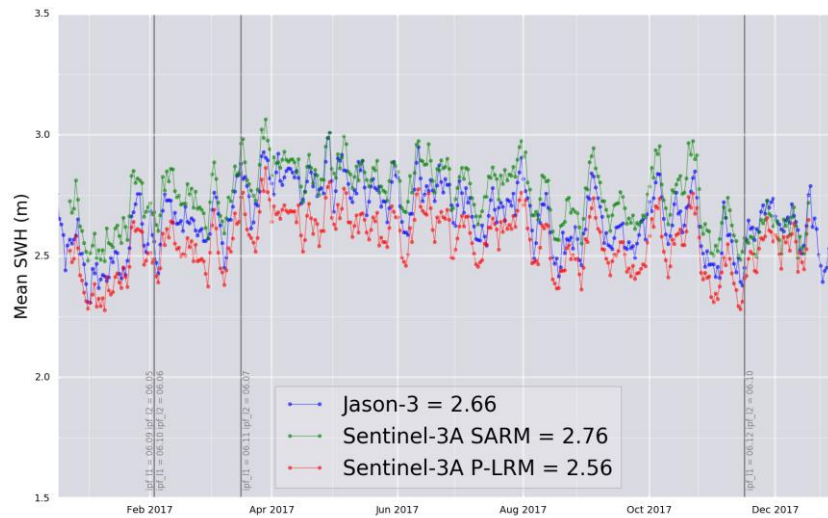


Figure 23: Daily monitoring of the Sentinel-3A SARM (green curve) P-LRM (red curve) and Jason-3 (blue curve) SWH.

The precise comparison of Sentinel-3A and Jason-3 SWH through the analysis of histograms and temporal averaging is not an exhaustive metric since the satellite ground tracks are different and the temporal variability of this parameter is very high. Thus, to precisely assess the Sentinel-3A SWH accuracy with respect to other altimetry mission, the differences are computed at crossovers for which the time lag between Sentinel-3A and Jason-3 sampling is lower than 3 hours. From these points, we compute the SWH difference between Sentinel-3A and Jason-3 as a function of the Jason-3 SWH (left panel Figure 24). This analysis shows a very good agreement between Sentinel-3A P-LRM and Jason-3 SWH with a mean bias lower than 5 cm and no significant dependency when SWH increase. However, the Sentinel-3A SARM compared to Jason-3 highlights a higher bias and a clear dependency as a function of SWH. For SWH around 1 m SARM and Jason-3 estimations are consistent. Then, differences increase with SWH values to reach a 25 cm bias for SWH higher than 3m. This kind of behaviour was already observed from Cryosat-2 SARM, investigations are ongoing to understand the content of SARM observations with respect to conventional altimetry.

The good performances obtained with Sentinel-3A P-LRM SWH is an important result. It means that despite of its higher level of noise, this processing mode allows to constitute a robust reference at global scales to assess the co-located SARM measurements. The map plotted in right panel Figure 24, illustrates the difference of SWH between Sentinel-3A SARM and P-LRM. It confirms the result derived from 3 hours crossover analysis: the SARM SWH estimations, at global scales, vary as a function of the wave height and are over estimated compared to P-LRM SWH.

Note that this result was obtained with SAMOSA 2.3 retracker and will be improved with SAMOSA 2.5 retracker.

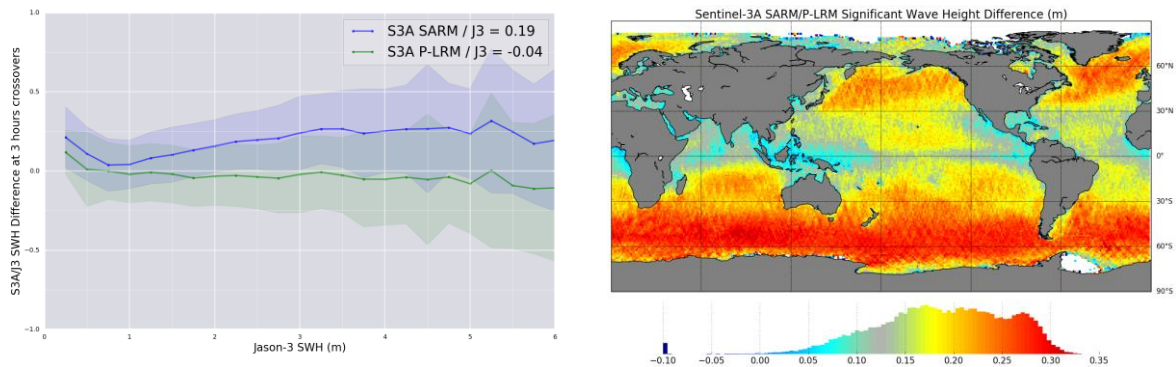


Figure 24: left panel shows the SWH differences computed at crossovers over the year 2017 between Sentinel-3A SARM and Jason-3 (blue curve) and between Sentinel-3A P-LRM and Jason-3 (green curve) as a function of the Jason-3 SWH. Due to the high temporal variability of the SWH parameters a selection was applied to select crossover time lags below 3 hours. Right panel shows the gridded map of collocated SWH differences between Sentinel-3A SARM and P-LRM over the year 2017.

7.2.2 Backscatter coefficient

The backscatter coefficient also called σ_0 , is computed from the power of the signal returned by the sampled surface. Over Ocean, it gives an information of the sea surface roughness. Over flat sea surfaces the σ_0 values are high, whereas over strong sea states (with for example high SWH values) the σ_0 values are lower. This parameter should be precisely estimated since it is used to compute the wind speed measured by the altimeter. Although the wind direction cannot be provided from altimeter measurements, the wind speed norm is of great importance for climatic applications.

Figure 25 shows the maps of Sentinel-3A SARM and P-LRM backscatter coefficients and the one derived from Jason-3. Same geographical structures are observed by both Sentinel-3A modes and both satellites: high values around Indonesia, in the Mediterranean Sea and in the Gulf of Mexico where the sea surface is usually flat; high values in the band of latitudes around 50°S where the SWH are in average higher. The mean values are different between Sentinel-3A and Jason-3 σ_0 . For Sentinel-3A, a bias is applied to the SARM and P-LRM σ_0 values to make them consistent with Envisat σ_0 mean value. Indeed, the algorithm used to compute the wind speed estimation, the Abdalla's algorithm, is inherited from Envisat mission and thus needs consistent inputs.

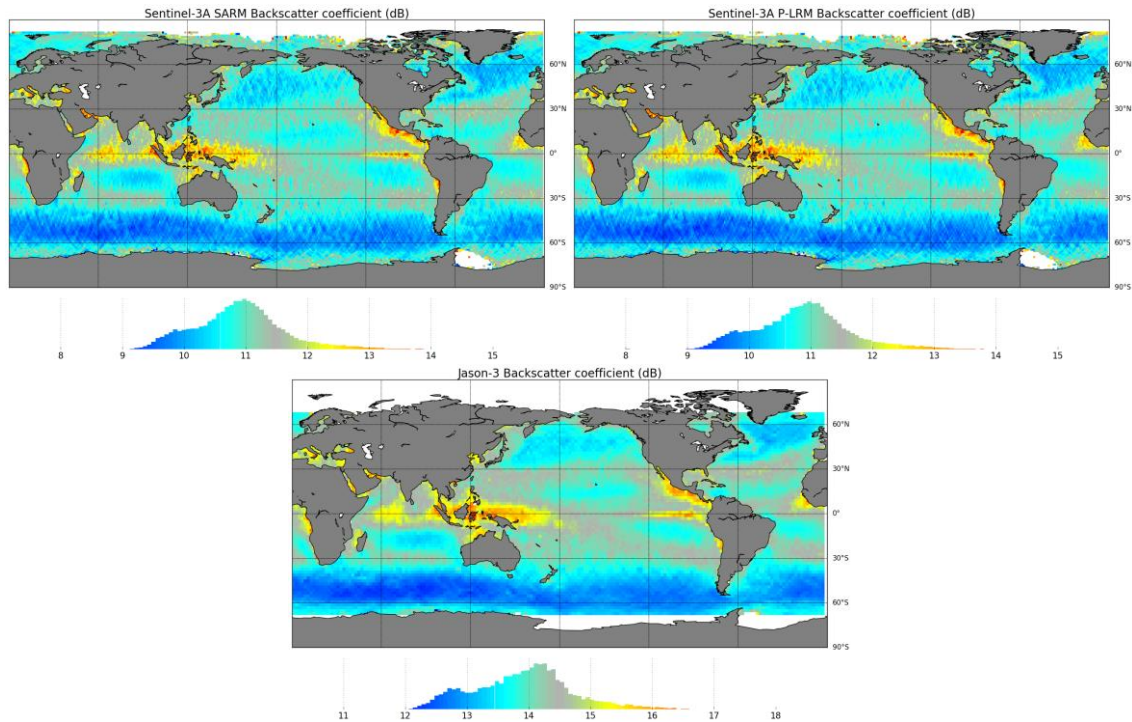


Figure 25: Gridded maps of Sentinel-3A SARM (top left panel) P-LRM (right left panel) and Jason-3 (bottom panel) backscatter coefficient computed over the year 2017.

The monitoring of the daily averaged backscatter coefficient (plotted in Figure 26) allows to detect abnormal events and potential significant drifts. In order to be consistent with Jason-3 global coverage, the Sentinel-3A data have been selected below 66° of latitude. The observed temporal variations are consistent between both Sentinel-3A modes and between both satellites. From beginning to mid of February the mean values of SARM and P-LRM σ_0 are slightly different. This is explained by the update of the SRAL calibrations management done in the Marine Centre ground processor. The other important event occurs on 13 December 2017, where the σ_0 is now corrected from the atmospheric attenuation: it explains the increase of 0.2 dB observed since the deployment of IPF 06.10. The other IPF updates did not impact the stability of the backscatter coefficients.

The difference of mean value between Sentinel-3 and Jason-3 is due to a system bias applied on Sentinel-3A to align the σ_0 mean value with the Envisat mean value.

- ❖ The system bias on P-LRM data is -2 dB which means that the true bias between Sentinel-3A and Jason-3 is closer to 0.7 dB, Sentinel-3A being lower than Jason-3 σ_0 .
- ❖ The system bias on SARM data is -18.9 dB which means that the true bias between Sentinel-3A and Jason-3 is closer to 16.1 dB, Sentinel-3A being higher than Jason-3 σ_0 .

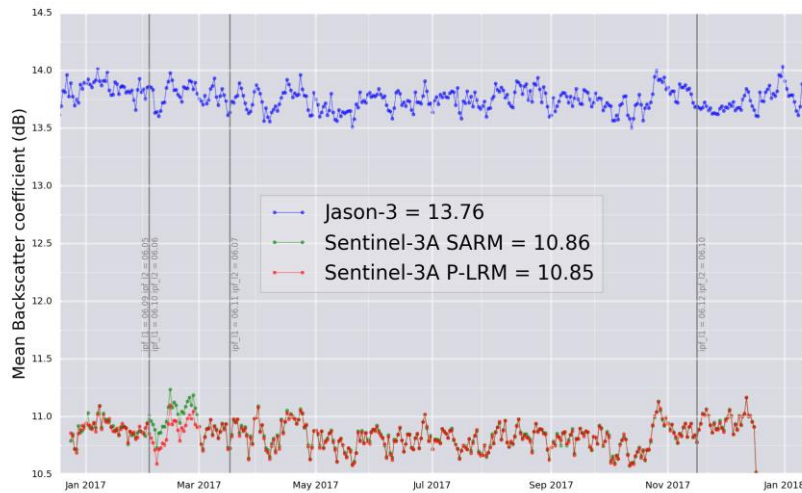


Figure 26: Daily monitoring of the Sentinel-3A SARM (green curve) P-LRM (red curve) and Jason-3 (blue curve) backscatter coefficient.

The co-located differences between Sentinel-3A SARM and P-LRM sigma0 (left panel Figure 27) highlights patterns that depends on the latitude. The mean difference is centred on 0 dB (as already shown on the temporal monitoring) but negative and positive values are respectively observed at low and high latitudes. These variations are strongly correlated with the Sentinel-3A altitude plotted in right panel Figure 27. This anomaly identified in the SARM processing is significantly reduced since the installation of the latest IPF version (IPF-SM-2 06.10). Note that this error of 0.3 dB magnitude on the SARM backscatter coefficient can be hardly detected on the altimeter wind speed (see section 7.7).

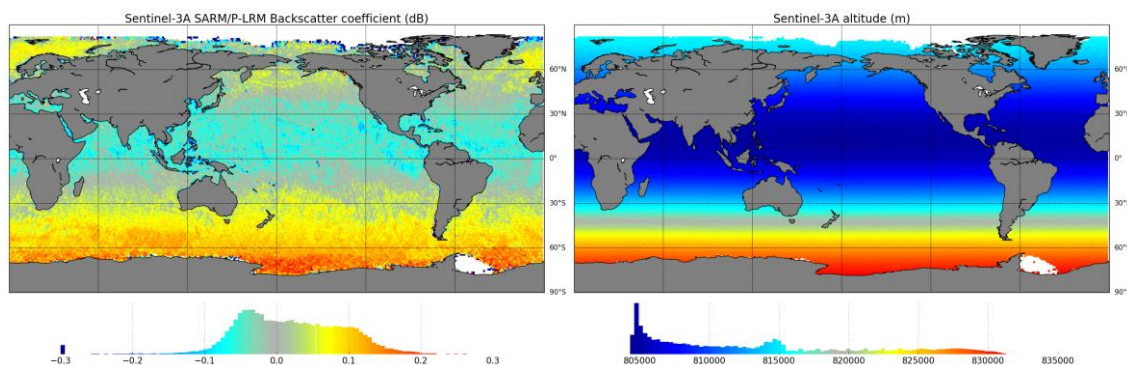


Figure 27: Gridded maps of the collocated backscatter differences between Sentinel-3A SARM and P-LRM over the year 2017 (left panel) and of the Sentinel-3A altitude computed over cycle 25 (right panel).

7.2.3 Dual-Frequency ionospheric correction

In addition to the nominal Ku-band transmit frequency, the SRAL altimeter interleaves a C-band signal. The purpose of this second frequency is to provide a collocated ranging measurement to correct for ionospheric path delay in the Ku-band range estimate. Indeed, both Ku and C-band have different sensitivity to the electron content in the atmosphere.

Figure 28 shows the maps of the delay induced by the electron content on the Ku-Band range for Sentinel-3A SARM (top left panel), P-LRM (top right panel) and Jason-3 (bottom panel). Note that the fields “iono_cor_alt_01_ku” and “iono_cor_alt_01_plrm_ku” provided in the L2 products are not filtered. Their level of noise is thus approximatively the sum of the Ku and C-band range noise. In order to improve the quality of the assessment, the dual-frequency ionosphere correction has been filtered at 300 km. The two maps obtained for both Sentinel-3A modes are very consistent. The slight discrepancies between SARM and P-LRM ranges (described in Figure 77) have a very low impact on the dual frequency ionosphere correction (-5 mm differences in strong SWH areas). The map derived from Jason-3 altimeter shows similar patterns but magnitudes slightly lower. It has been demonstrated that the ionosphere correction derived from Jason-3 altimeter is 5 mm higher with respect to Jason-2.

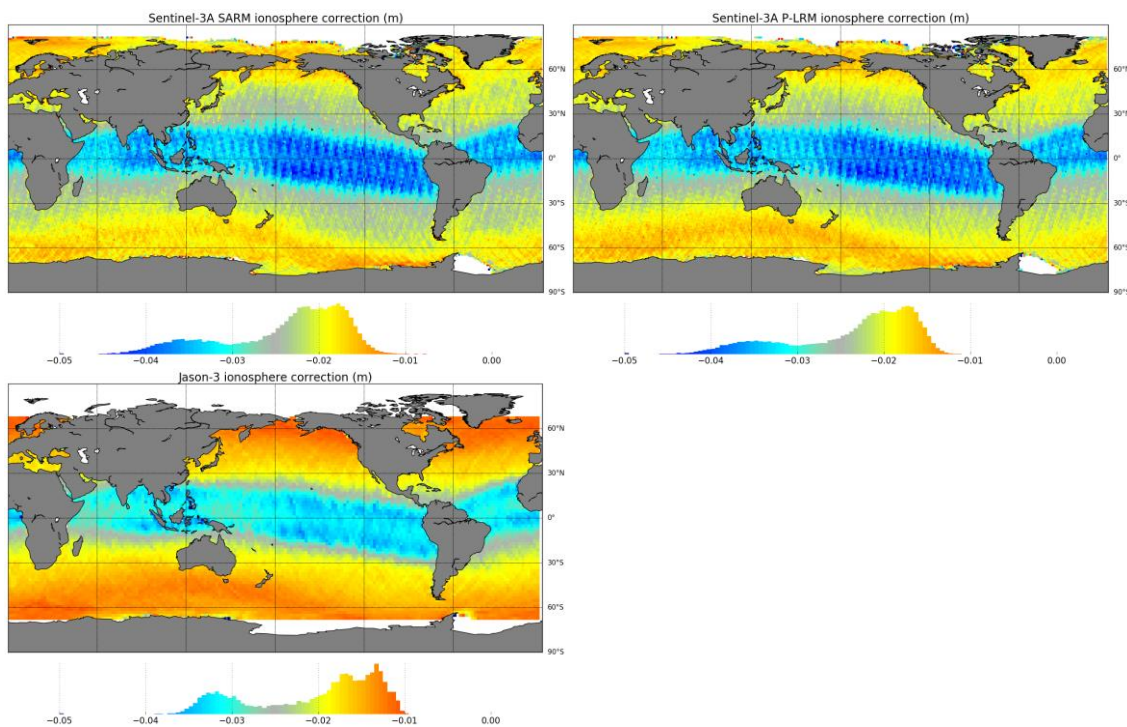


Figure 28: Gridded maps of Sentinel-3A SARM (top left panel) P-LRM (right left panel) and Jason-3 (bottom panel) dual frequency ionospheric correction computed over the year 2017.



The delay induced by the electron content can also be derived from the GPS global Ionosphere Maps (GIM) model. Jee et al. demonstrated that, although the GIM model is not as accurate as the dual-frequency metric, overall the GIM model is able to reproduce the spatial and temporal variations of the ionosphere. Figure 29 shows maps of differences between dual frequency and GIM model ionospheric correction for Sentinel-3A (top panels) and Jason-3 (bottom panels). Ascending (left panels) and Descending (right panels) passes have been plotted separately. The dual frequency ionosphere derived from Sentinel-3A is, in average, closer to the GIM model (differences centred on 0 cm) than the one derived from Jason-3 (7 mm bias). Discrepancies are observed between Sentinel-3A ascending and descending passes, whereas this is not the case for Jason-3. These differences are related to the local time. Indeed Sentinel-3A is sun-synchronous satellite, which means that for a given latitude and pass orientation, the local time is always the same. Figure 30 shows the Sentinel-3A local hours distribution for ascending and descending passes for cycle 26 (this result is the same whatever the chosen period):

- ❖ For ascending passes (left panel) and for latitudes below 70°, the local hours are ranged between 9:00 PM and 01:00 AM. For these local hours, the sun activity and thus the electron content in the atmosphere are lower.
- ❖ For descending passes (right panel) and for latitudes below 70°, the local hours are ranged between 8:00AM and 12:00 AM. For these local hours, the sun activity and thus the electron content in the atmosphere are higher.

On the other hand, Jason-3 is not a sun-synchronous satellite and revisits only every 12 cycles (120 days) the same local hours. Day and night hours are thus averaged in both Jason-3 maps, this explain the similarity between Jason-3 ascending and descending passes and the geographical differences with respect to Sentinel-3A.

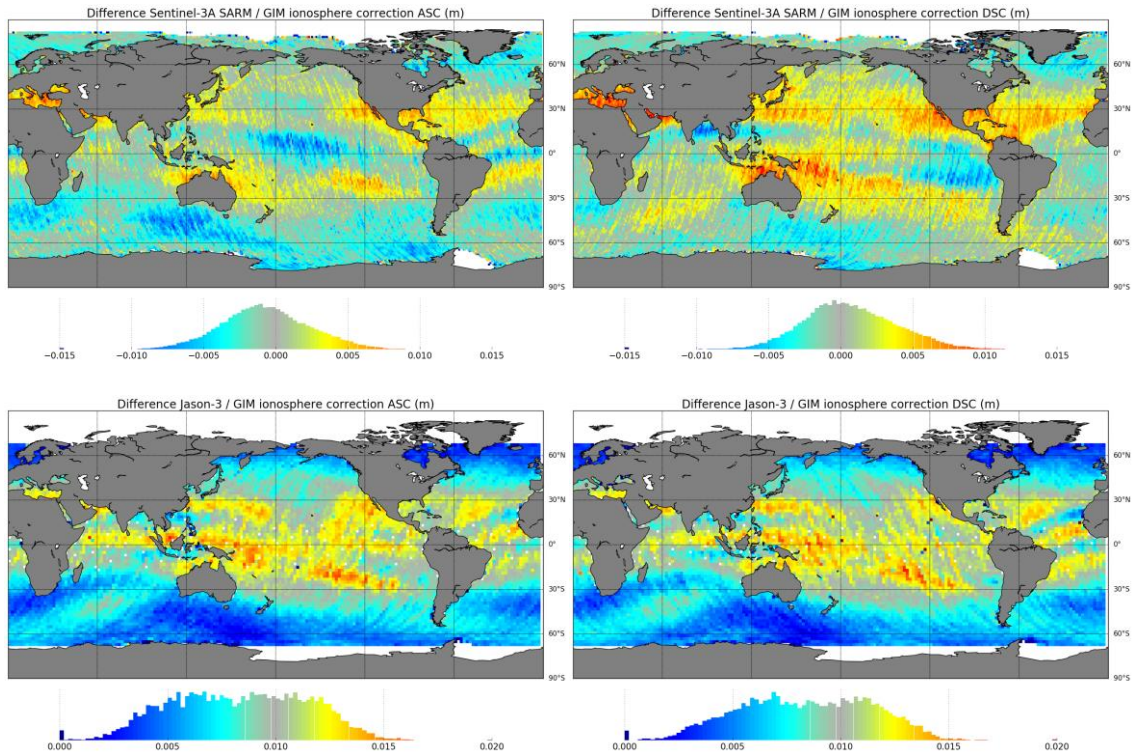


Figure 29: Top panels shows the gridded maps of the collocated differences between Sentinel-3A SARM dual frequency ionosphere correction and GIM model for ascending (left panel) and descending (right panel) passes. Bottom panels show the gridded maps of the collocated differences between Jason-3 dual frequency ionosphere correction and GIM model for ascending (left panel) and descending (right panel) passes. The ionosphere corrections derived from altimeter were filtered at 300km.

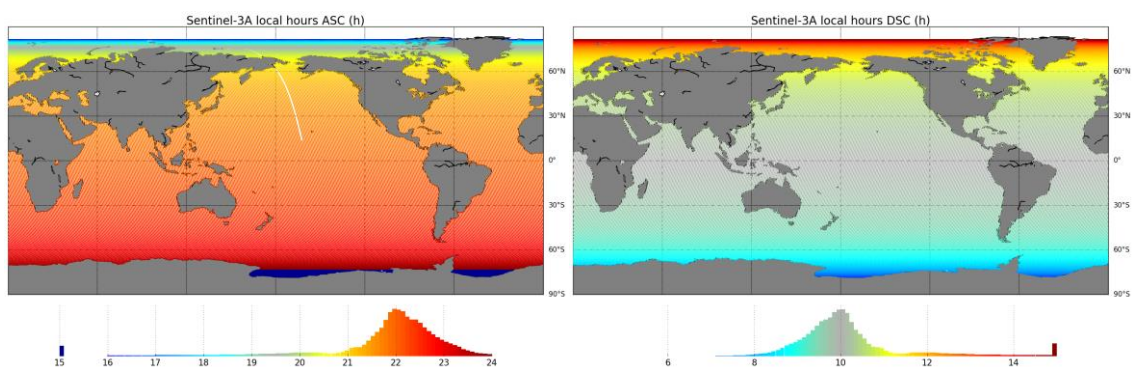


Figure 30: Along-track maps of the Sentinel-3A local hours for ascending (left panel) and descending (right panel) passes computed over cycle 25.

The monitoring of the Sentinel-3A dual frequency and GIM ionosphere corrections and their differences (Figure 31) presents a very good and stable agreement between the two solutions. The mean bias is centred on 0 cm and magnitudes of the variations do not exceed 6 mm. There is a slight jump of 3 mm observed mid November 2017 due to the change to the processing Baseline 2.24. The very small bias between both corrections is a good way to check that there is so significant bias on the SRAL C-band range. The curves plotted for different bins of local hours highlight slight differences between the months of May and September. For this period, the monitoring of the ionospheres corrections (bottom panel) shows an increase of the range delay and thus of the electron content in the atmosphere. This increase is higher for descending passes (day local hours) than for the ascending passes (night local hours).

Small temporal variations are observed in the two plots. The main period identified equals to 27 days which corresponds to the solar Dicke cycle. These temporal oscillations could be related to the lowest resolution of the GIM model with respect to the altimeter dual frequency ionosphere correction.

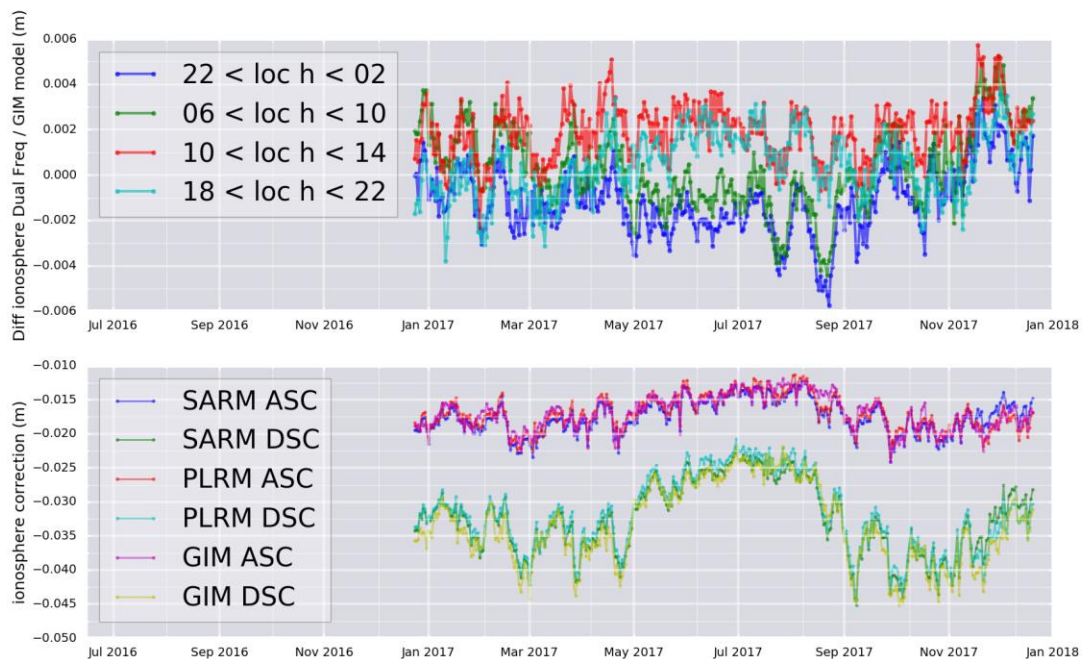


Figure 31: Top panel shows the daily monitoring of the collocated differences between Sentinel-3A SARM dual-frequency ionosphere correction and the GIM model. The Sentinel-3A local hours were split by four hours bins and plotted separately. Bottom panel shows the daily monitoring of the Sentinel-3A SARM, P-LRM dual-frequency ionosphere correction and the collocated GIM model. Ascending and Descending passes were plotted separately.

	Sentinel-3 MPC S3MPC STM Annual Performance Report - Year 1	Ref.: S3MPC.CLS.APR.002 Issue: 1.1 Date: 23/05/2018 Page: 44
--	--	---

7.2.4 Off-Nadir angle waveform

The off-nadir angle gives an information about the satellite attitude. It can either be the result of real platform mispointing (also seen by the Star-Tracker measurements) or of backscattering properties of the surface measured on the altimeter waveforms.

Figure 32 presents the maps of mispointing angles derived from Sentinel-3A waveforms (left top panel), Sentinel-3A Star-Tracker (right top panel), and from Jason-3 (bottom left panel) and AltiKa (bottom right panel) waveforms. The Sentinel-3A off-nadir angle is biased by -0.006 degrees^2 with respect to the one derived from star-trackers centred on 0 degrees^2 . Such a bias could be related to the value used for the antenna aperture angle in the P-LRM processing, this needs to be further investigated. For Sentinel-3A, off-nadir angle values derived from waveforms are available in P-LRM (and LRM) only since the SAMOSA DPM2.3 and DPM2.5 are MLE3 retracking. In SARM, the mispointing information is derived from star-tracker measurement and injected as input of the retracking. The map derived from platform off-nadir angles confirms that Sentinel-3A pointing is excellent. The along-track effects observed in the Pacific and East Indian Oceans are due to pointing manoeuvres.

Geographical variations are observed for the waveform mispointing. Indeed, this parameter is estimated through the waveform trailing edge slope which varies with the surface and the atmosphere perturbations (rain cells attenuation, high SWH, blooms, sea ice...). Between SARAL/AltiKa and Jason-3, similar geographical variations are observed, but with a higher dispersion for Jason-3 than for SARAL/AltiKa. This is explained by the Jason-3 larger antenna aperture angle: 1.29° against 0.6° for SARAL/AltiKa. For Sentinel-3A, the map of mispointing derived from P-LRM waveforms is not consistent with the two others: large scale variations are decreased and the off-nadir values decrease over calm seas such as in Mediterranean and Indonesian seas, whereas they increase for Jason-3 and SARAL/AltiKa. These differences could be explained by:

- ❖ The P-LRM waveforms higher level of noise. In P-LRM only 32 individual echoes are averaged to compute the 20Hz waveform, while 91 echoes are used in LRM.
- ❖ The length of the SRAL calibration averaging windows. Indeed, until the installation of the IPF-SM2 06.10, the SRAL calibrations are averaged over one day only. The monitoring of the Sentinel-3A off-nadir angle derived from P-LRM waveforms plotted in Figure 33 shows an important variability from one day to another. Since the last IPF installation, the calibrations are averaged over 10 days: the Sentinel-3A off-nadir angle temporal variations are now more consistent with Jason-3 and SARAL/AltiKa variations.

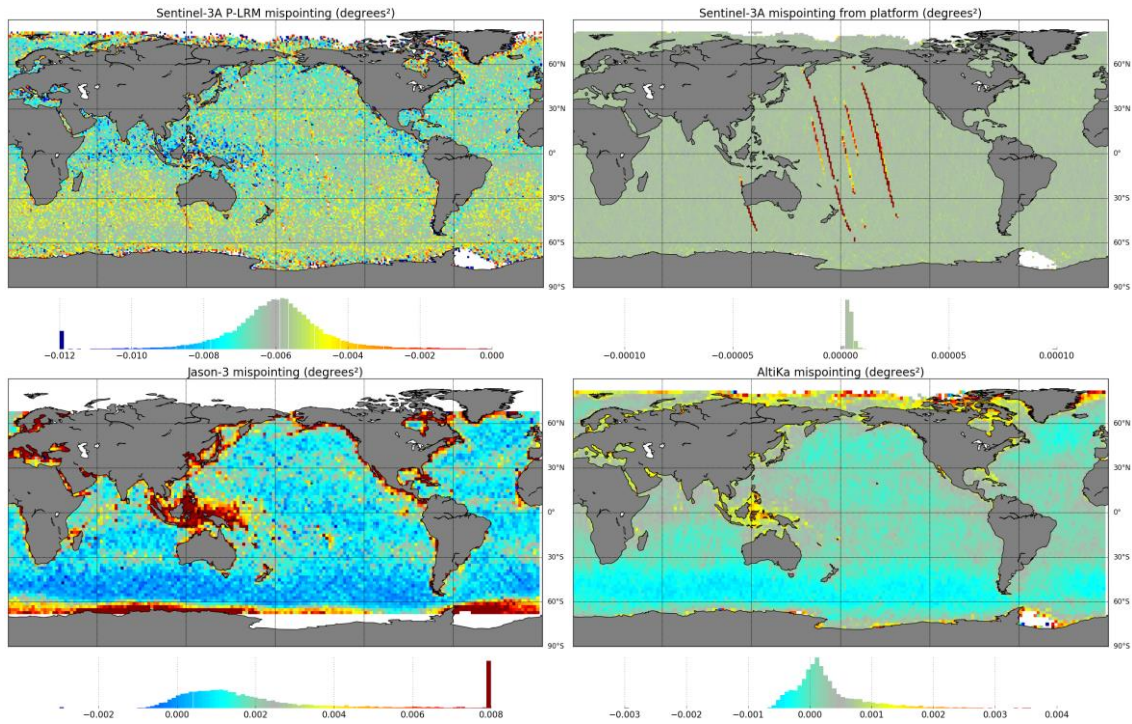


Figure 32: Top panels show the gridded maps of Sentinel-3A off-nadir angle derived from waveforms (left panel) and derived from Star-Trackers (right panel) over the year 2017. Bottom panels show the off-nadir angle derived from waveforms for Jason-3 (left panel) and SARAL/Altika (right panel) over their respective whole mission lifetime.

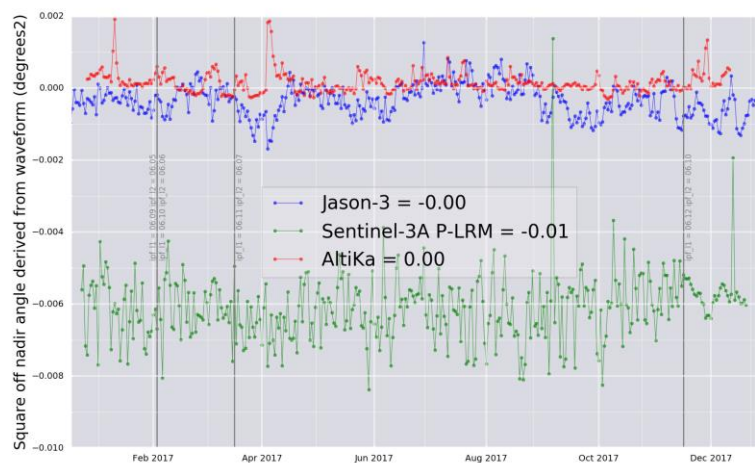


Figure 33: Daily monitoring of the Sentinel-3A P-LRM (green curve), Jason-3 (blue curve) and SARAL/Altika (red curve) off-nadir angle derived from waveforms.



7.3 Wet tropospheric correction

The wet tropospheric correction is a parameter retrieved from MWR brightness temperatures and the altimeter backscattering coefficient. It corrects for the radar excess path delay due to the presence of water vapor in the troposphere.

In Sentinel-3A processing, two retrieval algorithms based on neural networks are used for the retrieval of the wet tropospheric correction. First the classical three inputs algorithm (annotated 3P) using the two brightness temperatures from the microwave radiometer and the altimeter backscattering coefficient (σ_0). This type of algorithm is commonly used for European altimetry mission such as Envisat, or AltiKa. Secondly an enhanced algorithm (annotated 5P) is proposed taking as additional input parameter the sea surface temperature and the atmosphere temperature lapse rate (the so-called γ_{800}). The sea surface temperature brings additional information from the surface globally over ocean. The atmosphere temperature lapse rate is more useful over specific areas such as upwelling regions where the temperature lapse rate is very specific to these regions. These two additional parameters are provided to the processor by static maps: seasonal maps (one map for each season) for sea surface temperature, one map for γ_{800} .

7.3.1 Along-track analyses

The monitoring of the wet tropospheric correction is performed by comparison of the difference MWR-model of the wet tropospheric correction (Δwtc) for several instruments. Figure 34 shows this monitoring for Sentinel-3A, SARAL, and Jason-3 with the daily average of the Δwtc on the left panel, and the standard deviation on the right panel. As this monitoring is performed in a long-term perspective, we used delayed-time products: GDR products for SARAL and Jason3. For Sentinel-3A, the monitoring was started with Short Time Critical (STC) products. To be consistent with Jason-3 coverage, data for the three missions have been selected below 60° of latitude.

The monitoring of the daily averaged Δwtc allows to detect abnormal events and potential significant drifts. The first conclusion over the full period of study is that a global bias appears between SARAL, Jason3 which have a mean Δwtc around 0.6cm and Sentinel-3A around 0cm. This bias is considered small and more analysis are required to decide if it shall be corrected. One can notice the same variations of Δwtc for SARAL and Sentinel-3A Δwtc : a period with no trend from January to May 2017, followed with a period with a small trend up to October 2017, and finally a period with no trend. Jason3 shows slightly different variations: it is very similar to AltiKa until June2017, then the Δwtc seems to stay at the same level while AltiKa is increasing, and finally a negative trend is observed. These differences of variations are not yet explained. One has also to keep in mind the order of magnitude of these variations: about 2mm.

The daily Δwtc standard deviation allows to assess the performance of the correction. The instruments used in this study for the comparison have different configurations. First Jason3 benefits from its three channels radiometer (18.7GHz, 23.8GHz, 34GHz), providing a correction with a smaller deviation with respect to the model. SARAL/MWR is closer to Sentinel-3A/MWR in this context with its two channels

(23.8GHz, 37GHz). Then the standard deviation for SARAL is the closest reference. But the SARAL GDR products is issued from the so-called “Patch2” algorithms, known to have issues with the Sigma0 in Ka-band in the simulations used for the learning database. Then the difference between SARAL and Sentinel-3A has to be considered carefully. The standard deviation of Δwtc for Sentinel-3A is smaller than for SARAL meaning that we have a better estimation of the correction for Sentinel-3A according to these metrics. Jason-3 shows the best performances with the smallest deviation. Moreover, one can notice that both SAR and P-LRM corrections have very similar performances, as the two curves are almost on top of each other for both mean and standard deviation.

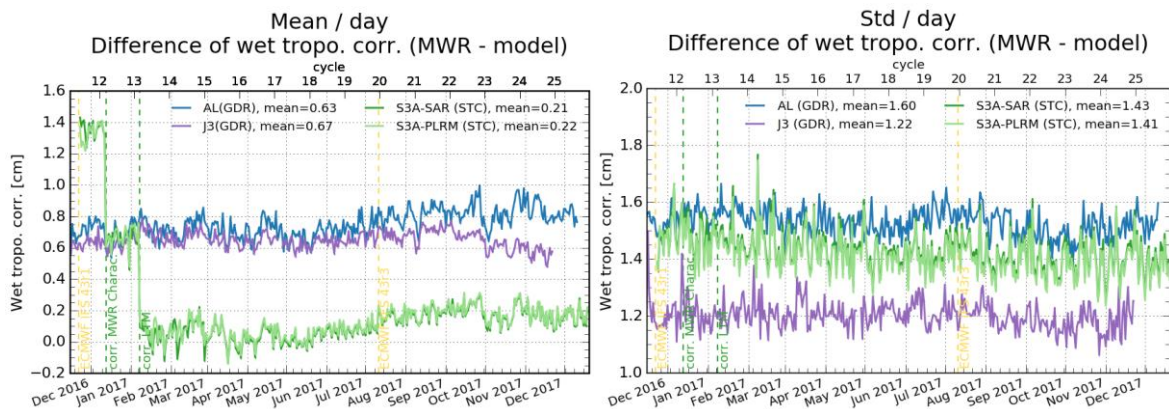


Figure 34: Monitoring of MWR (3P) - ECMWF wet tropospheric correction for Sentinel-3A, SARAL/AltiKa, Jason3/AMR: mean (left), standard deviation (right)

Figure 35 shows the map of the differences of SAR and P-LRM wet tropospheric corrections. The mean difference is very small, lower than 1mm, but it is not homogeneous. Some patterns appear on this map, driven by the differences of Sigma0 (Figure 27) that will be discussed later in this report. The band from -40° to -80° in latitude shows the strongest differences up to -1mm, where the difference of SAR/P-LRM Sigma0 shows its highest values.

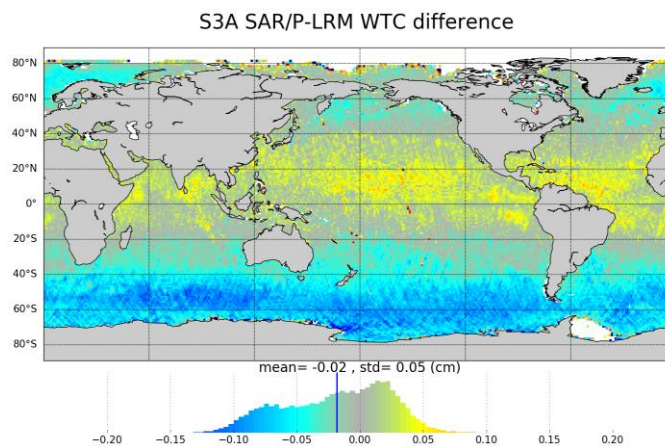


Figure 35: Difference of SAR/P-LRM wet tropospheric correction for Sentinel-3A, SARAL/AltiKa, Jason3/AMR

The enhanced retrieval algorithm of the WTC was not tuned correctly until version 6.10 of the IPF, operated since December 2017. Consequently, for the study presented here, this correction has been computed with an in-house tool using NTC data and the same auxiliary inputs than the IPF (sea surface temperature, γ_{800}). Figure 36 shows the monitoring of Δwtc for SAR and PLRM wet tropospheric corrections, using both 3P and 5P retrieval algorithms. First a small bias is observed between 3P and 5P retrievals of about 2mm. Secondly the variations of the daily averaged Δwtc is the same for almost all the period of study except for cycle 14. The standard deviation of 5P Δwtc is slightly smaller than 3P: for example for P-LRM, standard deviation Δwtc is around 1.37cm with the 5P algorithm, and 1.43cm with the 3P algorithm. This indicates that the 5P algorithm improve the retrieval with respect to 3P algorithm. This improvement will have to be quantified by another diagnosis such as the crossover analysis.

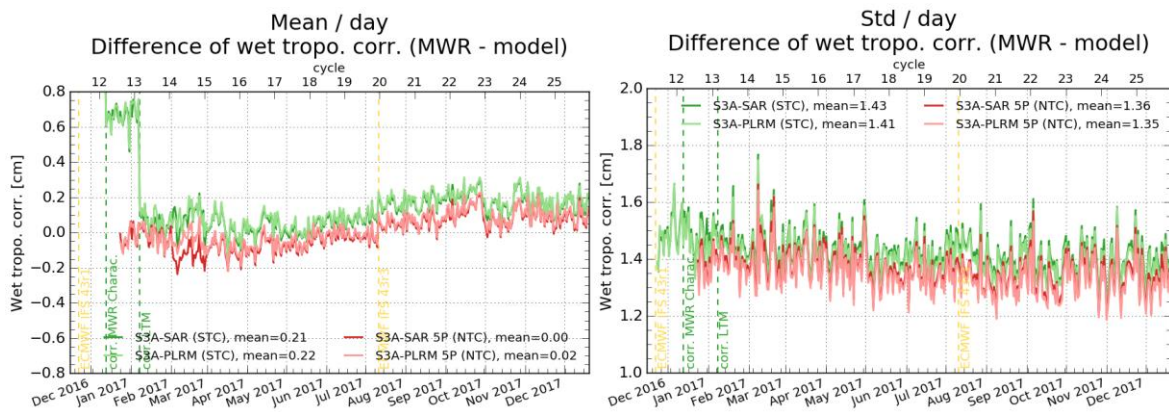


Figure 36: Monitoring of 3P and 5P MWR - ECMWF wet tropospheric correction for Sentinel-3A

Figure 37 shows the map of the difference between 5P and 3P algorithms. As seen before with Figure 36, the average difference is small of the order of mm, but Figure 37 highlights the geographical impacts of the enhanced algorithm. On this map, we retrieve the signature of the sea surface temperature.

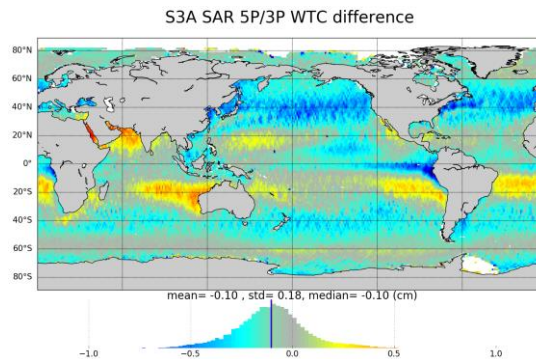


Figure 37: Map of the difference 5P - 3P wet tropospheric correction for Sentinel-3A (using NTC data)

7.3.2 Crossover analyses

The analysis of difference of variance of SSH at crossover points allows to assess the improvement or degradation of one correction with respect to the other. The SSH difference between the ascending and descending passes is composed of the variation of oceanic signal between the two passages, the measurement errors and estimation errors of the SSH. For a time lag below 10 days, one can consider that the oceanic variability is negligible. Then the SSH difference at crossover points approximates the errors of the corrections applied to the range for the estimation of the SSH. The lower the variance, the better the correction.

The usual reference for such a diagnosis for wet tropospheric correction is the model correction computed using ECMWF analysis. The computation of SSH is detailed on section 7.3. For this study, we compute the difference of variance when using the MWR WTC or the model correction:

$$\Delta Var = \text{Var}(\Delta\text{SSH with MWR WTC}) - \text{Var}(\Delta\text{SSH with model WTC})$$

When the correction computed using MWR measurements reduces the error on the SSH, ΔVar will be negative as the variance of ΔSSH using MWR correction will be smaller than the variance of ΔSSH when using the model correction. On the opposite when the correction computed using MWR measurements increases the error on the SSH, ΔVar will be positive.

We will start by analyzing the wet tropospheric correction retrieved from the classical algorithm (3P) (Figure 38). The analysis is performed here over the lowest oceanic variability areas. Jason-3 with its three channels AMR shows the best improvement with respect to the model correction with an average of -2.4cm^2 , Sentinel-3A is below with -1.6cm^2 for P-LRM correction, and finally SARAL using the Patch2 algorithm (see previous explanation) shows the smaller ΔVar (-1.3cm^2). Considering Sentinel-3A is a two channels radiometer and we analyze here a classical 3P algorithm, these results are good.

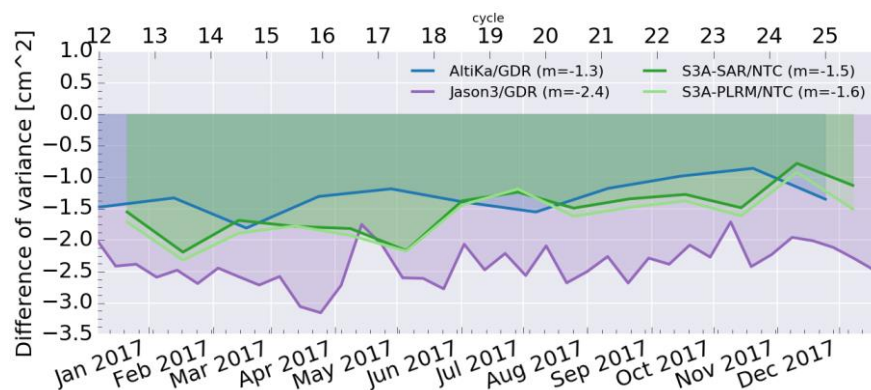


Figure 38: Difference of variance of ΔSSH at crossover points for Sentinel-3A, SARAL, Jason3 :
 $\text{var}(\text{SSH with WTC 3P MWR}) - \text{var}(\text{SSH with WTC ECMWF})$
 global ocean (top) and low oceanic variability (bottom)

Looking at the map of the ΔVar (Figure 39), we can see that we have a global improvement when using MWR correction. The map is quite noisy due to the small amount of data for this diagnosis.

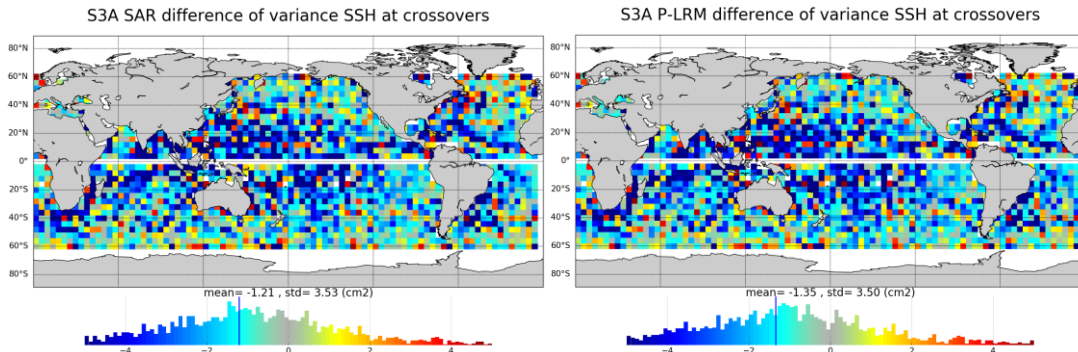


Figure 39: Difference of variance of SSH at crossover points SAR (left) / P-LRM (right)

We perform the same analysis for the enhanced algorithm (5P) again over the lowest oceanic variability areas (Figure 40). Jason-3 with its three channels AMR shows the best improvement with respect to the model correction with an average of -2.4cm², Sentinel-3A is below with -2.0cm² for P-LRM correction, and finally SARAL using the Patch3 algorithm (see previous explanation) shows similar results. The SARAL Patch3 algorithm is the next version of the retrieval algorithm based on measurements and not simulation, it corrects the issues seen with the previous algorithm and improves the retrieval using SST and $\gamma 800$. These are very good results but we know that there is room for Sentinel-3A as its algorithm is based on simulations.

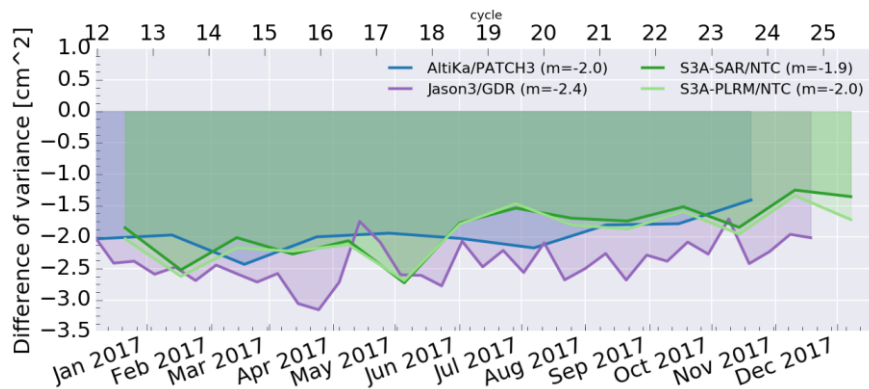


Figure 40: Difference of variance of SSH at crossover points for Sentinel-3A, SARAL/AltiKa, Jason3/AMR: $var(SSH \text{ with WTC } 5P \text{ MWR}) - var(SSH \text{ with WTC ECMWF})$

As for the 3P algorithm, the maps of the ΔVar (Figure 41) show a global improvement when using MWR correction.

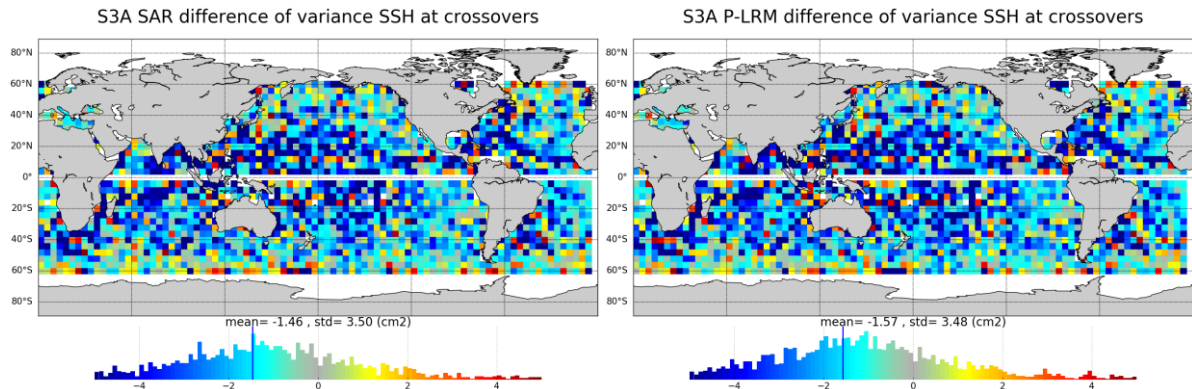


Figure 41: Difference of variance of SSH at crossover points SAR (left) / P-LRM (right)

7.4 Sea Level Performances

The Sea Level Anomaly is the most well-known parameter estimated from altimetry. It corresponds to the elevation of sea surface, with respect to a reference called Mean Sea Surface (MSS), generated by oceanic variability and climatic phenomena (such as Gulf stream current, El Nino, ...). It is computed as following:

$$SLA = Orbit - Altimeter Range - \sum Geophysical\ corrections - Mean\ Sea\ Surface$$

Where the geophysical corrections and the MSS are listed and described in the following table:

Table 6: Detail of the standard used to compute Sentinel-3A and Jason-3 SLA and SSH. For Sentinel-3A over the year 2017 some of these standards have been updated, thus they are detailed as a function of the IPF-SM2 versions.

Correction / mission and version	Sentinel-3A			Jason-3
	IPF-SM2 V06.05	IPF-SM2 V06.07	IPF-SM2 V06.10	GDR-D
Dry troposphere correction	ECMWF model			
Dynamical atmospheric correction	MOG2D			
Radiometer wet troposphere correction	3 parameters MWR WTC	3 parameters MWR WTC	3 parameters MWR WTC	AMR GDR-D
Ionospheric correction	Dual Frequency altimeter			
Sea State Bias	SSB Tran et al. (2012)			Jason-3 GDR D SSB
Ocean tide correction (including loading tide)	GOT 4.8		FES 2014	GOT 4.8
Earth tide height	Cartwright and Taylor			

Correction / mission and version	Sentinel-3A			Jason-3
	IPF-SM2 V06.05	IPF-SM2 V06.07	IPF-SM2 V06.10	GDR-D
Pole tide height	Wahr			
Mean Sea Surface	CNES_CLS_2011		DTU15	CNES_CLS_2011

Table 7: Detail of the standard used to compute Sentinel-3A and Jason-3 SLA and SSH. For Sentinel-3A over the year 2017 some of these standards have been updated, thus they are detailed as a function of the IPF-SM2 versions.

7.4.1 Along-track analyses

Figure 42 shows the maps of Sentinel-3A SARM and P-LRM SLA and the one derived from Jason-3. Same geographical structures are observed by both Sentinel-3A modes and both satellites. The SLA mean values and their dispersions are slightly different. They cannot be directly compared since Sentinel-3A coverage reaches latitudes around 81° (against 66° for Jason-3), the analysis of the biases between Sentinel-3A and Jason-3 is described in the next section.

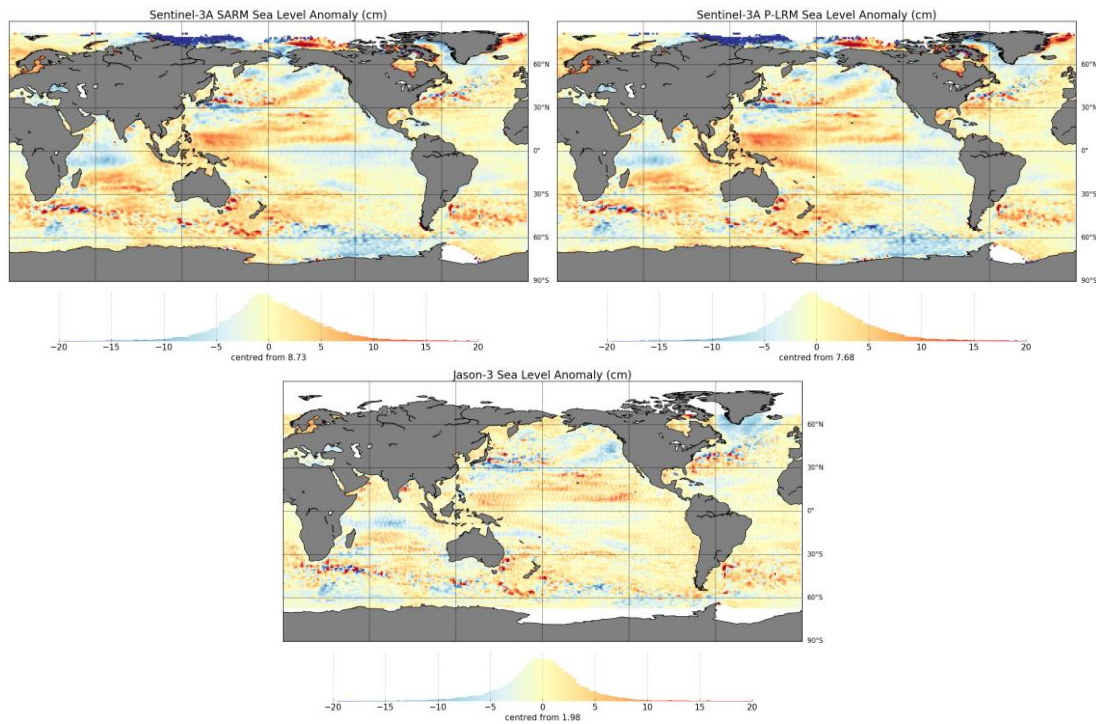


Figure 42: Gridded maps of Sentinel-3A SARM (top left panel) P-LRM (right left panel) and Jason-3 (bottom panel) SLA computed over the year 2017.

	Sentinel-3 MPC S3MPC STM Annual Performance Report - Year 1	Ref.: S3MPC.CLS.APR.002 Issue: 1.1 Date: 23/05/2018 Page: 53
---	--	---

The monitoring of the daily averaged SLA (plotted in Figure 43, left panel) allows to detect abnormal events and potential significant drifts. In order to be consistent with Jason-3 global coverage, the Sentinel-3A data have been selected below 66° of latitude. The observed temporal variations are consistent between both Sentinel-3A modes and between both satellites. At mid-November 2017, an important jump is observed for the Sentinel-3A SLA. It corresponds to the latest update of IPF version (installation of the IPF-SM2 06.10). This SLA jump of 4.93 cm in SARM and 2.48 cm in P-LRM was expected and is explained by the modifications listed in Table 8.

This monitoring of the mean SLA shows several interesting features:

- ❖ The bias between SARM and PLRM SLA is of 1 cm, SARM being higher with SAMOSA 2.3 retracker while it becomes lower with SAMOSA 2.5 retracker.
- ❖ Before the installation of the last IPF version, P-LRM bias is of 6cm against Jason-3, it falls to 3.5 cm with the update of the Sentinel-3A MSS (CNES-CLS11 to CNES-CLS15) whereas the MSS used to compute Jason-3 SLA is still the MSS CNES-CLS11.
- ❖ Before the installation of the last IPF version, the SARM bias is 7 cm against Jason-3, it falls to 2.1 cm with the update of the Sentinel-3A MSS (CNES-CLS11 to CNES-CLS15) whereas the MSS used to compute Jason-3 SLA is still the MSS CNES-CLS11 and the update of the SARM retracking (SAMOSA DPM2.3 to DPM2.5).

Note that the absolute bias is sensitive to the SSB model used. In this case, the product SSB models are used for Sentinel-3A and Jason-3 missions. The assessment of differences between Sentinel-3A and Jason-3 with updated or not SSB are described in the next section through crossover analyses.

The monitoring of the SLA variance allows to detect potential changes in the long-term stability of the altimeter's system performances. The metric between both Sentinel-3A modes and both satellites are consistent. The SARM SLA variance is slightly lower than for P-LRM and Jason-3, it could be explained by the range lower level of noise. After the installation of the IPF-SM2 version 06.10, Sentinel-3A SARM and P-LRM SLA variance decreased. This is explained by the use of the MSS CNESCLS15 instead of the MSS CNESCLS11 in the SLA computation. For Jason-3, the SLA is computed with the MSS CNESCLS11 over all the period assessed. This reduction of the variance is explained by the better quality of the latest model (Pujol et al., 2018).

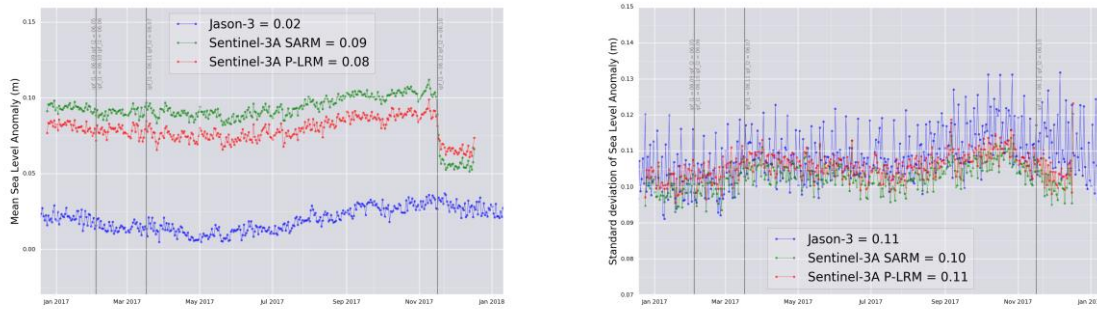


Figure 43: Daily monitoring of the Sentinel-3A SARM (green curve) P-LRM (red curve) and Jason-3 (blue curve) mean SLA (left panel) and its standard deviation (right panel).

Parameter	Difference between versions 06.10 and 06.07 in SARM	Difference between versions 06.10 and 06.07 in P-LRM
Range altimeter	1.63 cm	0.00 cm
Sea State Bias	0.47 cm	0.00 cm
Dual frequency ionosphere correction	0.30 cm	0.00 cm
Ocean tide	0.05 cm	0.05 cm
Mean Sea Surface	2.43 cm	2.43 cm

Table 8: List of the main parameters (involved in the SLA computation) impacted by the IPF-SM2 upgrade from version 06.07 to 06.10 and the corresponding impact on SARM parameters and P-LRM parameters.

7.4.2 Crossovers

The analysis of Sea Surface Height (SSH) computed at mono-mission crossovers allows to assess the consistency between ascending and descending passes. It also provides a robust metric of the system performances. Indeed, it consists on the analysis of the difference between two independent measurements (from the ascending and from the descending passes) over a same location for which we consider the oceanic signal constant during the time laps. To make this assumption as reliable as possible we applied criteria to select the crossovers with a time lag below 10 days and located in the lowest oceanic variability areas.

The monitoring of the mean SSH differences at mono-mission crossovers is computed cycle by cycle (Figure 44). The result shows a slight mean bias of 0.4 cm for Sentinel-3A, between ascending and descending passes. This unexpected bias is related to altitude estimation, since performing the same diagnosis with STC altitude gives a mean bias centred in -0.2 cm. For both missions, temporal variations are observed:

- ❖ An annual signal of 1.2 cm of amplitude is observed for Sentinel-3A SARM SSH.
- ❖ A 120 days signal of 2 cm of amplitude is observed for Jason-3 SSH. The explanation of this signal is detailed in the Jason-3 annual report.

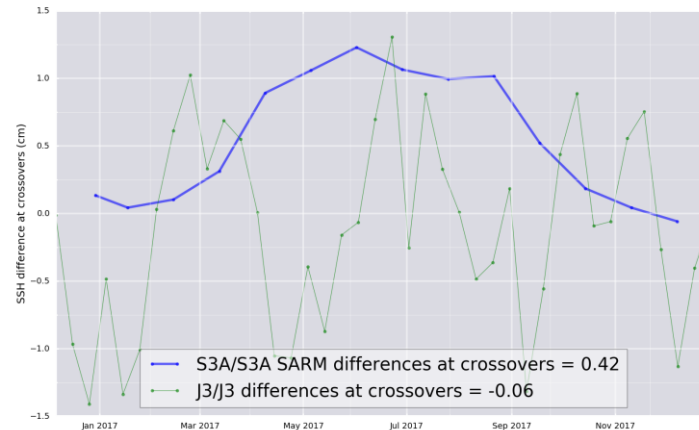


Figure 44: Cycle per cycle monitoring of the SSH differences computed at mono-mission crossovers for Sentinel-3A SARM (blue curve) and Jason-3 (green curve).

The Sentinel-3A SARM and P-LRM maps of SSH differences at crossovers are plotted in Figure 45. Once the global biases of 4.8 mm in SARM and 4.4 mm in P-LRM are removed, the SSH differences are low, ranging between -5 and 5 cm. The P-LRM map exhibits an excellent consistency between ascending and descending tracks. The residual patterns of 2 cm in the Atlantic and Pacific ocean could be possibly related to residual orbit errors. However, they are less homogeneous in SARM than in P-LRM. These geographical patterns could be explained by two main reasons:

- ❖ The 0.5 % of dependency of the SARM range with respect to SWH. This anomaly is illustrated Figure 77 where the SARM range increases with the SWH. Over a crossover location, if the wave height has changed between the two measurements, this anomaly creates an error. Differences with respect to Jason-3 SSH described in the next paragraph also highlight this error on SARM observations.
- ❖ The dependency of the SARM range as a function of the tracker variations. This anomaly is detailed in section 7.7.

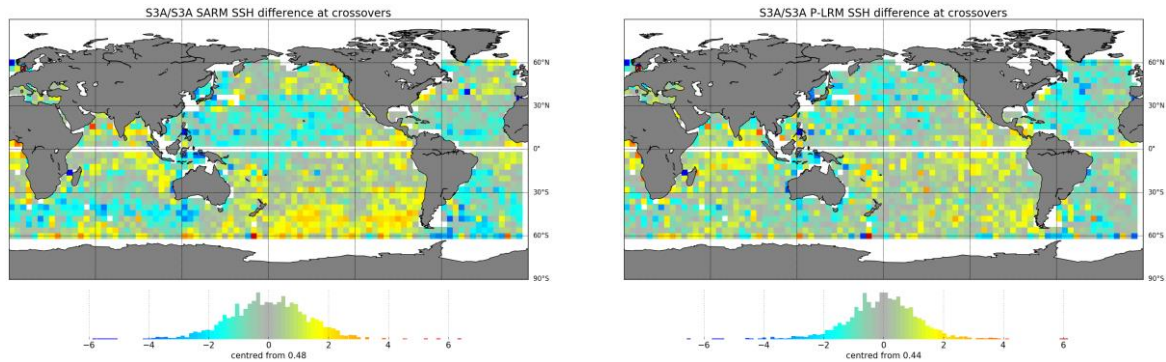


Figure 45: Gridded maps of Sentinel-3A SSH differences computed at mono-mission crossovers in SARM (left panel) and in P-LRM (right panel) over the year 2017.

As mentioned previously, the crossover analysis also allows to estimate the mission performance at spatial and temporal mesoscales. The monitoring of the systems error is plotted in Figure 46. The global standard deviation computed are the sum of the 2 arc errors (the ascending and the descending), thus the following metrics were divided by $\sqrt{2}$. A selection was applied on latitudes to make consistent the global coverage between Sentinel-3A and Jason-3. The SSH error is slightly higher for Sentinel-3A (4 cm) than for Jason-3 (3.5 cm). However, this estimation still includes a natural residual variation of the sea surface height between the two measurements at the crossover location. Computing the mean time lag for both missions, it was found that the mean delay is larger for Sentinel-3A (4.7 days) than for Jason-3 (3 days). It means that the ocean surface height has more probabilities to change in the case of Sentinel-3A crossovers, and thus adds more oceanic signal variability in this metric. Applying a specific selection, we reduced the Sentinel-3A mean time lag to make it consistent with Jason-3. The results (red curve) shows that Sentinel-3A and Jason-3 performances are now fully comparable and consistent with a mean value of 3.5 cm at global scale.

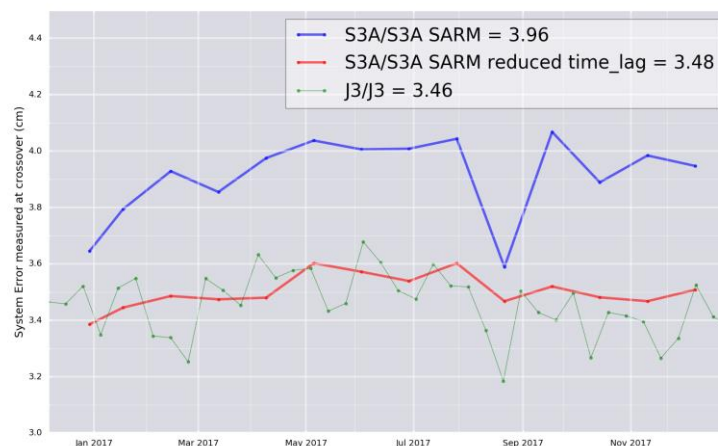


Figure 46: Cycle per cycle monitoring of the system error computed at mono-mission crossovers for Sentinel-3A (blue curve) and Jason-3 (green curve). The system error is computed through the cyclic SSH differences standard deviation at crossovers and divided by $\sqrt{2}$ because of the cumulation of the ascending and descending errors. The red curve shows the Sentinel-3A SARM system error when the mean time lag at crossovers is consistent with the Jason-3 one.

The crossover analysis is also a relevant tool to perform cross calibration between two missions. The following plot (Figure 47) shows the differences at crossovers between Sentinel-3A and Jason-3 in SARM (left panel) and in P-LRM (right panel). It shows a very good consistency between the two missions with differences ranging between -4 and 2 cm (once the mean bias is removed). However, the discrepancies are less homogeneous in SARM than in P-LRM. In SARM, positive differences are observed in the South and North hemispheres whereas they are mainly negative between the tropics. These geographical patterns are strongly correlated with the SWH signal which is consistent with the result of Figure 77.

In P-LRM, differences are homogenous and very low, a small negative signal is observed between the tropics, the source being still under investigation. Nevertheless, this map does not highlight the same patterns than the map of S3A/S3A crossovers. This confirms that these two metrics complete each other to further understand the residual errors that can affect Sentinel-3A sea level observations.

The mean biases specified under the histograms of the maps give the global SSH bias between Sentinel-3A and Jason-3: 7.1 cm for the SARM, 5.8 cm for the P-LRM which is consistent with the mean SLA monitoring before the installation of the last IPF version.

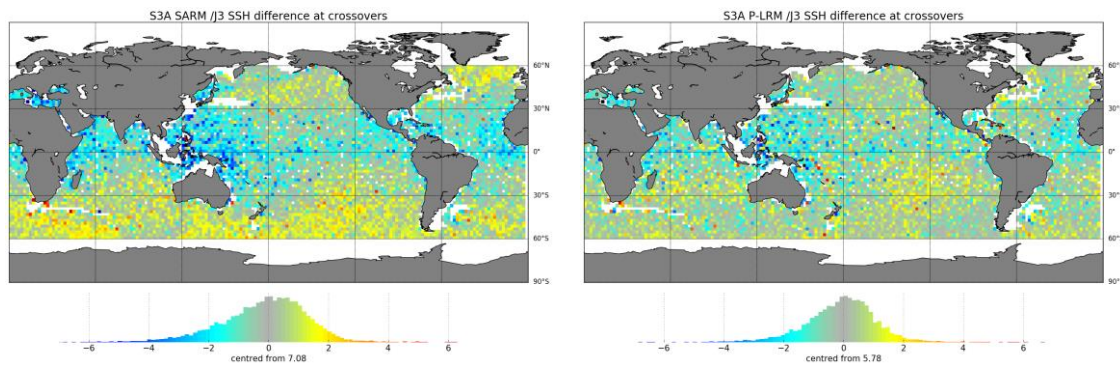


Figure 47: Gridded maps of SSH differences computed at Sentinel-3A and Jason-3 crossovers in SARM (left panel) and in P-LRM (right panel) over the year 2017.

The following plot (Figure 48) shows the monitoring of the mean bias between Sentinel-3A and Jason-3 at crossovers.

Before the installation of IPF-SM2 version 06.10:

- ❖ The bias between SARM and Jason-3 equals 7.5 cm which is consistent with previous analyses.
- ❖ The bias between P-LRM and Jason-3 equals 5.8 cm which is consistent with previous analyses.
- ❖ When the Jason-3 SSB is updated with the latest version available (Tran et al., 2012) these biases decrease by 2.6 cm.

After the installation of the latest IPF-SM2 version (version 06.10):

- ❖ The bias between SARM and Jason-3 equals 2.5 cm when using updated SSB for Jason-3 mission. SARM parameters impacted by the update are listed in Table 8. Note that the MSS is never taken into account in the SSH computation at crossovers. Taking into account that Jason-3 SSH is biased by 3 cm (Jason-3 SSH being too low by 3 cm compared to Jason-2 SSH), we are left with a bias for Sentinel-3A SARM SSH close to -0.5 cm with the new Processing Baseline. Note that this figure is more in agreement with the mean range bias observed with the transponder (see section 11.1)
- ❖ The bias between P-LRM and Jason-3 is not changed, since the IPF update has very low impact on P-LRM SSH computation.

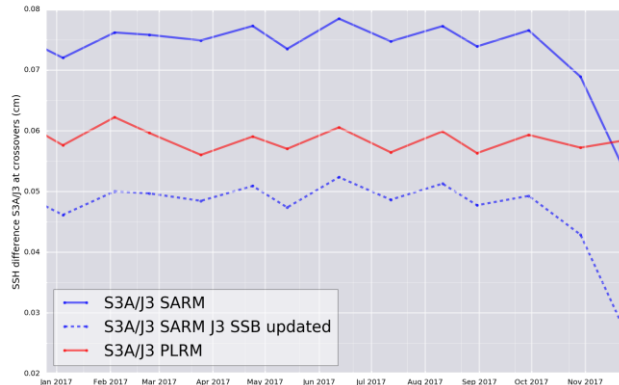


Figure 48: Cycle per cycle monitoring of the SSH differences computed at Sentinel-3A and Jason-3 crossovers in SARM (blue filled curve) and in P-LRM (red curve). The dashed blue curve shows the evolution of the bias when the Jason-3 SSH is computed using an updated SSB (SSB Tran et al. 2012 instead of GDR-D SSB).

The mono-mission crossover analysis also allows to compute a pseudo time tag bias by computing the regression between SSH differences and orbital altitude rate (\dot{H}), also called satellite radial speed:

$$\Delta\text{SSH} = \alpha \dot{H}$$

This method allows to estimate the time tag bias but it can also absorb other errors correlated with \dot{H} as for instance orbit errors. Therefore it is called pseudo time tag bias. Figure 49 shows the monitoring of the pseudo datation bias for Sentinel-3A, SARAL/AltiKa and Jason-3 on a cyclic basis. In average Sentinel-3A SARM has slightly higher pseudo time tag bias than Jason-3 and AltiKa (respectively 41 us against -18 us and 8 us). Moreover Sentinel-3A pseudo time tag bias, as Jason-3, presents temporal variations:

- ❖ An annual signal for Sentinel-3A as observed for the monitoring of the SSH differences between ascending and descending tracks.
- ❖ A 60 days signal for Jason-3

These temporal variations are under investigations.

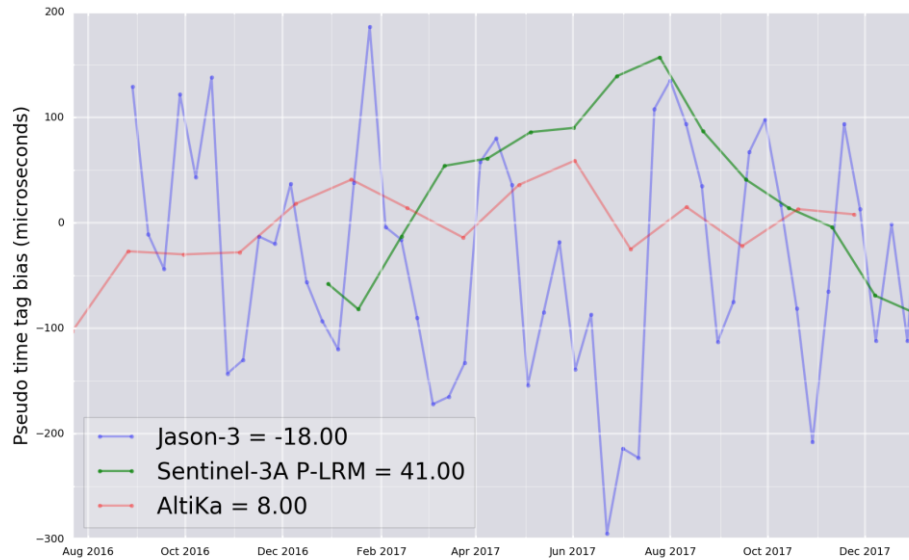


Figure 49: Cycle per cycle monitoring of the pseudo time tag bias for Sentinel-3A (green curve), Jason-3 (blue curve) and SARAL/AltiKa (red curve). The pseudo time tag biases are computed at mono-mission crossovers.

7.5 Global Mean Sea Level

The Global Mean Sea Level (GMSL) is one of the most important indicator of the climate change. In the past two decades, sea level has been routinely measured from space using satellite altimetry techniques. This indicator is computed from the SLA measurements applying then specific methods to estimate precisely the slope and the corresponding uncertainty. These methods are described in Ablain et al. (2017).

The GMSL trend was computed using these processing methods for Sentinel-3A and Jason-3 over the same period. To extend the Sentinel-3A time series and make this analysis more relevant, a homogeneous Sentinel-3A dataset was concatenated from reprocessed and on the fly products. For this dataset, the IPF version is the 06.07, with consistent geophysical corrections between both satellites. The global trend of 3.9 mm/year measured by Sentinel-3A is consistent with the one derived from the reference time series based on Jason-3. The level of uncertainty is slightly higher for Sentinel-3A, this is mainly explained by the longer repetitive period of the satellite (27 days against 10 days for Jason-3). This result allows to affirm that with a one and half year dataset, no significant drift or abnormal behavior is observed on Sentinel-3A sea level.

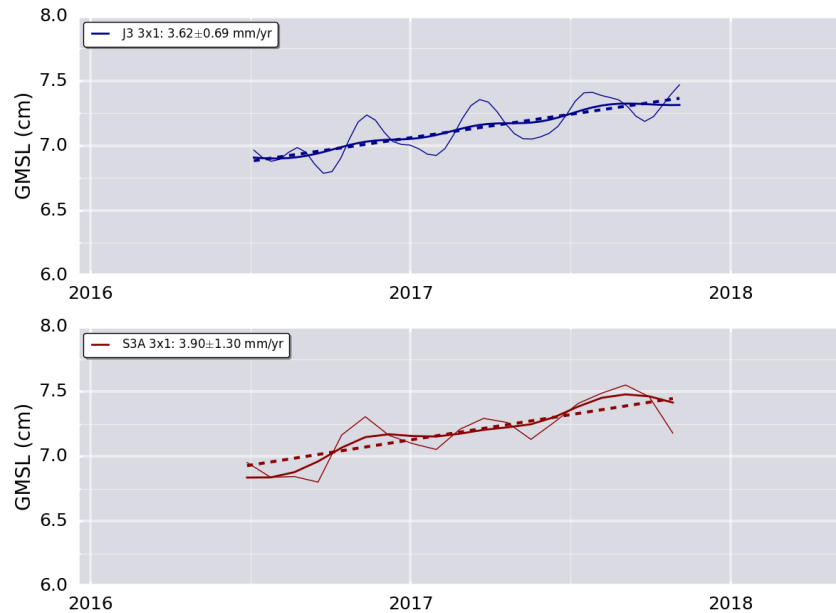


Figure 50: Evolution of the Global Mean Sea Level computed with Jason-3 (top panel) and Sentinel-3A SARM (bottom panel) SLA.

7.6 Wind/Wave Performance

Radar backscatter (σ_0), surface wind speed (WS) and significant wave height (SWH) from product S3A_SR_2_WAT are monitored and validated using the procedure used successfully for the validation of the equivalent products from earlier altimeters. The procedure is described in Appendix A of the cyclic reports. The procedure composed of a set of self-consistency checks and comparisons against other sources of data. Model equivalent products from the ECMWF Integrated Forecasting System (IFS) and in-situ measurements available in NRT through the Global Telecommunication System (GTS) are used for the validation.

The validation is based on the NRT operational Sentinel-3A Surface Topography Mission Level 2 (S3-A STM L2) wind and wave marine products (S3A_SR_2_WAT) product. For the time being, the product distributed by EUMETSAT in netCDF through their Online Data Access (ODA) system is used after converting into ASCII format but this will be replaced by the formal BUFR (Binary Universal Form for the Representation of meteorological data) format whenever becomes operationally available. The raw data product is collected for 6-hourly time windows centred at synoptic times (00, 06, 12 and 18 UTC).

The data are then averaged along the track to form super-observations with scales compatible with the model scales of around 75 km. It is worthwhile mentioning that the model scale is typically several (4~8) model grid spacing. This corresponds to 11 individual (1 Hz) Sentinel-3 observations (7 km each).



Sentinel-3 MPC
S3MPC STM Annual Performance
Report - Year 1

Ref.: S3MPC.CLS.APR.002
Issue: 1.1
Date: 23/05/2018
Page: 61

To achieve this, the stream of altimeter data is split into short observation sequences each consisting of 11 individual (1-Hz) observations. A quality control procedure is performed on each short sequence. Erratic and suspicious individual observations are removed and the remaining data in each sequence are averaged to form a representative super-observation, providing that the sequence has enough number of “good” individual observations (at least 7). The super-observations are collocated with the model and the in-situ (if applicable) data. The raw altimeter data that pass the quality control and the collocated model and in-situ data are then investigated to derive the conclusions regarding the data quality. The details of the method used for data processing, which is an extension to the method used for ERS-2 RA analysis and described in Abdalla and Hersbach (2004), can be found in Appendix A of the cyclic reports.

This annual assessment of wind and wave products focuses on the 1-year period spanning from 13 December 2016 till 12 December 2017. Selecting this period enables the assessment to avoid the abrupt change in performance due to the major SRAL Processing Baseline (PB) version 2.24 which was introduced on 13 December 2017. However, the time-series plots extend beyond the PB 2.24 date and thus showing the impact of this PB.

7.6.1 Backscatter coefficient

The ice-free ocean normalised Radar backscatter coefficient (backscatter, σ^0 or Sigma-0) from Sentinel-3A S3A_SR_2_WAT product seems to be reasonable and compares well with that from other altimeters. The backscatter global histogram (or the probability density function, PDF) of Sentinel-3A SRAL for a full year spanning between 13 December 2016 and 12 December 2017 is shown in **Figure 76**. Sentinel-3 backscatter PDF compares quite well with those of other Ku-band altimeters as shown in **Figure 52**. This can be clearly seen after applying proper shift of each PDF as shown in the legend of lower panel of **Figure 52**.

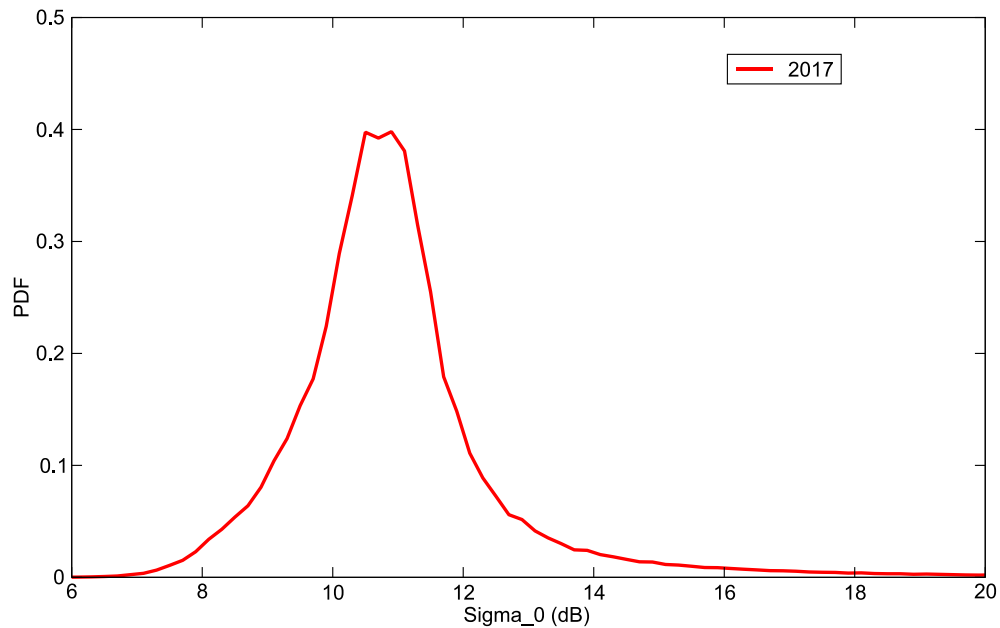


Figure 51: Sentinel-3A SRAL backscatter coefficient PDF over the whole global ocean for one year from 13 December 2016 to 12 December 2017.

The time series of the global (ice-free ocean only) mean and standard deviation (SD) of backscatter coefficients from SRAL of Sentinel-3A are shown in **Figure 53**. The temporal change in the mean and the SD of backscatter is not much different than the other altimeters (not shown). The plot shows the average of a moving window of 7 days moved by one day at a time to produce smooth plots. Both the mean and the SD of the backscatter are stable (within ~ 0.2 dB) over the whole year from 13 December 2016 till 12 December 2017. There was a slight increase in the mean value (and a possible decrease in SD) of the backscatter after the implementation of PB 2.24 on 13 December 2017. This is due to the change in backscatter coefficient that is now corrected for the radiometer atmospheric correction. The highest ever global mean backscatter value was attained towards the end of December 2017 (see the upper panel of **Figure 53**).

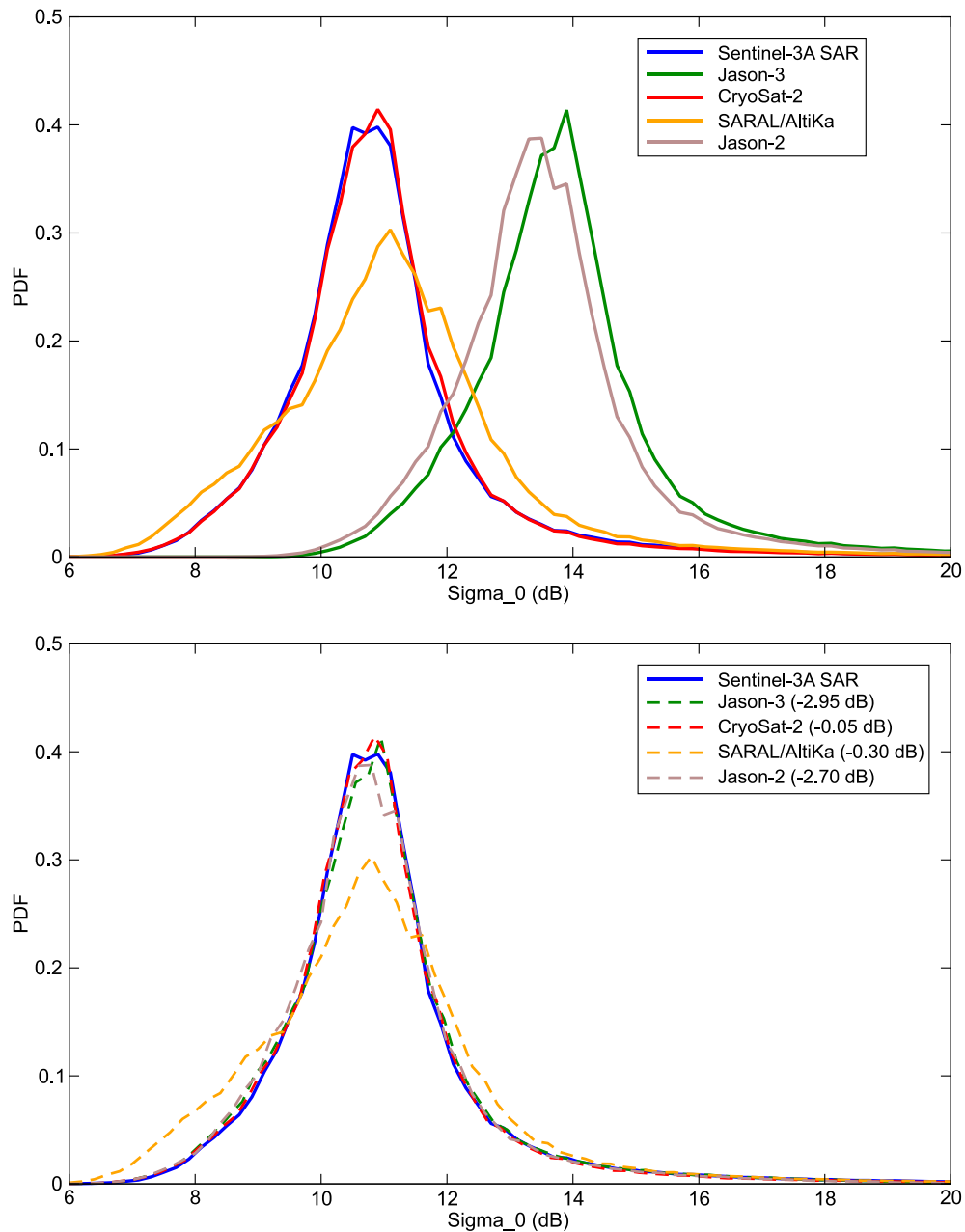


Figure 52: Comparison between backscatter PDF's of various altimeters over the year from 13 December 2016 to 12 December 2017 is shown in the upper panel. Better comparison can be carried out when PDF's are shifted to have their peak estimates coincide with that of Sentinel-3A (lower panel). The amount of shift is given in the legend of the lower panel.

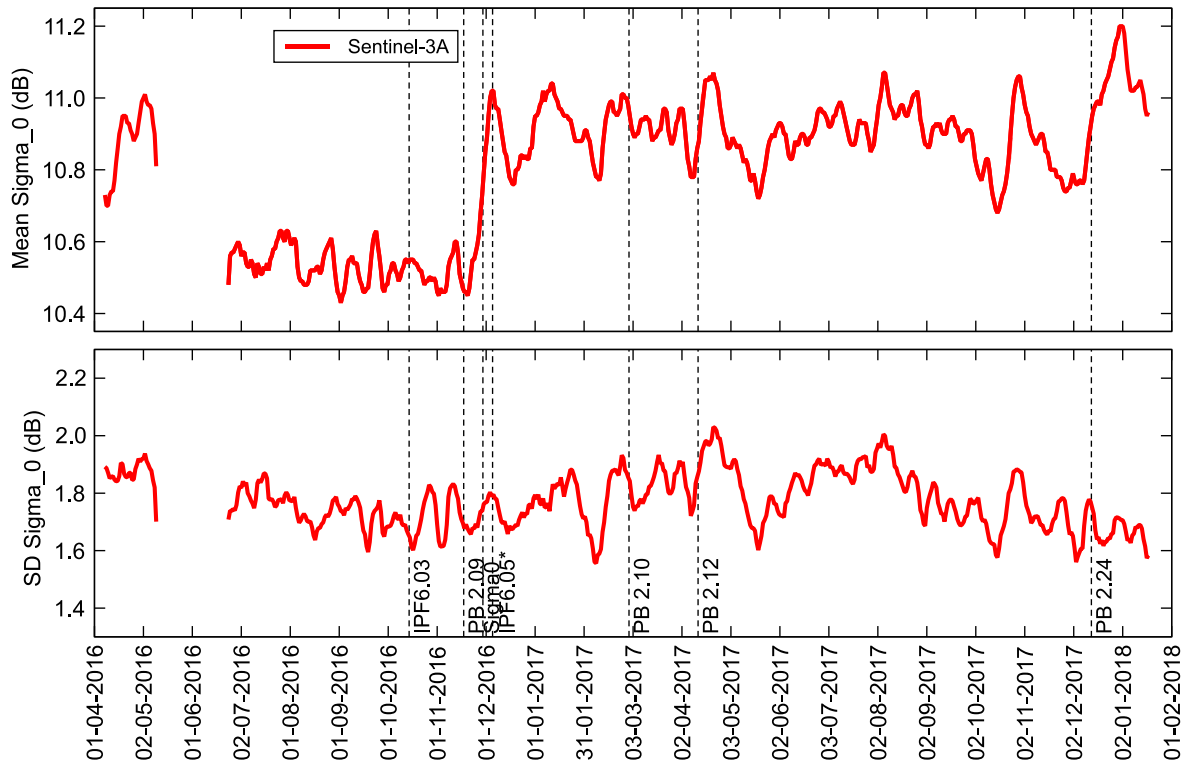


Figure 53: Time series of global mean (top) and standard deviation (bottom) of backscatter coefficient of SRAL Ku-band after quality control. Mean and SD are computed over a moving time window of 7 days. Vertical dashed lines show events which may have impact on the comparison. This includes Sentinel-3 STM Instrument Processing Facility (IPF) and Processing Baseline (PB) changes.

7.6.2 Altimeter Wind Speed

Figure 54 shows the global wind speed probability density function (PDF) of Sentinel-3A SAR mode for the year running from 13 December 2016 to 12 December 2017. The PDF of the ECMWF Integrated Forecast System (IFS) model wind speed collocated with Sentinel-3 during the same period is also shown. Although the PDF of Sentinel-3 wind speed is close to that of the model, there are some deviations especially around the peak of the PDF.

The deviation between Sentinel-3A PDF and those of the other altimeters are more pronounced as can be seen in the upper panel of **Figure 55**. The PDF's of model collocations with each satellite are shown in the lower panel of **Figure 55**. The deviation among the model PDF's as sampled along the ground track of each altimeter (i.e. the collocation with the altimeter super-observations) is not large. This suggests that the wind speed measurements from various altimeters show non-negligible deviations (at least in their PDF distributions).

The time series of the global mean and standard deviation (SD) of the wind speed from Sentinel-3 over a 7-day time window moving by 1 day at a time are shown in the upper and lower panels, respectively, of **Figure 56**. The corresponding time series of the model are also shown for comparison. It is clear that

global mean of Sentinel-3 SAR wind speed is very close to that of the ECMWF model. The processing change in late November 2016 that involved sigma-0 calibration (part of the Processing Baseline, PB 2.09 and IPF 6.05) played the major role to bring Sentinel-3 global mean and standard deviation values closer towards the corresponding model values with a very small difference. However, after the implementation of PB 2.09, Sentinel-3A altimeter showed lower wind speed variability (standard deviation) compared to the ECMWF model. It is unusual for the instrumental measurements to show lower variability compared to the model. Note that at the scale of the super-observations (~75 km is used for this assessment) one would expect comparable SD values.

According to **Figure 56**, PB 2.24 has no obvious impact on the wind speed measurements. However, due to natural variability it is still too early to have a clear conclusion.

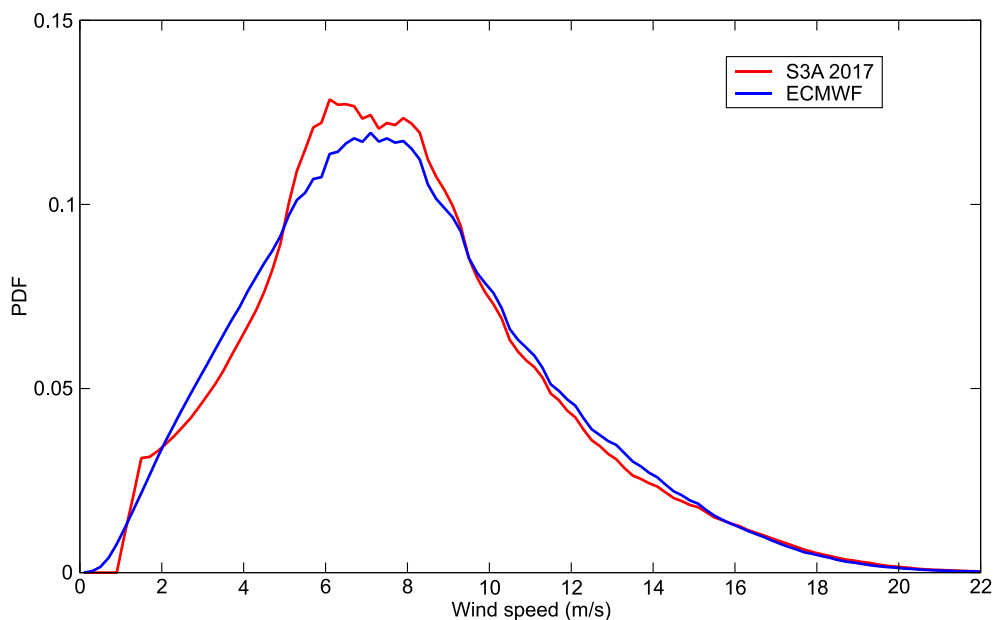


Figure 54: Sentinel-3A SRAL surface wind speed PDF over the whole global ocean for the year running between 13 December 2016 and 12 December 2017. The corresponding ECMWF (collocated with Sentinel-3) PDF is also shown for the same period for comparison purposes.

Collocated pairs of altimeter super-observation and the analysed (AN) ECMWF model wind speeds are plotted in a form of a density scatter plot in **Figure 57** for the whole globe over the one-year period from 13 December 2016 to 12 December 2017. The scatter plots in **Figure 57** and other similar wind speed scatter plots that appear hereafter represent two-dimensional (2-D) histograms showing the number of observations in each 2-D bin of 0.5 m/s × 0.5 m/s of wind speed. It is clear that the agreement between Sentinel-3 winds and their model counterpart is very good with virtually no bias (except for slight bias at high wind speed values). The standard deviation of the difference (SDD) with respect to the model, which can be used as a proxy to the random error, is about 1.1 m/s. The correlation coefficient is higher than 0.95. These values are similar to those of the other altimeters.

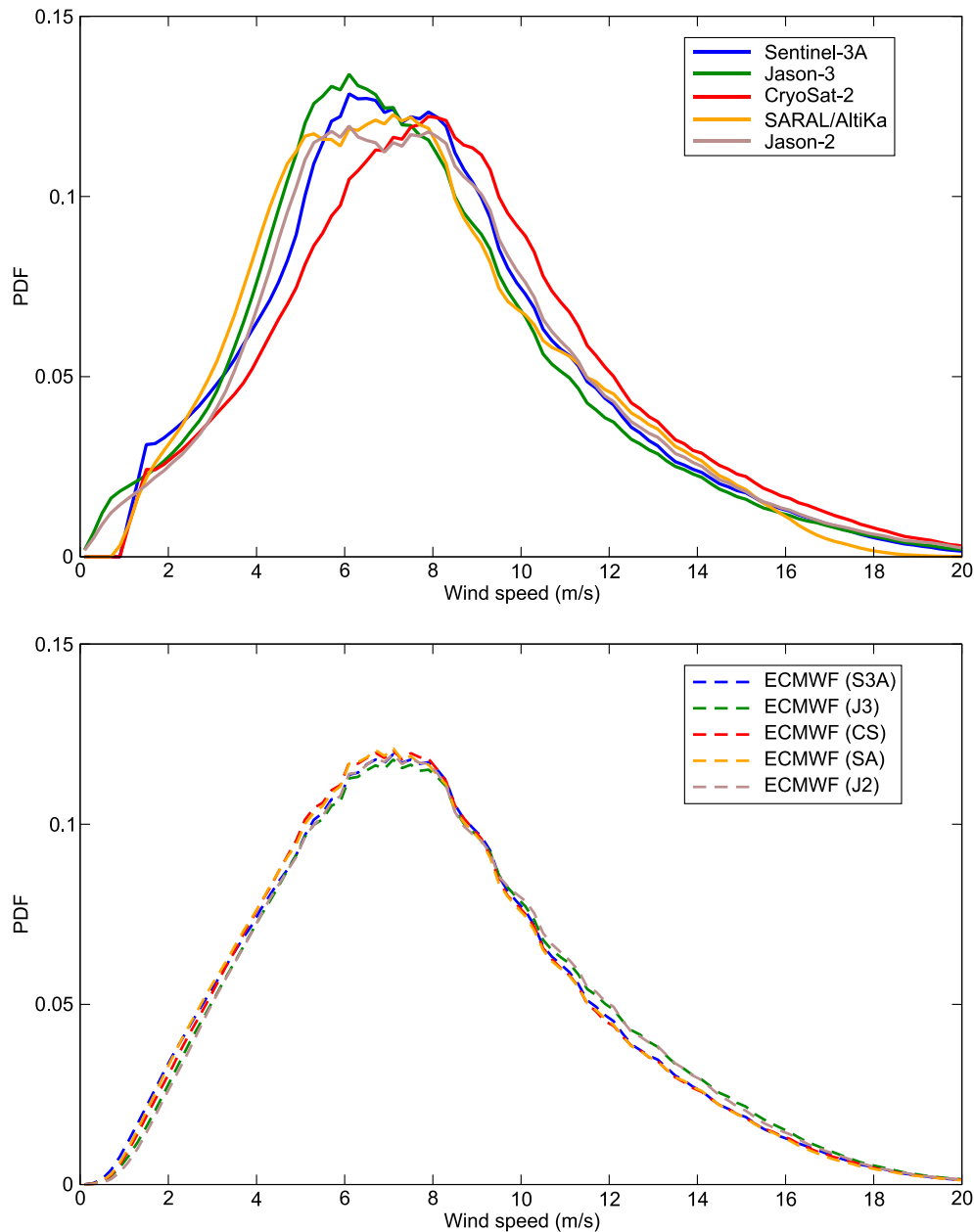


Figure 55: Comparison between wind speed PDF's of various altimeters over the year from 13 December 2016 to 12 December 2017 is shown in the upper panel. The corresponding model PDF's as collocated with the measurements used for the upper panel are shown in lower panel. The abbreviations are as follows: .S3A: Sentinel-3A, J3: Jason-3, CS: CryoSat-2, SA: SARAL/AltiKa and J2: Jason-2

The comparison against in-situ (mainly buoy) observations for the same period is shown in **Figure 58**. The bias against in-situ observation for this period is rather small (about 0.1 m/s). The SDD is about 1.4 m/s which is about 17% of the mean. The correlation coefficient is higher than 0.92. These figures are comparable to same statistics emerging from the comparison of wind speeds from other altimeters

against in-situ observations (not shown). It is important to state that most of in-situ observations are located in the Northern Hemisphere around the American and European coasts.

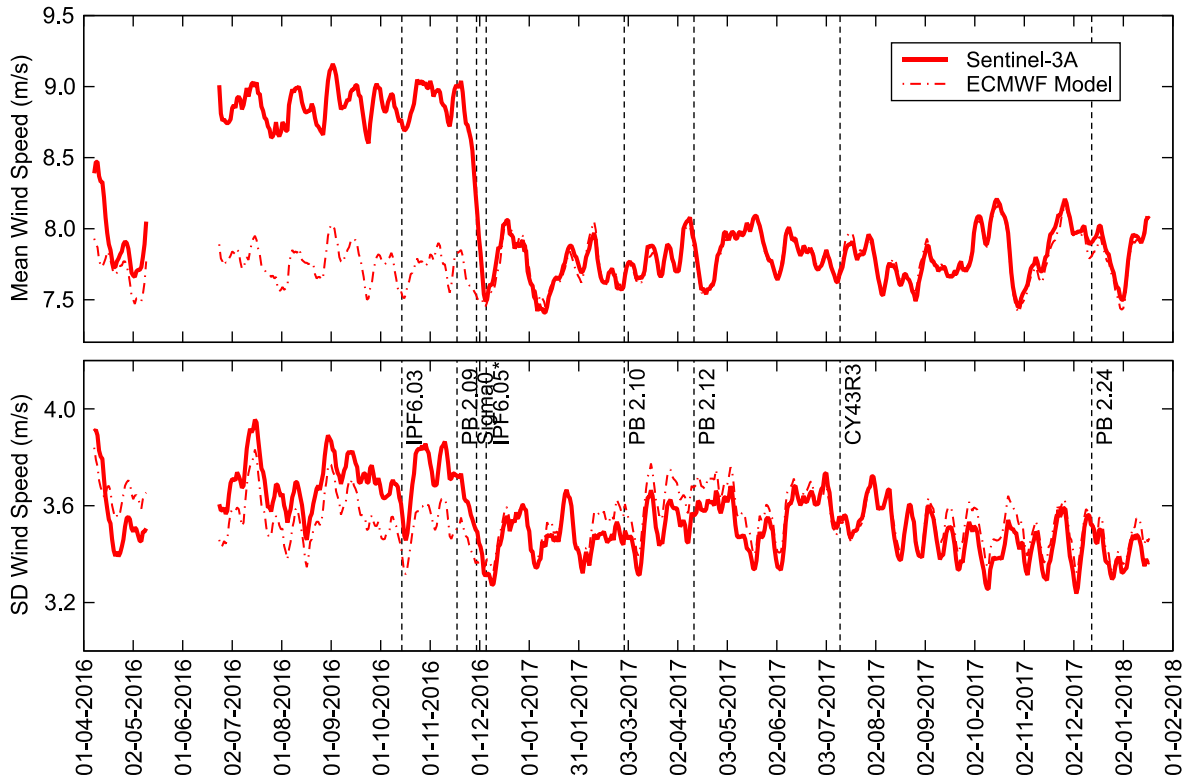


Figure 56: Time series of global mean (top) and standard deviation, SD, (bottom) of SAR wind speed from SRAL after quality control. The collocated model wind speed mean and SD are also shown. Mean and SD are computed over a moving time window of 7 days. Vertical dashed lines show events which may have impact on the comparison. This includes Sentinel-3 STM Instrument Processing Facility (IPF) and Processing Baseline (PB) changes as well as ECMWF IFS model changes like CY43R3.

The time series of the wind speed weekly bias (defined as the altimeter – model) and the standard deviation of the difference (SDD) of SRAL compared to the ECMWF model analysis (AN) are shown in the upper and lower panels, respectively, of **Figure 59**. Before the end of November 2016, the global wind speed bias was stable at about 1 m/s. The impact of the processing change known as PB 2.09 / IPF 6.05, which was implemented between late November and early December 2016, is very evident in **Figure 59**. This improvement was driven mainly by the change in the backscatter (see the upper panel of **Figure 53**). The bias in Northern Hemisphere (NH, area to the north of latitude 20°N), Tropics (the area confined between latitudes 20°N and 20°S) and Southern Hemisphere (SH, area to the south of latitude 20°S) collapsed to very small values (well within ± 0.5 m/s). The bias and SDD with respect to the model in the NH and SH follow seasonal cycles which peak during the hemispheric winter and becomes lowest during the summer. The amplitude of the bias seasonal cycle is about 1 m/s and 0.5 m/s in the NH and

SH, respectively. On the other hand, the amplitude of the SDD seasonal cycle is about 0.4 m/s and 0.2 m/s in the NH and SH, respectively. The bias and the SDD in the Tropics have been fairly constant since early December 2016.

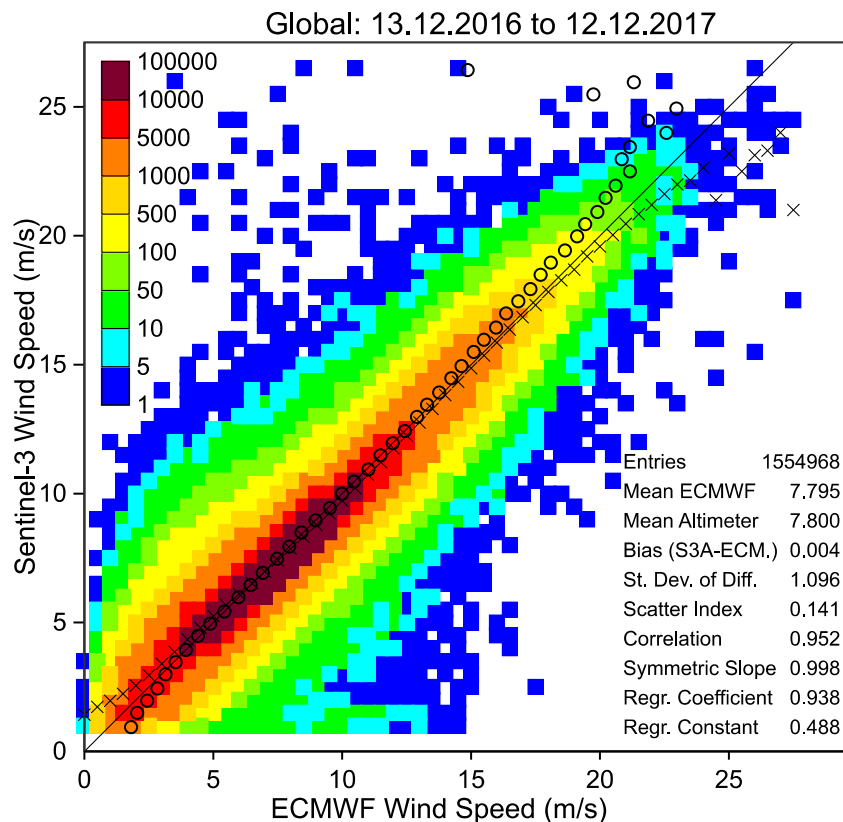


Figure 57: Global comparison between Sentinel-3A SRAL and ECMWF model analysis surface wind speed values over one-year period from 13 December 2016 to 12 December 2017. The number of collocations in each 0.5 m/s x 0.5 m/s 2D bin is color-coded as in the legend. The crosses are the means of the bins for given x-axis values (model) while the circles are the means for given y-axis values (Sentinel-3).

The time series of the wind speed monthly bias (defined as the altimeter – in situ) and the SDD of SRAL compared to the in-situ measurements are shown in the upper and lower panels, respectively, of **Figure 60**. Similar picture to that of the comparison against the model emerges. Noting that most of the buoy measurements are carried out in the NH, the “global” buoy comparison is nothing but a NH comparison. The impact of the processing change (PB 2.09 / IPF 6.05) in late November and early December 2016 is very evident in **Figure 60** as well. Similar seasonal cycles to those seen in the model comparison (**Figure 59**) for the NH can be also seen in **Figure 60**.

The time series of the global wind speed weekly bias and SDD of 5 altimeters (including SRAL) compared to the ECMWF model AN are shown in the upper and lower panels, respectively, of **Figure 61**. It is clear that the wind speed from Sentinel-3A shows the best agreement with the ECMWF model winds. It has

the lowest global bias (almost zero) and one of the lowest SDD values. However, there seems to be minor increase in the SDD (possible degradation) during the months of November and December.

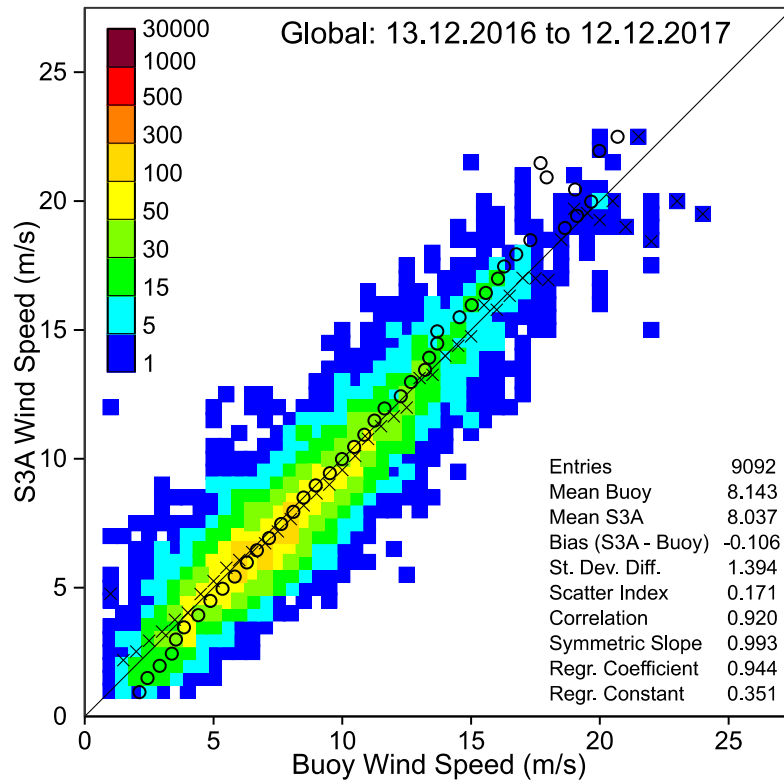


Figure 58: Same as Figure 57 but the comparison is done against in-situ observations (mainly in the NH).

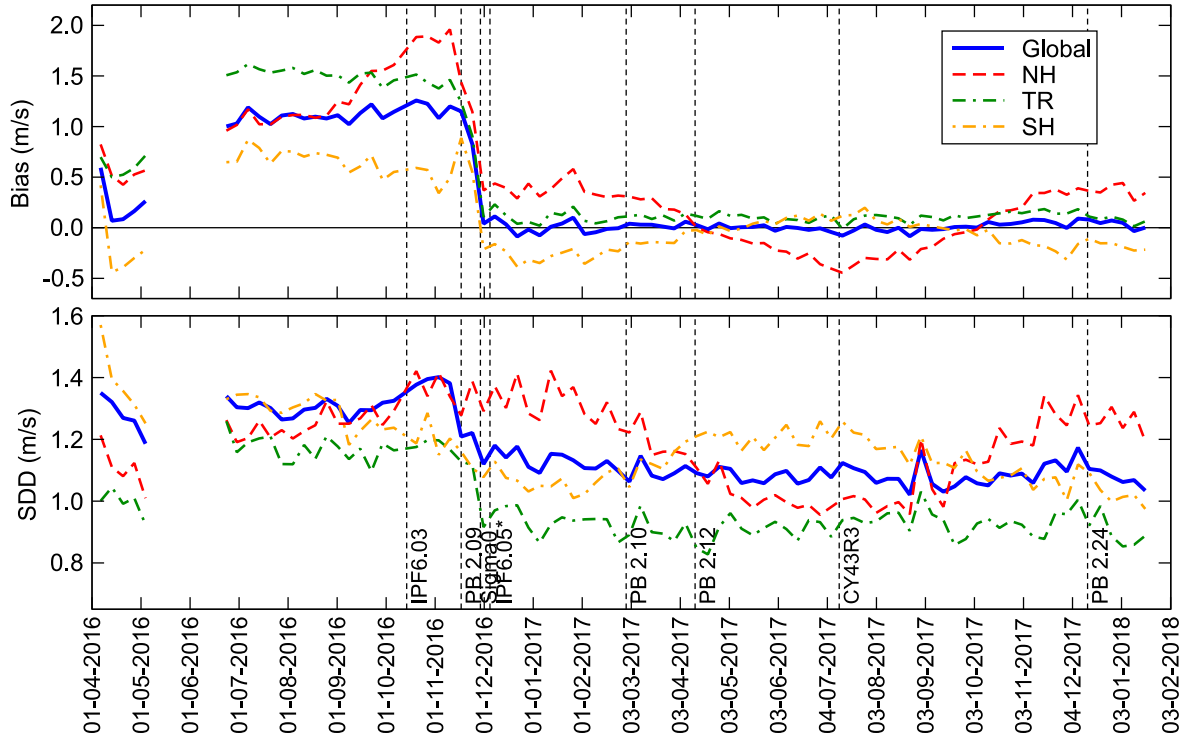


Figure 59: Time series of weekly wind speed bias defined as altimeter - model (top) and standard deviation of the difference (bottom) between SRAL Ku-band and ECMWF model analysis.

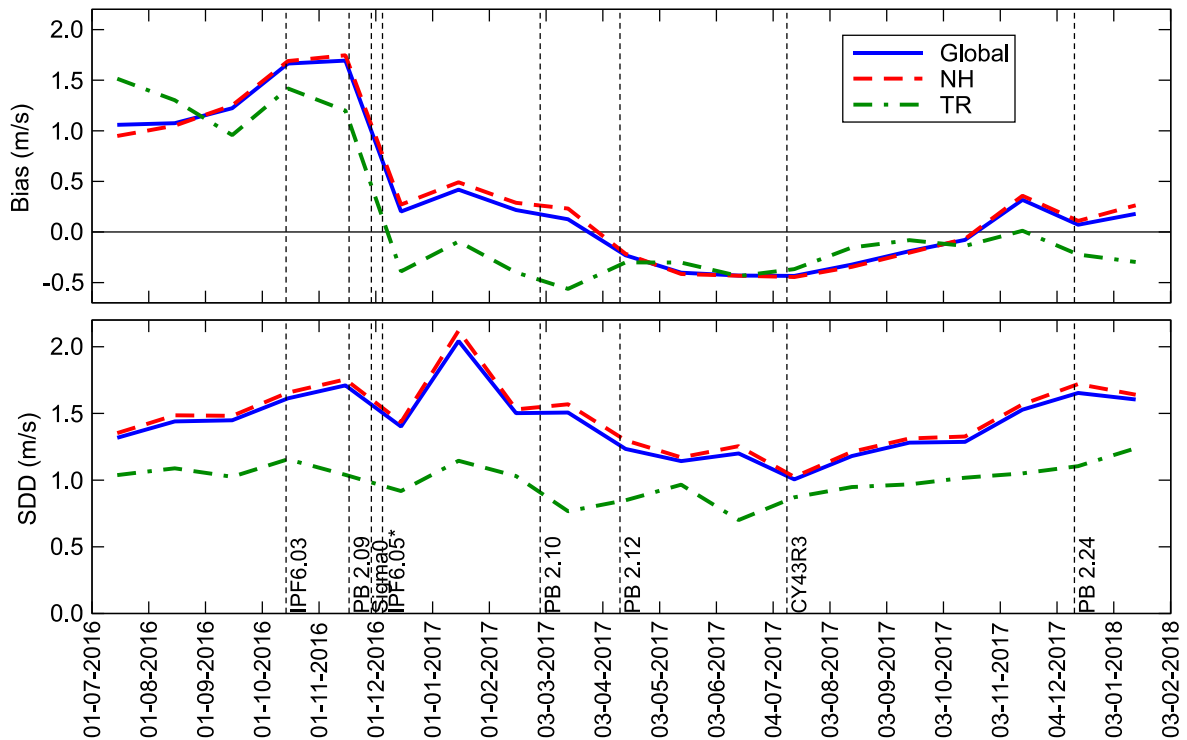


Figure 60: Time series of weekly wind speed bias defined as altimeter - buoy (top) and standard deviation of the difference (bottom) between SRAL Ku-band and in-situ (buoy) measurements.

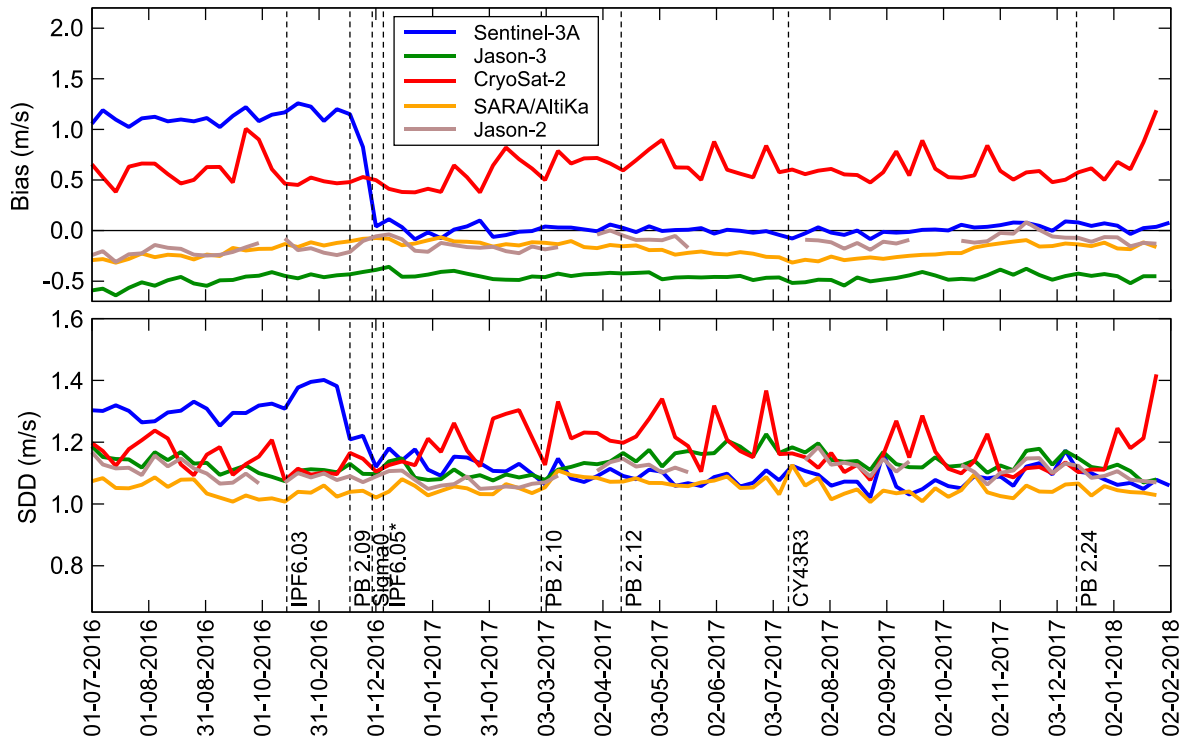


Figure 61: Time series of weekly global wind speed bias defined as altimeter - model (top) and standard deviation of the difference (bottom) between various altimeters (including SRAL) and ECMWF model analysis. SRAL curves are same as the global curves in Figure 59.

Keeping in mind that Jason-3, CryoSat-2, SARAL/AltiKa and Jason-2 are all conventional altimeters (the CryoSat-2 statistics in **Figure 61** are for LRM only), it is possible to conclude that Sentinel-3A SAR wind speed is as good as (if not slightly better than) its counterpart from the conventional altimeters.

It seems that PB 2.24 has no obvious impact on the quality of Sentinel-3A wind speed measurements as can be inferred from **Figure 61**. However, there is a hint of wind speed improvement if one compares the SDD of January 2018 to that of January 2017. In any case, it is still too early to reach a sound conclusion regarding this due to the natural variability of statistics.

The geographical distribution of the mean Sentinel-3 wind speed values and the wind speed bias, SDD and scatter index (SI, defined as the SDD divided by the model mean and expressed in percentage) with respect to the ECMWF model averaged over the one-year period from 13 December 2016 to 12 December 2017 are shown in **Figure 62**. While the mean wind speed, the SDD and SI distributions all look similar to their counterparts from other altimeters (not shown), the bias in panel (b) is rather low almost everywhere.

(a) **Satellite: Sentinel-3**
Sat. Mean Wind Speed [m/s]
For period between 21:09:33UTC on 12.12.2016 and 20:59:49UTC on 12.12.2017

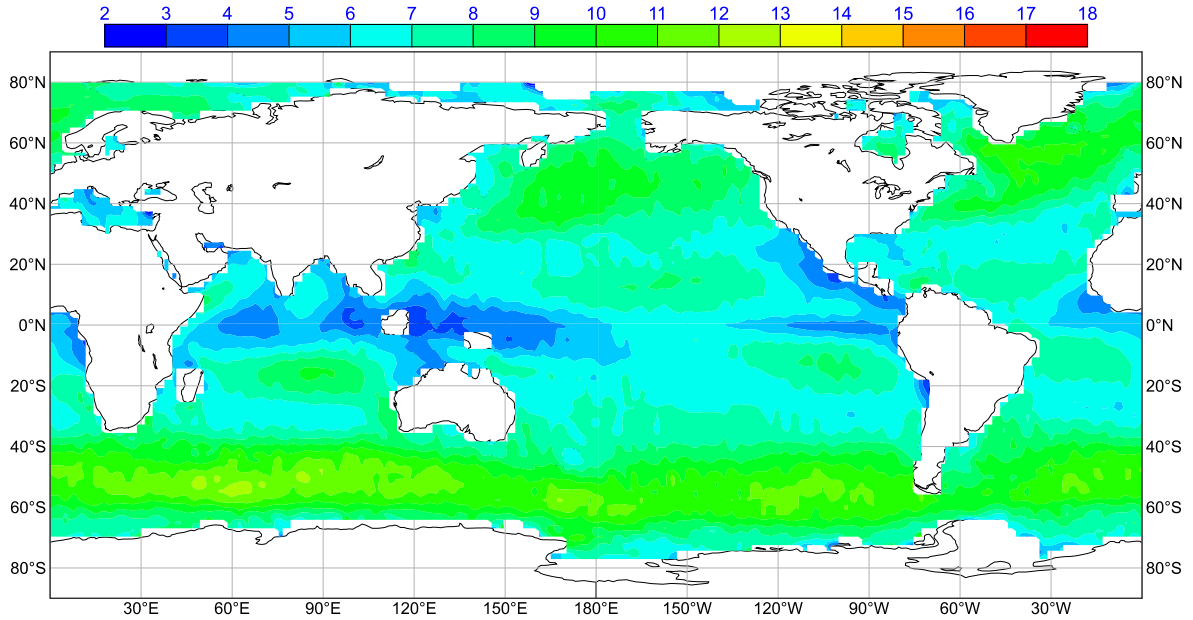
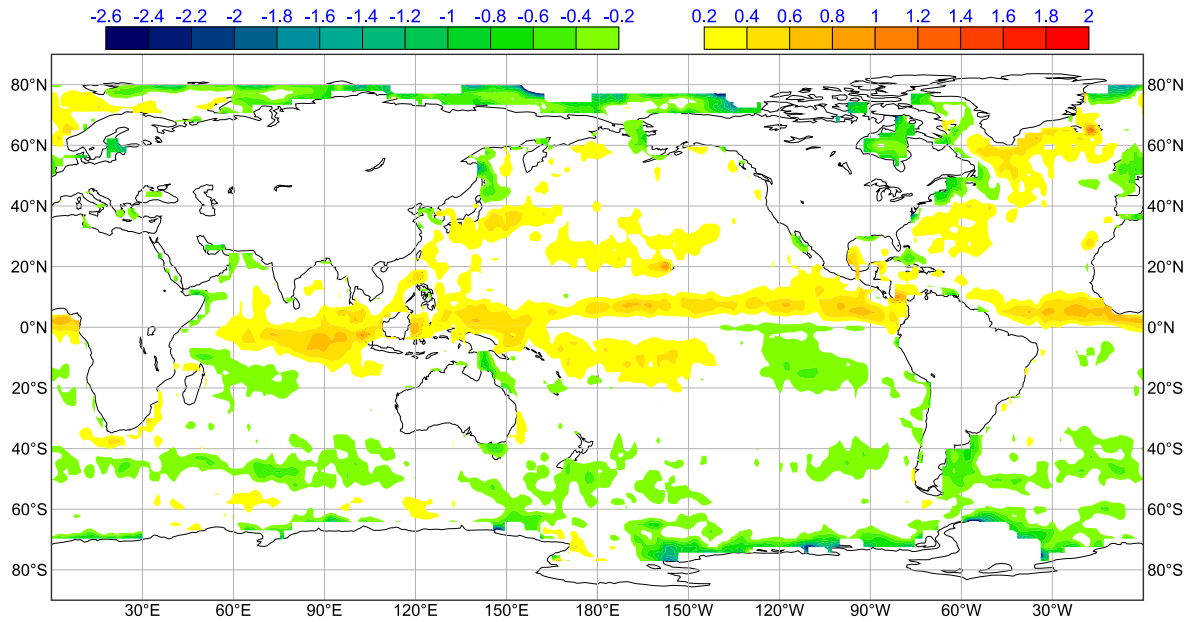


Figure 62: Geographical distribution of mean Sentinel-3 wind speed (a) as well as the bias (b); the SDD (c) and the SI (d) between Sentinel-3 and ECMWF model AN during the period from 13 December 2016 to 12 December 2017. Bias is defined as altimeter - model.

(b) **Satellite: Sentinel-3**
Wind Speed Bias (Sat-Mod) [m/s]
 For period between 21:09:33UTC on 12.12.2016 and 20:59:49UTC on 12.12.2017



(c) **Satellite: Sentinel-3**
Wind Speed SDD (Sat-Mod) [m/s]
 For period between 21:09:33UTC on 12.12.2016 and 20:59:49UTC on 12.12.2017

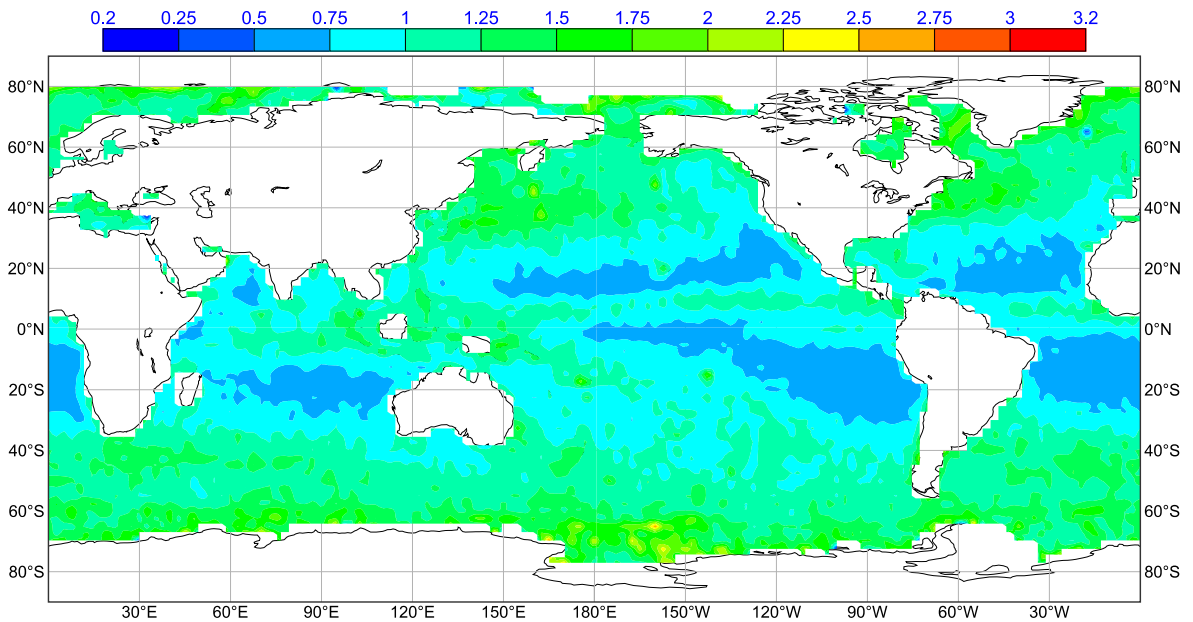


Figure 62: Continued.

(d) **Satellite: Sentinel-3**
Wind Speed SI (Sat-Mod) [%]
 For period between 21:09:33UTC on 12.12.2016 and 20:59:49UTC on 12.12.2017

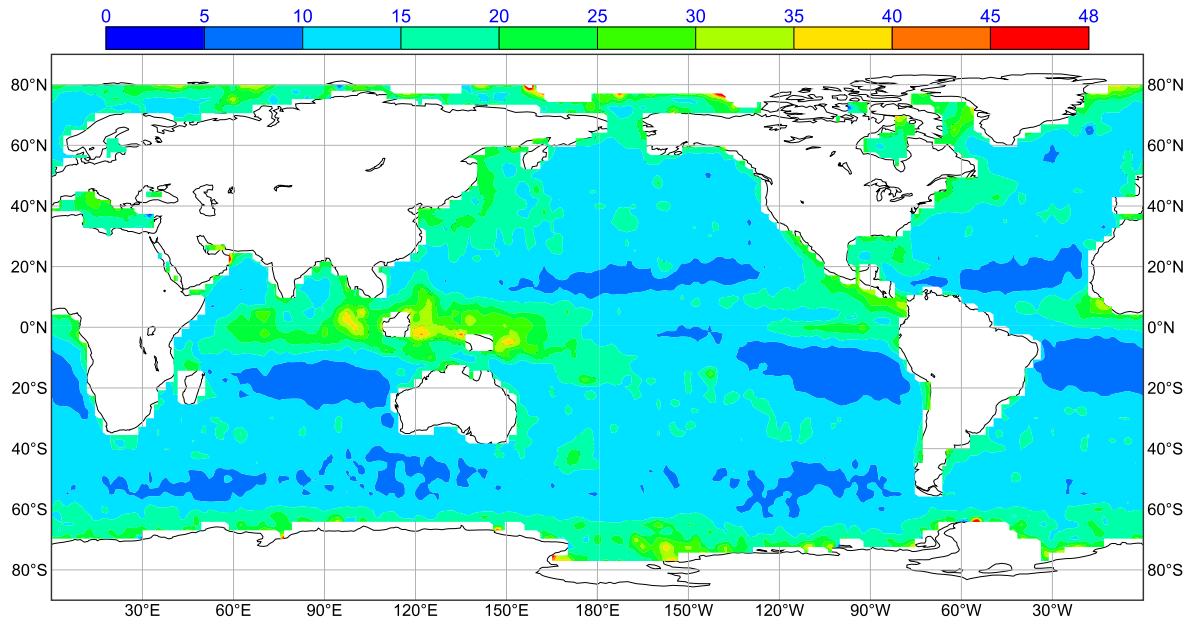


Figure 62: Continued.

PLRM Wind Speed:

Collocated pairs of Pseudo Low-bit Rate Mode (PLRM) wind speed super-observation and the analysed (AN) ECMWF model wind speeds are plotted in a form of a density scatter plot in **Figure 63** for the whole globe over the one-year period from 13 December 2016 to 12 December 2017. It is clear that the agreement between PLRM winds and their model counterpart is very good. The PLRM is globally unbiased when compared to the model although small regional biases do exist (see for example the upper panel of **Figure 64**). The SDD between SRAL PLRM wind and the model for the same period is 1.43 m/s (about 18% of the mean) which is slightly higher than that of SAR winds (see **Figure 57**). The correlation coefficient is 0.924 which is slightly lower than that of the SAR-mode wind comparison (see **Figure 57**).

The time series of the weekly bias and the SDD between PLRM wind speed and that of the model are shown in **Figure 64**. It is clear that there was an important improvement in PLRM wind speed associated with the implementation of PB 2.09 during the second week of November 2016. This change, which includes an increase of PLRM backscatter, resulted in almost zero bias between the altimeter and the model. The bias and the SDD time series in the NH and SH shown in **Figure 64** follow seasonal cycles similar to seasonal cycles followed by the corresponding time series of the SAR-model wind speed bias and SDD (**Figure 59**).

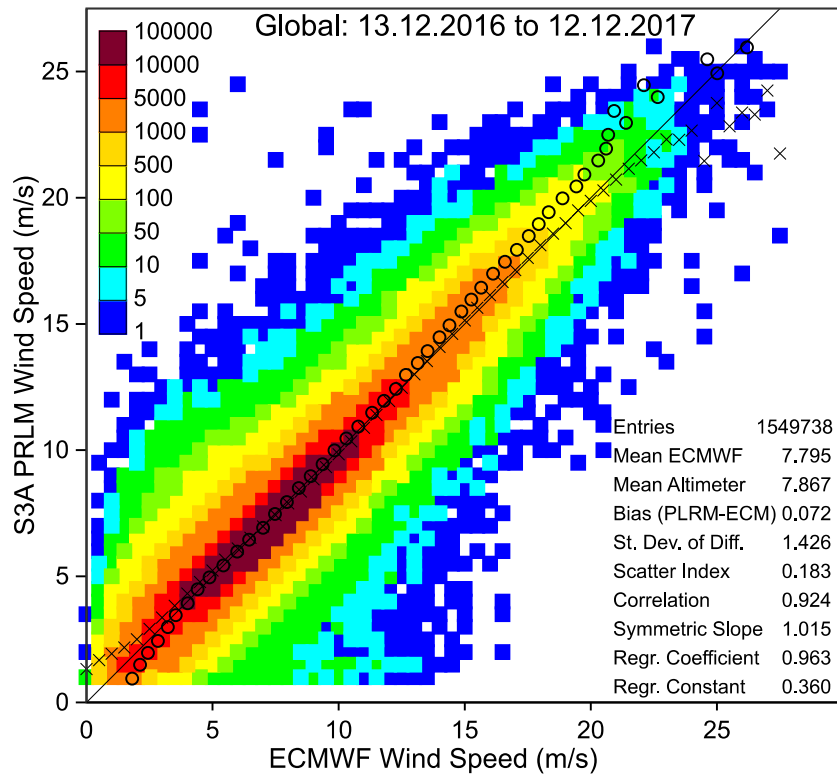


Figure 63: Global comparison between Sentinel-3A PLRM and ECMWF model analysis wind speed values over the one-year period from 13 December 2016 to 12 December 2017. Refer to Figure 57 for the meaning of the crosses and the circles as well as the colour coding.

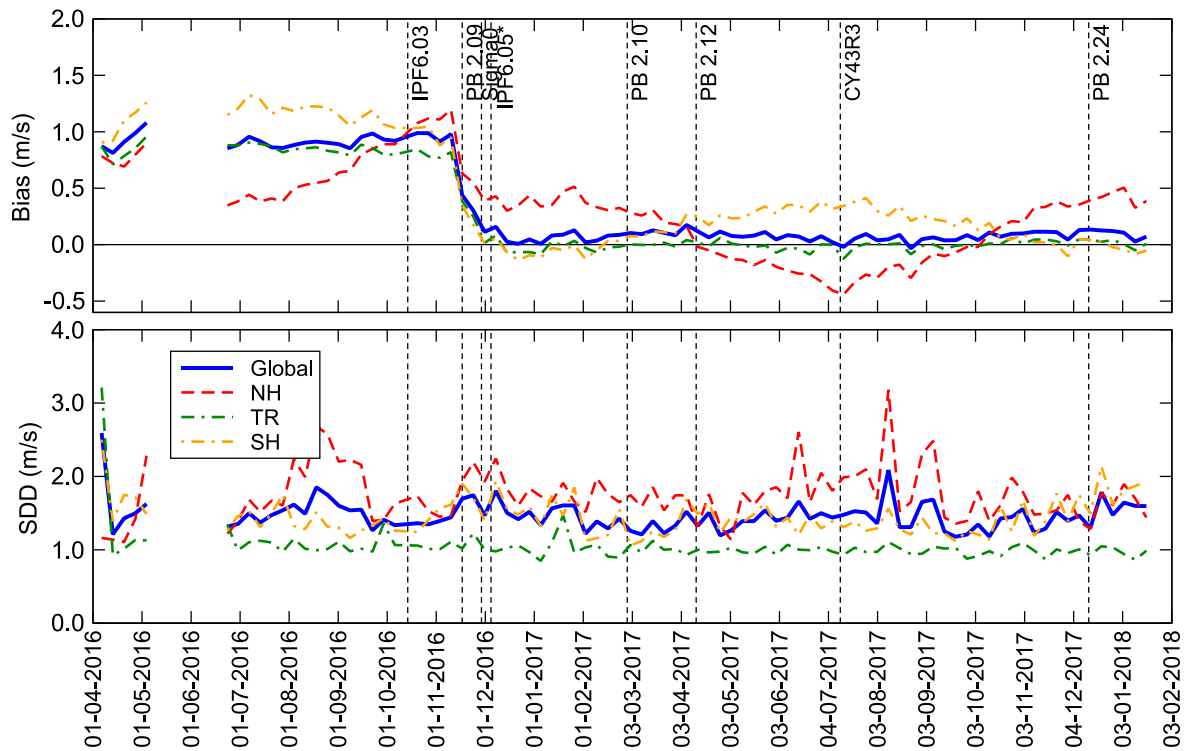


Figure 64: Time series of weekly PLRM wind speed bias defined as altimeter - model (top) and standard deviation of the difference (bottom) between SRAL PLRM and ECMWF model analysis.

There is a noticeable deterioration (increase in SDD) of the PLRM wind speed in the NH during the months of June-August of 2017. In fact, there was also a clear degradation in the NH during the month of August 2016. This may be an indication of a potential PLRM wind speed degradation in the NH during the summer period (roughly from June to August). However, at this stage this can be only a speculation based on very limited observations (two summer periods).

7.6.3 Significant Wave Height

At the time of writing, the altimeter significant wave height (SWH) from Cryosat-2, Jason-2, and SARAL/AltiKa are assimilated in the ECMWF model. Therefore, instead of the model analysis (which is the best available state of the atmosphere), the model first-guess (FG, which is practically a short model forecast) is used for the validation against the model to reduce the impact of error correlation between the model and Sentinel-3 SRAL that may be conveyed through sharing the same principle of measurement with the other altimeters whose SWH products are being assimilated.

Figure 65 shows the global SWH PDF of Sentinel-3A for the one-year period from 13 December 2016 to 12 December 2017. The PDF of the ECMWF model FG SWH collocated with Sentinel-3A during the same

period is also shown for comparison. Although Sentinel-3A SWH PDF agrees very well with its model counterpart, there are some deviations especially around the peak of the PDF (at SWH of about 2 m).

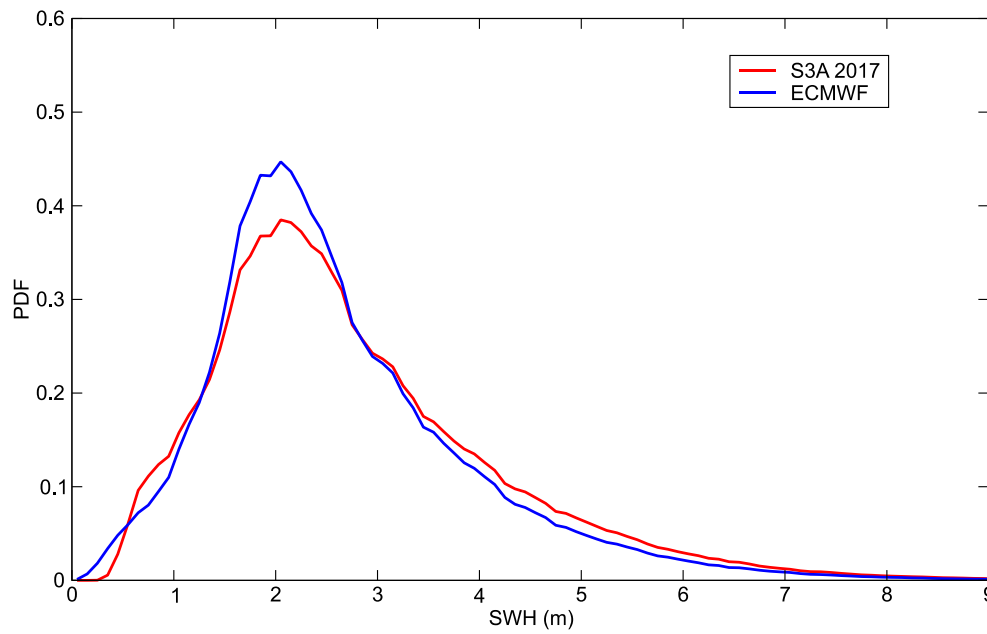


Figure 65: Sentinel-3A SRAL SWH PDF over the whole global ocean for the one-year period from 13 December 2016 to 12 December 2017. The corresponding ECMWF (collocated with Sentinel-3A) PDF is also shown for comparison.

The SWH PDF's from the altimeters on-board Jason-3, CryoSat-2 (only LRM data are used here), SARAL/AltiKa and Jason-2, which are all conventional altimeters or, in the case of CryoSat-2, operating in a conventional mode, are shown in upper panel of **Figure 66** together with the corresponding Sentinel-3A SAR PDF. The SWH PDF's for model collocations with each altimeter are shown in the lower panel of **Figure 66**. The deviation among the model PDF's as sampled along the ground track of each altimeter (i.e. only the model points that are collocated with the altimeter super-observations) is not large. However, the deviation between Sentinel-3A SWH PDF and those of the other altimeters is very clear. With the exception of that of CryoSat-2, SWH PDF's of the other altimeters are in better agreement with their corresponding model PDF's than that of Sentinel-3A. To eliminate the impact of the possible geographical sampling (as Jason-2 and Jason-3 cannot visit areas beyond latitudes 66°), the PDF's for the global ocean region extending between 65°N and 65°S (which is common for all altimeters considered here) are shown in **Figure 67**. The SWH PDF's of **Figure 67** (between 65°N and 65°S) show marginal differences from those of **Figure 66** (whole globe). This suggests that Sentinel-3A SAR (and CryoSat-2) SWH products deviate from those of other altimeters and from the model counterparts.

The time series of the global mean and standard deviation (SD) of the SWH from Sentinel-3 averaged over a 7-day time window moved by 1 day at a time are shown in the upper and lower panels,

	Sentinel-3 MPC S3MPC STM Annual Performance Report - Year 1	Ref.: S3MPC.CLS.APR.002 Issue: 1.1 Date: 23/05/2018 Page: 78
---	--	---

respectively, of **Figure 68**. The corresponding time series of the model as collocated with Sentinel-3 are also shown for comparison. Sentinel-3 mean and standard deviation are not much different than those of the model (and the other altimeters). The slightly higher Sentinel-3 SWH standard deviation compared to the model and the other altimeters (not shown) cannot be attributed to the fact that SAR mode has higher resolution compared to the conventional altimetry (LRM). The comparison is done at the scale of the super-observations (about 75 km) and, therefore, the impact of the high frequency variability in the SAR altimetry (below the 1-km scale) is eliminated. Therefore, this enhanced Sentinel-3 SWH variability and higher mean values indicate that fine tuning to SWH retrieval may be needed. **Figure 68** suggests that the SRAL SWH statistics compared to the model have changed in mid-November 2016 with the implementation of PB 2.09. Sentinel-3 mean started to be higher than that of the model. This has changed after the implementation of PB 2.24 in December 2017. Sentinel-3A mean SWH has reduced and became similar to the model mean value since then.

Collocated pairs of altimeter super-observation and the ECMWF model SWH FG are plotted in a form of a density scatter plot in **Figure 69** for the whole globe over the one-year period from 13 December 2016 to 12 December 2017. The SWH scatter plots (**Figure 69** and other similar wave height scatter plots that appear hereafter) are plotted similar to those of the wind speed (e.g. **Figure 57**) except for the size of the 2-D bin which is $0.25 \text{ m} \times 0.25 \text{ m}$ in the case of SWH. It is clear from **Figure 69** that the agreement between Sentinel-3 SWH and its model counterpart is very good except for a slight underestimation at SWH values below $\sim 2 \text{ m}$ and an overestimation at moderate to high SWH's (above $\sim 4 \text{ m}$). The underestimation at lower wave heights, although less noticeable, is not noticed in the case of other altimeters. In general, compared to ECMWF model, Sentinel-3A overestimates SWH by about 0.14 m. The SDD between the pair is about 0.27 m (or 11% of the mean value). The correlation coefficient is 0.983 which is quite high. These figures indicate that Sentinel-3A SAR SWH products are what is expected from radar altimeter SWH.

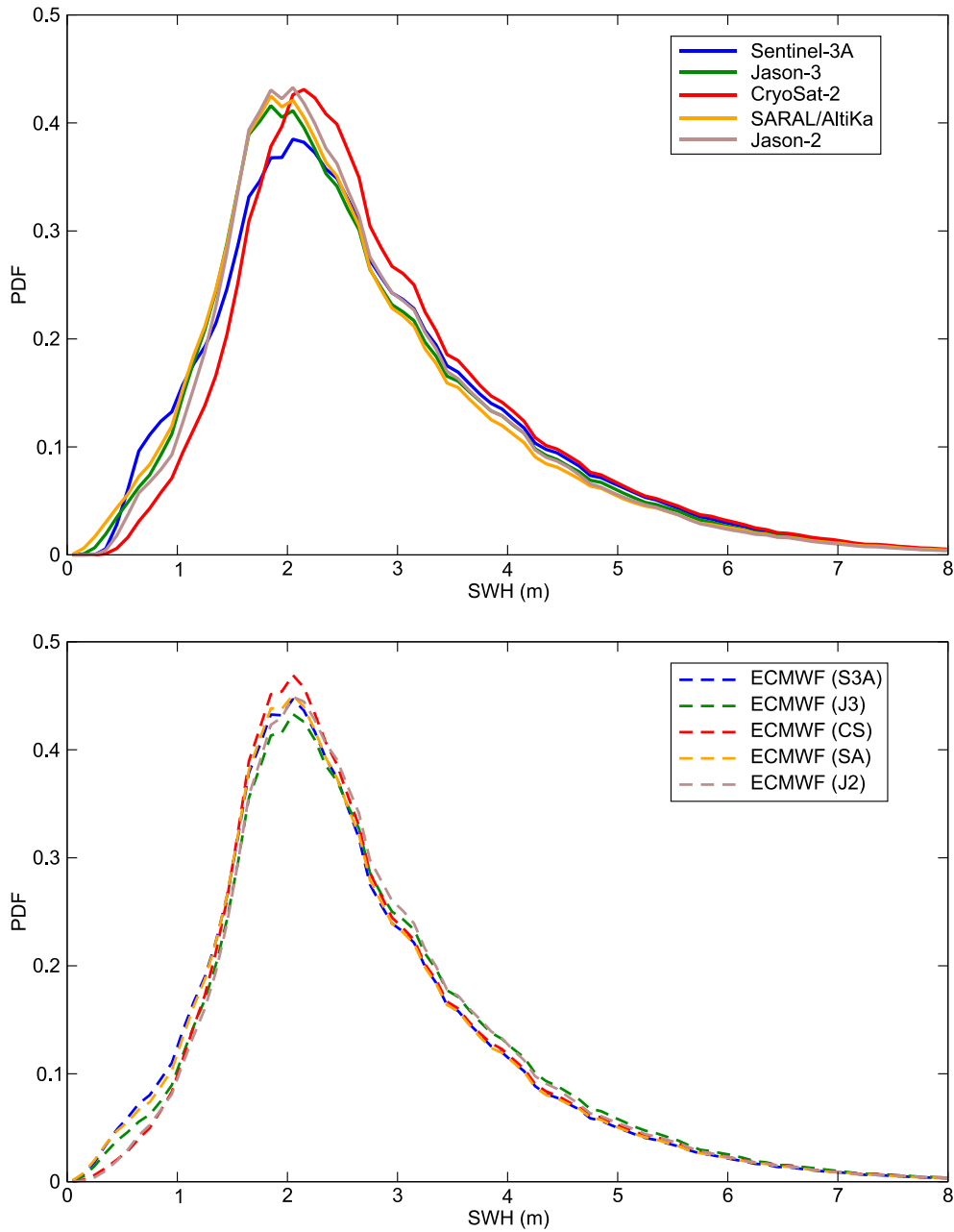


Figure 66: Global SWH PDF's from 5 altimeters for the one-year period from 13 December 2016 to 12 December 2017 (upper panel). The corresponding ECMWF (collocated with Sentinel-3) PDF's are shown in the lower panel for comparison.

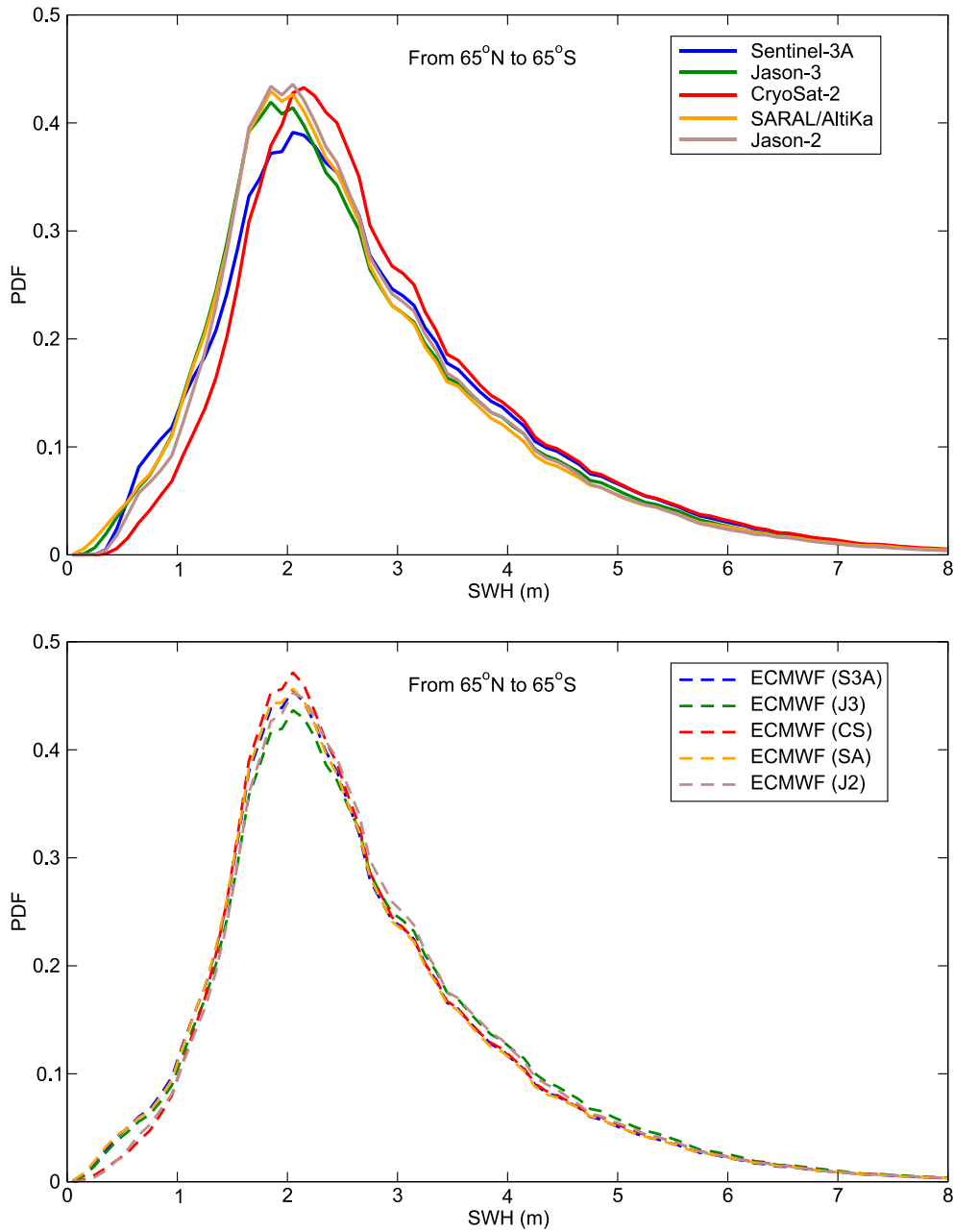


Figure 67: Same as in Figure 66 but for the global ocean region extending from 65°N to 65°S which is common for all altimeters considered here.

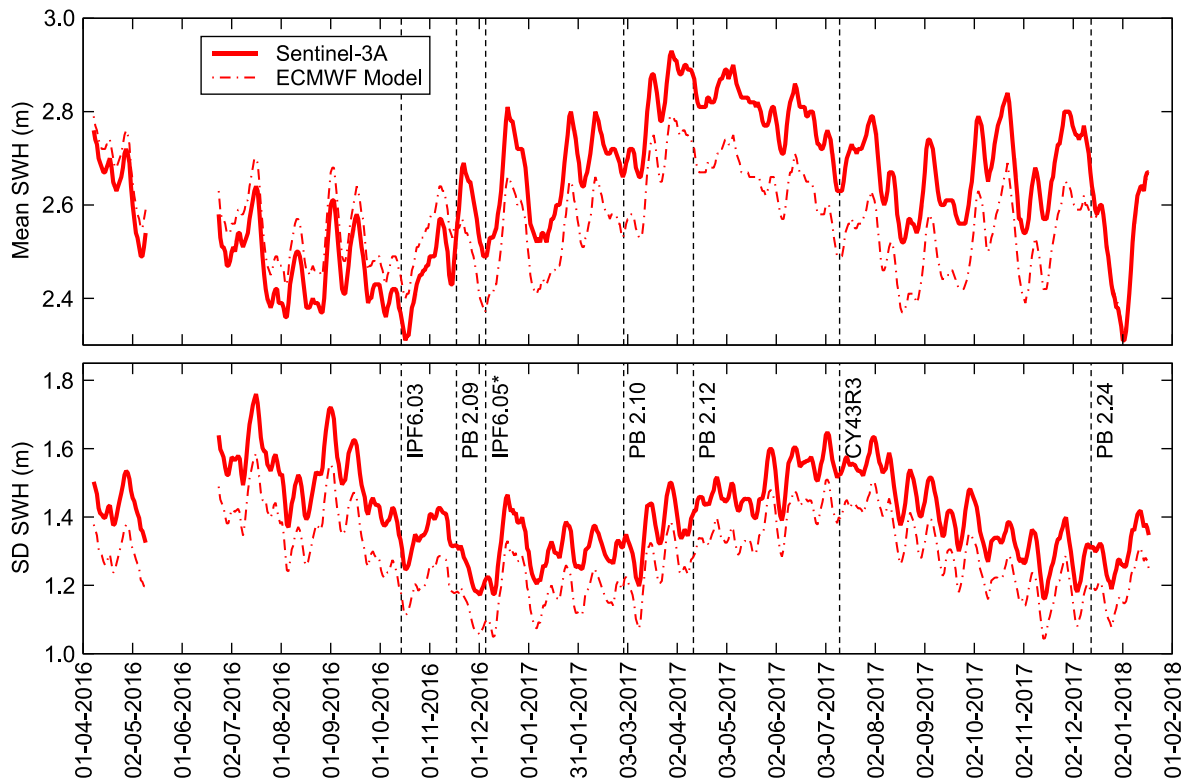


Figure 68: Time series of global mean (top) and standard deviation (bottom) of significant wave height from SRAL Ku-band after quality control. The collocated ECMWF model SWH mean and SD are also shown. The mean and SD are computed over a moving time window of 7 days.

The wave height comparison against in-situ (mainly buoy) observations for the one-year period from 13 December 2016 to 12 December 2017 is shown in **Figure 70**. SRAL SWH is 0.16 m higher than the in-situ observations for this period. The SDD (a proxy to the random error) is 0.30 m which is ~13% of the mean. The correlation coefficient is 0.978. These numbers indicate that Sentinel-3A SAR SWH products are now very close their counterparts from other altimeters (not shown). It is important to state that most of in-situ observations are located in the Northern Hemisphere around the American and European coasts.

The time series of the SWH bias (altimeter – model) and SDD of Sentinel-3 compared to the ECMWF model FG are shown in the upper and lower panels, respectively, of **Figure 71**. Until the first week of November 2016, Sentinel-3 used to underestimate (negative bias) SWH by about 0.05 m globally and about 0.15 m in the Northern Hemisphere and the Tropics while it used to overestimate SWH in the Southern Hemisphere by few centimetres. PB 2.09 caused the increase in Sentinel-3A SWH making it biased high. However, this change has minor impact on the SDD. Later changes associated to PB 2.10 and 2.12 do not seem to have any impact on SWH statistics.

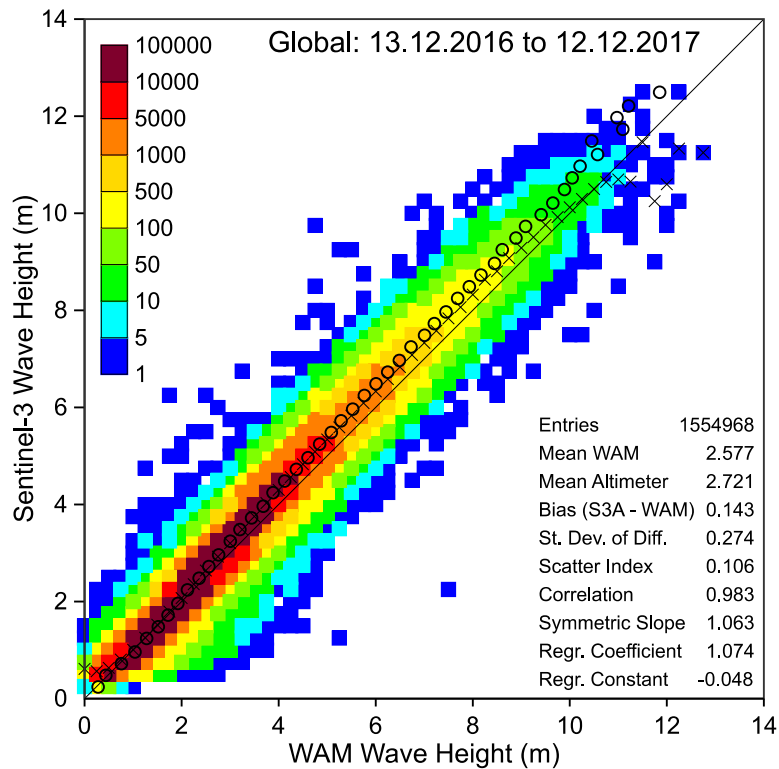


Figure 69: Global comparison between Sentinel-3A and ECMWF model first-guess SWH values over the one-year period from 13 December 2016 to 12 December 2017. The number of collocations in each 0.25 m x 0.25 m 2D bin is coded as in the legend. Refer to Figure 57 for the crosses and the circles.

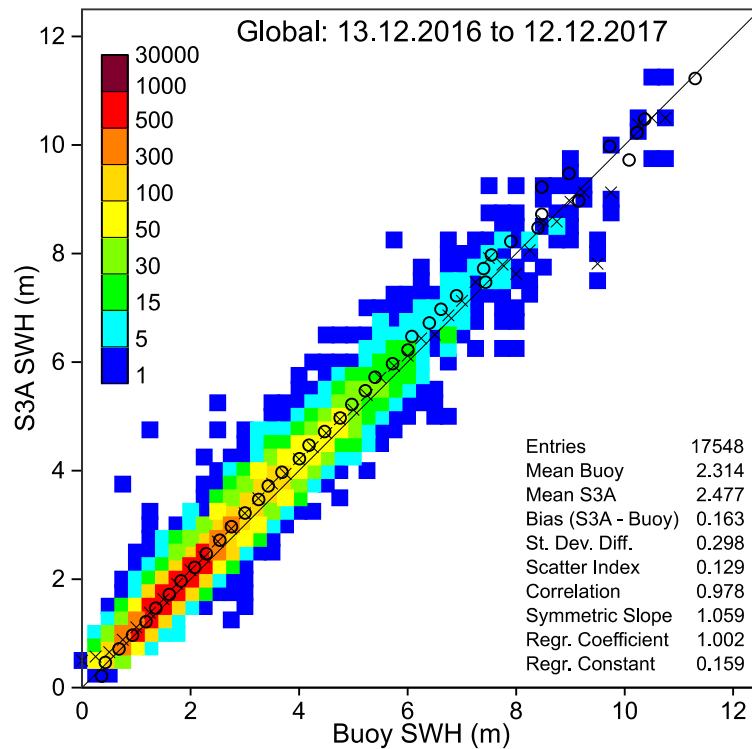


Figure 70: Same as Figure 69 but the comparison is done against in-situ observations (mainly in the NH).

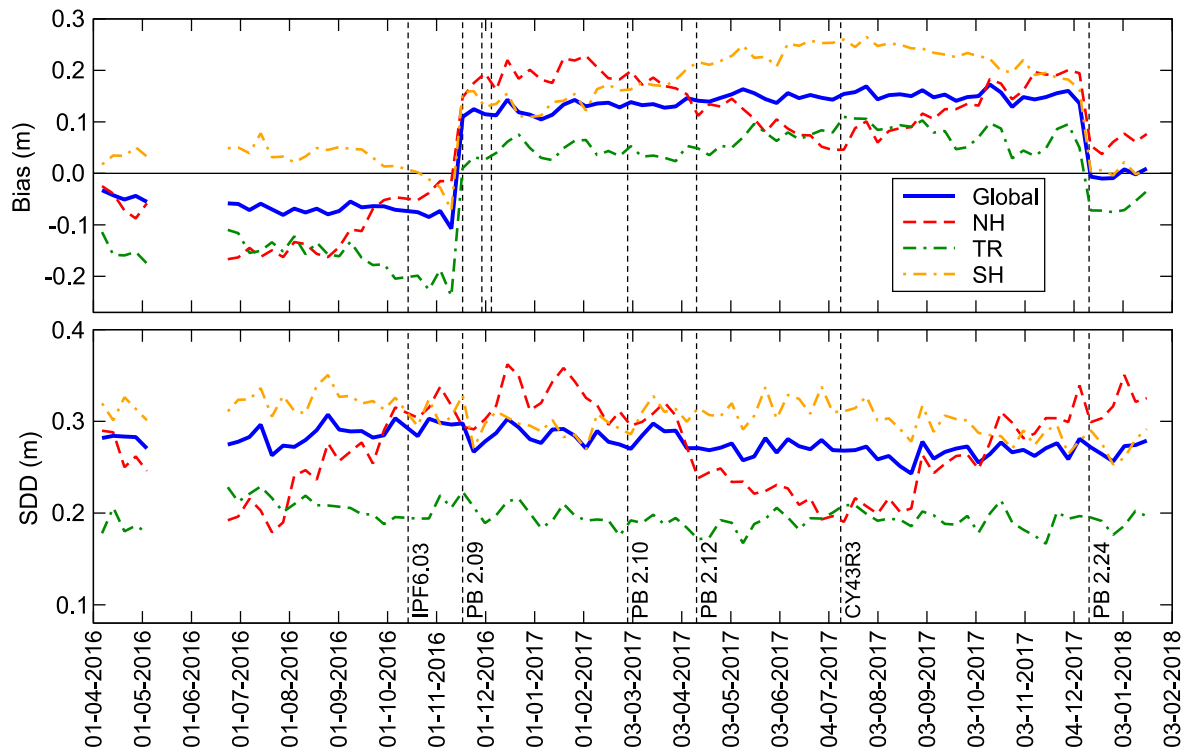


Figure 71: Time series of weekly global significant wave height bias defined as altimeter - model (top) and standard deviation of the difference (bottom) between SRAL and ECMWF model first-guess.

On the other hand, the implementation of PB 2.24 on 13 December 2017 has an obvious positive impact on Sentinel-3A SAR mean SWH. The bias with respect to the model dropped to almost zero. However, there seems to be no impact on the SDD.

Careful inspection of **Figure 71** reveals possible seasonal cycles in the bias and SDD with respect to the model in extra-tropics. The bias and the SDD seem to be highest during the hemispheric winter and lowest during the hemispheric summer.

The time series of the SWH monthly bias (defined as the altimeter – in situ) and the SDD of SRAL SAR compared to the in-situ measurements are shown in the upper and lower panels, respectively, of **Figure 72**. The impact of various PB's noticed in **Figure 71** also show themselves in **Figure 72**. Noting that most of the used buoys are in the NH, the “global” buoy comparison is nothing but a NH comparison. Similar seasonal cycles to those “seen” in the model comparison (**Figure 71**) for the NH can be also seen in **Figure 72**.(the outlier SDD value in August 2017 should be ignored as it can be attributed to erroneous measurements in one of the buoys).

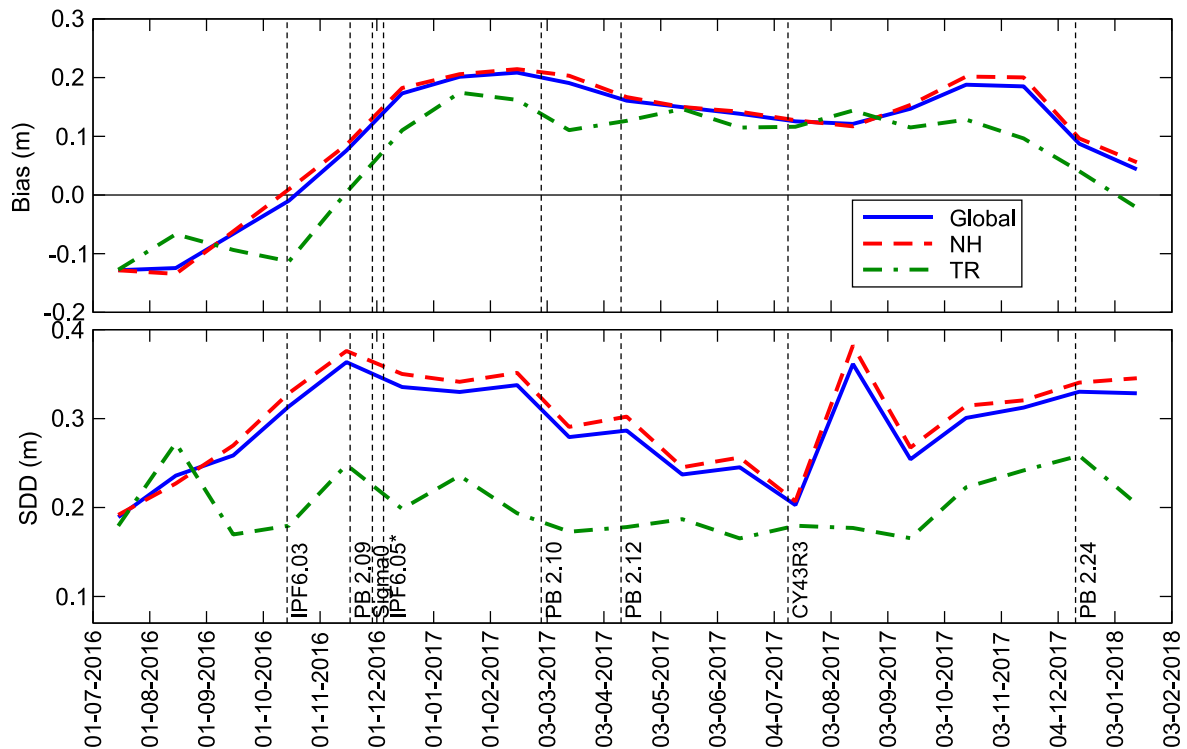


Figure 72: Time series of monthly global significant wave height bias defined as altimeter - buoy (top) and standard deviation of the difference (bottom) between SRAL and in-situ measurements.

The time series of the global SWH weekly bias and SDD of 5 altimeters (including SRAL) compared to the ECMWF model FG are shown in the upper and lower panels, respectively, of **Figure 73**. The bias in Sentinel-3A SAR SWH was one of the highest among the 5 operational altimeters between December 2016 (PB 2.09) and December 2017 (PB 2.24). PB 2.24 reduced SRAL SWH bias to almost zero. However, the SDD between Sentinel-3A SAR and the model is the highest among all altimeters irrespective of the various processing changes.

It is possible to conclude that although Sentinel-3 provides practically very good SAR SWH product, it is still in need of fine tuning. Irrespective of the SWH improvement due to PB 2.24, fine tuning is still needed to make SRAL SWH one of the best altimeter SWH products.

The geographical distribution of the mean Sentinel-3 SWH and the SWH bias, SDD and SI with respect to the ECMWF model FG averaged over the one-year period from 13 December 2016 to 12 December 2017 are shown in **Figure 74**. All the four plots look similar to their counterparts from other altimeters (not shown) apart from the positive bias in panel (b).

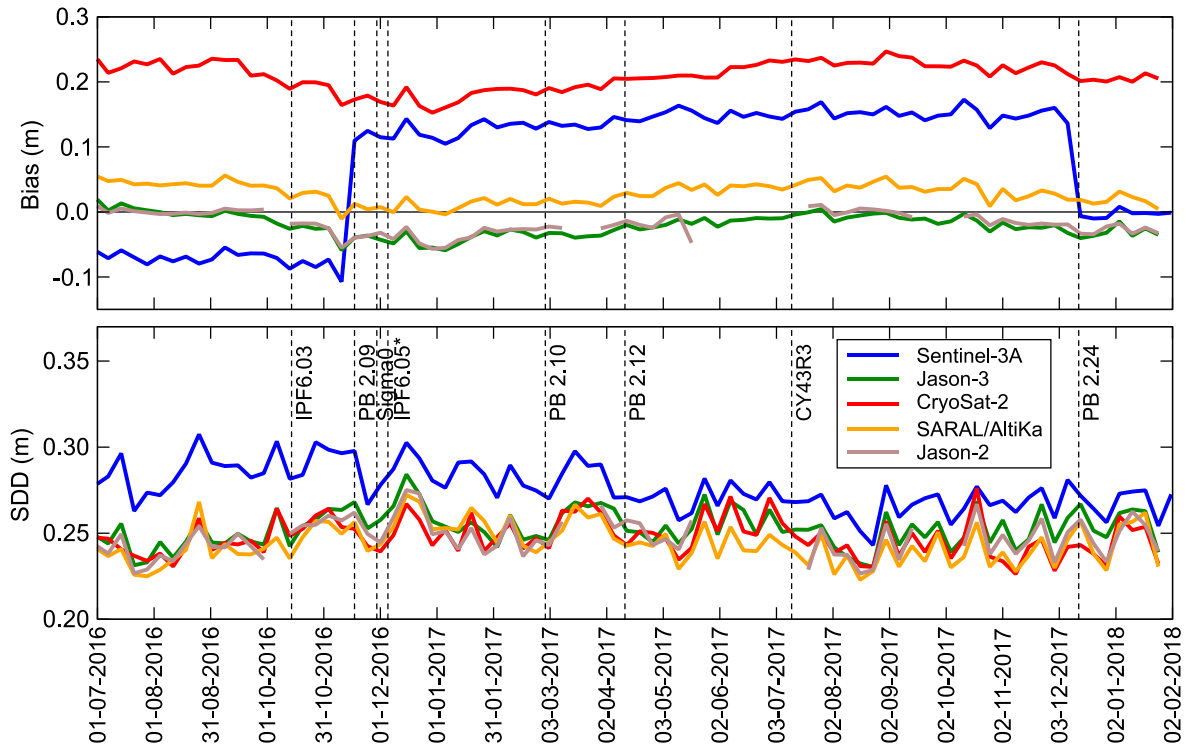


Figure 73: Time series of weekly global significant wave height bias defined as altimeter - model (top) and standard deviation of the difference (bottom) between 5 altimeters including Sentinel-3A SRAL (same as the global curves in Figure 71) and the ECMWF model first-guess.

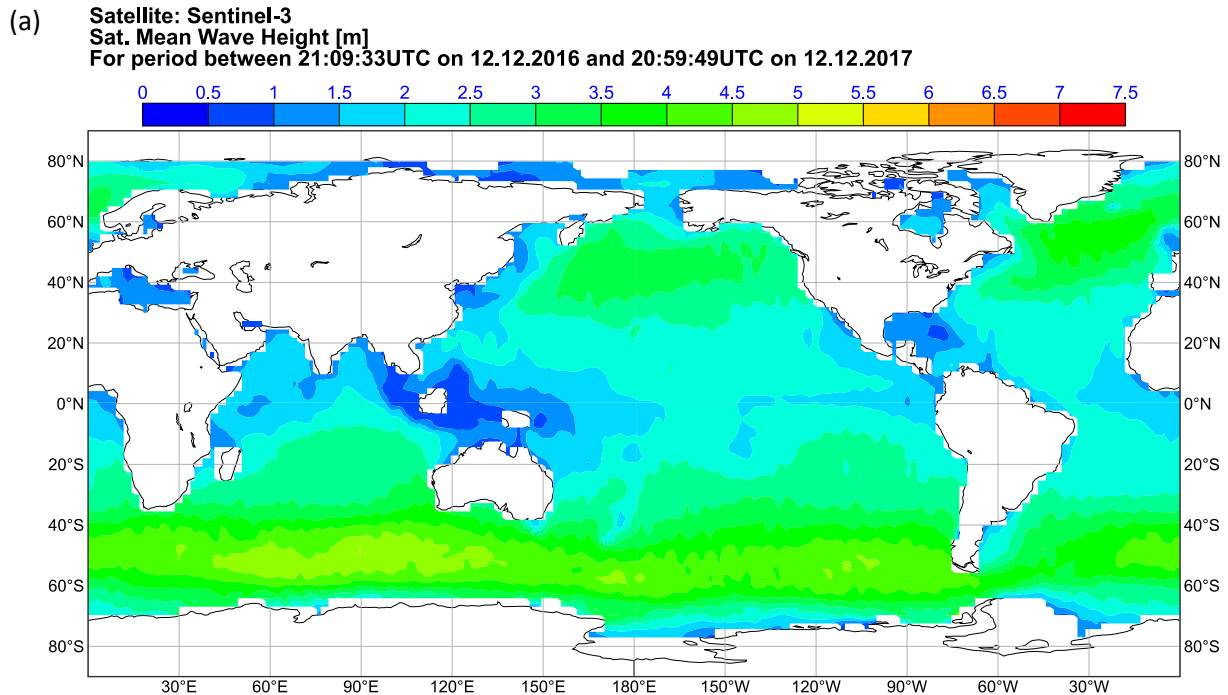
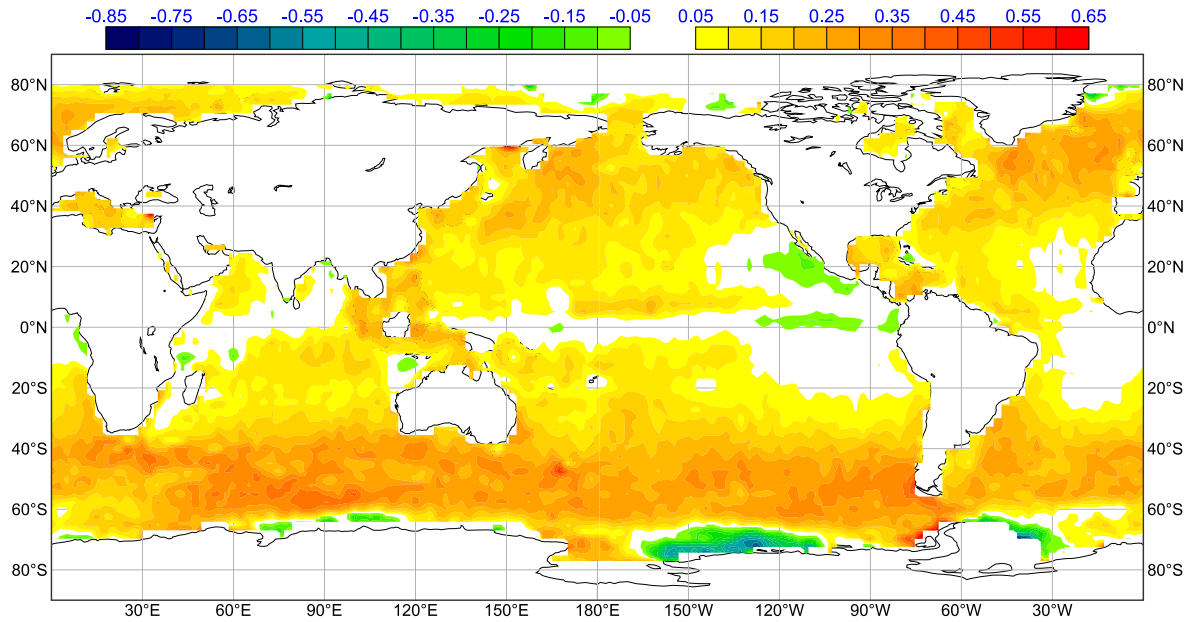


Figure 74: Geographical distribution of mean Sentinel-3A SWH (a) as well as the bias (b); the SDD (c) and the SI (d) between Sentinel-3A and ECMWF model FG during the one-year period from 13 December 2016 to 12 December 2017. Bias is defined as altimeter - model.

(b) **Satellite: Sentinel-3**
Wave Height Bias (Sat-Mod) [m]
 For period between 21:09:33UTC on 12.12.2016 and 20:59:49UTC on 12.12.2017



(c) **Satellite: Sentinel-3**
Wave Height SDD (Sat-Mod) [m]
 For period between 21:09:33UTC on 12.12.2016 and 20:59:49UTC on 12.12.2017

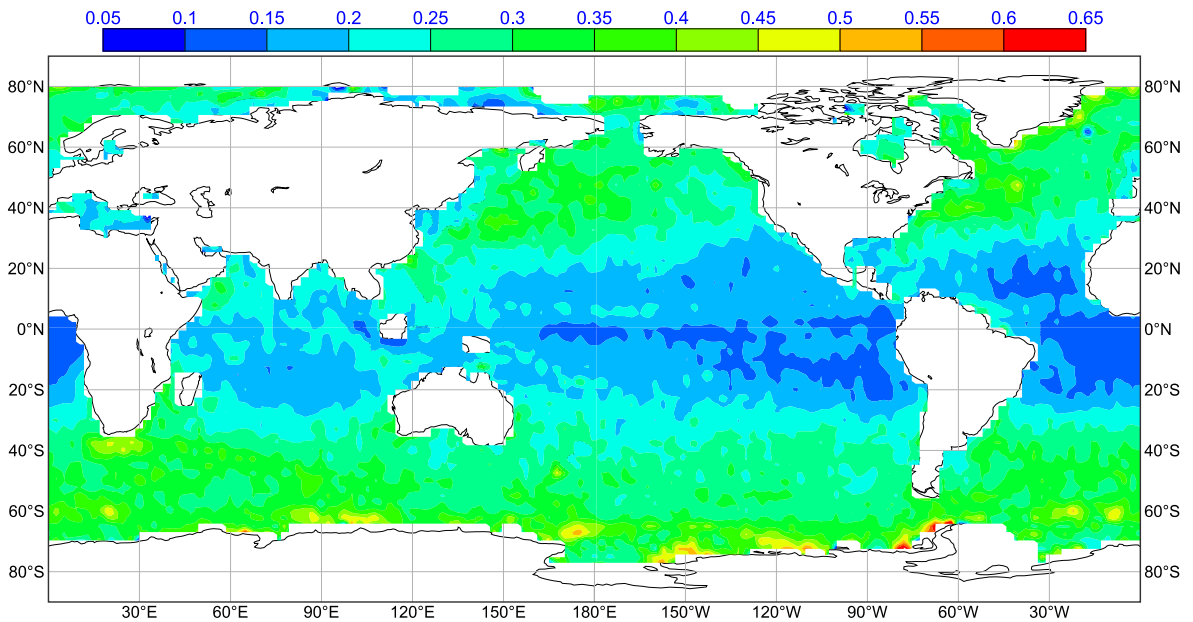


Figure 74: Continued.

(d) **Satellite: Sentinel-3**
Wave Height SI (Sat-Mod) [%]
For period between 21:09:33UTC on 12.12.2016 and 20:59:49UTC on 12.12.2017

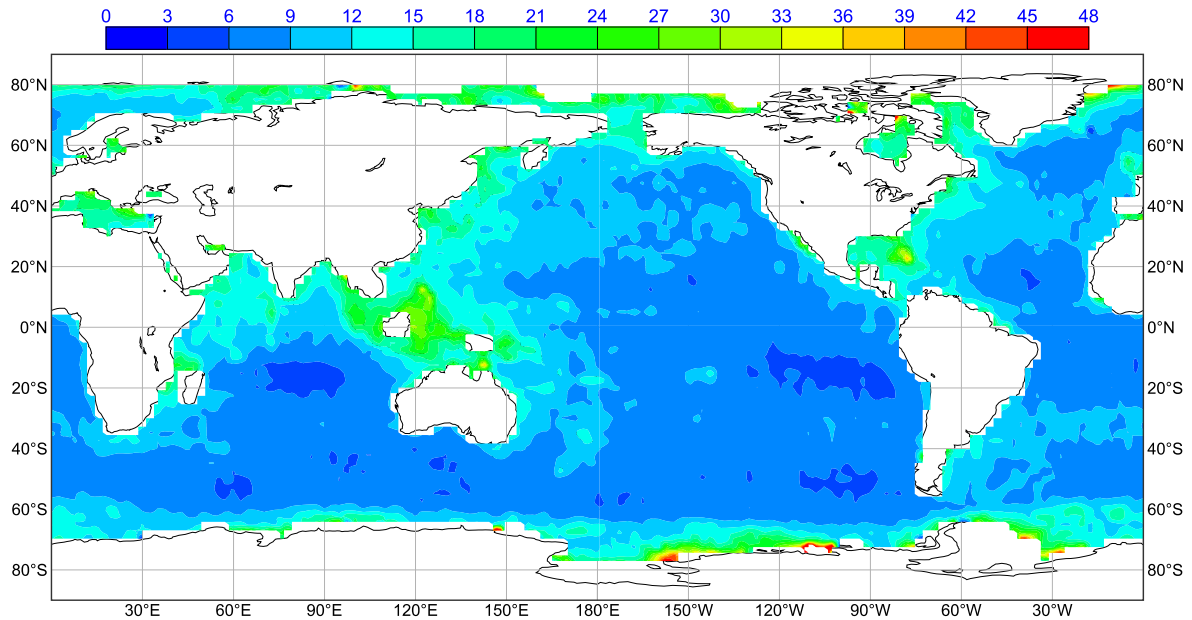


Figure 74: Continued.

Summary:

By the end of 2017, SAR wind speed is globally unbiased compared the wind speeds from the model and the in-situ measurements. The standard deviation of the difference (SDD) between SRAL and model wind speeds is one of the lowest among all operational altimeters.

The PLRM wind speed is now globally unbiased. The SDD with respect to the model improved considerably since Cycle 012. However, it is slightly higher than that of SAR winds (and other altimeters). There is a tendency of PLRM wind speed to degrade slightly in the Northern Hemisphere during the summer months (June to August). This can be only confirmed during the coming years.

The SRAL Processing baselines introduced so far (especially PB 2.24) improved the already good SAR SWH. By the end of 2017, the SWH bias with respect to the model and the in-situ measurements is almost zero. However, some fine tuning of the SAR SWH product is still needed to make it one of the best altimeter SWH products.

	Sentinel-3 MPC S3MPC STM Annual Performance Report - Year 1	Ref.: S3MPC.CLS.APR.002 Issue: 1.1 Date: 23/05/2018 Page: 88
---	--	---

7.7 Investigation: SARM Sensitivity to the tracker command

By plotting the SAMOSA sigma0 differences between Sentinel-3A SARM and P-LRM for ascending and descending passes, different geographical patterns are observed with discrepancies of 0.3 dB compared to P-LRM and with a different signature between ascending and descending maps. It is mentioned in 7.2.2 that the SARM sigma0 is sensitive to the satellite altitude, however the observed differences on the maps of Figure 75 could not be related to the altitude since they vary if we consider ascending or descending tracks. After investigation it has been found that these patterns are correlated with the position of the waveform leading edge in the tracking window (Figure 75). Indeed, over ocean, SRAL operates in Open-Loop mode, the tracking command is given by a Digital Elevation Model (DEM) loaded onboard. This model, over ocean, is based on the MSS and does not take into account the effects of the atmosphere on the range and the effects of the tides on the surface elevation. Thus, the echoes positions vary following the difference between the SSH measured and the corresponding MSS. This is not an anomaly and this behavior was expected, it is identical as for other altimetry missions. However, it seems that the SARM model implemented in the IPF i.e. SAMOSA DPM 2.3 is sensitive to this parameter. Comparison with P-LRM measurements (which are not impacted by this effect) allows to quantify this error for all the retrieved parameters (Figure 76):

- ❖ 0.2 dB of amplitude on the SARM sigma0. But this metric should be taken with care since it also includes the dependency as a function of the altitude.
- ❖ 2 cm of amplitude on the SARM range. But this metric should be taken with care since it also includes the dependency as a function of SWH.
- ❖ 10 cm of amplitude on SARM SWH. But his metric should be taken with care since it also includes the dependency as a function of SWH.

With the installation of the IPF latest version (on the 13th of December 2017, version 06.10) the ocean retracker was updated with the implementation of SAMOSA DPM 2.5. Comparisons between the estimated parameters derived from both retracking showed that the SARM range, SWH and Sigma0 estimated from SAMOSA DPM2.5 retracker are significantly less sensitive to the echo position in the tracking window. However, due to the short time series available (in IPF-SM2 version 06.10), it cannot be affirmed that this error is no more present.

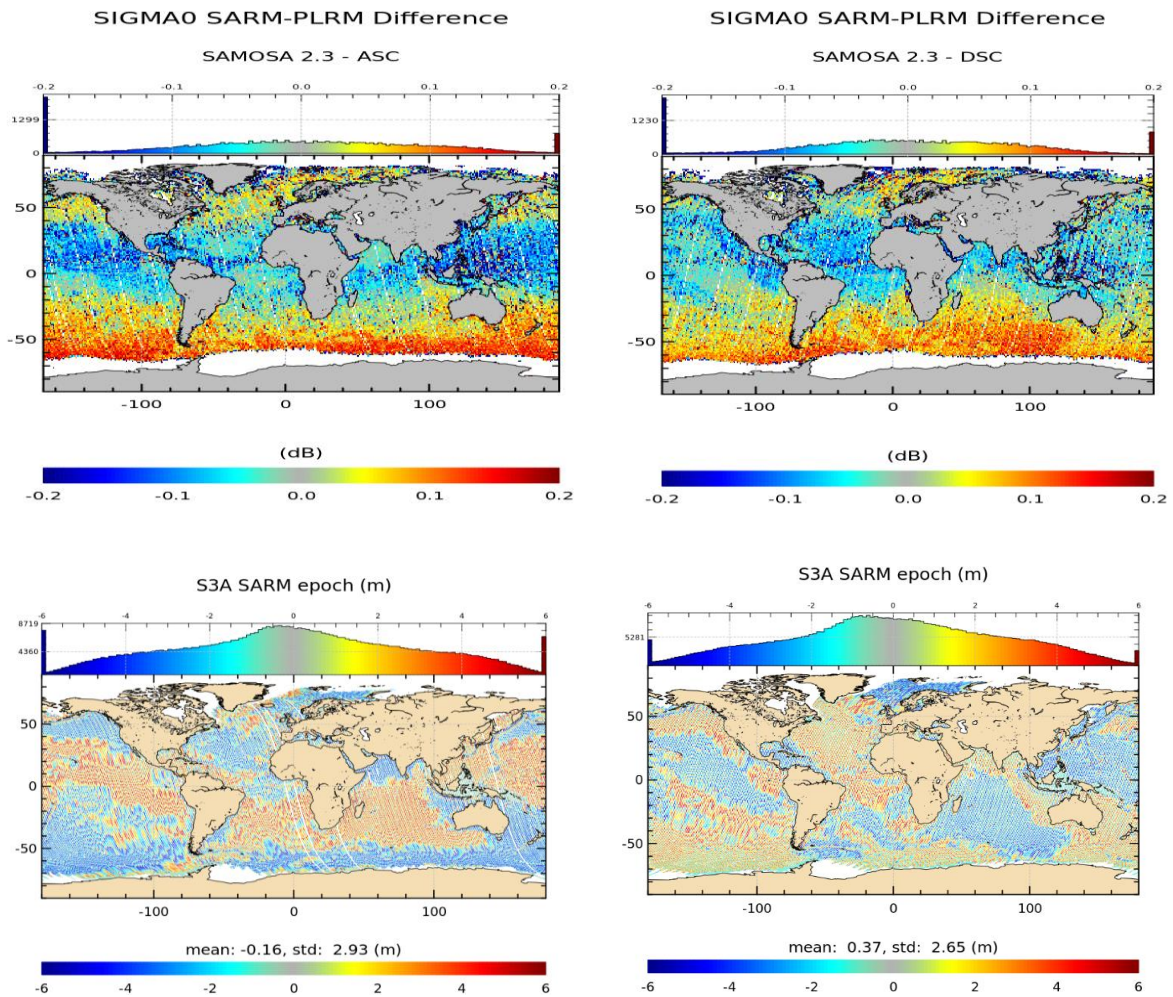


Figure 75: top panels shows the Gridded map of the Sentinel-3A collocated backscatter coefficient differences between SARM and P-LRM for ascending (left panel) and descending (right panel) passes. These maps were computed using L2 measurements derived from SAMOSA DPM2.3. Bottom panels shows the corresponding variation of the epoch for ascending (left panel) and descending (right panel) passes.

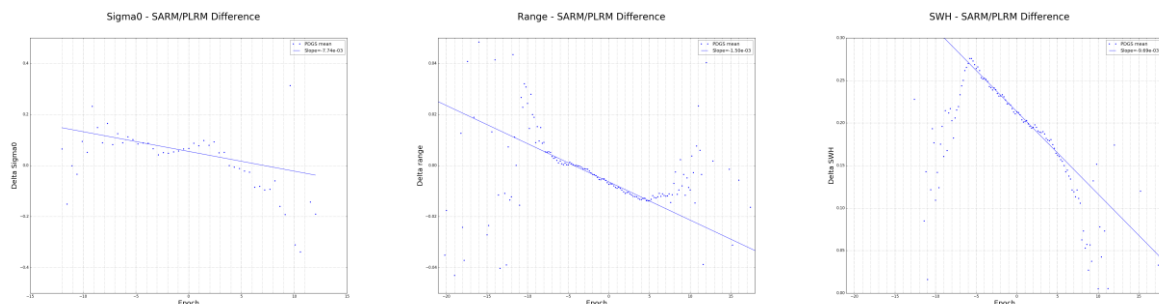


Figure 76: Differences between Sentinel-3A SARM and P-LRM backscatter coefficients (left panel, in dB), ranges (middle panel, in meters) and SWH (right panel, in meters) as a function of the epoch variations (in meters).

	Sentinel-3 MPC S3MPC STM Annual Performance Report - Year 1	Ref.: S3MPC.CLS.APR.002 Issue: 1.1 Date: 23/05/2018 Page: 90
---	--	---

7.8 Investigation : Quality assessment of SAMOSA 2.5 ocean retracker

The main achievements brought by the implementation of SAMOSA 2.5 retracker for SARM observations are summarised below:

- ❖ The SARM range dependency with SWH is decreased as shown on the Figure 77. We observe now a discrepancy reduced to 0.3% SWH for waves greater than 4 m, compared to PLRM. Note that the SSB correction has not yet been tuned for Sentinel-3A and contains Jason-2 SSB solution. With this new version of the retracker, the results are very similar to the ones obtained with the CNES prototype (which is a completely independent processing), except for a constant bias of 1 cm between both processing.
- ❖ The SARM SWH values are decreased by 14 cm in average as shown on the Figure 78, which provides values closer to the PLRM mode, but also to the ECMWF model and to the Jason-3 altimeter (not shown). The dependency wrt to SWH is also improved for the stronger waves greater than 5 m. With this new version of the retracker the results are also very similar to the ones obtained with the CNES prototype, except for a constant bias of 7 cm between both processing.
- ❖ The SARM backscatter coefficient showed an error correlated with the altitude in the previous version, that is now reduced to 0.1 dB in the regions where strong radial velocities dominate (between 30S and 60S). This is evidenced when comparing the SARM and PLRM backscatter coefficient for both Processing Baseline versions in the Figure 79. Note that this reduction of the error in the SARM sigma0 has only a slight improvement on the resulting altimeter wind speed in SARM. The SARM wind speed bias is reduced by 0.4 m/s in the region below 50S where the error on the SARM sigma0 was the greater (regions of stronger altitude).

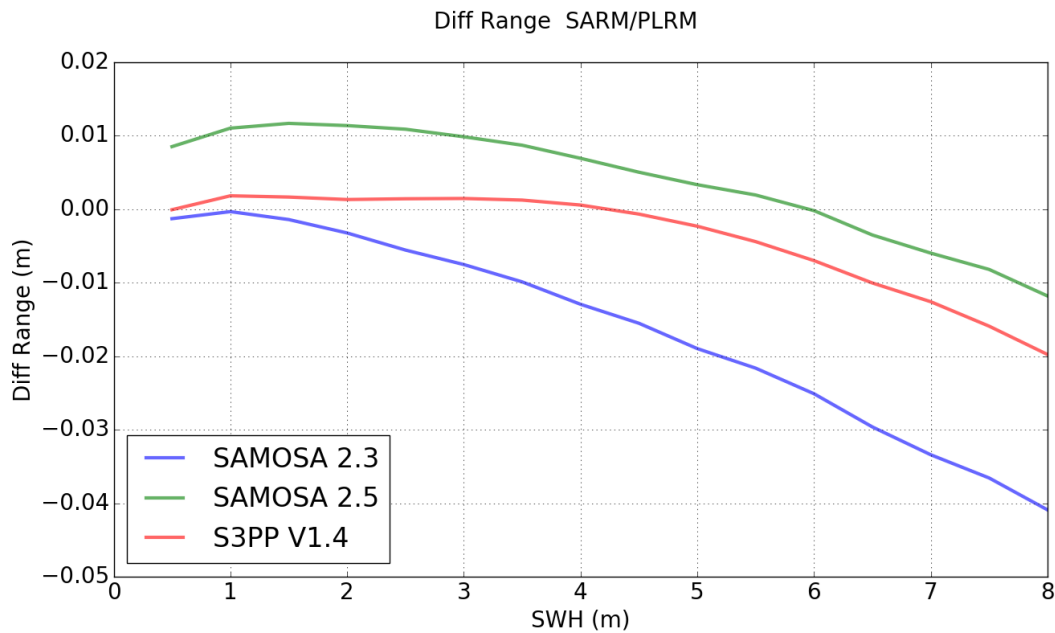


Figure 77 Difference between SARM Ku band and PLRM Ku band range wrt SWH for previous processing baseline (blue curve) and Processing Baseline 2.24 (green curve). The curve obtained for the CNES S3 prototype (red curve) is also represented to provide an external reference.

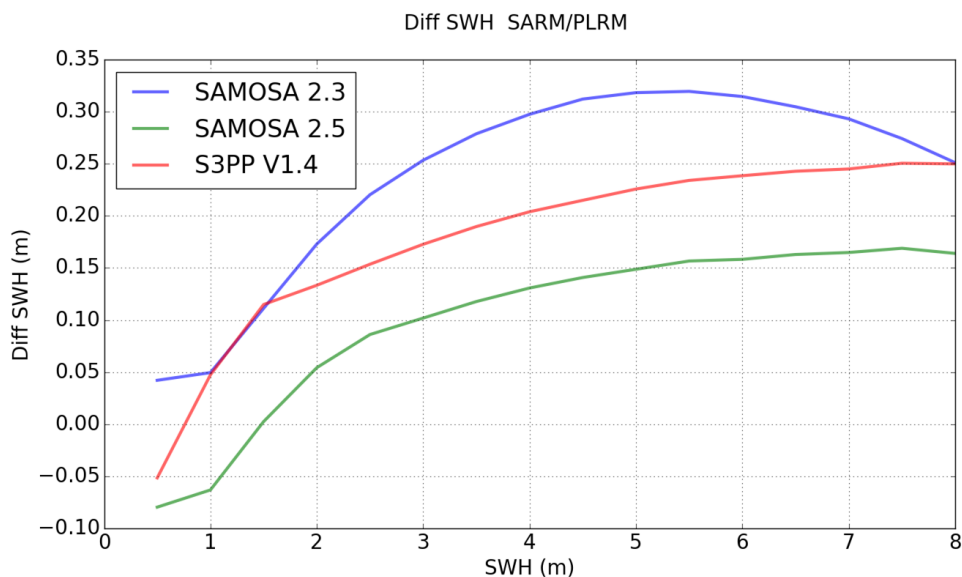


Figure 78 Difference between SARM Ku band and PLRM Ku band SWH wrt SWH for previous processing baseline (blue curve) and Processing Baseline 2.24 (green curve). The curve obtained for the CNES S3 prototype (red curve) is also represented to provide an external reference.

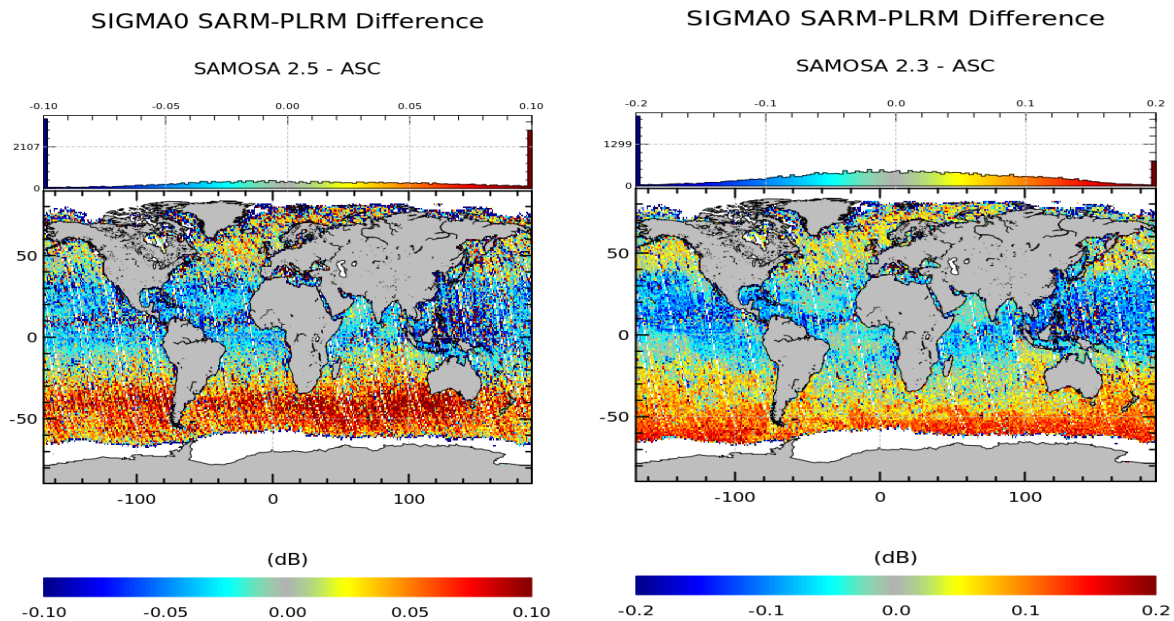


Figure 79 Difference between SARM Ku band and PLRM Ku band backscatter coefficient for previous processing baseline (right map) and Processing Baseline 2.24 (left map). The maps display only the ascending tracks to better highlight the finer details of the difference in the maps.

7.9 Investigation: SRAL Sensitivity to the Swell Waves

The first evidence of impact of swell on SARM altimetry real data was shown by Aouf and Phalippou in 2015. Through the comparison between the MFWAM model and the Cryosat-2 SARM SWH, they demonstrated that the altimeter measurements are likely biased by ocean swell, and most noticeably for longest waves and swell fields propagating in a direction parallel to the satellite track. More recently, Moreau et al. (2018) were able to go a bit further in our understanding and explanation of the phenomenon, showing a high correlation between the 20-Hz noise of the altimeter-derived estimates and the swell parameters (namely the period, the swell height and the direction of swell propagation), without however clearly determined errors in SARM estimates due to the restricted number of ocean areas operated in this radar mode.

Unlike Cryosat-2, Sentinel-3A operates in full SARM orbit. This global coverage gives the opportunity to better understand and characterize the specificities of the SARM technique using real data. The impact on biases and noise of the altimeter parameters assessed in this section were computed by using collocation between Sentinel-3A data and WaveWatch3 wave model.

The Figure 80 shows polar plots of the average range noise for wave heights ranged between 2 and 3 m. The radial distance of the plot corresponds to the mean period and the angle of the plot represents the azimuth angle difference between the track and the mean swell direction. A zero angle means the track

and the swell are collinear and for 180° , they are anti-collinear. The whole period available (1 year) was used to compute the SARM (left panel) and the P-LRM (right panel) results.

The SARM and P-LRM range noise increase with the mean wave period whatever the azimuth angle between swell and track directions. However, from the lowest to the highest period, the SARM range noise is approximately twice higher whereas in P-LRM it is only $\sim 10\%$ higher. This strong sensitivity of the SARM range noise to the swell long waves is mainly due to the footprint resolution.

The SARM range noise increases faster when the waves propagate in the along-track direction (0° and 180°) than in the across-track direction (90° and 270°). There is a ratio of 12% between range noise in along-track and across-track configurations (for wave periods higher than 6s). Regarding the P-LRM SWH noise, the increase is homogeneous as a function of the angle which means that swell direction has no impact. As for the range noise, this difference of sensitivity to the swell direction between SARM and P-LRM approaches is related to the footprint shape.

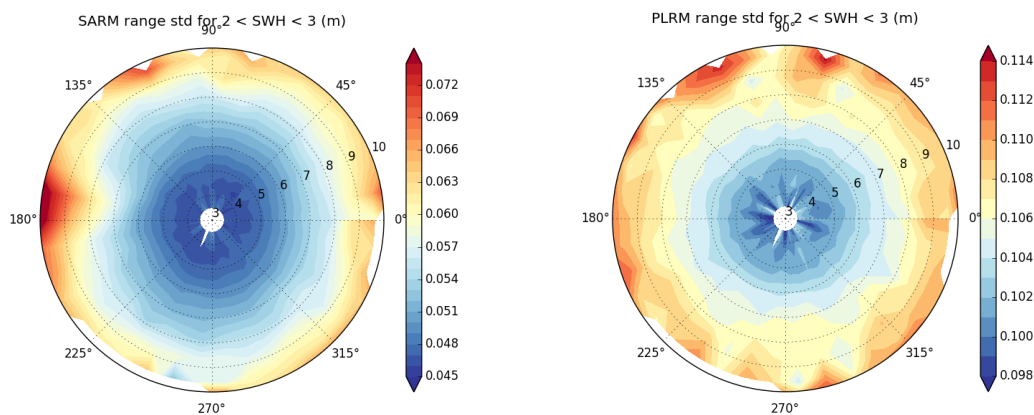


Figure 80: Polar plot of the SARM (left panel) and P-LRM (right panel) range noises as a function of the mean swell period and as a function of the azimuth angle between swell and track directions. The wave height was fixed between 2 and 3 m.

The analyses performed previously demonstrate the sensitivity of the SARM approach to the swell waves characteristics for very short wavelengths below 7 km. Figure 81 shows the polar plots of the difference between SARM and P-LRM SWH at long wavelength for wave heights ranged between 2 and 3 m. The radial distance of the plot corresponds to the mean period and the angle of the plot represents the azimuth angle difference between the track and the mean swell direction. A zero angle means the track and the swell are collinear and for 180° , they are anti-collinear.

It is clear that the bias between SARM and P-LRM SWH decreases while the swell period increases:

- ❖ For the lowest swell periods, the SWH bias is around 25 cm, which is consistent with Figure 78.
- ❖ For the highest swell periods, the SWH bias decrease to 15 cm.

Thus, it is clear that, at long wavelength, the SARM SWH parameter is sensitive to the swell period. This result confirms the observations made by Abdalla (2017) and Moreau et al. (2018) by comparing the SARM SWH to model outputs. This plot also demonstrates the impact of the relative azimuth angle on the SARM SWH values. When SWH are ranged between 2 and 3 m and the swell mean period equals 8 s, the bias between SARM and P-LRM SWH is around 25 cm when the swell propagation is perpendicular to the satellite direction. In the same SWH and T02 conditions, it reaches 18 cm if the two directions are parallel.

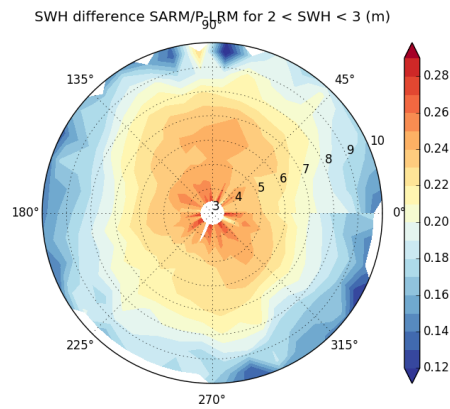


Figure 81: Polar plot of the SWH differences as a function of the mean swell period and the azimuth angle between swell and track direction.

7.10 Performance over Coastal areas

All the SRAL processing for both sea surface height (SSH) and for significant wave height (SWH) is the same in the coastal zone as in the open ocean; however, there is the potential that land within the instrument footprint may give rise to anomalous values for SSH or SWH; thus there is a need for special evaluation within the coastal zone. Since the SAMOSA 2.5 reprocessing (PB 2.24 onwards) was not available at the time of this report, the data used are from an earlier version of the processing. The focus of our coastal validation efforts is the waters around the southwest of the United Kingdom, where we have access to "in situ" data from both moorings and from a HF radar system (see Figure 82).

Firstly comparisons have been made of SRAL's SWH records against those from a meteorological buoy within the Western Channel Observatory off Plymouth. Figure 83 shows a scatter plot of the matched observations for two tracks near the E1 buoy, with the extent of the horizontal and vertical lines showing the spread of observations by the altimeter and the buoy respectively. With these data (June 2017 processing), there is close agreement of the mean values for track 415, but S-3A appears to read slightly high for track 256. However the latter is further from the buoy and in slightly more exposed conditions. At the time of analysis there were insufficient data match-ups to give a statistically useful estimate of the Sentinel-3A bias. This analysis will be repeated with more match-ups once the SAMOSA 2.5 data are available.

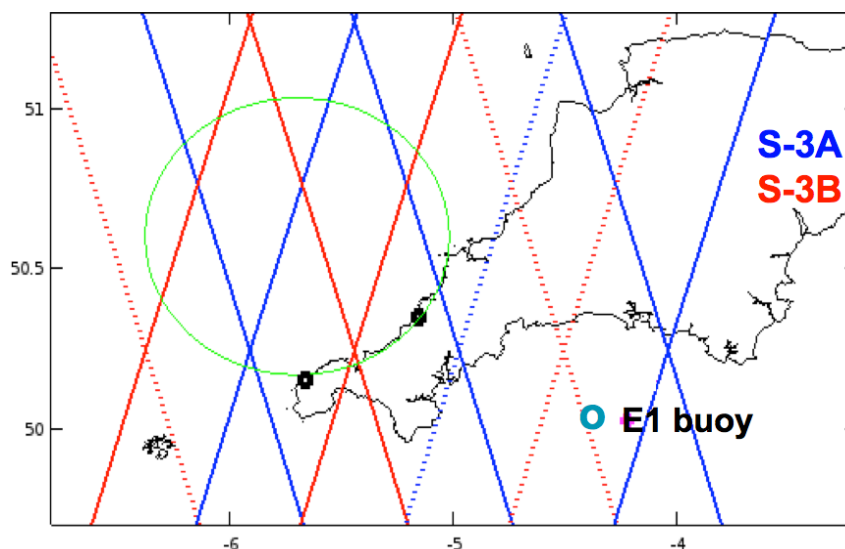


Figure 82 Pattern of Sentinel-3 ground tracks over the southwest UK for the interleaved phase. E1 is the location ($4^{\circ}22.5'W$, $50^{\circ}2.6'N$) of a meteorological buoy and a long-term sampling station as part of the Western Channel Observatory, implying that many ancillary data are available. The green circle indicates the rough coverage of the HF radar system, with transmitters at Pendeen and Perrenporth (marked by the black dots).

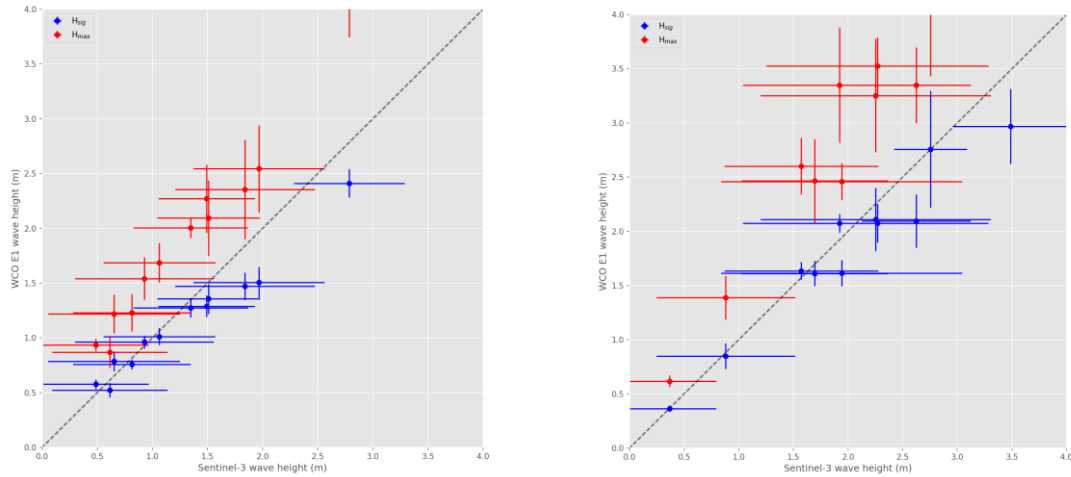


Figure 83 Comparison of data from S-3A (x-axis) with meteorological buoy. (left) Orbit 128, (track 256) which passes 36 km to west of buoy (Right) Orbit 208 (track 415), which passes 15 km to the east of the buoy. Altimeter data are the 20 Hz records within 45 km of the buoy, and buoy data are the 5 nearest hourly values to the time of the overpass, with mean SWH in blue and maximum wave height in red.

The second aspect of the analysis looks at the consistency of retrievals from independent waveforms. This is shown in characterised σ_H s and σ_h (the r.m.s. variations in SWH and SSH within the 20 measurements recorded in a second). Figure 84 shows the mean values of σ_H s from a number of Sentinel-3A repeat cycles over the region of interest. Clearly there are higher wave values nearer the coast, but there is a lot of spatial variation due to the differences in coastal topography.

To provide a more quantitative comparison, values of σ_H s and σ_h are averaged in bins representing different distances from the coast. In this case the data used are global, in order to provide more points for comparison, and thus more robust statistics. The variability varies with wave height, but the values for SAR processing are roughly 30% less than PLRM processing for σ_H s and almost 50% less for σ_h , with negligible difference (for the SAR processing) on going from open ocean to within 3-5 km of the coast.

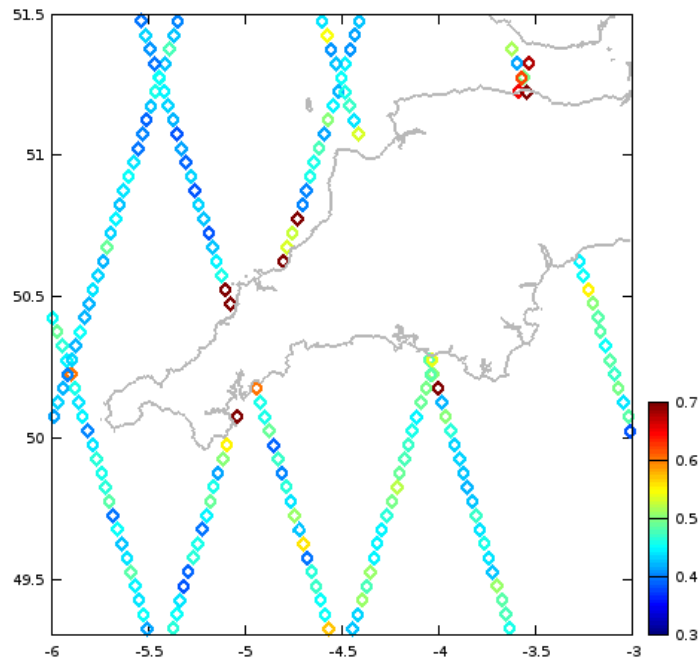


Figure 84 Mean values of SAR mode σ_{H_s} (in metres) for repeat cycles of Sentinel-3A over the southwest UK.

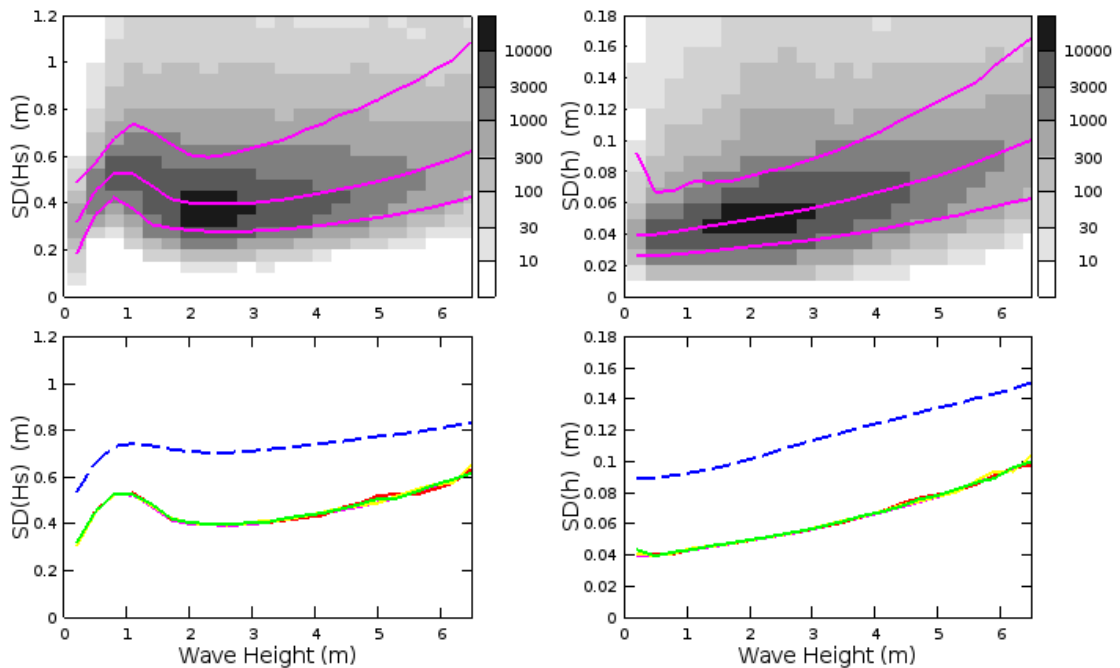


Figure 85 Measures of uncertainty in wave height (σ_{H_s}) and range (σ_h) as a function of H_s . The top row shows 2-D histograms for open ocean conditions, with the population density shown by grey shading (using a logarithmic scale) and the magenta lines indicating the 5th, 50th and 95th percentiles in each narrow H_s bin. The bottom row shows how the median values increase as the coast is approached, with the different coloured solid lines for >25 km; 11-13 km, 7-9 km and 3-5 km being indistinguishable). This indicates that the median performance in SAR mode is as good at 3-5 km from coast as in open ocean. However, there are differences at the higher percentiles, because a small proportion of the coast are high enough to have an effect within the SAR footprint. For comparison, the uncertainty estimates obtained from the Pseudo-LRM (PLRM) processing for >25 km from the coast are shown by the blue dashed lines.

	Sentinel-3 MPC S3MPC STM Annual Performance Report - Year 1	Ref.: S3MPC.CLS.APR.002 Issue: 1.1 Date: 23/05/2018 Page: 98
---	--	---

8 Performance Mission over Sea Ice

Sentinel-3A SRAL altimeter operates in SAR mode over areas of sea ice and ocean and shares a common heritage with Cryosat, the first altimetry mission to operate predominantly in this mode over sea ice.

Unlike Cryosat, whose ground segment was optimized from launch primarily for ice surfaces, Sentinel-3A STM is an operational mission with a single ground segment shared between all surface types (ocean, sea ice, land ice, ice shelves, inland waters, coastal zones) which all have very different properties and processing requirements at each ground processor level. For this reason, commissioning and tuning the processors specifically for sea ice is more complex than simply replicating the Cryosat sea ice processors, which have also been significantly upgraded since the Sentinel-3A ground segment was specified.

Tuning of sea ice algorithms for a new altimetry mission is a multi-stage process, which requires stable cycles of data acquired over one or more full Arctic winter seasons (Oct-May). Since Sentinel-3A was launched in February 2016, it was not possible to start all the sea ice commissioning tasks until reprocessed data from the winter of Oct 2016 - May 2017 became available during the summer of 2017. Since then good progress has been made in the key stages of sea ice surface type discriminator tuning and sea ice retracker validation and testing. Following analysis of Sentinel-3A sea ice data in autumn 2017, and an in-depth comparison with contemporaneous results and upgraded algorithm methods from Cryosat, a number of essential sea ice processor upgrades (from the forthcoming Cryosat baseline-D) and tasks have been identified as a requirement in order to complete Sentinel-3A sea ice commissioning. These include replacement of the diffuse echo retracker, optimised waveform filtering and outlier removal, an upgrade of the MSS to DTU15 (completed in PB2.24 in Dec 2017) and retracker bias calibration. These tasks have been scheduled for the first half of 2018, after which it should be possible to produce a high-quality Sentinel-3A sea ice Arctic winter freeboard in the L2 product equivalent to the excellent results available from the Cryosat mission. Due to sea ice conditions in Antarctica, where thin sea ice and snow loading are an issue, producing accurate freeboard measurements from either Sentinel-3A or Cryosat is still an area of active research. It is currently not possible to measure freeboard from SAR altimetry during the polar summer months (June-Sept in the Arctic) as summer melt creates pooling in the sea ice which makes discrimination between sea ice leads and floe echoes impossible.

The following sections detail the performance of key L2 sea ice parameter in products released during 2017, culminating in product baseline 2.24 (Dec 2017).

8.1 SRAL Instrument Mode over Sea Ice

For sea ice and ocean surfaces the SRAL instrument operated in both SAR open loop and closed loop mode during the operational phase depending on the fixed mode mask. Note that the mode mask is does not dynamically change from cycle to cycle. In open loop the range window is positioned using a 1-D along track DEM with a-priori knowledge of the surface height. In Antarctica areas of sea ice are predominantly covered by the closed loop mask, whereas in the Arctic open loop is the predominant mode.

Flag: instr_op_mode_20_ku

Mode: all

Cycle: 25 NTC SR_2_WAT

Rel. Orbits: 1 to 385

First Time: 2017-11-23T22:22

Last Time: 2017-12-20T21:27

IPF Version: IPF-SM-2 D6.10

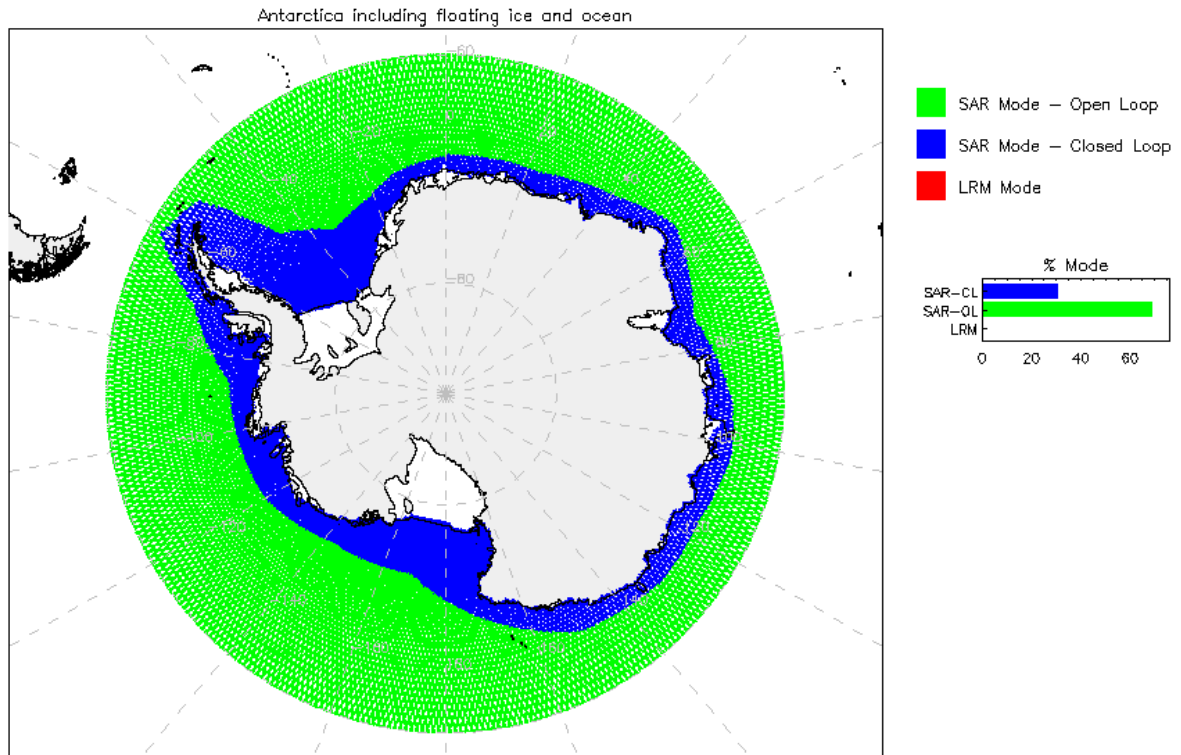


Figure 86: Map of SRAL mode over the Antarctic sea ice for cycle 25 NTC

Flag: instr_op_mode_20_ku

Mode: all

Cycle: 25 NTC SR_2_WAT

Rel. Orbits: 1 to 385

First Time: 2017-11-23T22:22

Last Time: 2017-12-20T21:27

IPF Version: IPF-SM-2 D6.10

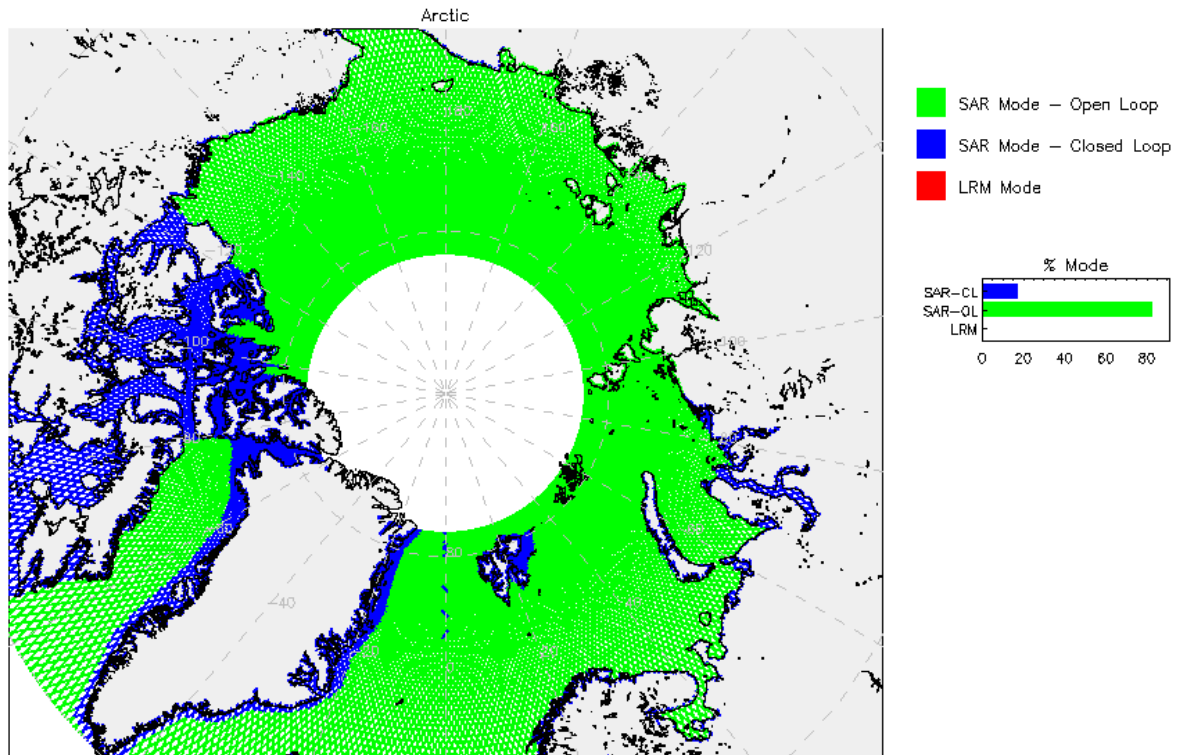


Figure 87: Map of SRAL mode over the Arctic sea ice for cycle 25 NTC

8.2 20Hz Ku Band Surface Classification (surf_class_20_ku)

This parameter is computed from a mask built with MODIS and GlobCover data. Over areas of sea ice, typical maps from the latest marine product baseline in 2017 (PB 2.24) are as follows:

Flag: surf_class_20_ku

Mode: all

Cycle: 25 NTC SR_2_WAT

Rel. Orbits: 1 to 345

First Time: 2017-11-23T22:22

Last Time: 2017-12-18T02:06

IPF Version: IPF-SM-2 D6.10

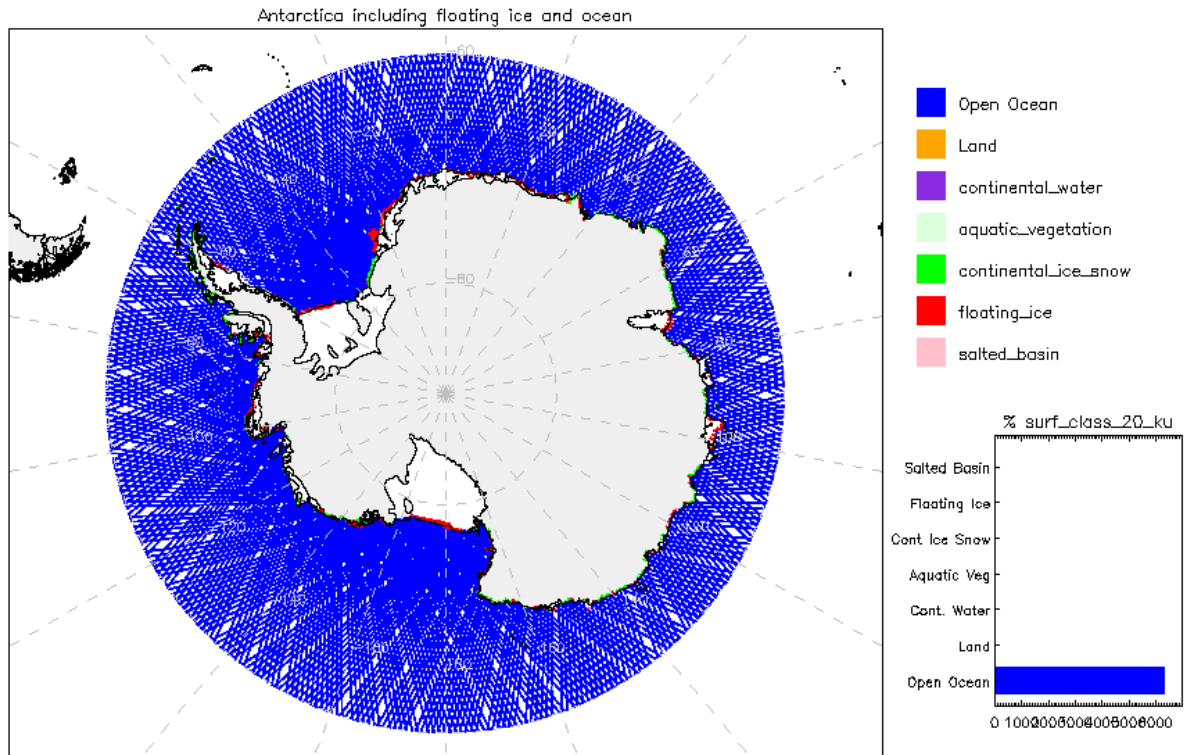


Figure 88: Maps of 20Hz Ku Band Surface Classification (surf_class_20_ku)

Flag: surf_class_20_ku

Mode: all

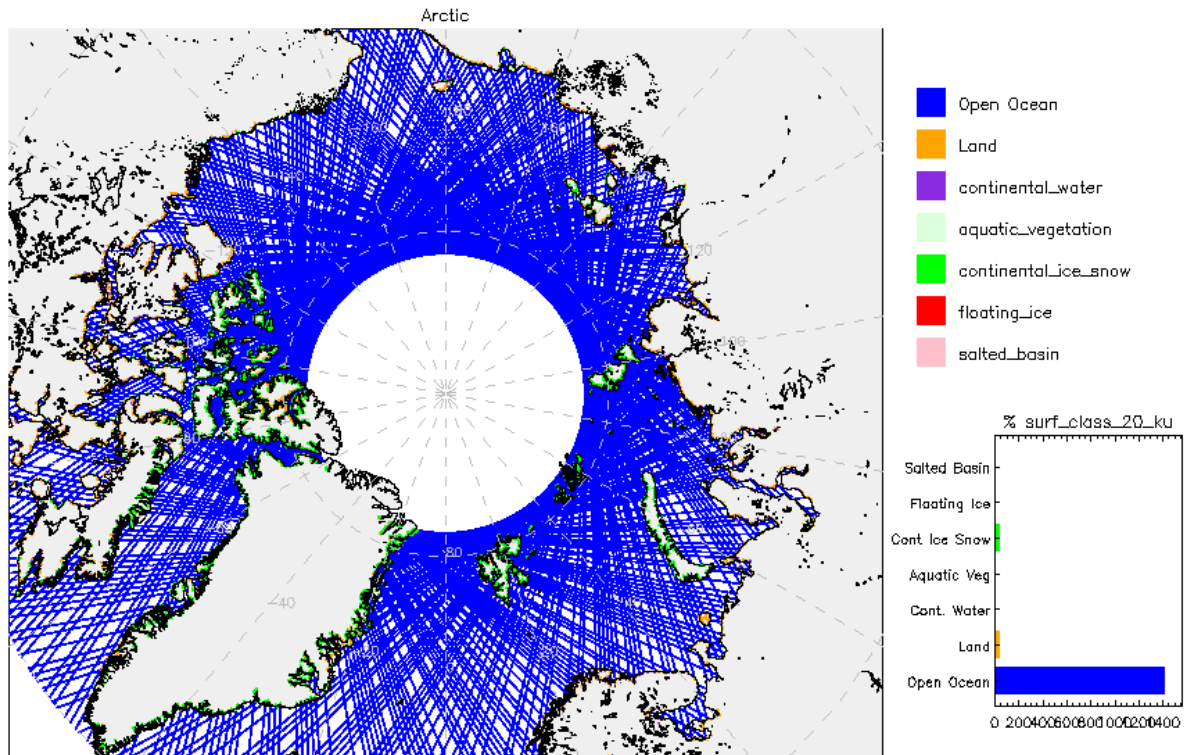
Cycle: 25 NTC SR_2_WAT

Rel. Orbits: 1 to 345

First Time: 2017-11-23T22:22

Last Time: 2017-12-18T02:06

IPF Version: IPF-SM-2 06.10



8.3 20Hz Ku Band Altimeter Derived Surface Type (surf_type_class_20_ku)

This parameter is the output of the sea ice echo discriminator which classifies SAR echoes as either leads, floes, open ocean or unclassified, based on their waveform shape (peakiness), SAR beam behaviour statistics and % sea ice concentration. During summer 2017 the discrimination thresholds were tuned to match those of Cryosat during a full winter season and discrimination results were validated against contemporaneous Sentinel-1 imagery. The new discriminator thresholds were implemented in product baseline PB2.24 (13 December 2017). Tuning of these thresholds will continue to be improved as more Arctic winter data becomes available and a planned evolution to include the SAR stack standard deviation in the tuning is implemented in 2018.

Typical maps of discriminator type from the final product baseline in 2017 (PB2.24) are as follows:

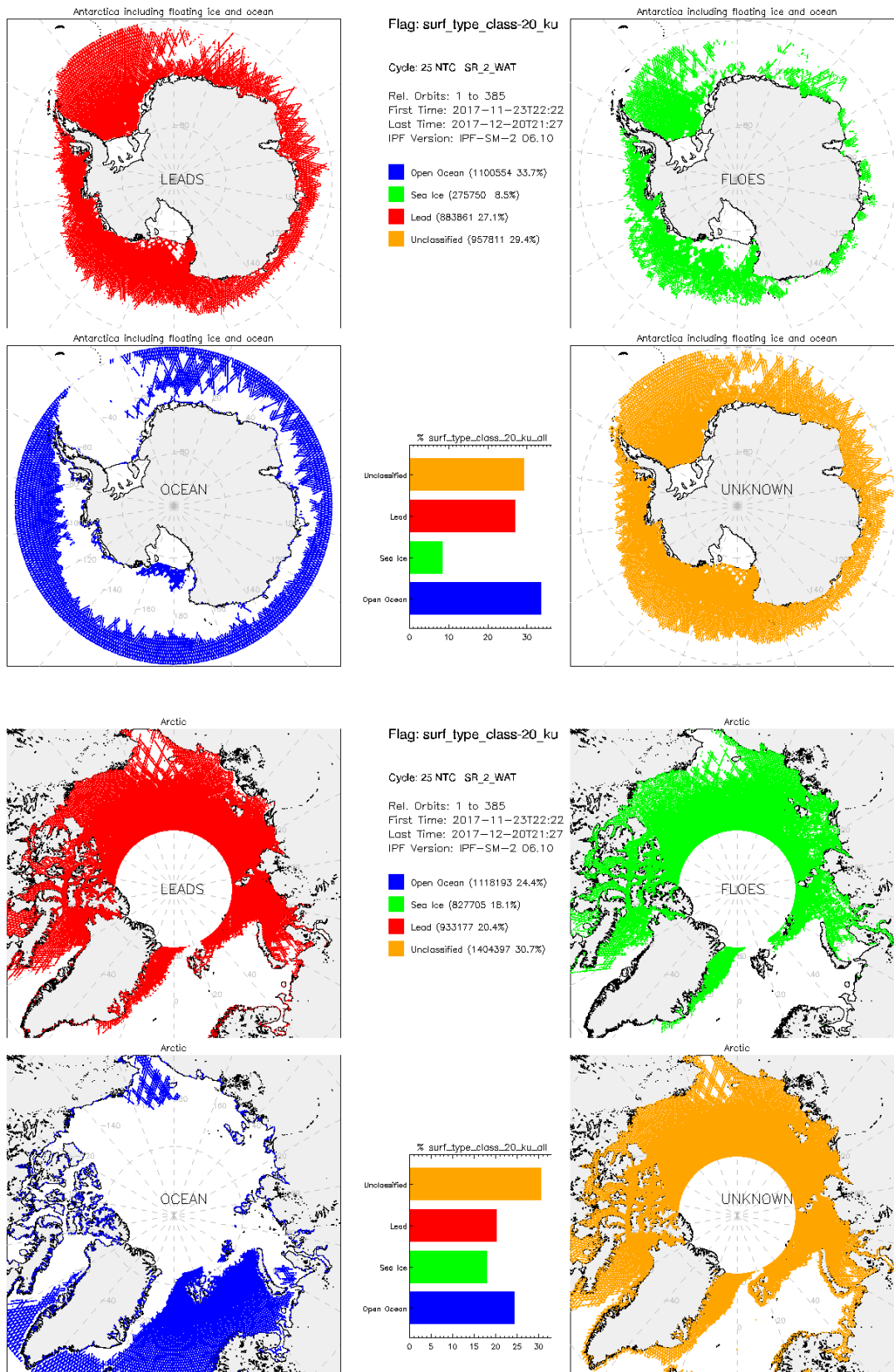


Figure 89: Maps of 20Hz Ku Band Altimeter Derived Surface Type (surf_type_class_20_ku)

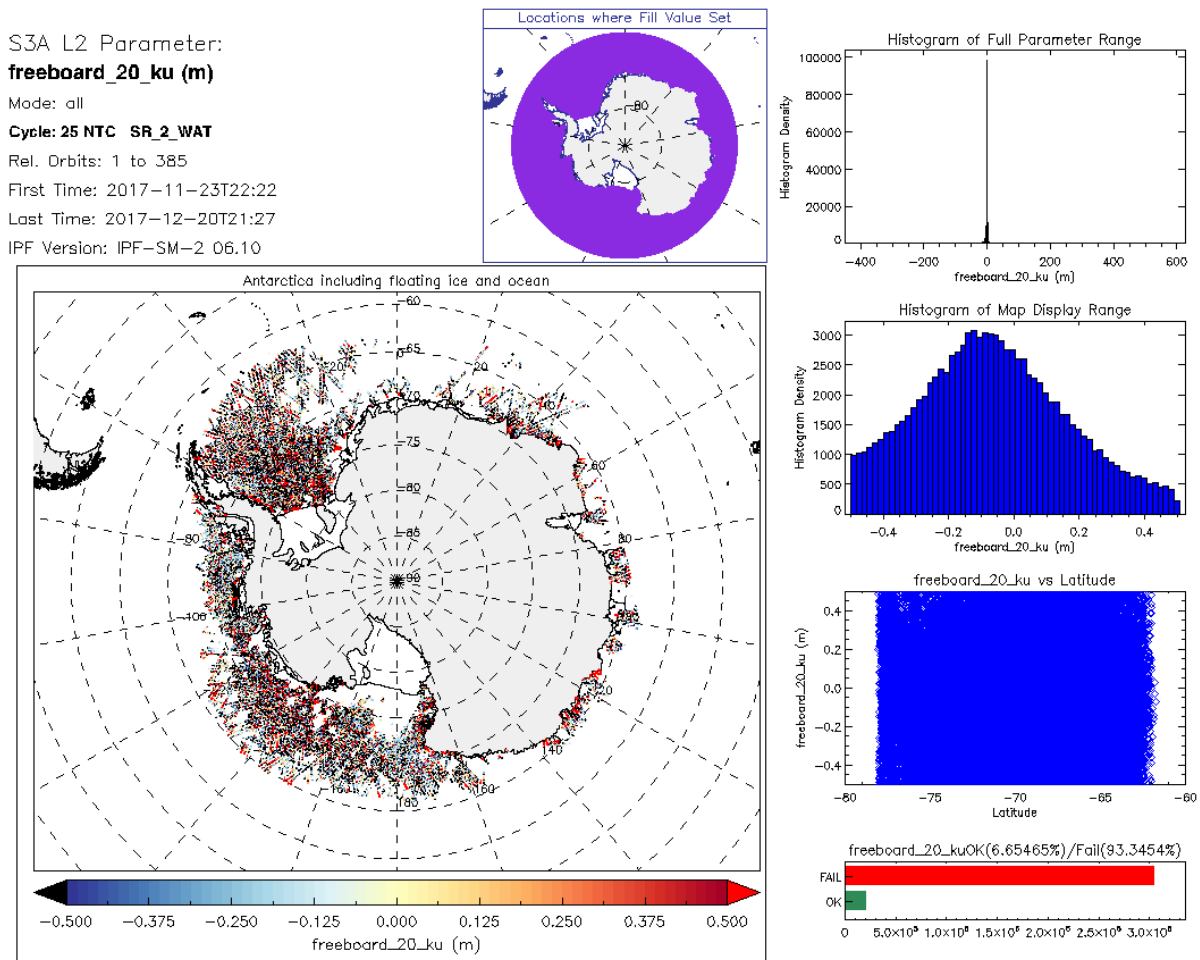
8.4 20Hz Ku band Freeboard (freeboard_20_ku)

Sea ice freeboard is the final output of the Sentinel-3A L2 sea ice processing and when validated can be used in combination with sea ice type, snow depth and density data to calculate sea ice thickness and volume which are essential climate variables.

The histogram of freeboard results from the latest product baseline in 2017 show a greater proportion of negative freeboard values and a wider spread of freeboard than would be expected. Although negative freeboard is possible due to snow loading, this spread of values is likely to be erroneous.

Analysis of results has shown that valid freeboard will not be achieved until the diffuse echo retracker (used to correct the range measurements of waveforms discriminated as sea ice floes) has been upgraded to a TMFRA retracker, as used in the latest Cryosat baseline-D and a lead and floe retracker bias calibrated. Replacement of this retracker and calibration is scheduled for the first half of 2018.

Typical maps of freeboard, showing a negative freeboard histogram from the latest product baseline in 2017 (PB 2.24) are shown below:



S3A L2 Parameter:
freeboard_20_ku (m)

Mode: all

Cycle: 25 NTC SR_2_WAT

Rel. Orbits: 1 to 385

First Time: 2017-11-23T22:22

Last Time: 2017-12-20T21:27

IPF Version: IPF-SM-2 06.10

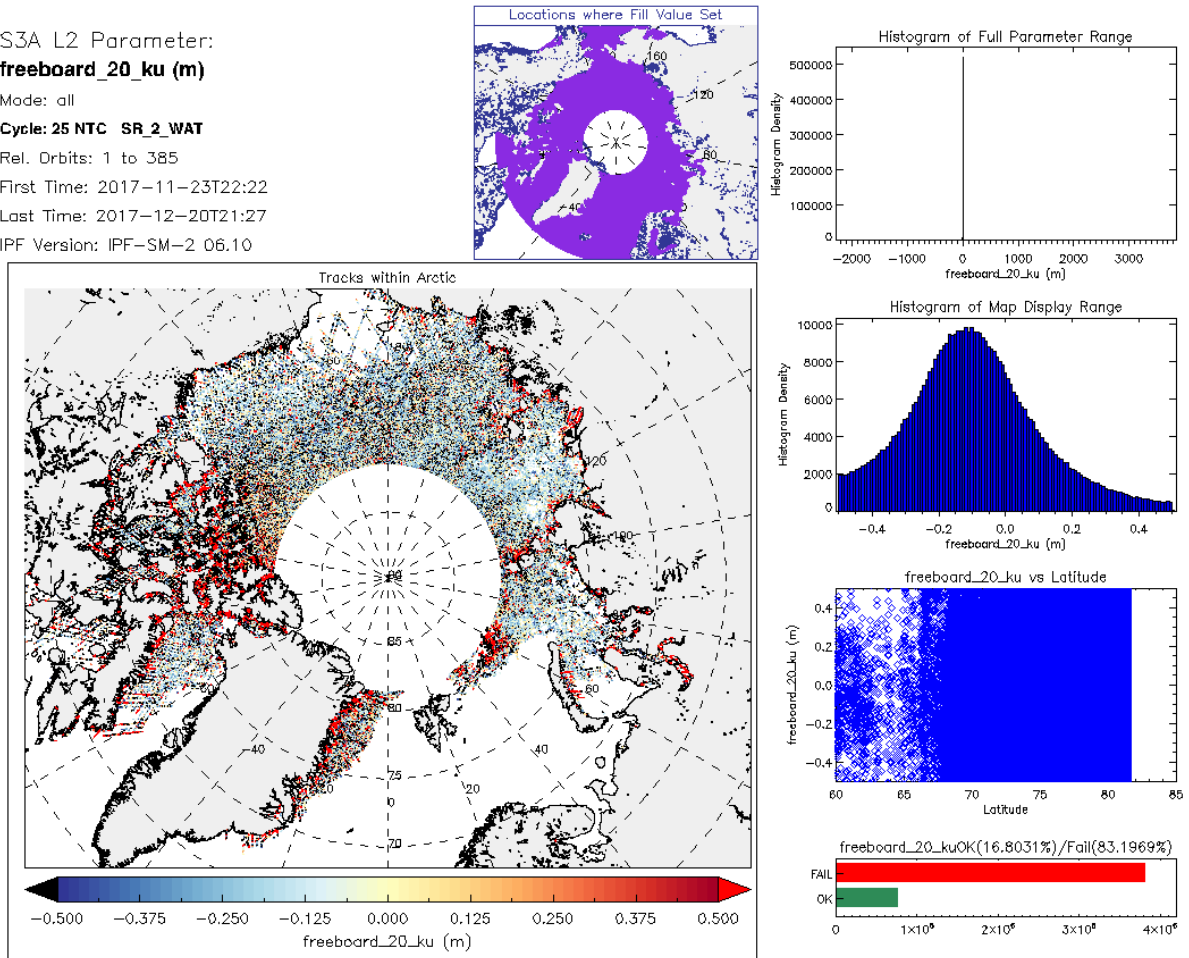


Figure 90: Maps of 20Hz Ku band Freeboard (freeboard_20_ku)

8.5 Sea Surface Height Anomaly (sea_ice_ssha_20_ku)

This parameter is the sea surface height with respect to the mean sea surface. Note that an anomalous band exists to the west of Greenland and east of Antarctica where values exceed -3 m: this is due the GIM ionospheric correction default value which is not well taken into account in the ssha calculation. This will be corrected in the next IPF version in 2018.

Note that higher than expected failure rates exist in this parameter due to erroneous waveform filtering of some lead echoes. This will be corrected in a product baseline evolution in early 2018.

Typical maps of SSHA from the final product baseline in 2017 (PB2.24) are as follows:

S3A L2 Parameter:
sea_ice_ssha_20_ku (m)

Mode: all

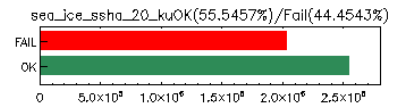
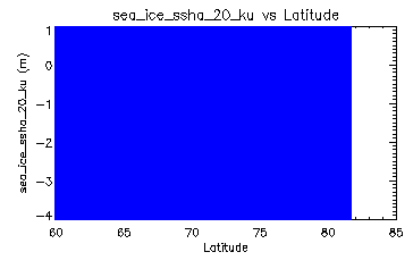
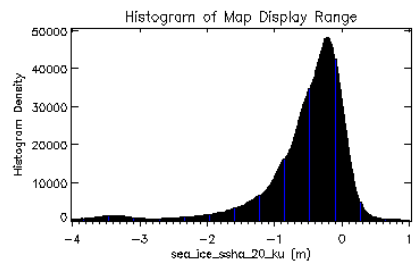
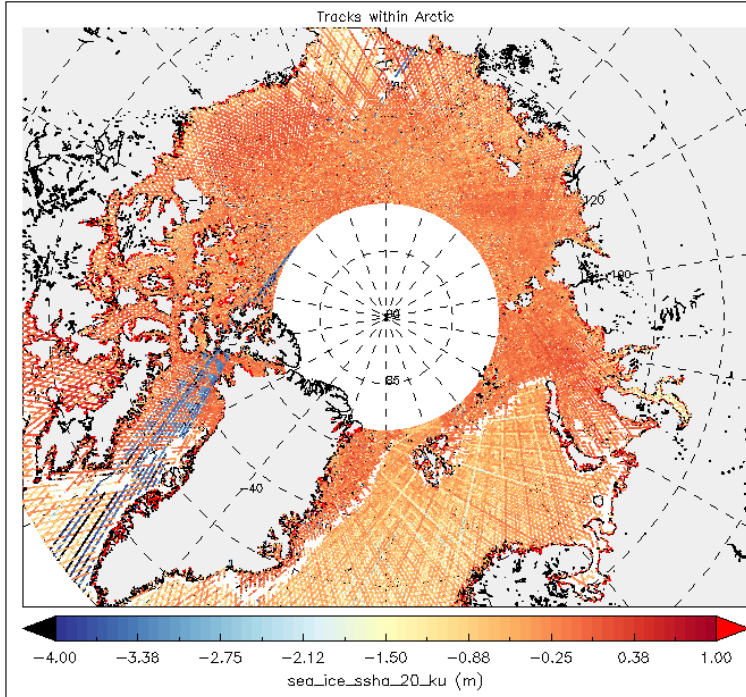
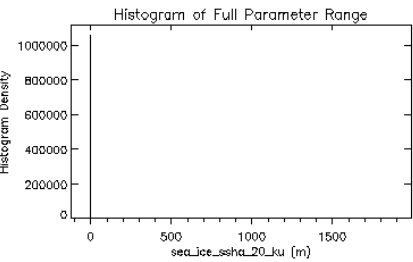
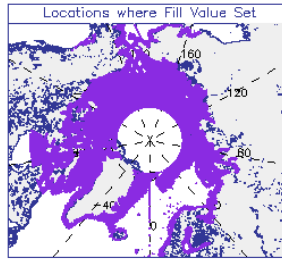
Cycle: 25 NTC SR_2_WAT

Rel. Orbits: 1 to 385

First Time: 2017-11-23T22:22

Last Time: 2017-12-20T21:27

IPF Version: IPF-SM-2 06.10



S3A L2 Parameter:
sea_ice_ssha_20_ku (m)
 Mode: all
 Cycle: 25 NTC SR_2_WAT
 Rel. Orbits: 1 to 385
 First Time: 2017-11-23T22:22
 Last Time: 2017-12-20T21:27
 IPF Version: IPF-SM-2 06.10

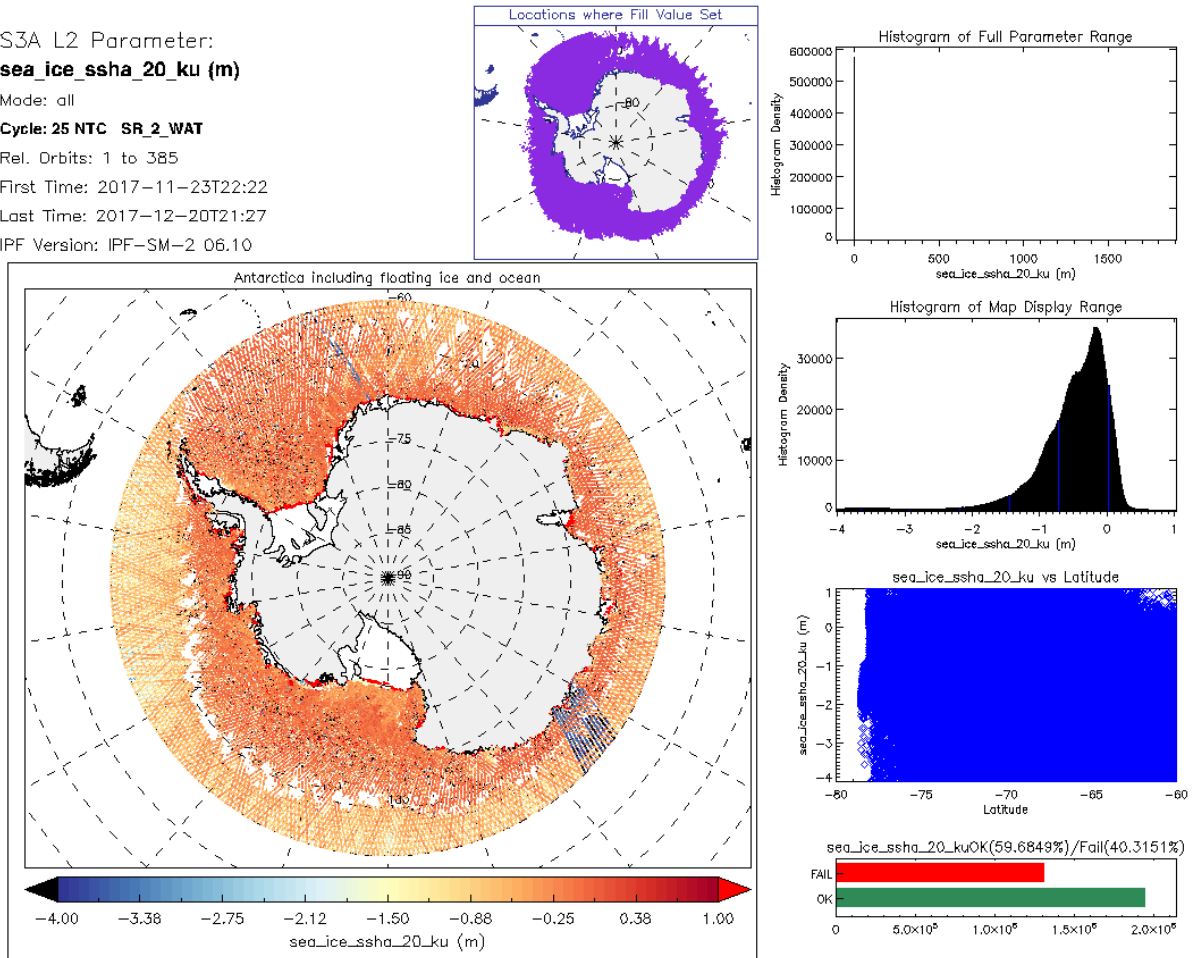


Figure 91: Maps of 20Hz Ku band Sea Ice SSHA (m)

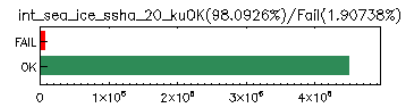
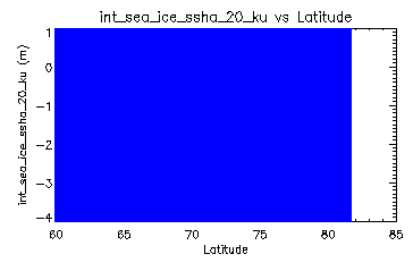
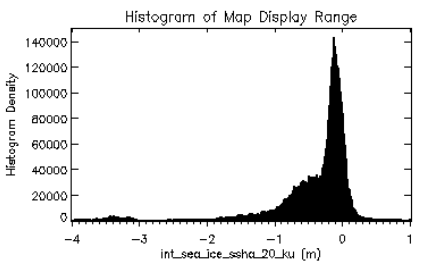
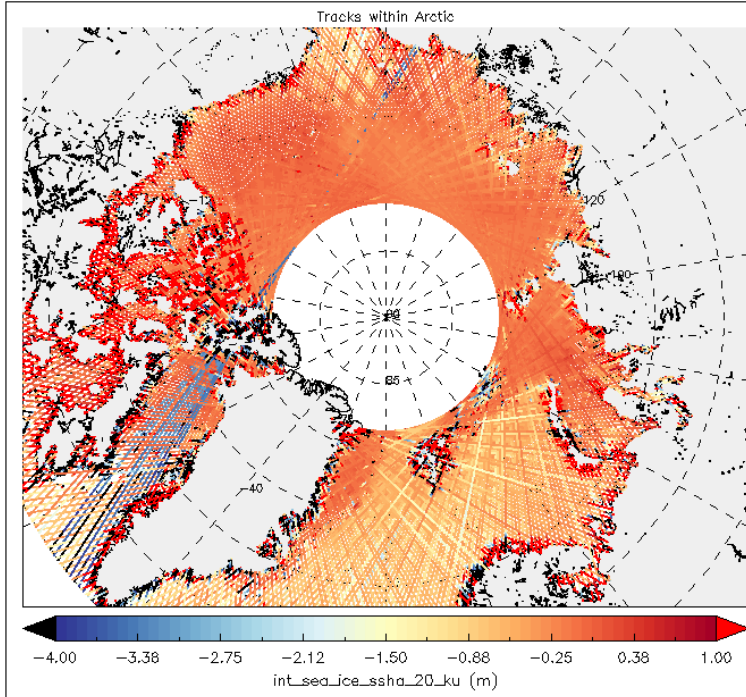
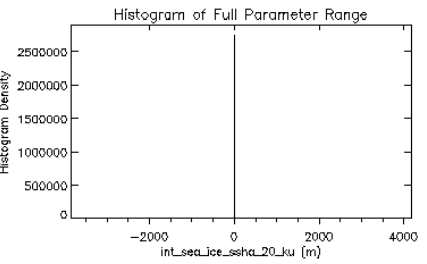
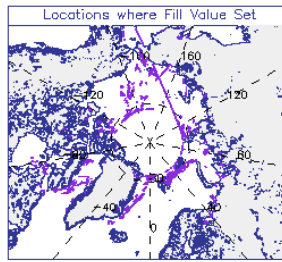
8.6 20Hz Ku Band Interpolated Sea Surface Height Anomaly (int_sea_ice_ssha_20_ku)

This parameter is the sea surface height with respect to the mean sea surface interpolated between leads in the sea ice (ie represents the SSHA underneath the sea ice floes).

Plots of this parameter show an anomalous region to the west of Greenland where incorrect values of the GIM ionospheric correction have been used, as for the sea ice ssha maps. Anomalous high values are also noted around the edge of land surfaces due to contamination of the SSHA interpolation with land elevations. This issue will be corrected in a future IPF evolution.

Typical maps of interpolated SSHA from the final product baseline in 2017 (PB2.24) are as follows:

S3A L2 Parameter:
int_sea_ice_ssha_20_ku (m)
 Mode: all
 Cycle: 25 NTC SR_2_WAT
 Rel. Orbits: 1 to 385
 First Time: 2017-11-23T22:22
 Last Time: 2017-12-20T21:27
 IPF Version: IPF-SM-2_06.10



S3A L2 Parameter:

int_sea_ice_ssha_20_ku (m)

Mode: all

Cycle: 25 NTC SR_2_WAT

Rel. Orbits: 1 to 385

First Time: 2017-11-23T22:22

Last Time: 2017-12-20T21:27

IPF Version: IPF-SM-2 06.10

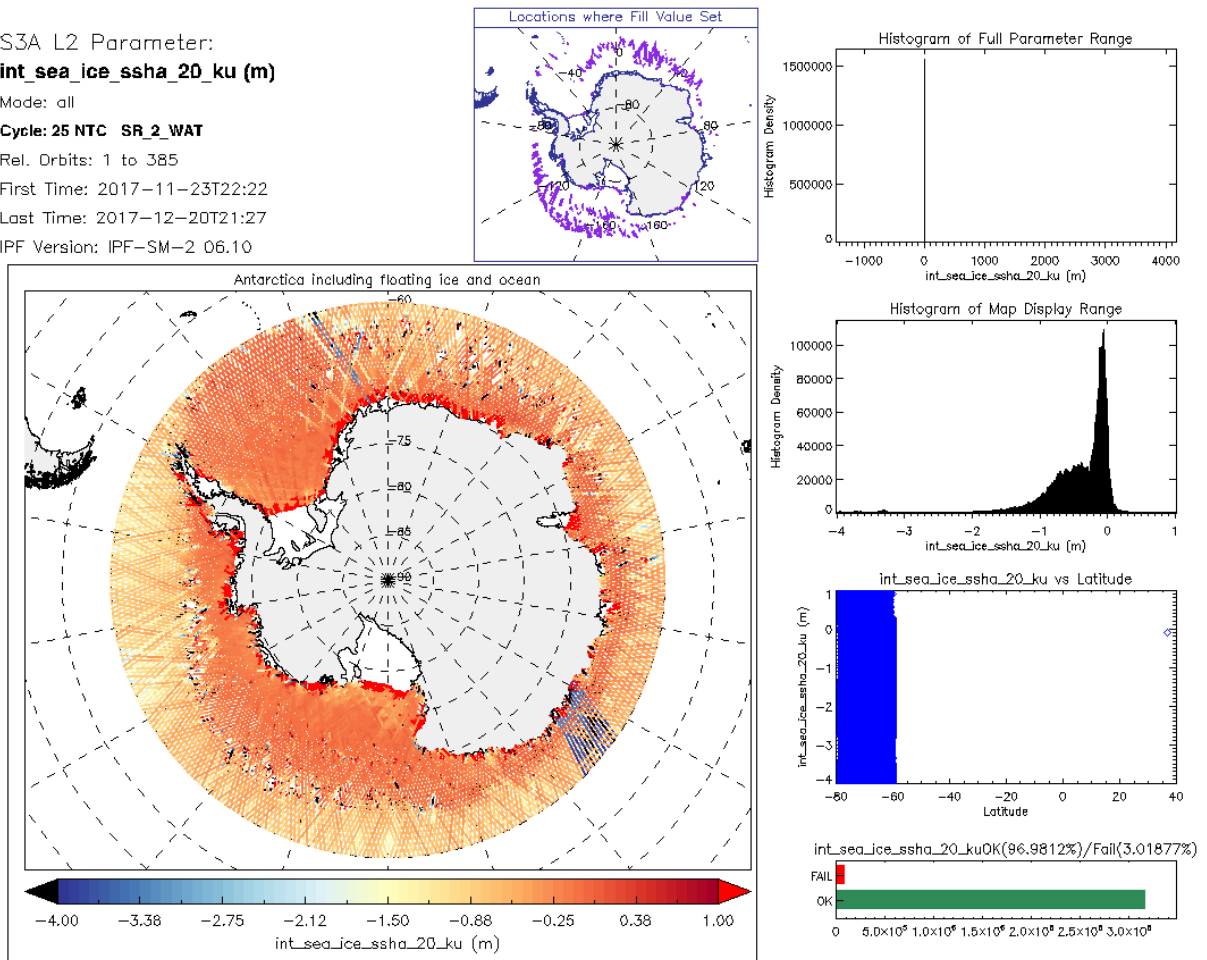


Figure 92: Maps of 20Hz Ku band Interpolated Sea Ice SSHA (m)

8.7 20Hz Ku band Sea Ice Concentration (sea_ice_concentration_20_ku)

Sea ice concentration data is available in 100% of records in products in 2017. Sea Ice Concentration is derived from a dynamic 3 day average of sea ice concentration calculated from SSM/I daily brightness temperature data and this map is consistent with external sea ice extent maps for these periods.

Note that sea ice concentration values in the L2 product are currently set to low values at locations on the coastal boundary. This is due to an interpolation of sea ice concentration with zero values over land. This issue will be corrected in a future evolution in 2018.

Typical maps of sea ice concentration from the final product baseline in 2017 (PB2.24) are as follows:

S3A L2 Parameter:
sea_ice_concentration_20_ku (%)

Mode: all

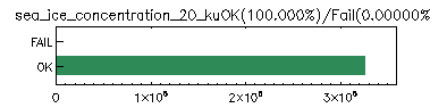
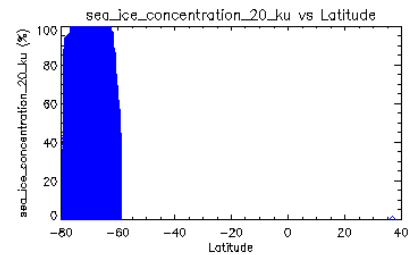
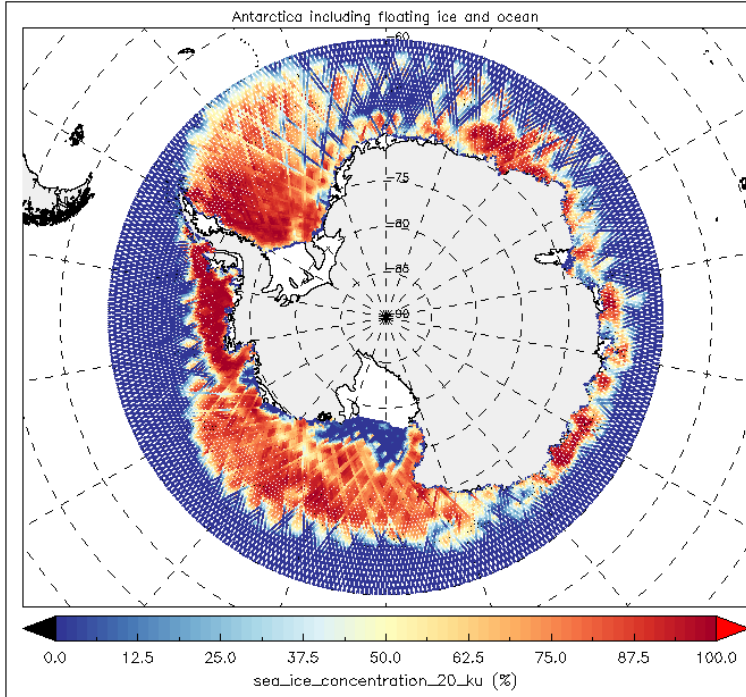
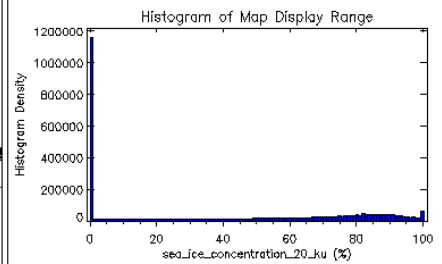
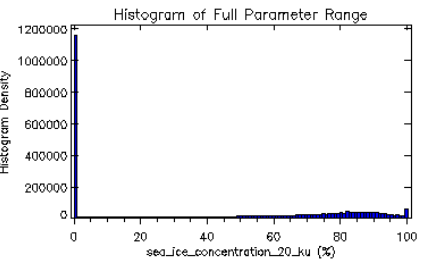
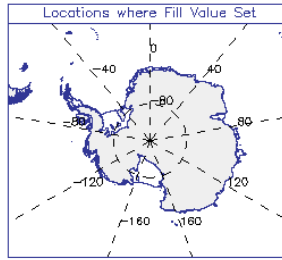
Cycle: 25 NTC SR_2_WAT

Rel. Orbits: 1 to 385

First Time: 2017-11-23T22:22

Last Time: 2017-12-20T21:27

IPF Version: IPF-SM-2 06.10



S3A L2 Parameter:
sea_ice_concentration_20_ku (%)
 Mode: all
 Cycle: 25 NTC SR_2_WAT
 Rel. Orbits: 1 to 385
 First Time: 2017-11-23T22:22
 Last Time: 2017-12-20T21:27
 IPF Version: IPF-SM-2 06.10

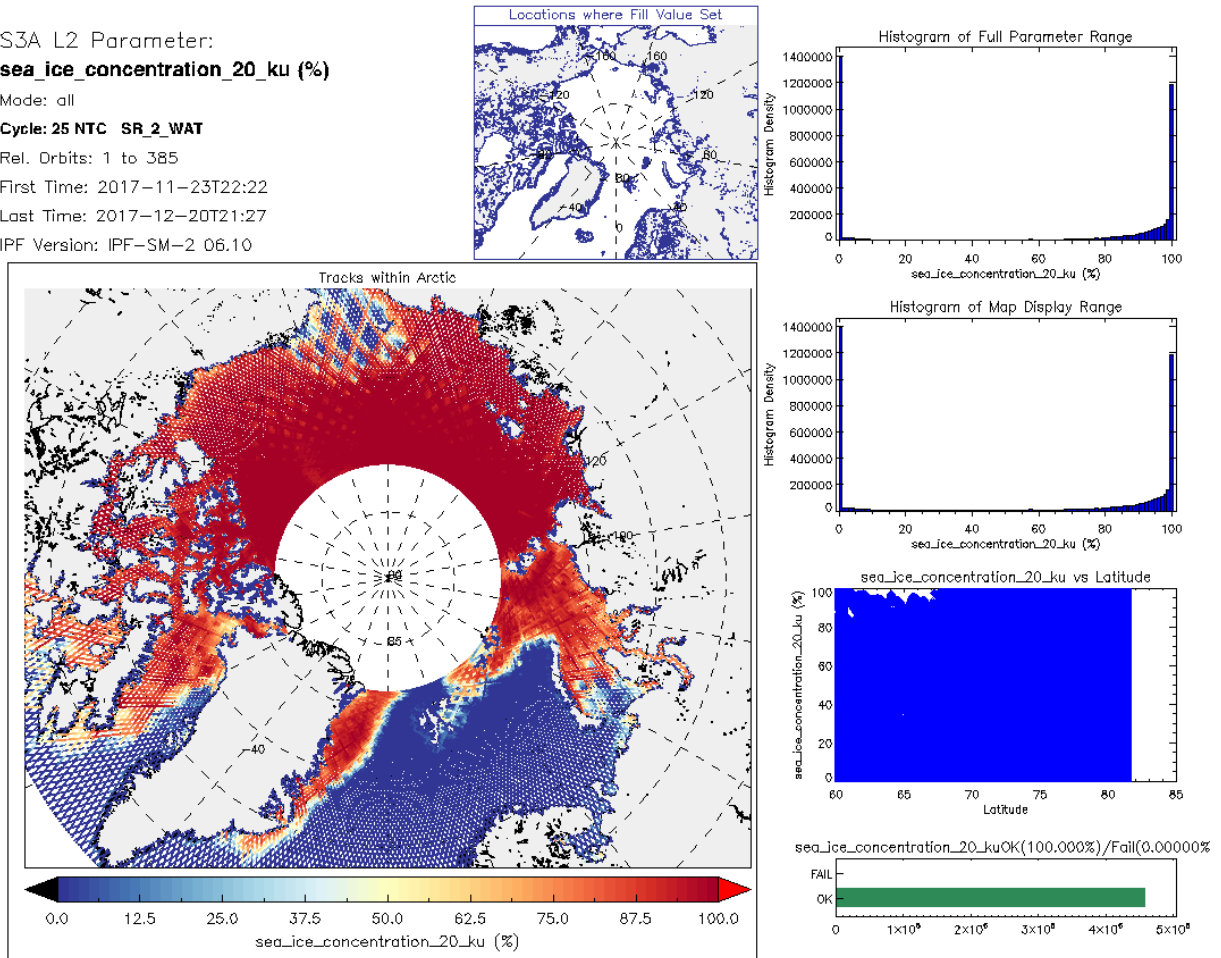


Figure 93: Maps of 20Hz Ku band Sea Ice Concentration (sea_ice_concentration_20_ku)

8.8 Availability of Geophysical Corrections over Sea Ice

Over sea ice the model dry tropospheric, model wet tropospheric, ionospheric, solid earth tide, pole tide and ocean tide and inverse barometric corrections are applied in the NTC L2 Marine product.

For the final product baseline in 2017 (PB 2.24), the percentage availability of geophysical corrections over sea ice was:

Cycle: 25 NTC SR_2_WAT

Rel. Orbits: 1 to 385
 First Time: 2017-11-23T22:22
 Last Time: 2017-12-20T21:27
 IPF Version: IPF-SM-2 06.10

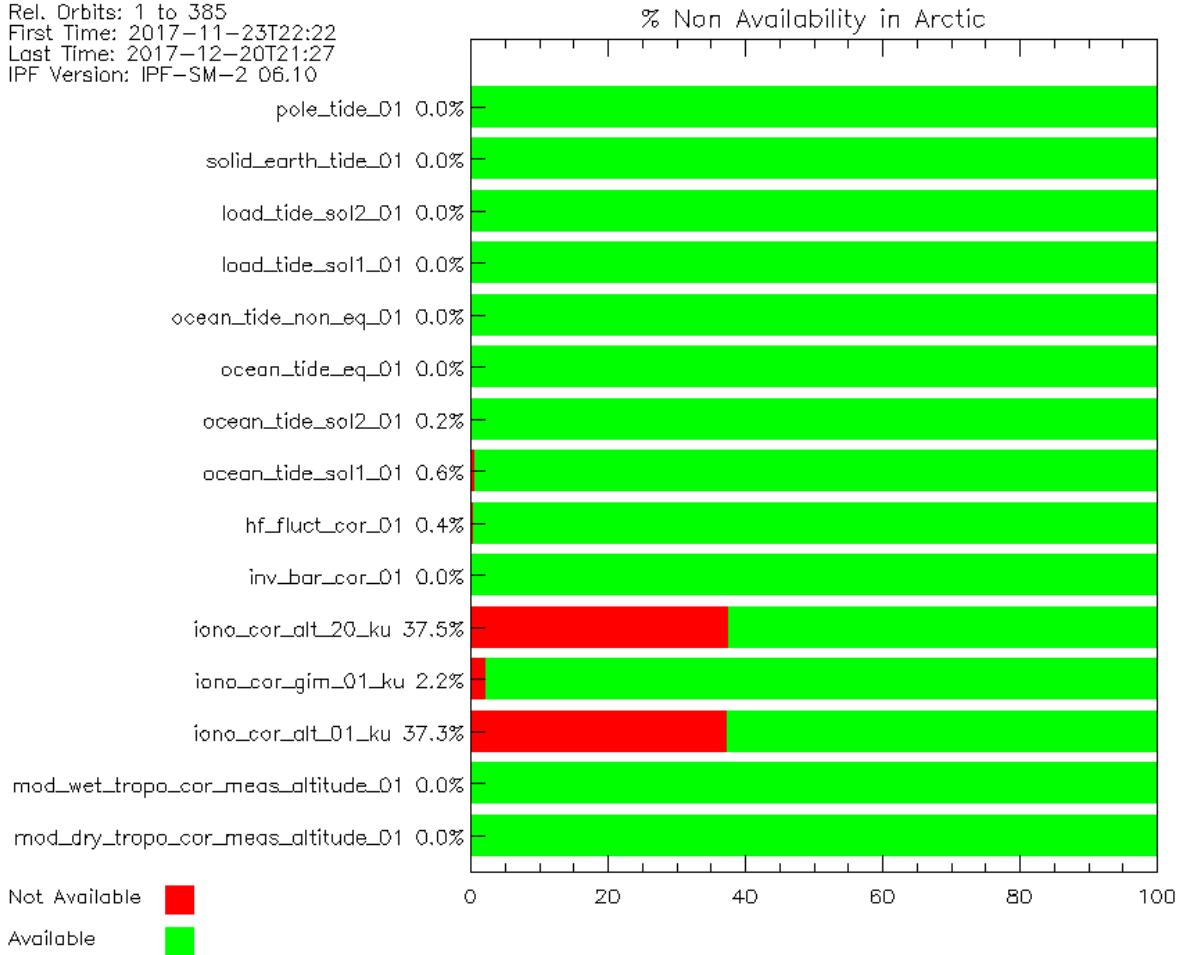


Table 9: % Non Availability of Geophysical Corrections over Sea Ice (NTC)



8.9 Availability of Snow Density, Snow Depth and Sea Ice Concentration over Sea Ice

For the product baselines in 2017 (PB 2.24), the percentage availability of sea ice concentration, snow depth and snow density data was:

Correction	% Availability Arctic Sea Ice	% Availability Antarctic Sea Ice
Sea Ice Concentration ³	100	100
Snow Density ¹	100	100
Snow Depth	100	100 ²

Table 10: % Availability of Snow Density, Snow Depth, Sea Ice Concentration over Sea Ice

¹Snow Density is set to a single value of 400 Kg/m³ as expected.

² Snow depth over Antarctic sea ice is set to zero as expected.

³Sea Ice Concentration is derived from a dynamic 3 day average of sea ice concentration calculated from SSM/I daily brightness temperature data.



9 Performance Mission over Land Ice

Sentinel-3A STM is the first altimetry mission to operate in SAR mode over all surfaces including ice sheets, ice sheet margins and ice shelves. Sentinel-3A shares a common heritage with the Cryosat polar altimetry mission, but over land ice surfaces, the operational modes and ground segment processing of Cryosat are quite different (Cryosat operates in LRM over the ice sheets and SARin over the ice margins) and hence the full commissioning of Sentinel-3A over land ice requires new methods, algorithm tuning, and validation.

Unlike Cryosat, whose ground segment was optimized from launch primarily for ice surfaces, Sentinel-3A STM is an operational mission with a single ground segment shared between all surface types (ocean, sea ice, land ice, ice shelves, inland waters, coastal zones) which all have very different properties and processing requirements at each ground processor level. For these reasons commissioning and tuning the processors specifically for land ice is a complex and still ongoing task.

Good progress was made in 2017 identifying key performance issues, tuning land ice algorithms, introducing new L2 land ice product parameters requested by users, and specifying requirements for evolutions of the low-level ground processing, which should result in reaching a good level of performance over land ice surfaces in 2018. Studies using prototype processors have tested many of these improvements and shown performance comparable with or exceeding previous missions over ice sheets.

Due to the complexity of the multi-surface type Sentinel-3A ground segment, some evolutions to land ice processing identified during 2017 are still to be phased in to future product baseline releases in 2018, and users should take note of current issues with product quality detailed below and available in the product notices.

The following sections detail the performance of key L2 land ice parameter in products released during 2017, culminating in product baseline 2.24 (Dec 2017).

9.1 SRAL Instrument Mode over Land Ice

Sentinel-3A has three different possible operating modes (LRM, SAR open loop, SAR closed loop). Over land ice surfaces the SRAL altimeter operated in SAR closed loop (autonomous) tracking mode for all operational cycles since Dec 2016 (from cycle 12).

Flag: instr_op_mode_20_ku

Mode: all

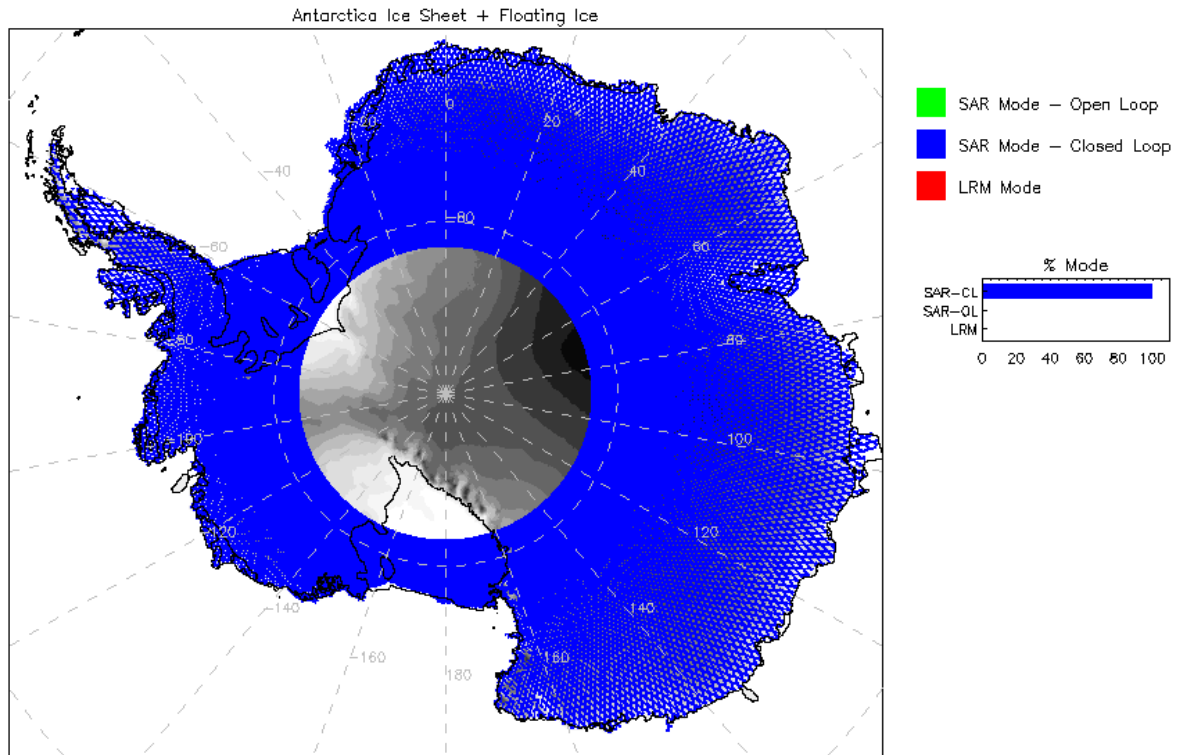
Cycle: 25 NTC SR_2_LAN

Rel. Orbits: 1 to 385

First Time: 2017-11-23T22:22

Last Time: 2017-12-20T21:32

IPF Version: IPF-SM-2 D6.10



Flag: instr_op_mode_20_ku

Mode: all

Cycle: 25 NTC SR_2_LAN

Rel. Orbits: 1 to 385

First Time: 2017-11-23T22:22

Last Time: 2017-12-20T21:32

IPF Version: IPF-SM-2 D6.10

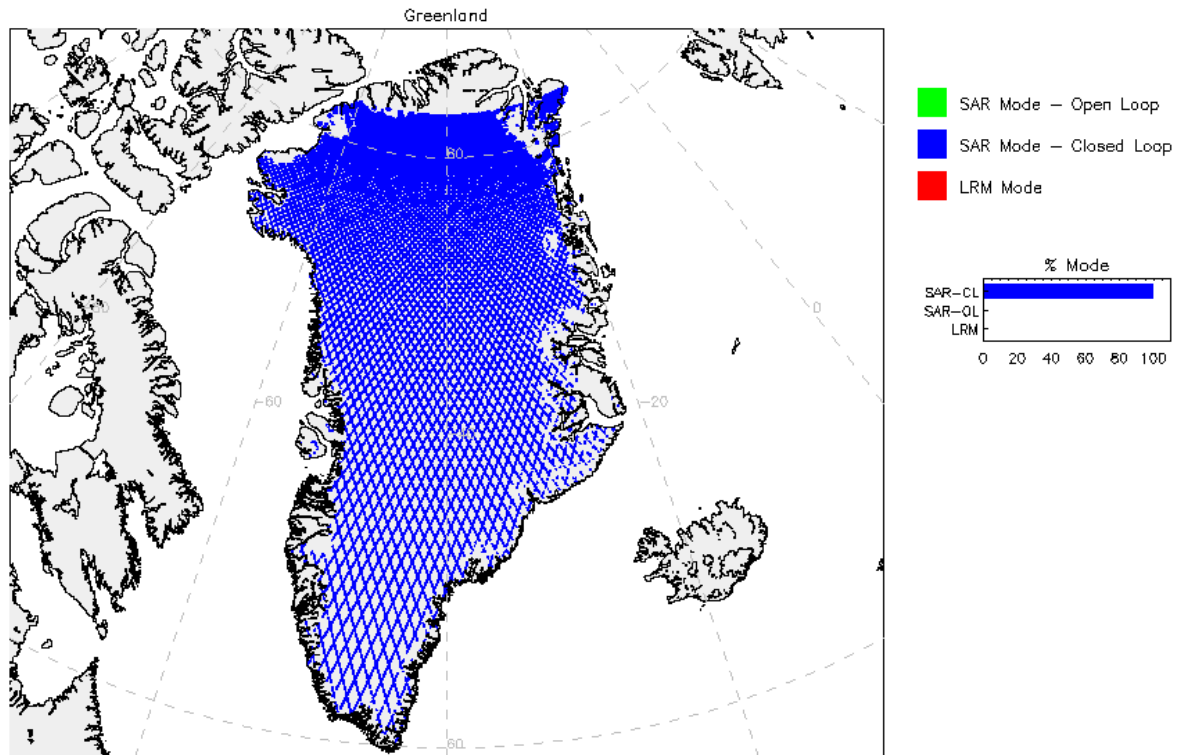


Figure 94: Maps of SRAL Instrument Mode, Antarctica and Greenland (Cycle 25, Nov/Dec 2017)

Users should note that during the commissioning phase of Sentinel-3A, the operational mode over the ice sheet margins was SAR open loop for cycles 3 (Apr-2016) -11 (Dec 2016). SAR open loop mode was found to have problems correctly tracking the surface over sloping terrain and this mode was switched to closed loop over the margins in Dec 2016. Therefore, measurement density over the margins during cycles 3-11 was severely reduced and it is unlikely that these measurements can be recovered by future ground processing.

Flag: instr_op_mode_20_ku

Mode: all

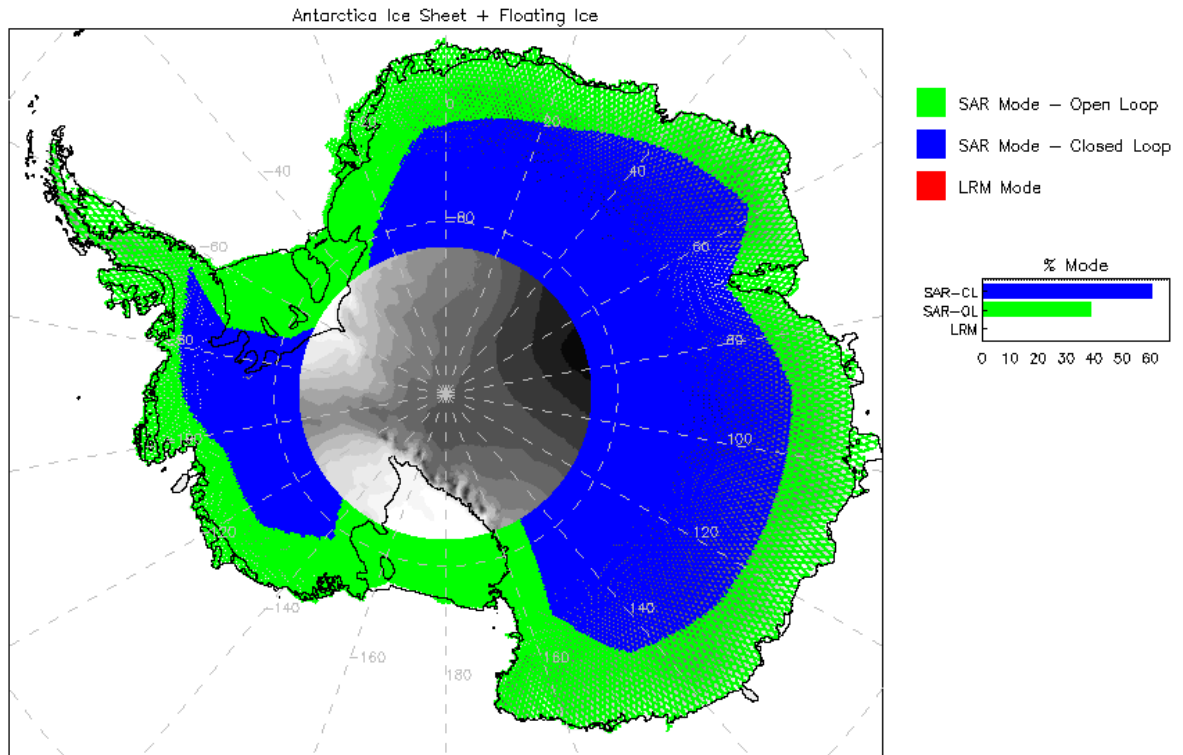
Cycle: 10 NTC SR_2_LAN

Rel. Orbits: 1 to 385

First Time: 2016-10-14T22:22

Last Time: 2016-11-10T21:32

IPF Version: IPF-SM-2 D6.07



Flag: instr_op_mode_20_ku

Mode: all

Cycle: 10 NTC SR_2_LAN

Rel. Orbits: 1 to 385

First Time: 2016-10-14T22:22

Last Time: 2016-11-10T21:32

IPF Version: IPF-SM-2 D6.07

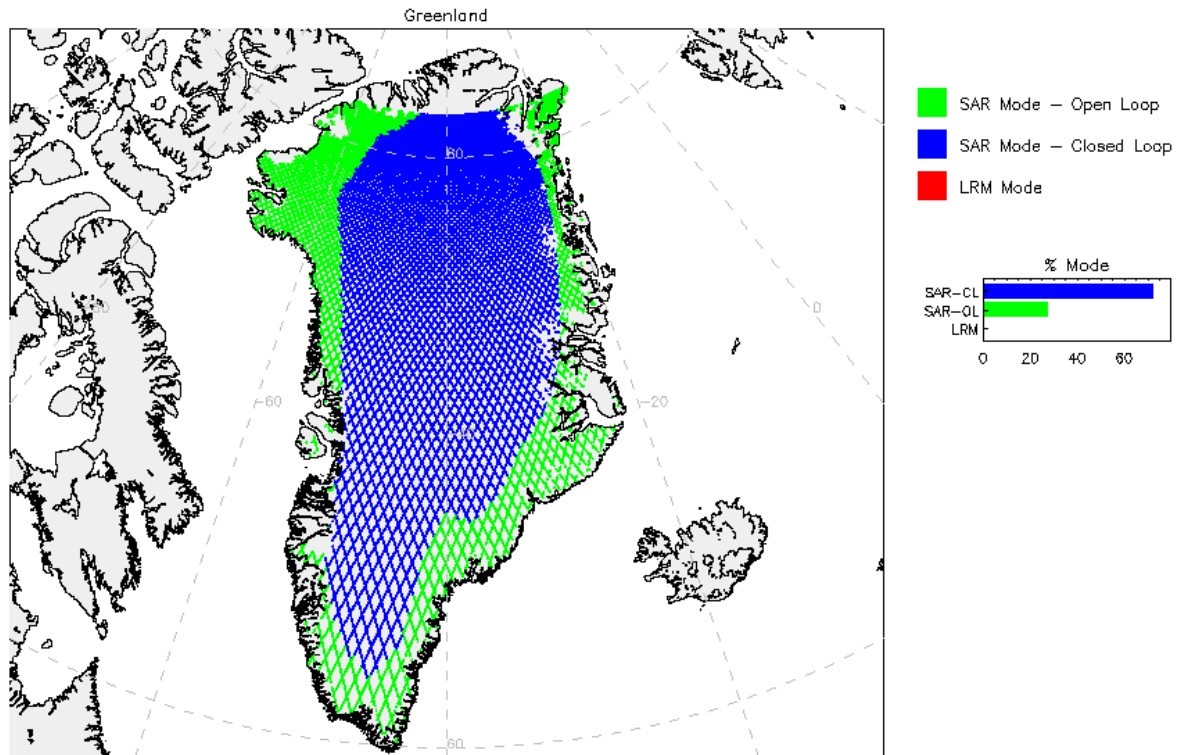


Figure 95: Maps of SRAL Instrument Mode, Antarctica and Greenland (Cycle 10, Oct/Nov 2016)

9.2 20Hz Ku-band Ice Sheet Elevation

The primary L2 geophysical parameter processed from Sentinel-3A STM data for monitoring land ice surfaces is the 20Hz Ku-band surface elevation (elevation_ice_sheet_20_ku). Elevation is calculated by subtracting the corrected range of the SAR echoes from the satellite altitude above the geoid, and then applying a slope correction across track to identify the point on the sloping ice sheet of closest approach. For this parameter, the fine correction to the range (retracking correction) is calculated by fitting a physical ice sheet model to each composite SAR waveform to find the precise location of the ice surface. For Ku-band the radar echo can penetrate the snow to reflect off the ice layer, and the waveform is composed of both surface and volume scattering.

Analysis of this parameter from the final product baseline in 2017, shows that the map of elevation over the ice sheets is as expected but there is a high rate of parameter failure (22-31%), particularly over the

ice sheet margins (40%) in both Antarctica and Greenland. This is partially due to complex waveform shapes over rough terrain which are difficult to model, and also due to the waveforms that are not maintained within the centre of the range window over areas of sloping terrain such as the continental margins. This results in waveforms being located towards the edge of the range window, outside the ice margin retracker's central fit window. Over areas of low ice sheet slope such as Dome-C or Lake Vostok failure rates are much lower (1%) as the waveform shape and position are much more stable.

For Cryosat-2 mission, the SAR window analysis is artificially extended and waveforms are finally centred by the L1 ground processing. The waveform centering ensures the stability of the waveform main leading edge position within the window analysis. A similar evolution of the Sentinel-3A L1 processor is planned during 2018. This shall recover some margins acquisitions and significantly reduces the failure ratio of the ice margin retracker.

Tuning of the ice margin retracker to partially correct for issues in the waveforms centering by the MPC during 2017 has reduced the failure rate of the elevation parameter by approximately 20% over the ice sheets. Further tuning of the ice margin retracker will be performed once the L1 processing is updated to provide centred waveforms.

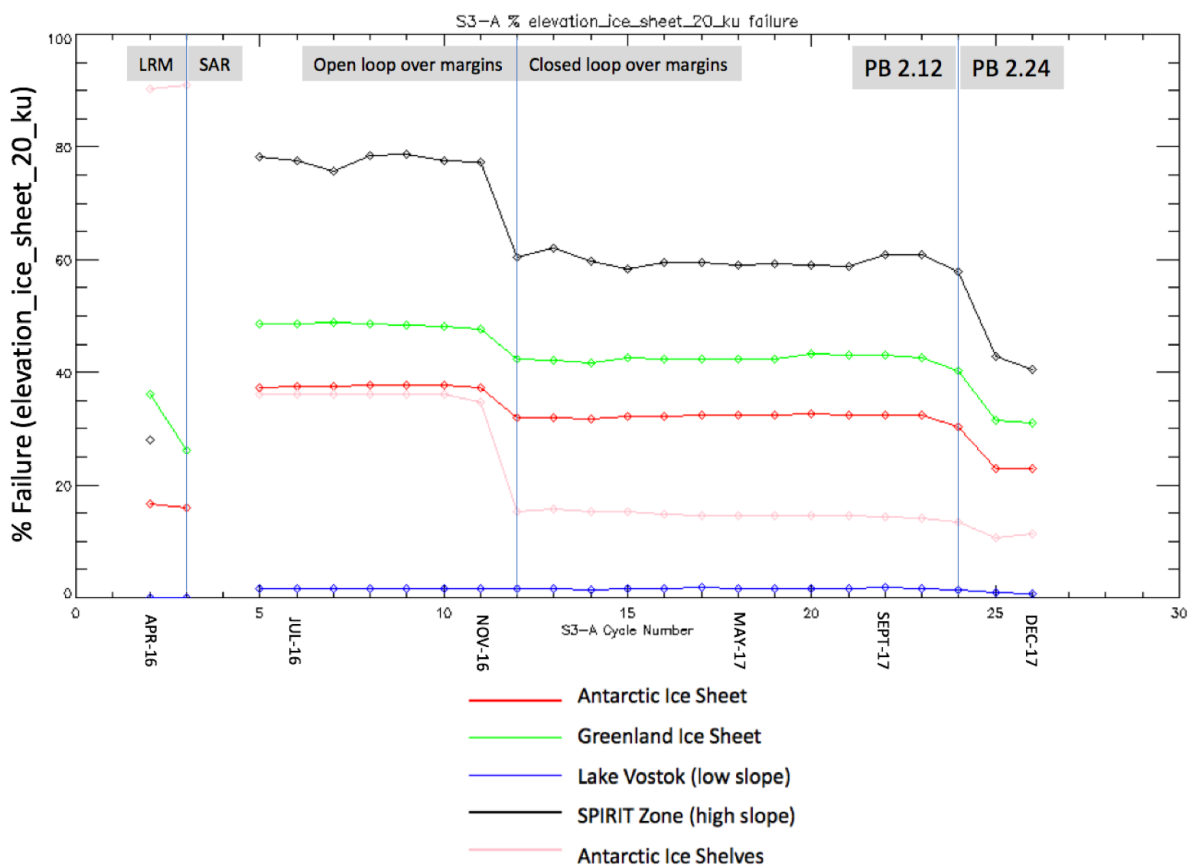


Figure 96: Failure rate of ice sheet elevation over different ice surfaces since start of mission

Statistics of elevation failure rate since start of mission indicate a reduction in failure rate over all ice surface types and regions of low and high slope due to L2 IPF evolutions during 2017. The time series (Figure 96) also shows the improvement after the change from open loop to closed loop tracking over

the margins. Statistics from LRM mode in cycles 2 and 3 are based on only a small number of orbits available during commissioning.

Additionally, tests indicate that an error in the SAR slope correction is present in all product baselines in 2017. This causes a resulting error in elevation (of 30 cm to several metres, dependent on slope) and an error in the slope corrected location parameters. This is corrected in Processing Baseline 2.27 which was deployed on 14 February 2018 and used for the Reprocessing 2.

S3A L2 Parameter:

elevation_ice_sheet_20_ku (m)

Mode: all

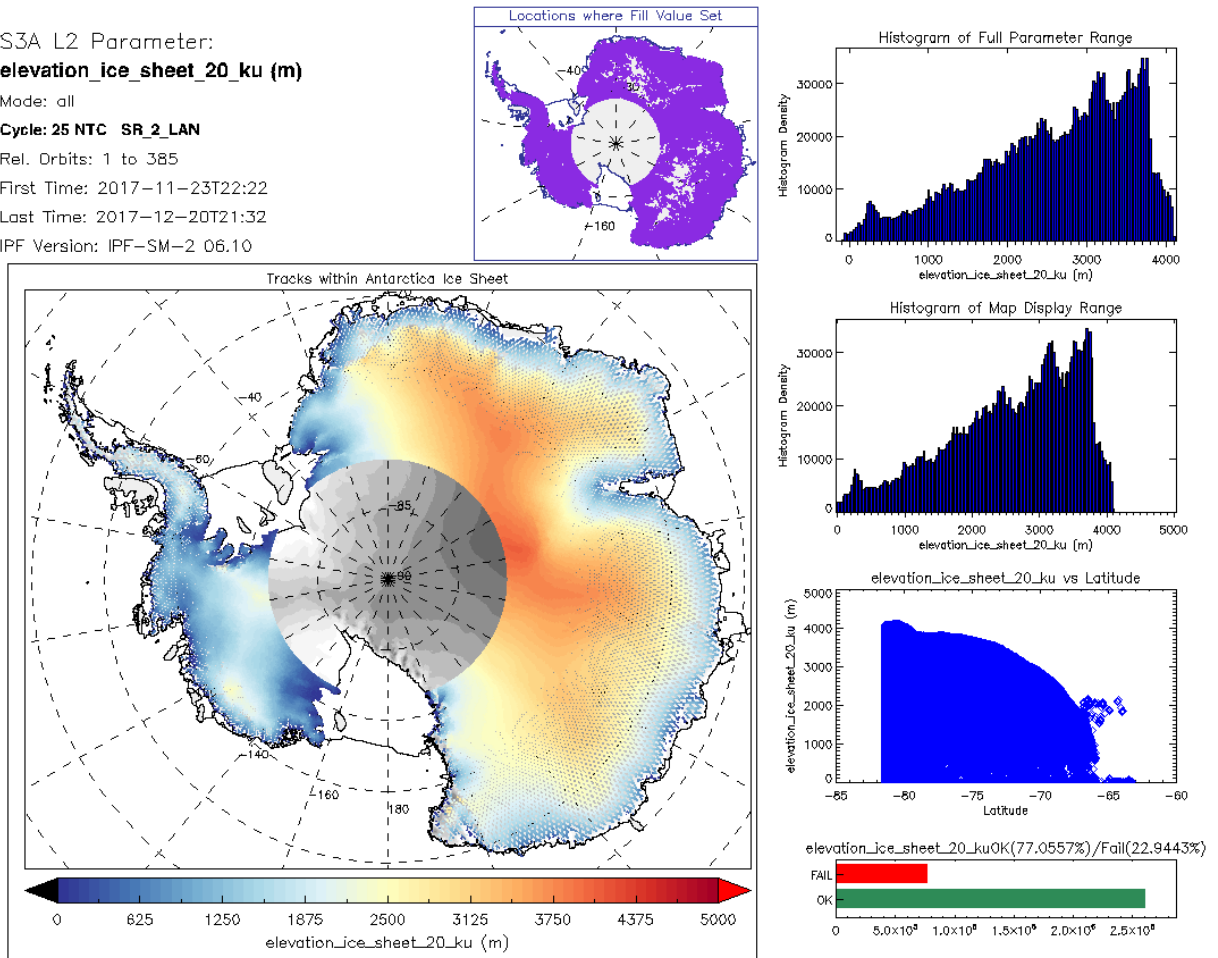
Cycle: 25 NTC SR_2 LAN

Rel. Orbits: 1 to 385

First Time: 2017-11-23T22:22

Last Time: 2017-12-20T21:32

IPF Version: IPF-SM-2 06.10



S3A L2 Parameter:
elevation_ice_sheet_20_ku (m)

Mode: all

Cycle: 25 NTC SR_2_LAN

Rel. Orbits: 1 to 385

First Time: 2017-11-23T22:22

Last Time: 2017-12-20T21:32

IPF Version: IPF-SM-2 06.10

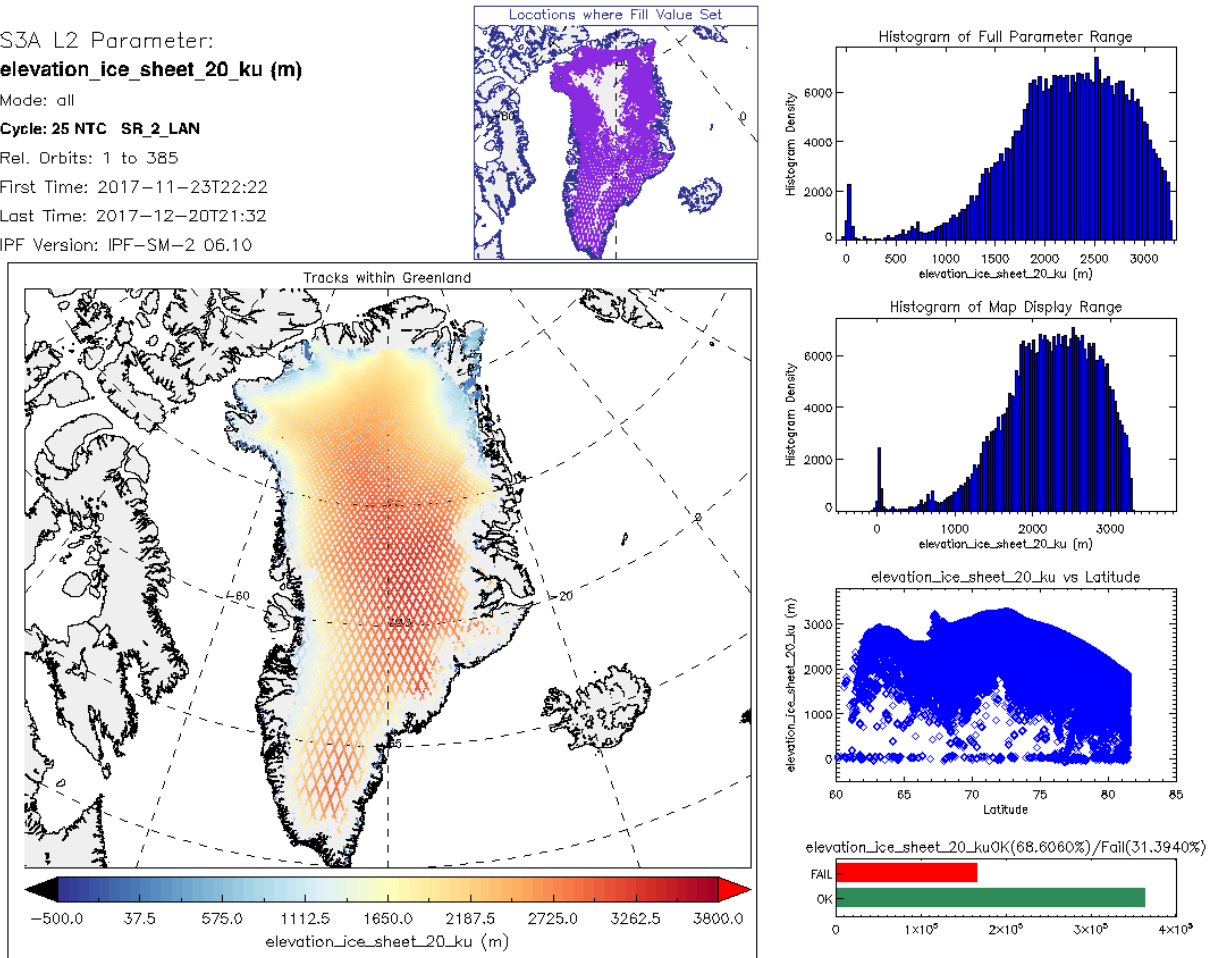


Figure 97: Maps of Ku band Ice Sheet Elevation, Antarctica and Greenland (Cycle 25, Nov/Dec 2017)

Maps of elevation over areas of low slope such as Dome-C in Antarctica (mean slope 0.04 degs) show very low failure rates. Whereas maps of elevation over the SPIRIT zone in the margins of Antarctica show failure of 42% of measurements.

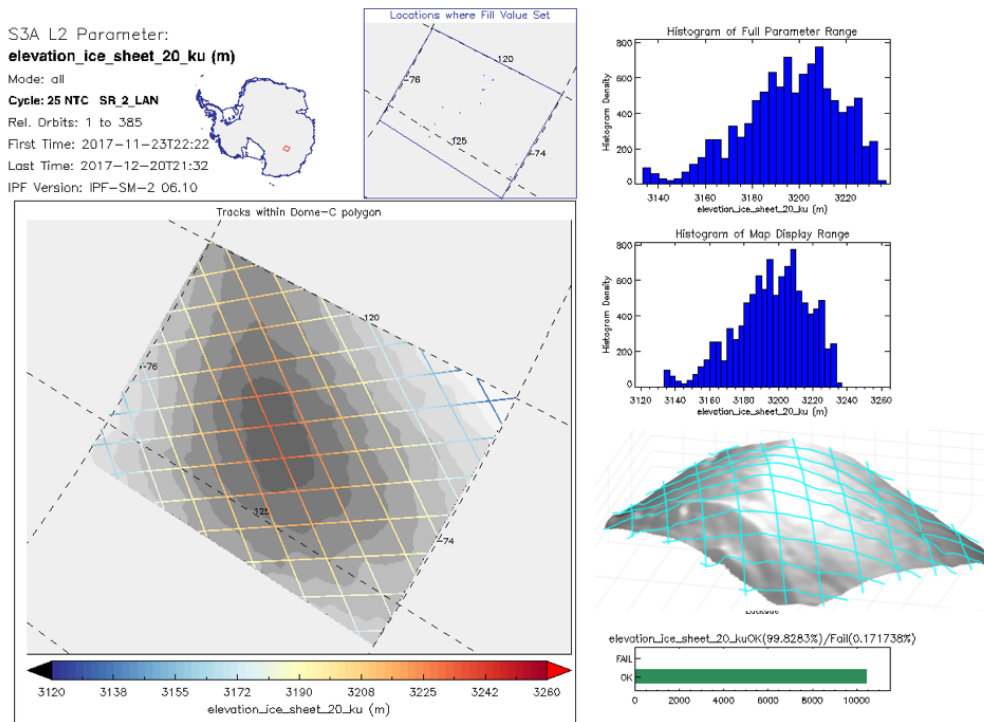


Figure 98: Maps of Ku band Ice Sheet Elevation, Dome-C, Antarctica (Cycle 25, Nov/Dec 2017)

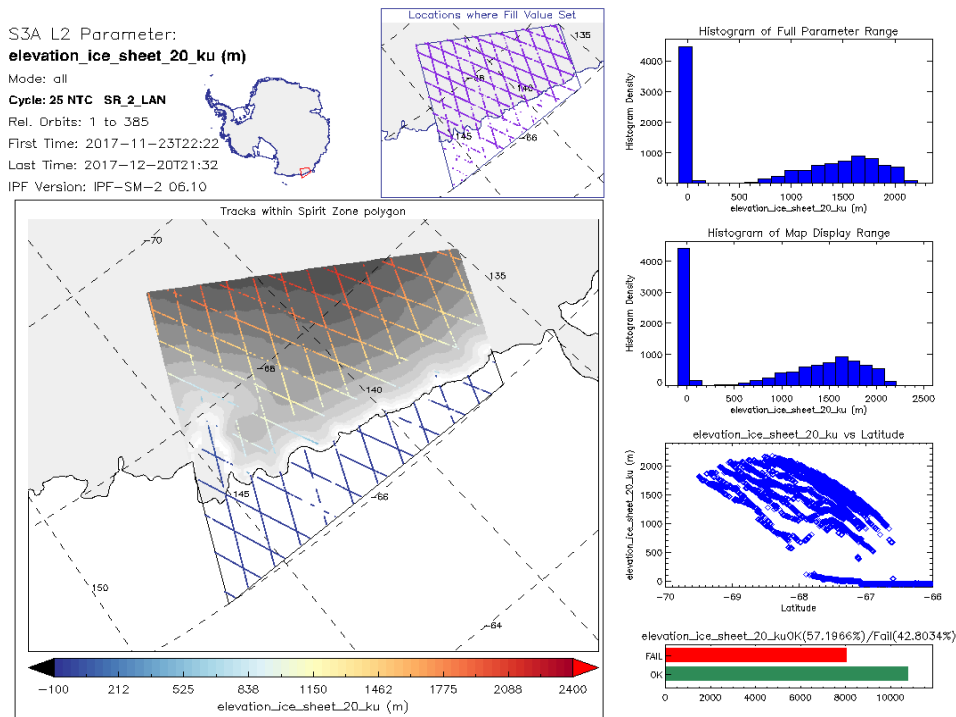


Figure 99: Maps of Ku band Ice Sheet Elevation, SPIRIT Zone, Antarctica (Cycle 25, Nov/Dec 2017)

9.3 20Hz Ku-band OCOG Elevation

Following user feedback in 2017 the MPC have added a new 20Hz Ku-band elevation parameter, processed using an empirical retracker (Ice-1, OCOG) to the L2 product in the Processing Baseline 2.27. The OCOG centre of gravity retracking algorithm will retrack a wider range of waveform shapes and leading edge positions than the model fit approach used by the SAR ice margin retracker. This results in greater measurement density, but in some areas lower accuracy. Elevation from the Ice-1 OCOG retracker is available from all previous radar altimetry missions providing a continuity of measurement technique that makes long term multi-mission studies of ice sheet surface elevation change and mass balance possible.

The following maps show the 20Hz Ku-band OCOG range measurements (provided in all baselines) which is used to process the new elevation parameter. Failure rates of 2-4% are significantly lower than for the SAR ice sheet elevation parameter which is more sensitive to waveform shape and lack of stability.

S3A L2 Parameter:
range_ocog_20_ku (km)

Mode: all

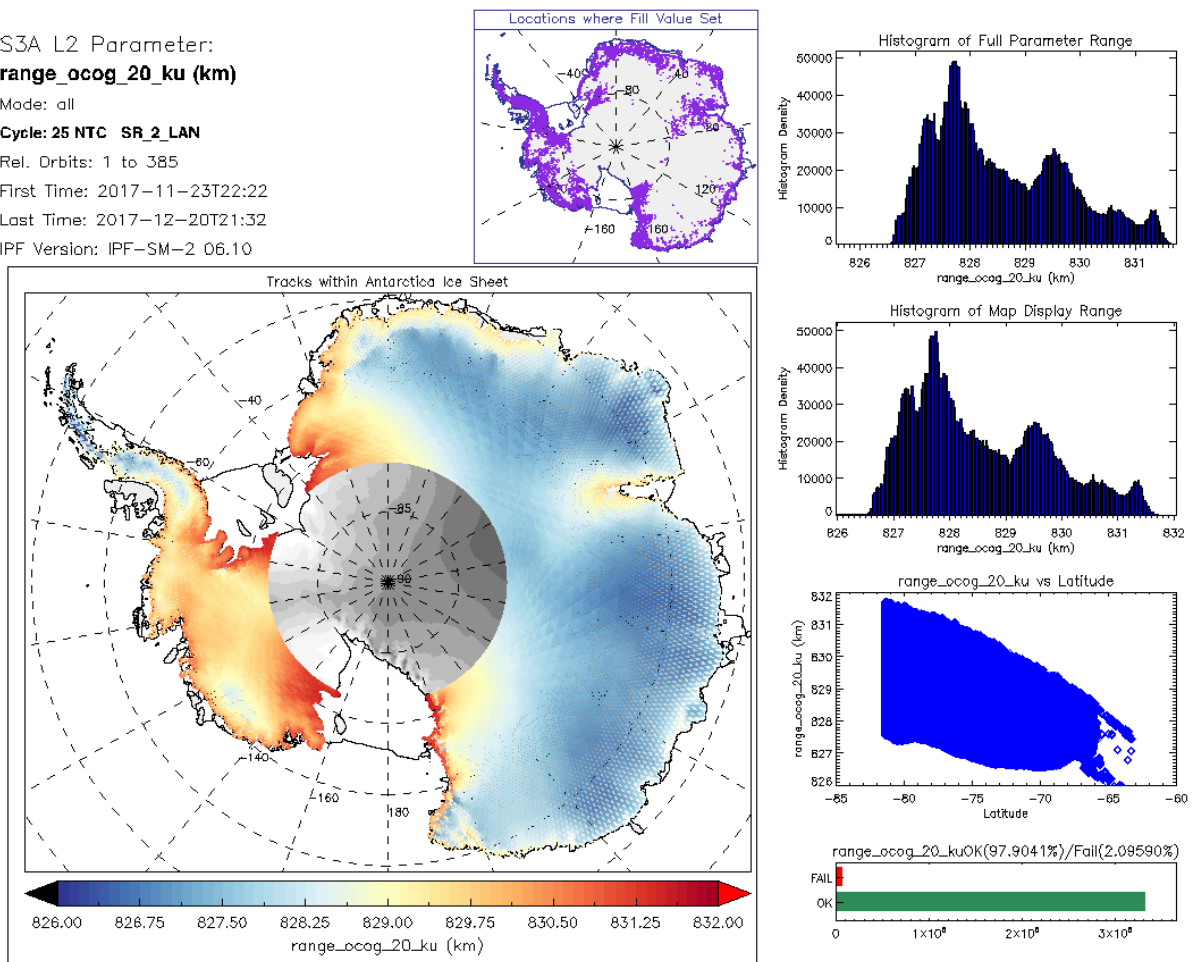
Cycle: 25 NTC SR_2_LAN

Rel. Orbits: 1 to 385

First Time: 2017-11-23T22:22

Last Time: 2017-12-20T21:32

IPF Version: IPF-SM-2 06.10



S3A L2 Parameter:
range_ocog_20_ku (km)

Mode: all

Cycle: 25 NTC SR_2_LAN

Rel. Orbits: 1 to 385

First Time: 2017-11-23T23:13

Last Time: 2017-12-20T22:22

IPF Version: IPF-SM-2 06.10

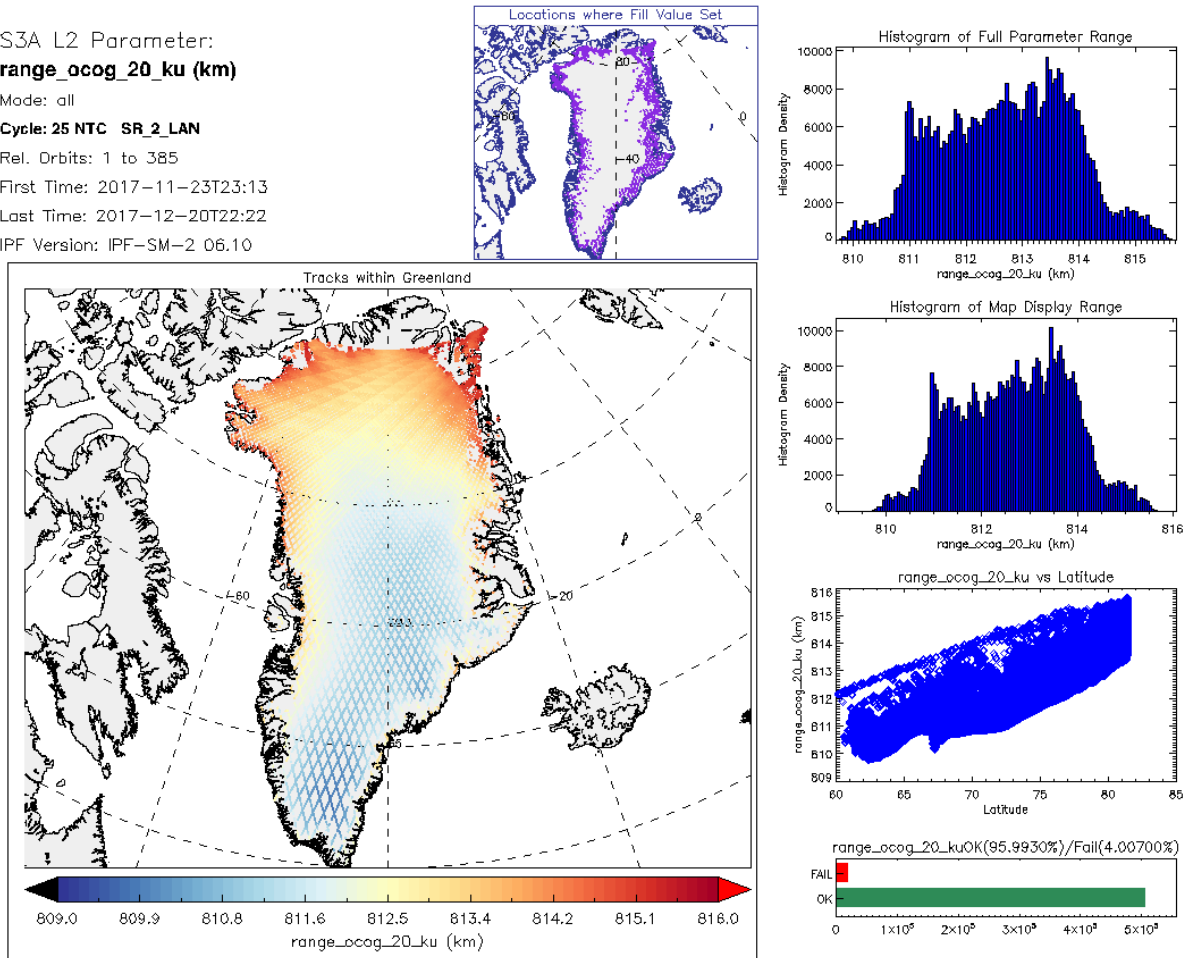


Figure 100: Maps of Ku band OCOG range, Antarctica, Greenland (Cycle 25, Nov/Dec 2017)

9.4 20Hz Ku-band Waveform Quality Flag for Ice Sheets

In the latest product baseline in 2017 (PB2.24), a new L2 parameter (waveform_qual_ice_20_ku) was added to indicate the results of a set of waveform quality tests optimized for ice sheet waveforms. Users can test the value of flag bits within this parameter to filter individual measurements or to indicate the reason for parameter failure.

Note that the Ice Sheet Elevation parameter (and associated ice sheet range and sigma0) are already filtered (with a fill value set) from the result of these waveform quality tests. Parameters derived from the Ice-1 (OCOg) retracker are not filtered, but users should use the results of the quality flag as an advisory.

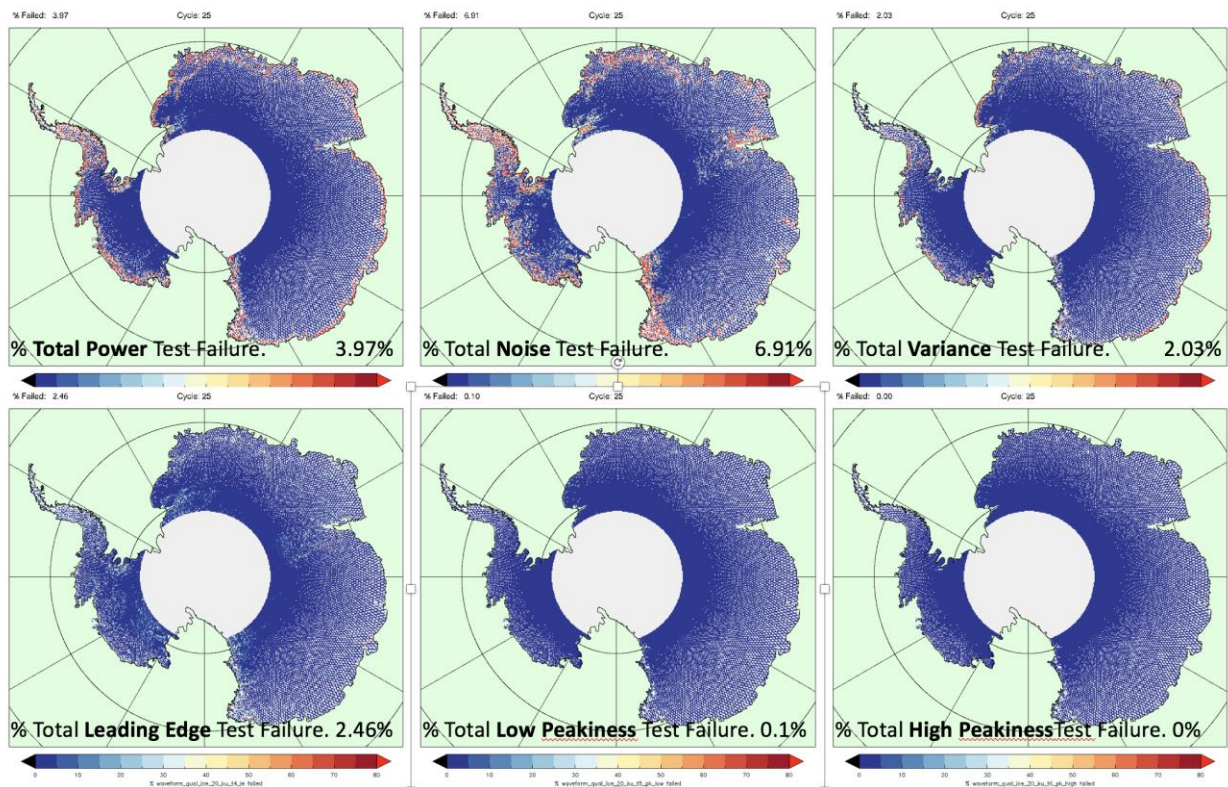
The tests comprise:

- ❖ Total power test to detect low power in the echo.
- ❖ Noise power test to detect high levels of noise at the start of the echo.
- ❖ Variance test to detect unstructured waveforms
- ❖ Leading edge detection to check waveform power distribution indicates a leading edge.
- ❖ Peakiness test to detect waveforms of too low or high peakiness value.

Users should note that in this product baseline, SAR radar echoes are not centred in the extended range window during L1 processing as required by the waveform test specification and the SAR ice margin retracker, and subsequently over regions of high slope such as the ice sheet margins the position of the waveform can move around the range window causing waveform truncation and higher rates of test failure than would be expected. This will be corrected in a future evolution of the L1 processing.

An anomaly relating to the calculation of noise power is also present in product baseline PB2.24, causing higher than expected failure rates of the noise power test. This will be fixed in the next baseline in early 2018.

Overall % quality flag failure rates shown below are higher in Greenland than in Antarctica because Greenland has a higher % area of high slope margins to low slope ice sheet in the areas shown.



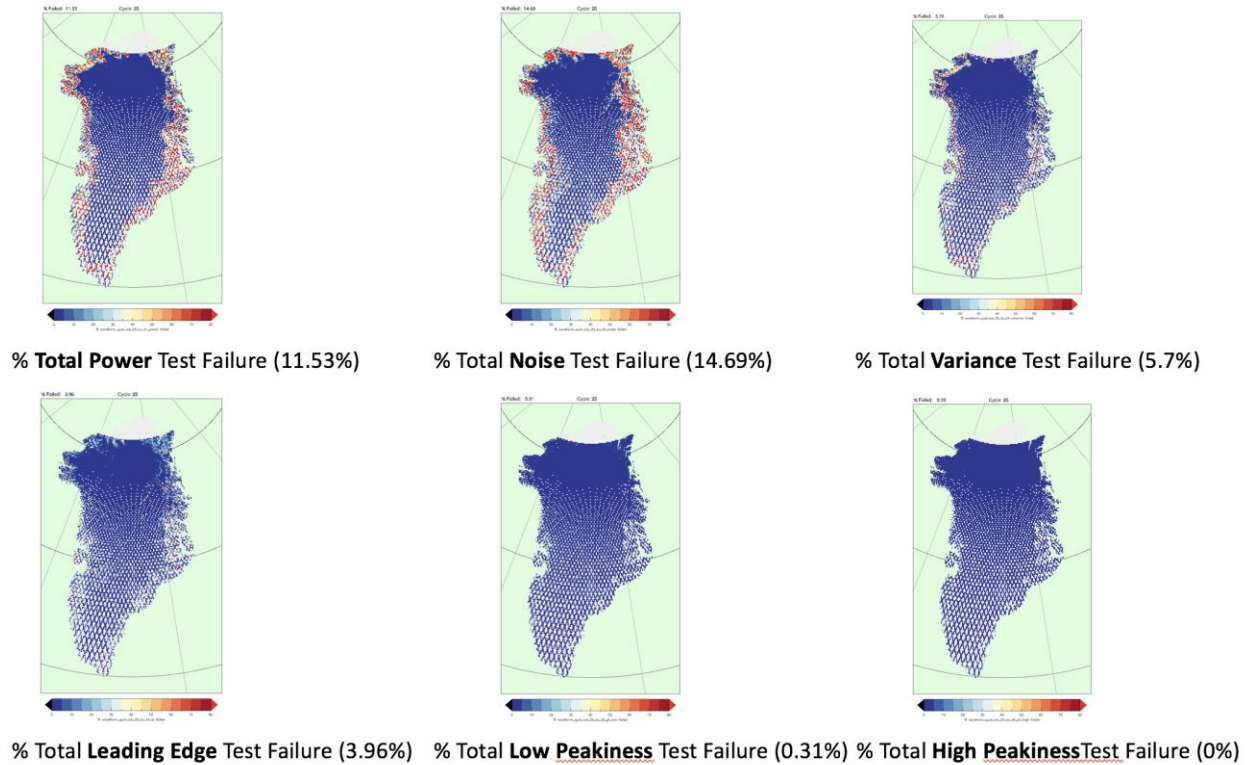


Figure 101: Maps of % 20Hz Ku Waveform Quality Flag Test Failure Densities (in 10 km² grid) for cycle 25, Antarctica and Greenland Ice Sheets

9.5 Slope Correction Assessment

A slope correction from a slope model derived from Antarctic (RAMP v2) and Greenland (Bamber 2001) DEMs is applied to 20Hz Ku band elevation over ice sheets to relocate the SAR echo to the point of closest approach across track. Note that no slope correction is performed if the SAR Ice Margin retracker fails.

In cycle 25, due to the high failure rate of the SAR Ice Margin retracker, the slope correction is not performed on more than 22 (AIS) -32 (GIS) % of range measurements over the ice sheets.

An additional error in the SAR slope correction is present in all product baselines before Processing Baseline 2.27. This causes a resulting error in elevation (of 30cm to several metres, dependent on slope) and an error in the slope corrected location down slope. This is corrected in Processing Baseline 2.27 which was deployed on 14 February 2018 and used for the Reprocessing 2.

New slope models based on latest Cryosat DEMs will be used in future evolutions of the product.

% Failed: 22.85

Cycle: 25

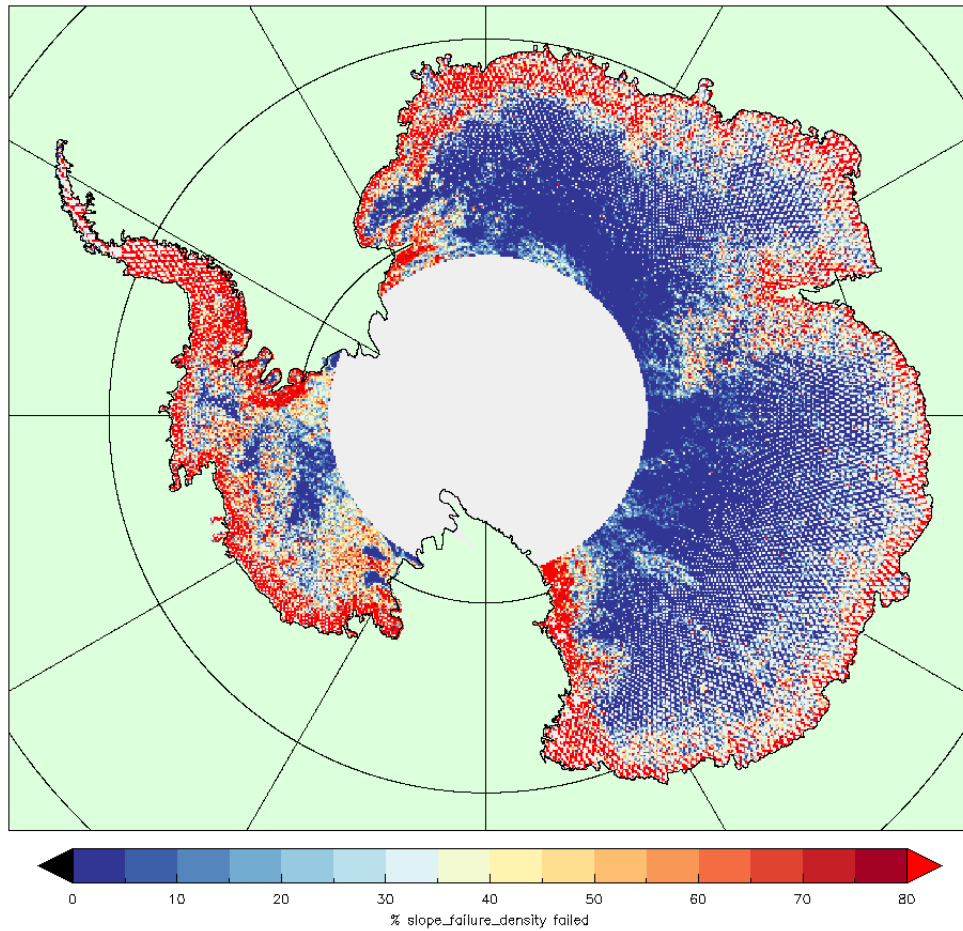


Figure 102: Maps of % Slope Correction Failure Density in a 10km grid

9.6 20Hz Ku-band Ice Sheet Range (range_ice_sheet_20_ku)

The ice sheet range is retracked using the SAR ice margin physical model retracker and is the primary range used to calculate elevation in the L2 product.

There are higher than expected rates of failure in this parameter over the ice sheet margins. An explanation of this is given in the preceding section on ice sheet elevation.

S3A L2 Parameter:
range_ice_sheet_20_ku (km)

Mode: all

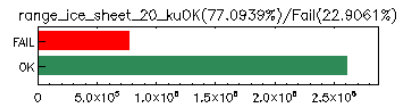
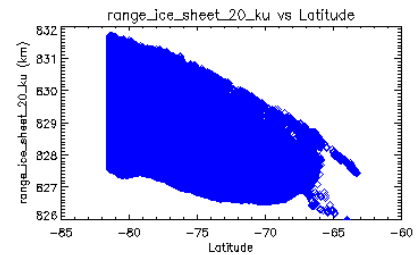
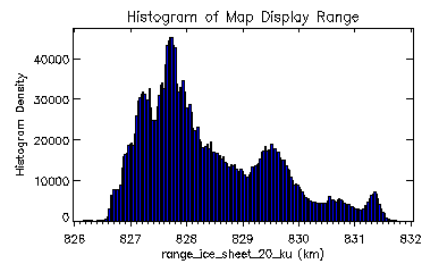
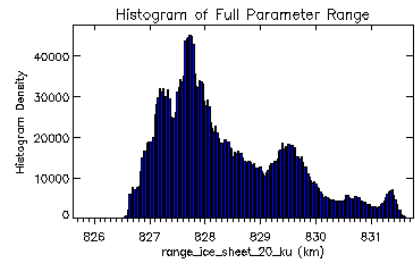
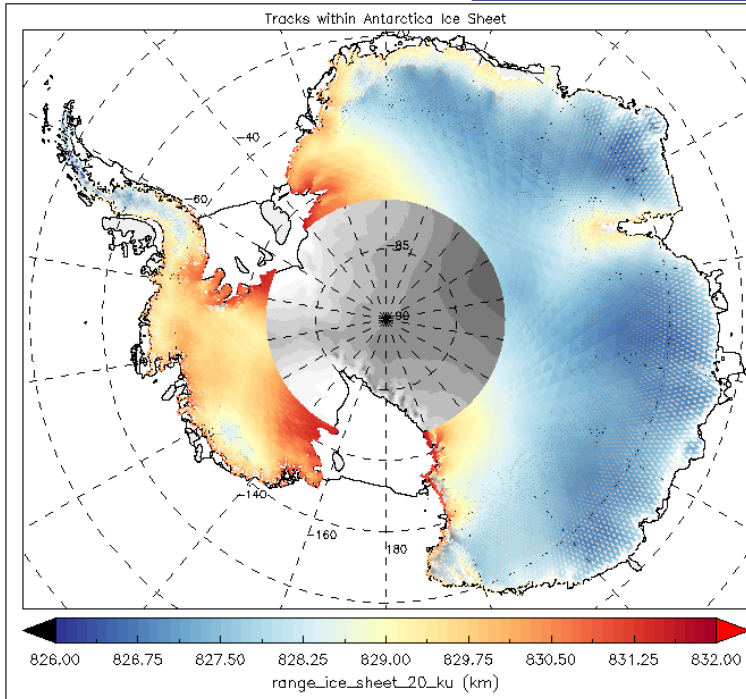
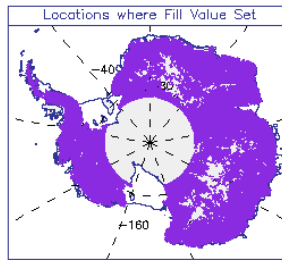
Cycle: 25 NTC SR_2_LAN

Rel. Orbits: 1 to 385

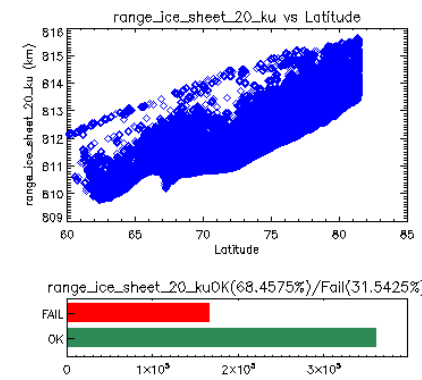
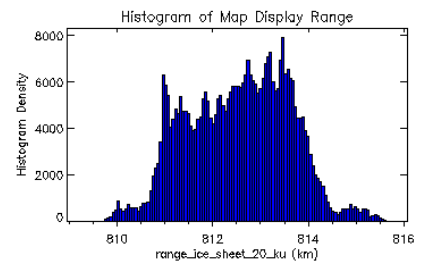
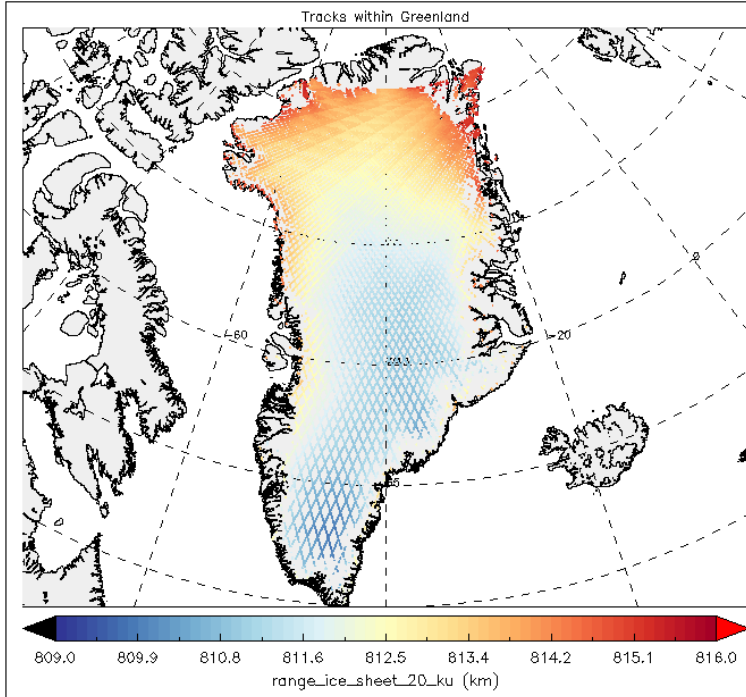
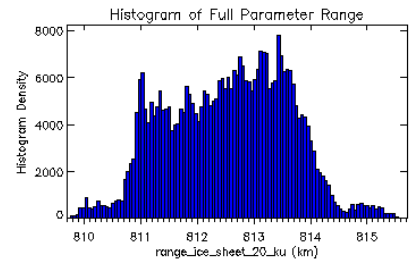
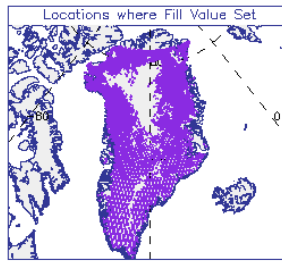
First Time: 2017-11-23T22:22

Last Time: 2017-12-20T21:32

IPF Version: IPF-SM-2 06.10



S3A L2 Parameter:
range_ice_sheet_20_ku (km)
 Mode: all
Cycle: 25 NTC SR_2 LAN
 Rel. Orbits: 1 to 385
 First Time: 2017-11-23T23:13
 Last Time: 2017-12-20T22:22
 IPF Version: IPF-SM-2 06.10

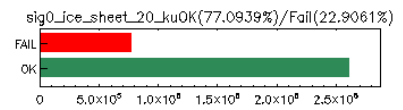
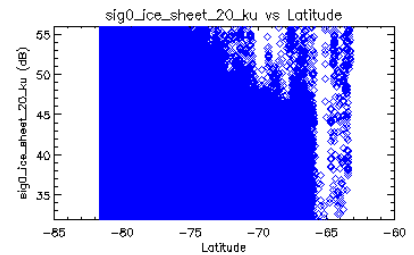
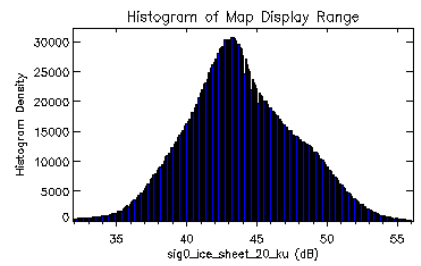
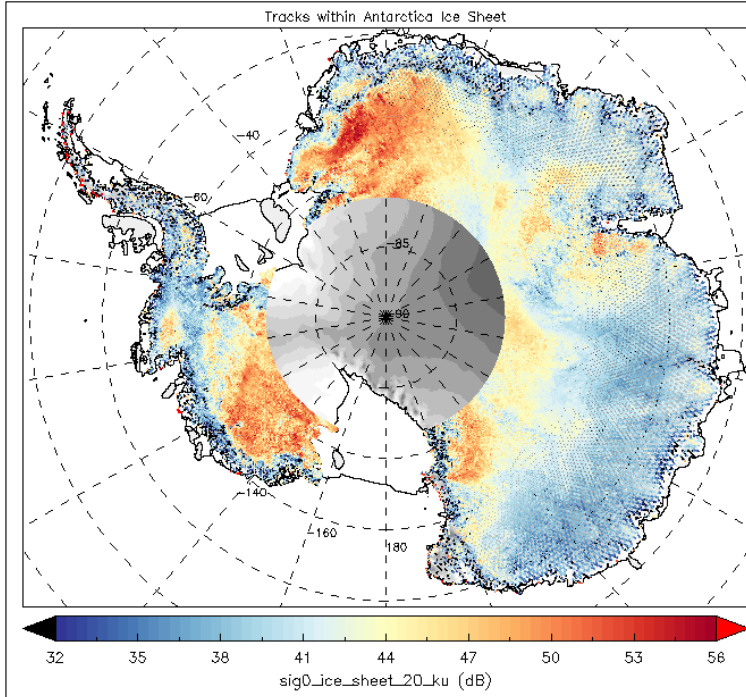
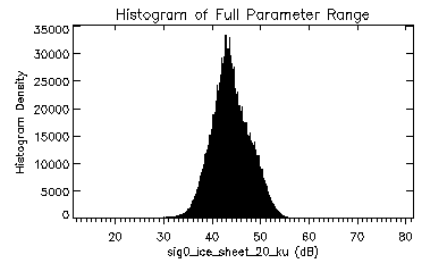
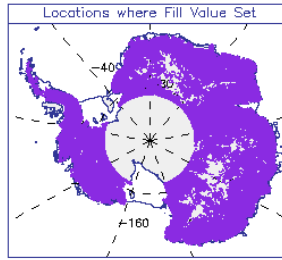


9.7 20Hz Ku Band Ice Sheet Sigma0 (sig_ice_sheet_20_ku)

The Ku band ice sheet sigma0 backscatter parameter is derived from the SAR ice margin retracker. The map of sigma0 over the ice sheets shows similar patterns of backscatter values to previous missions. Backscatter values are controlled by surface roughness characteristics, surface slope and differences in surface and volume echo. Over the ice sheet margins backscatter is low due to high surface slope, and over the East Antarctic ice sheet it is also low due to strong winds causing high surface roughness. Over the West Antarctic ice sheet and areas of Dronning Maud land there are high backscatter returns due to very smooth surfaces. In Greenland the ice sheet surface is smoother due to lower winds and regular melt events causing higher backscatter values.

There are higher than expected rates of failure in this parameter over the ice sheet margins. An explanation of this is given in the preceding section on ice sheet elevation.

S3A L2 Parameter:
sig0_ice_sheet_20_ku (dB)
 Mode: all
 Cycle: 25 NTC SR_2 LAN
 Rel. Orbits: 1 to 385
 First Time: 2017-11-23T22:22
 Last Time: 2017-12-20T21:32
 IPF Version: IPF-SM-2 06.10



S3A L2 Parameter:
sig0_ice_sheet_20_ku (dB)
 Mode: all
Cycle: 25 NTC SR_2 LAN
 Rel. Orbits: 1 to 385
 First Time: 2017-11-23T22:22
 Last Time: 2017-12-20T21:32
 IPF Version: IPF-SM-2 06.10

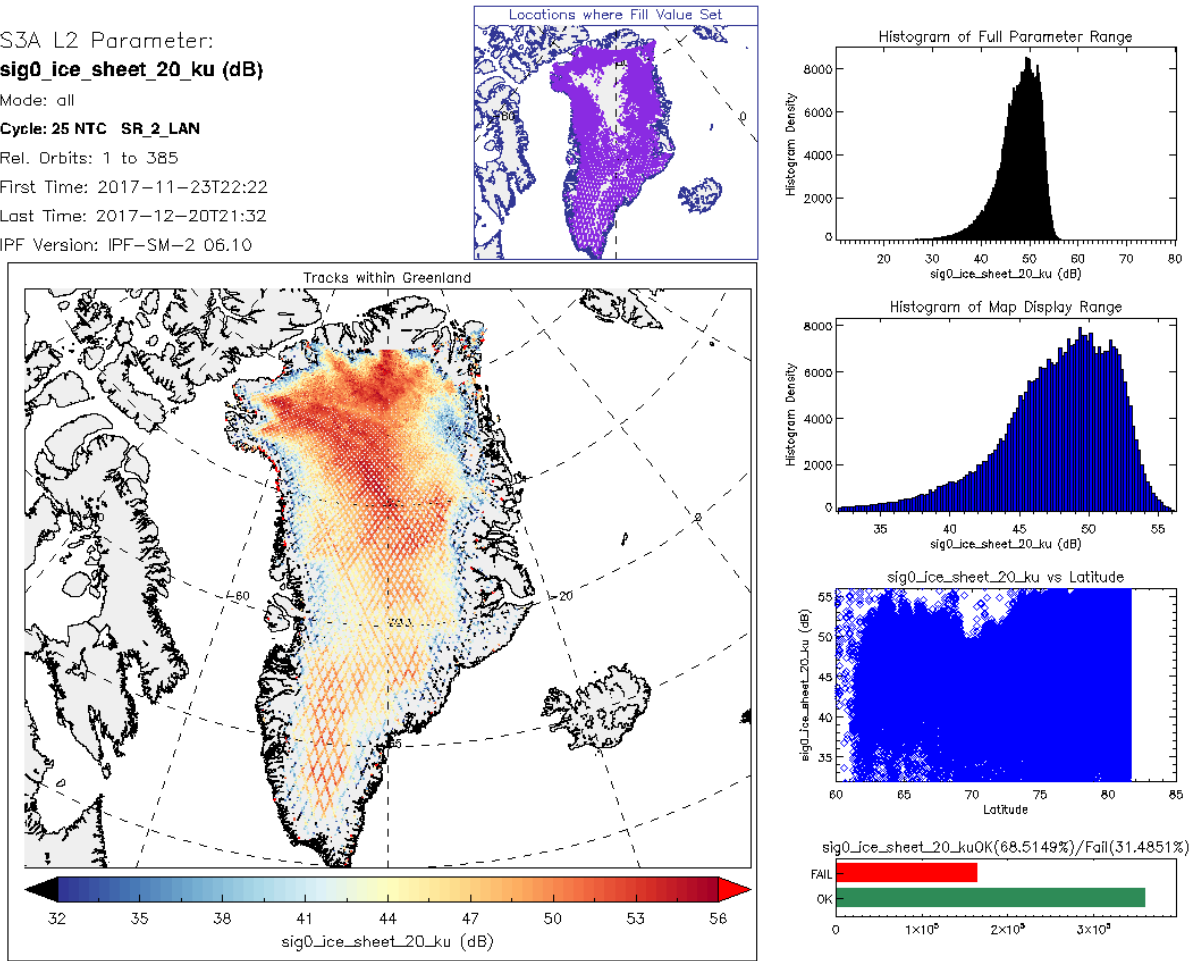


Figure 103: Maps of 20Hz Ku Band Ice Sheet Sigma0 (sig0_ice_sheet_20_ku)

9.8 20Hz Ku Band OCOG (Ice-1) Sigma0 (sig0_ocog_20_ku)

The Ku band OCOG sigma0 backscatter parameter is derived from the OCOG (Ice-1) retracker. The map of sigma0 over the ice sheets shows similar patterns of backscatter values to previous missions. Backscatter values are controlled by surface roughness characteristics, surface slope and differences in surface and volume echo. Over the ice sheet margins backscatter is low due to high surface slope, and over the East Antarctic ice sheet it is also low due to strong winds causing high surface roughness. Over the West Antarctic ice sheet and areas of Dronning Maud land there are high backscatter returns due to very smooth surfaces. In Greenland the ice sheet surface is smoother due to lower winds and regular melt events causing higher backscatter values.

There are higher than expected rates of failure in this parameter over the margins, West Antarctica and the Antarctic Peninsula, but much lower failure rates than for the SAR ice margin retracker. This is because the OCOG centre of gravity retracking algorithm will retrack a wider range of waveform shapes than the model fit approach used by the SAR ice margin retracker. This results in greater measurement density, but in some areas lower accuracy.

S3A L2 Parameter:
sig0_ocog_20_ku (dB)

Mode: all

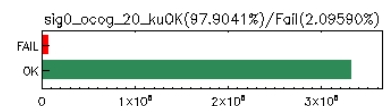
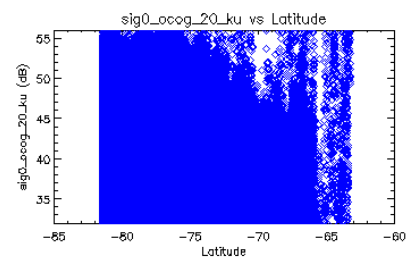
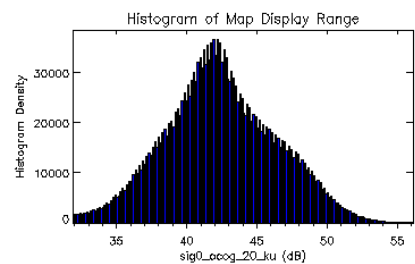
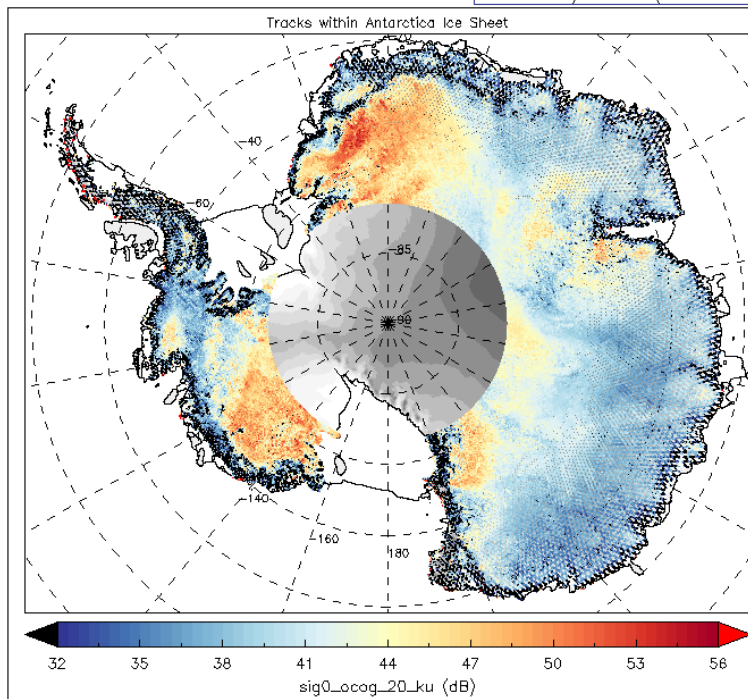
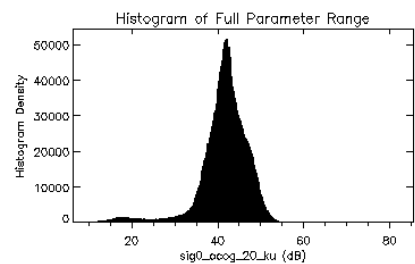
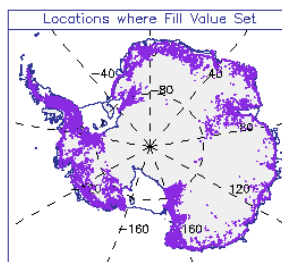
Cycle: 25 NTC SR_2_LAN

Rel. Orbits: 1 to 385

First Time: 2017-11-23T22:22

Last Time: 2017-12-20T21:32

IPF Version: IPF-SM-2_06.10



S3A L2 Parameter:
sig0_ocog_20_ku (dB)
 Mode: all
 Cycle: 25 NTC SR_2_LAN
 Rel. Orbits: 1 to 385
 First Time: 2017-11-23T23:13
 Last Time: 2017-12-20T22:22
 IPF Version: IPF-SM-2 06.10

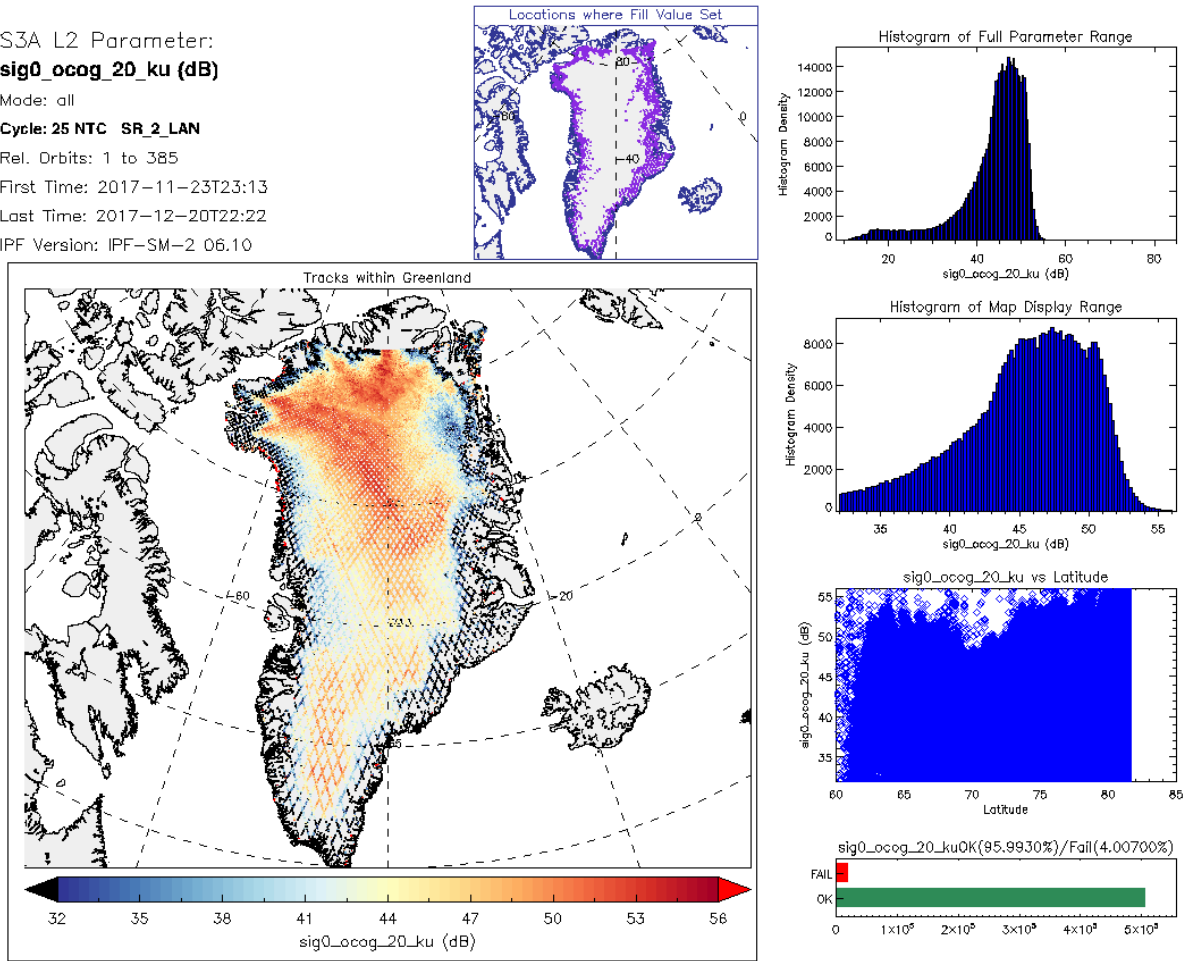


Figure 104: Maps of 20Hz Ku Band OCOG (Ice-1) Sigma0 (sig0_ocog_20_ku)

9.9 20Hz Ku Band PLRM Ice Range (range_ice_20_plrm_ku)

Range measurements derived from the PLRM waveforms and Ice2 retracker show similar but slightly higher failure rates than for the SAR OCOG retracked range.

Note that PLRM measurements are referenced to C-band (and not Ku-band) time in the L2 product.

S3A L2 Parameter:

range_ice_20_plrm_ku (km)

Mode: all

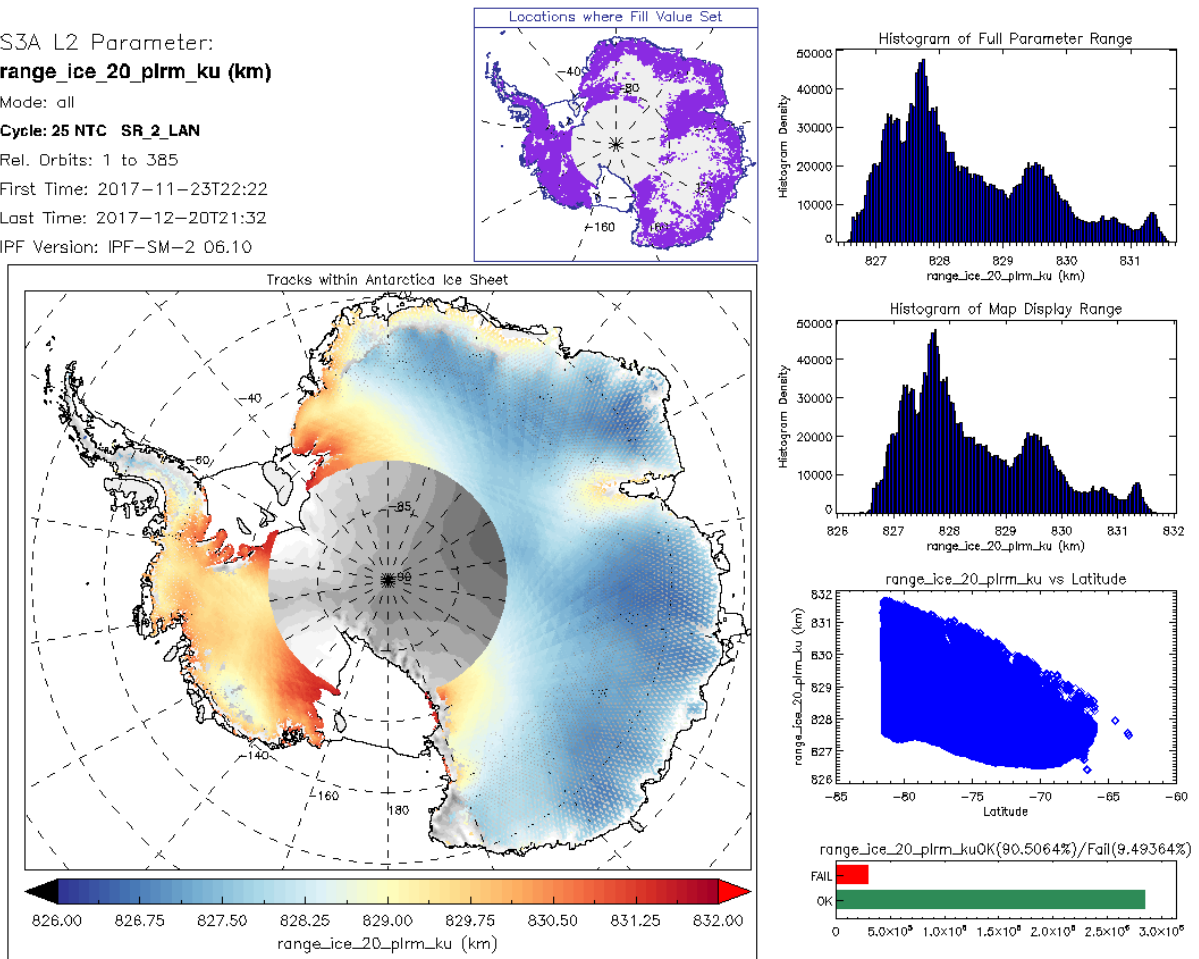
Cycle: 25 NTC SR_2_LAN

Rel. Orbits: 1 to 385

First Time: 2017-11-23T22:22

Last Time: 2017-12-20T21:32

IPF Version: IPF-SM-2_06.10



S3A L2 Parameter:
range_ice_20_plrm_ku (km)
 Mode: all
 Cycle: 25 NTC SR_2 LAN
 Rel. Orbits: 1 to 385
 First Time: 2017-11-23T23:13
 Last Time: 2017-12-20T22:22
 IPF Version: IPF-SM-2 06.10

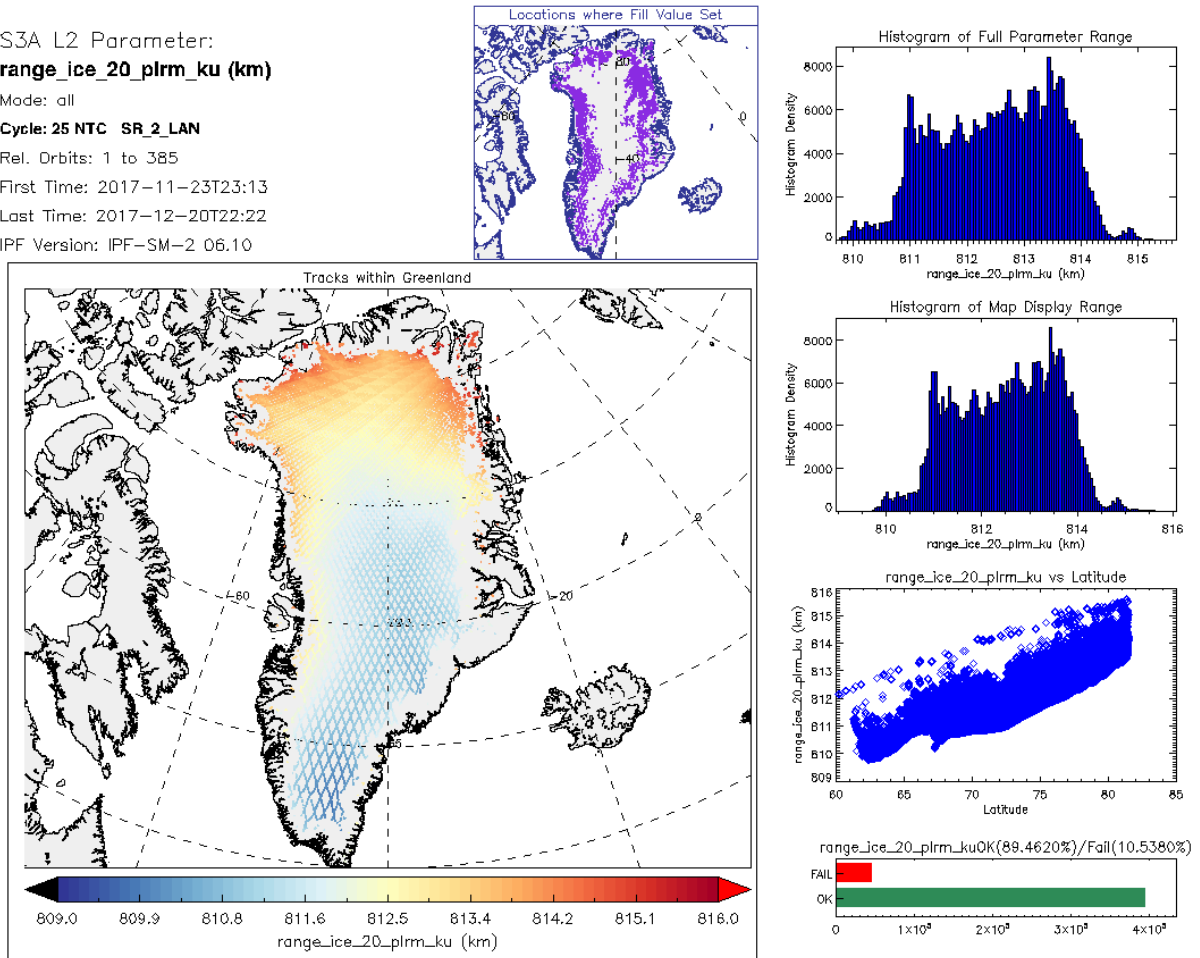


Figure 105: Maps of 20Hz Ku Band PLRM Ice Range (range_ice_20_plrm_ku)

9.10 20Hz Ku Band PLRM Sigma0 (sig0_ice_20_plrm_ku)

Backscatter sigma0 derived from the 20Hz Ku PLRM waveforms are shown below.

Note that PLRM measurements are reference to C-band (and not Ku-band) time in the L2 product.

S3A L2 Parameter:

sig0_ice_20_plrm_ku (dB)

Mode: all

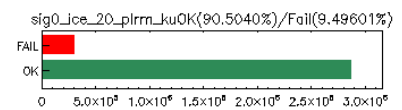
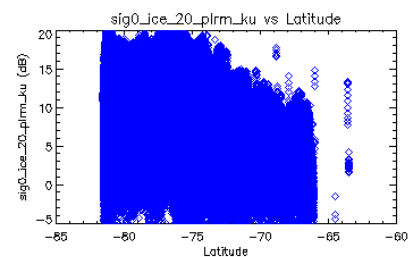
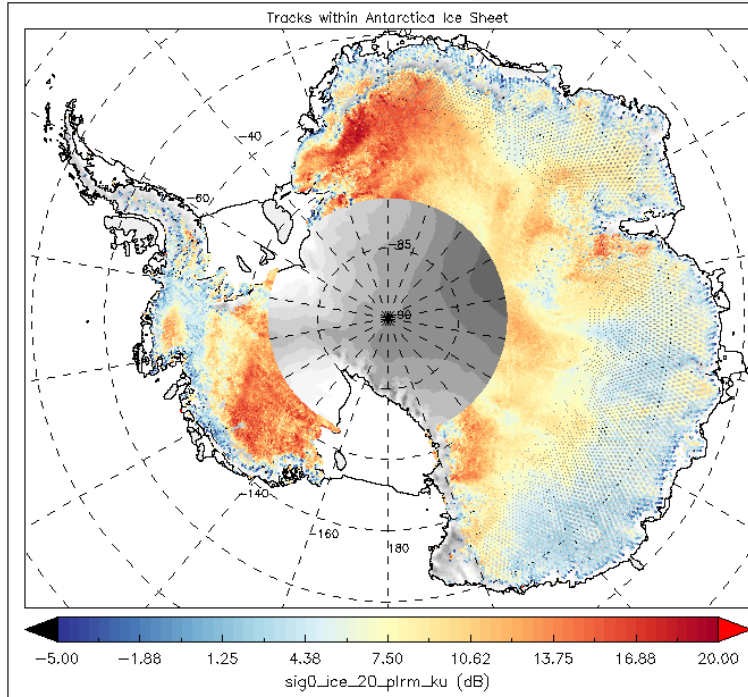
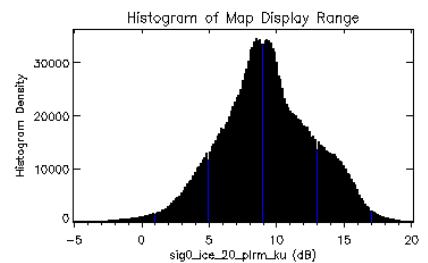
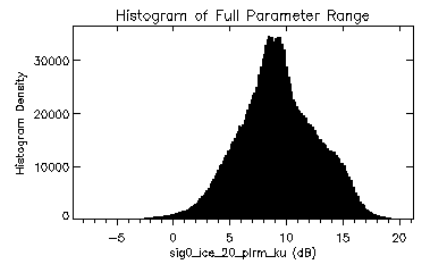
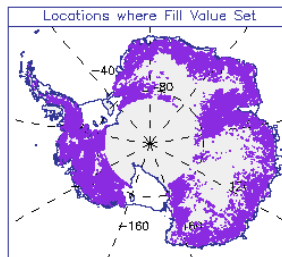
Cycle: 25 NTC SR_2_LAN

Rel. Orbits: 1 to 385

First Time: 2017-11-23T22:22

Last Time: 2017-12-20T21:32

IPF Version: IPF-SM-2 06.10



S3A L2 Parameter:
sig0_ice_20_plrm_ku (dB)
 Mode: all
 Cycle: 25 NTC SR_2_LAN
 Rel. Orbits: 1 to 385
 First Time: 2017-11-23T23:13
 Last Time: 2017-12-20T22:22
 IPF Version: IPF-SM-2 06.10

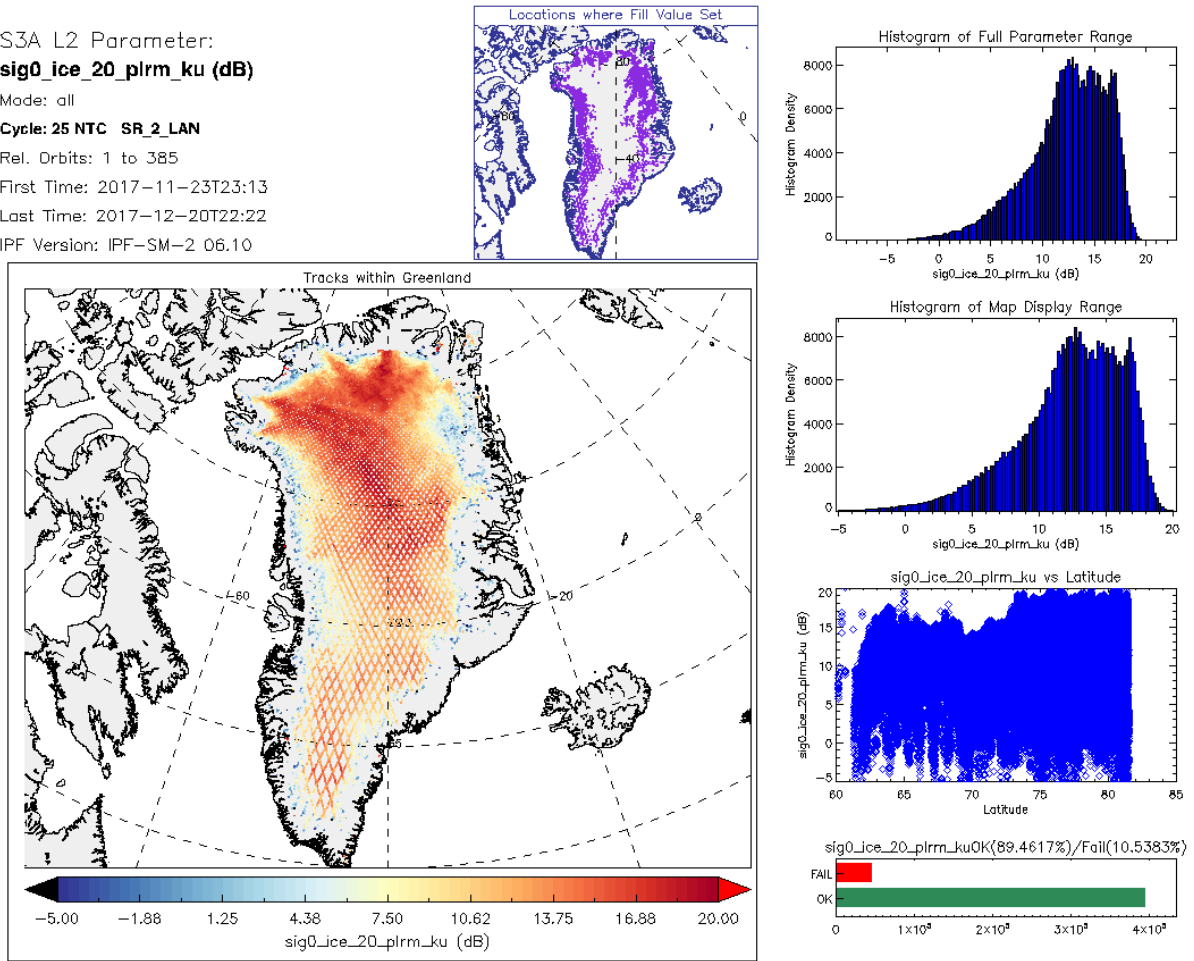


Figure 106: Maps of 20Hz Ku Band PLRM Sigma0 (sig0_ice_20_plrm_ku)

9.11 20Hz Ku Band Surface Class (surf_class_20_ku)

The 20Hz Ku surface classification parameter is derived from MODIS and GlobCover data. Users of the data requiring high resolution ice sheet glacier grounding line and calving front locations should consider applying their own surface type masks.

Flag: surf_class_20_ku

Mode: all

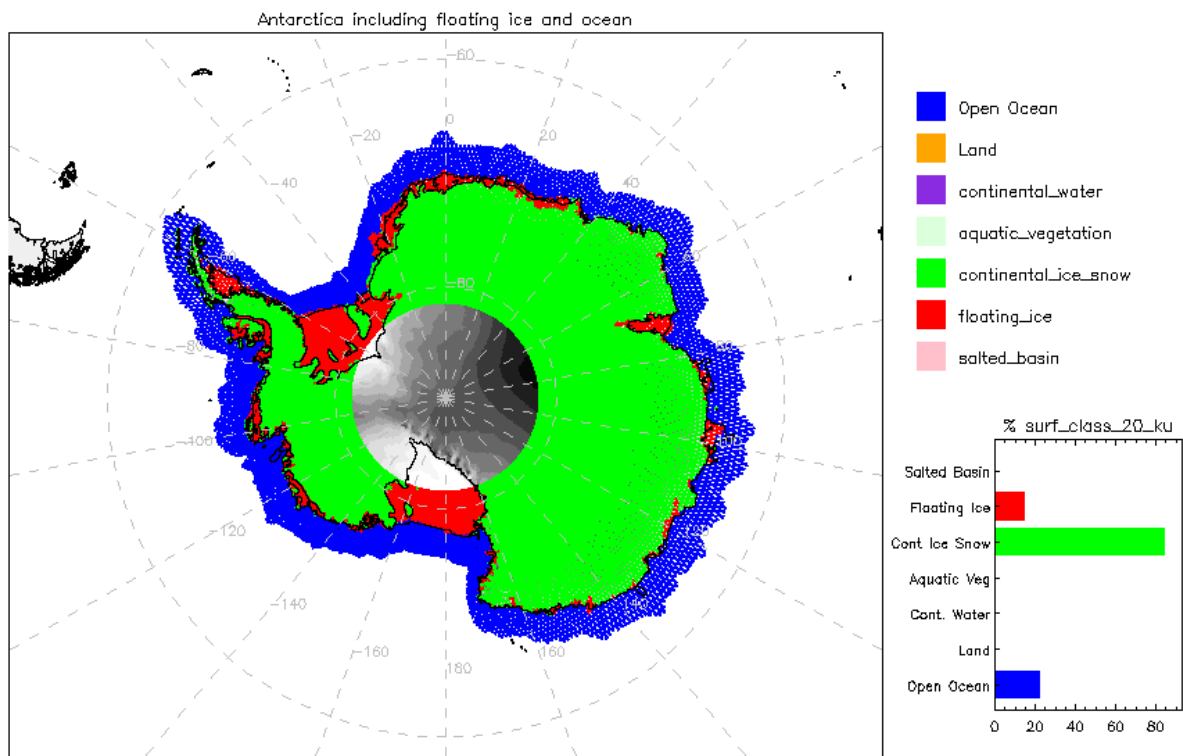
Cycle: 25 NTC SR_2_LAN

Rel. Orbits: 1 to 385

First Time: 2017-11-23T22:22

Last Time: 2017-12-20T21:32

IPF Version: IPF-SM-2 D6.10



Flag: surf_class_20_ku

Mode: all

Cycle: 25 NTC SR_2_LAN

Rel. Orbits: 1 to 385

First Time: 2017-11-23T22:22

Last Time: 2017-12-20T21:32

IPF Version: IPF-SM-2 D6.10

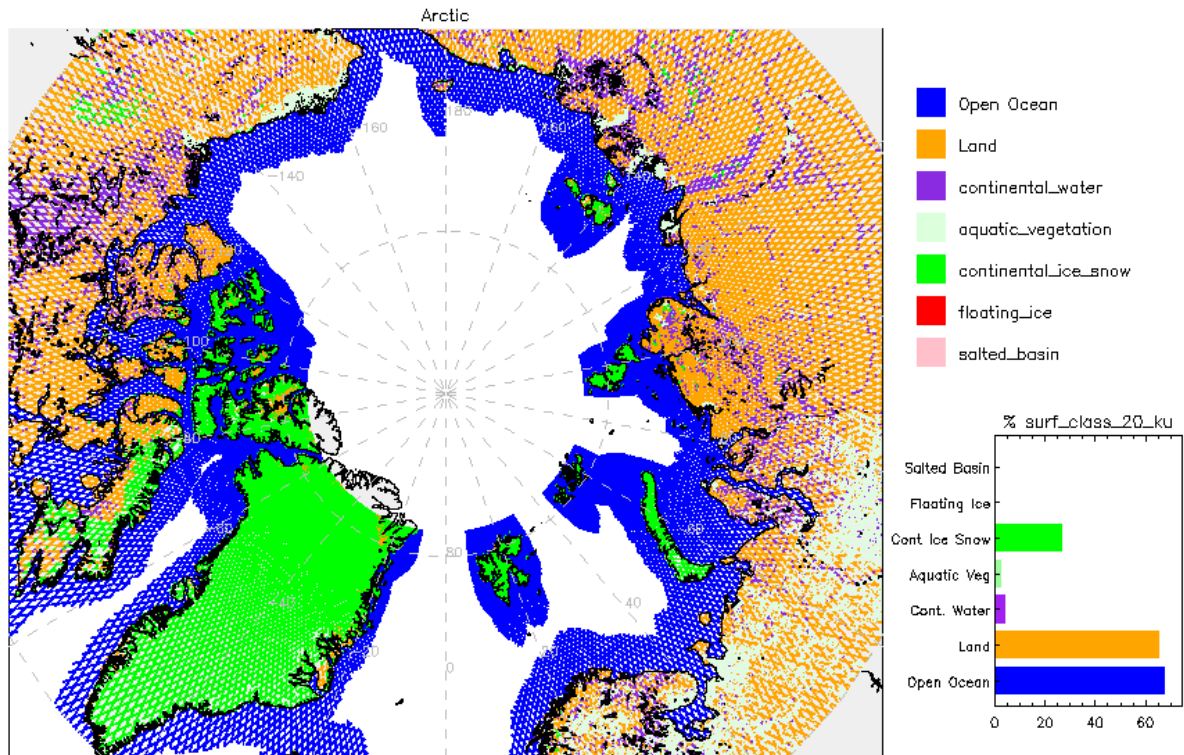


Figure 107: Maps of 20Hz Ku Band Surface Class (surf_class_20_ku)

9.12 Availability of Geophysical Corrections over Ice Sheets (NTC Products)

For polar ice sheets, the primary geophysical corrections applied to the range are model dry tropospheric, model wet tropospheric, GIM ionospheric, solid earth tide, pole tide and ocean loading tide. We would normally expect 100% availability of all corrections except the altimeter derived ionospheric corrections (iono_cor_alt_01_ku, iono_cor_alt_20_ku).

For the latest product baseline in 2017 (PB2.24, cycle 25 NTC) the percentage of non-available geophysical corrections over Antarctic ice sheets was:

Cycle: 25 NTC SR_2_LAN

Rel. Orbits: 1 to 385
 First Time: 2017-11-23T22:22
 Last Time: 2017-12-20T21:32
 IPF Version: IPF-SM-2 06.10

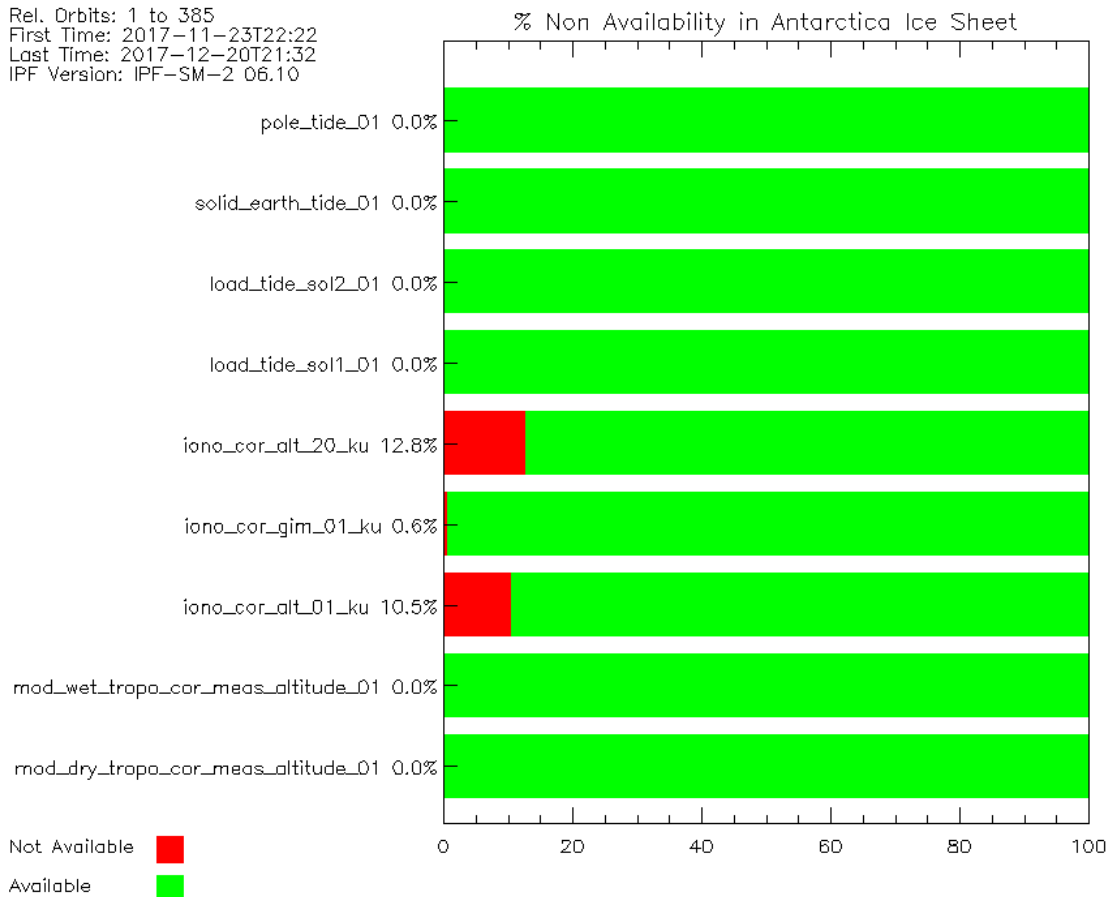
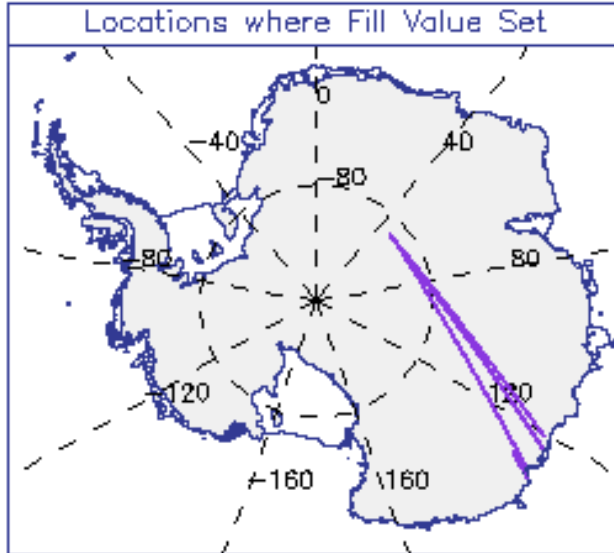


Figure 108: Percentage of Geophysical Correction Non-availability over Antarctic Ice Sheets

The GIM ionospheric correction has been found to be missing from several orbits over Antarctica:



For the latest product baseline in 2017 (PB2.24, cycle 25 NTC) the percentage of non-available geophysical corrections over the Greenland ice sheet was:

Cycle: 25 NTC SR_2_LAN

Rel. Orbits: 1 to 385
 First Time: 2017-11-23T22:22
 Last Time: 2017-12-20T21:32
 IPF Version: IPF-SM-2 06.10

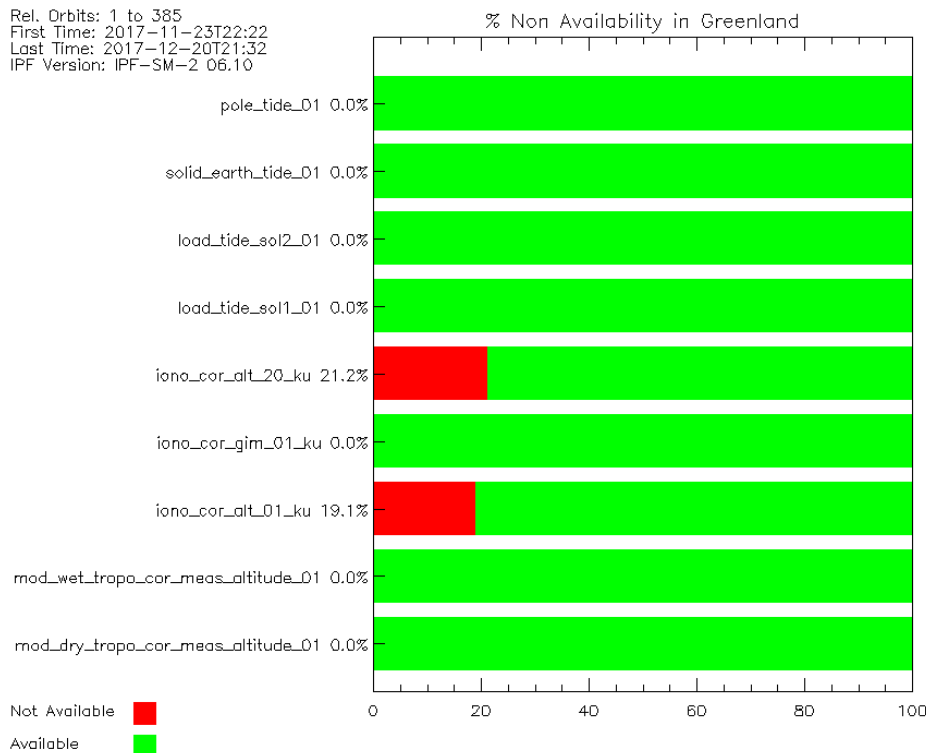


Figure 109: Percentage of Geophysical Correction Non-availability over the Greenland Ice Sheet

9.13 Availability of Geophysical Corrections over Ice Shelves (NTC Products)

For polar ice shelves, the primary geophysical corrections applied to the range are as for ice sheets plus ocean tide and inverse barometric corrections.

For the latest product baseline in 2017 (PB2.24, cycle 25 NTC) the percentage availability of geophysical corrections over Antarctic ice shelves was:

Cycle: 25 NTC SR_2_LAN

Rel. Orbits: 1 to 385
 First Time: 2017-11-23T22:22
 Last Time: 2017-12-20T21:32
 IPF Version: IPF-SM-2 06.10

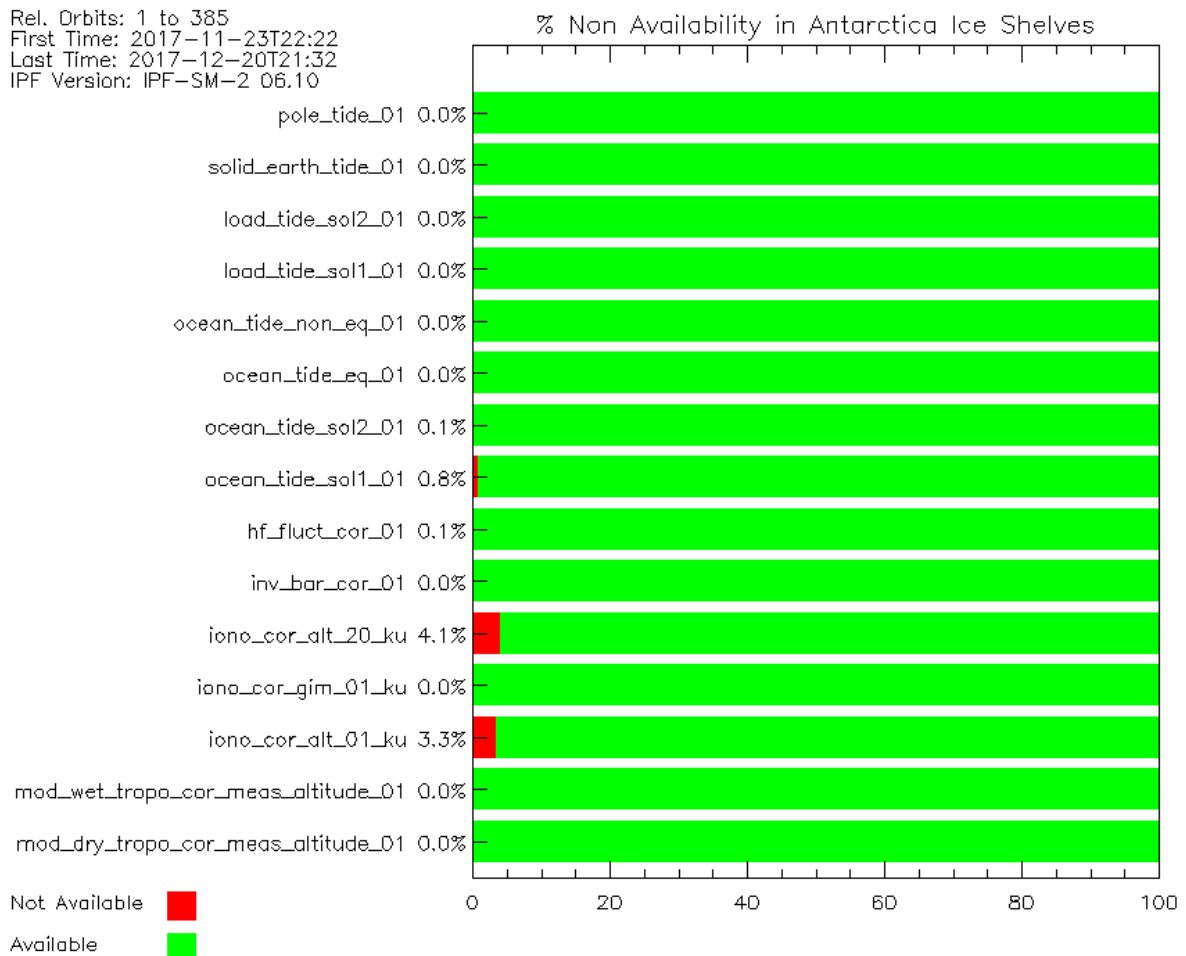


Figure 110: Availability of Geophysical Corrections over Antarctic Ice Shelves

For ice shelf studies it is recommended that users replace the ocean tide correction (Ocean Tide Solution 2 in cycle 25) where it is valid in the L2 NTC products over Antarctic ice shelves with a more accurate high resolution circumpolar ocean tide model correction such as the Circum Antarctic Tidal Simulation (CATS 2008a), Padman et al (2008).

	Sentinel-3 MPC S3MPC STM Annual Performance Report - Year 1	Ref.: S3MPC.CLS.APR.002 Issue: 1.1 Date: 23/05/2018 Page: 143
---	--	--

10 Performance Mission over Inland waters

10.1 Products used for the analysis

Validation has been performed in 2017 with NTC L2 Land products generated with IPF 6.07 from cycles 6 to 20 (more than one year of data). This analysis showed that the two problems below which were identified by LEGOS in the IPF 6.05 products have now been solved with the new version of the processing.

- ❖ OCOG range set to onboard tracker range when the retracker not activated
- ❖ OCOG is not as robust as expected, with a lot of failure observed compared to the ocean retracker

The third reported observation has not been taken into account (as it does not impact the performance of the retracked range, but only the raw measurements, ie the waveforms):

- ❖ The “tracker range” evolves by “steps”. This makes the leading edge discontinuous in the radargrams even when it could be continuous (as on the smooth surfaces of land ice sheets or lakes)

This latter behavior will be corrected in future evolutions of the SRAL ground processor.

10.2 Validation over Issykkul lake

LEGOS experts report results from in-situ measurements available over the lake Issykkul (4 sentinel-3A tracks intersect this large lake, see Figure 111 below):

- ❖ Continuous measurements which are available for each overpass of the Sentinel3-A satellite. They allow us to assess the precision of Sentinel-3A over about a one-year long period (from cycle 5 to cycle 16, see Figure 112).
- ❖ Measurements performed during dedicated campaigns, one in October 2016, the other in July 2017. These campaigns allow us to assess the absolute bias of Sentinel-3 (see Figure 113) and also show that the SAR mode available on Sentinel-3A provide accurate measurement very close to the coast of the lake.

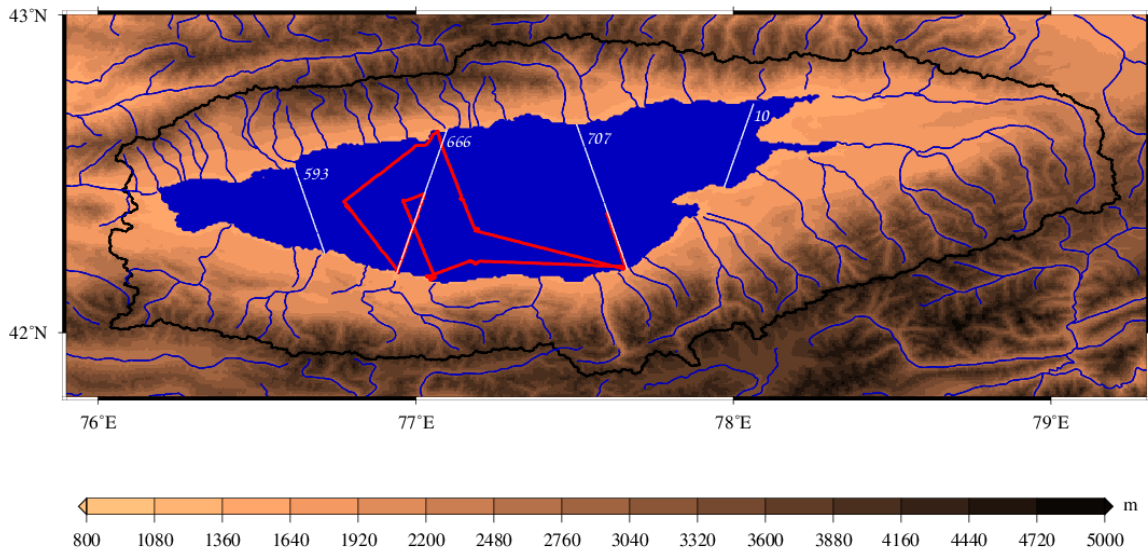


Figure 111 Campaign done in 2016 (October).
Track 666 and 707 were followed by the boat carrying the GPS receiver.

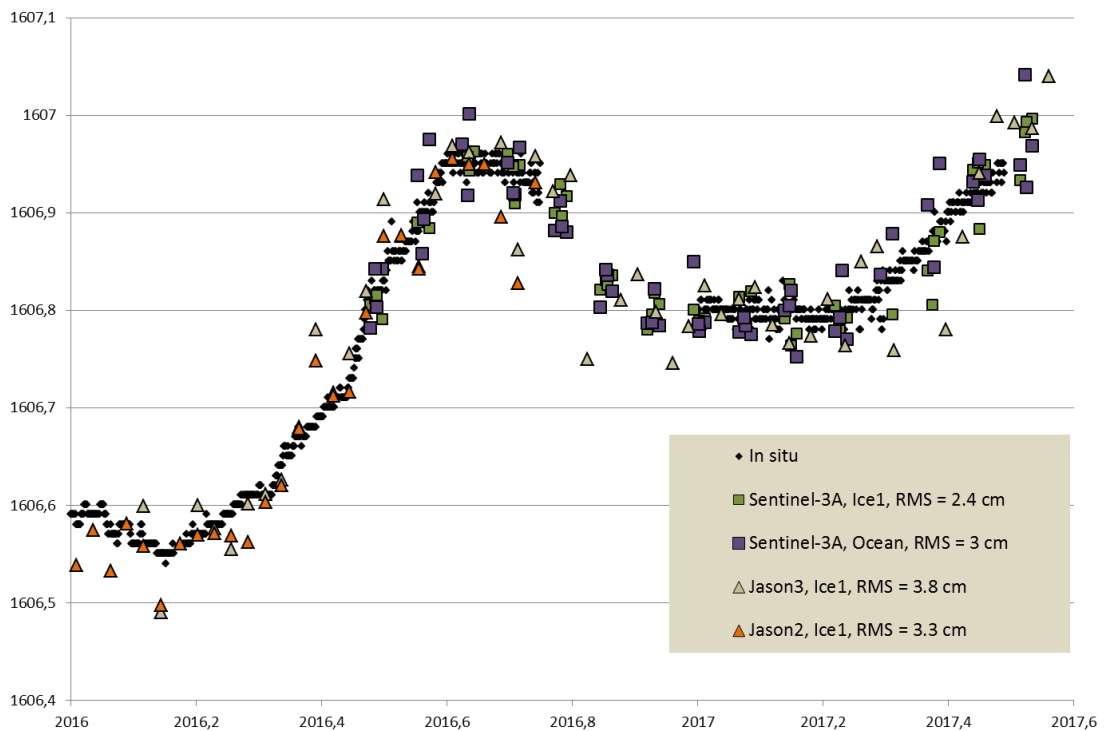


Figure 112 Accuracy of Jason2, Jason-3 and Sentinel-3A determined over the period from January 2016 to July 2017 using satellite water height of the lake at each pass and the in situ measurements of the permanent gauge.

The Figure 112 shows the Sentinel-3A data compared to in-situ measurements and to Jason2 and Jason3 measurements over a common period. A constant bias has been removed from each time series as the absolute bias calibration is done differently as described in next paragraph.

As seen on Figure 112, the results from the ice1 (OCOG) retracker are more precise (2.4 cm rms) than those of the ocean retracker (3 cm rms). This has already been observed for other missions as the ice1 retracker proves very robust for non-standard waveforms such as those encountered frequently over inland waters.

The second observation is that the precision of Sentinel-3A data is very good (2.4 cm rms) even when compared to the Jason2 measurements (3.3 cm rms).

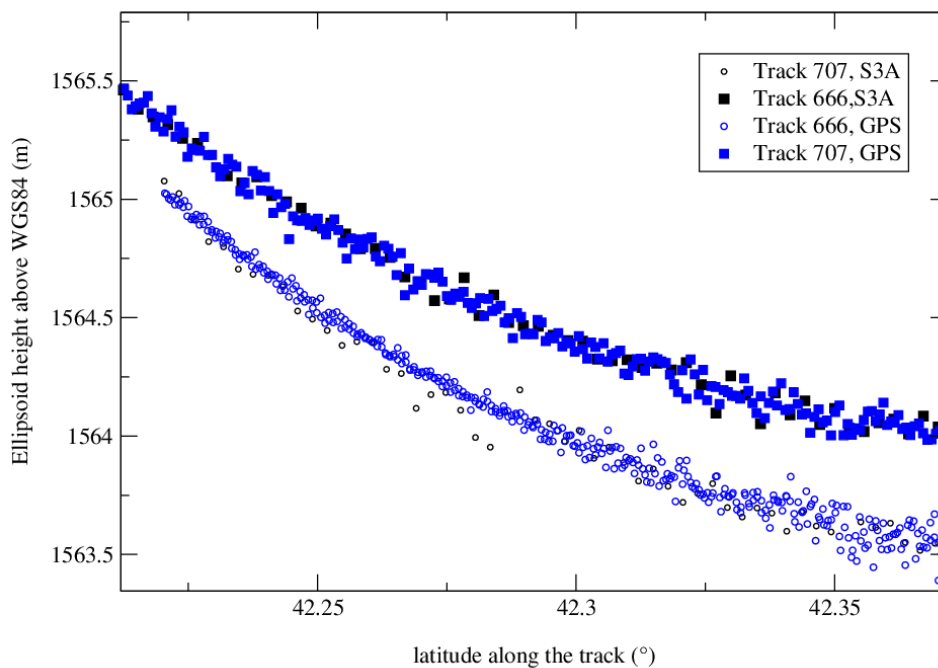


Figure 113 Absolute bias of Sentinel-3A with the tracker ocean over the cycle 9 (October 2016) for the two tracks (666 and 707) where the boat has measured the water height above ellipsoid at the date of pass of the satellite. The absolute bias observed was -14 +/-20 mm)

The Figure 113 shows the comparison between Sentinel-3A measurements and height of the lake surface measured from a boat cruising along the same track at the same time (except for the duration of the cruise induced by the slower speed of the boat).

The atmospheric corrections have been carefully computed and characterized thanks to in-situ measurements available during the campaigns.

This result is remarkably good with an absolute bias on the SSH for the ocean retracker of -1.4 cm +/- 2 cm. For the OCOG retracker, an absolute bias of +28.5 cm +/- 2 cm is observed. Even if this bias is higher than the ocean retracker bias, the OCOG bias is of the same order of magnitude than what is observed for the OCOG retracker with other missions.



10.3 Behaviour of the OLTC (open loop Tracking Command)

Sentinel3 altimeter can be operated in two tracking modes:

1. In the classic, so-called Close Loop mode (CL), the altimeter defines autonomously the position of the tracking window so that the radar is indeed tracking the surface.
2. In the new, so-called Open Loop mode (OL), the altimeter uses tables giving the surface altitude for each position along-track to compute the position of the tracking window. In this process, it uses the position of the satellite estimated in real time onboard.

The aim of the OL mode is to overcome some problems observed over continental surfaces when the altimeter is in CL mode. First, the tracking can be lost when there is a rapid modification of the topography, this implies that the measurements are interrupted. Second, even if the instrument is able to keep tracking, the tracking window can be positioned so that the altimeter is not observing a river but the surrounding topography. Using the OL mode can force the altimeter to observe the river. However, it requires that the knowledge of the water surface is known with an accuracy of about +/- 10 meters.

During the commissioning of Sentinel3 early 2016, we have defined a database of hydrology targets over Europe that were used to build the version 4.2 of the OLTC onboard tables.

During this year we have assessed the accuracy over Europe. It was found that the fraction of targets that were correctly observed in the CL mode is between 57 % (France) and 73 % (Europe). These figures are comparable with what is observed on other missions. The percentage is smaller over France because we have computed targets over smaller rivers in France than in the other parts of Europe (because we had available a public hydrology database with better resolution over France).

With more than one year of data in OL mode, these fractions become 83% (France) and 98% (Europe, larger rivers). This is much better than with the classic Close Loop mode and it is expected that the improvement will be much higher when the density of the target database will be improved (defining more small targets).

It has to be noted that narrow rivers (between 100 and 200 meters wide) which were never observed when the Sentinel3 altimeter were operated in CL mode (during the very first cycles of the commissioning phase) are now observed when the Open Loop mode was activated. And since then, they have been observed for all the overpasses.



11 Range and Sea Level Absolute calibration

11.1 Calibration with Crete transponder

isardSAT has processed the TRP data from a list of L1A products. The L1A products are official products from PDGS centres, processed with IPF-SR-1 version 06.11.

The range bias results are of the order of millimetres. The datation bias is of the order of hundreds of microseconds.

The analysis has been completed for Cycles 3 to 26 except cycle 5 (due to lack of L2 data), cycle 13 (TRP not switched on due to heavy snowing conditions) and cycle 21 (TRP not switched on due to high temperatures).

Table 11 and Table 12 present the results from the TRP passes processing. The range bias is computed as measured minus theoretical. The results show a positive range bias, 7.72 mm larger than expected (elevation 7.72 mm shorter than expected), and a datation bias of -161.90 microseconds, both extracted from the minimisation of the RMS between theoretical and measured series, and from the stack misalignment estimation. They also show a ~ 0.77 mm stack noise.



Sentinel-3 MPC
S3MPC STM Annual Performance
Report - Year 1

Ref.: S3MPC.CLS.APR.002
 Issue: 1.1
 Date: 23/05/2018
 Page: 148

Cycle	Date	Range bias [mm]	Datation bias [microseconds]	Alignment [mm/beam]	Noise [mm]	IPF-SR-1 Version
3	2016/04/09	2.53	-140.07	-0.08	0.35	06.11
4	2016/05/06	18.77	-114.60	-0.07	0.36	06.11
5	Lack of L2 data.					
6	2016/06/29	0.83	-152.81	-0.07	0.93	06.11
7	2016/07/26	-2.68	-152.81	-0.08	0.99	06.11
8	2016/08/22	-0.20	-127.34	-0.10	0.78	06.11
9	2016/09/18	1.24	-216.48	-0.13	0.73	06.11
10	2016/10/15	8.64	-178.27	-0.12	0.61	06.11
11	2016/11/11	19.90	-140.07	-0.09	0.82	06.11
12	2016/12/08	22.30	-127.34	-0.08	0.77	06.11
13	Transponder not switched on due to heavy snow.					
14	2017/01/31	26.01	-140.07	-0.09	0.73	06.11
15	2017/02/27	2.47	-152.81	-0.10	0.85	06.11
16	2017/03/26	-0.09	-216.48	-0.14	0.78	06.11
17	2017/04/22	12.75	-191.01	-0.12	0.40	06.11
18	2017/05/19	28.34	-127.34	-0.06	1.10	06.11
19	2017/06/15	-5.11	-203.74	-0.10	1.22	06.11
20	2017/07/12	-16.79	-127.34	-0.10	0.70	06.11
21	Transponder not switched on due to high temperatures.					
22	2017/09/04	18.61	-178.27	-0.12	0.72	06.11
23	2017/10/01	11.39	-152.81	-0.10	0.72	06.11
24	2017/10/28	0.31	-229.21	-0.15	0.92	06.11
25	2017/11/24	15.63	-203.74	-0.15	0.83	06.11
26	2017/12/21	-2.65	-127.34	-0.06	0.79	6.11
Mean		7.72	-161.90	-0.10	0.77	-
Standard Deviation		11.76	35.60	0.03	0.22	-

Table 11: Results of TRP passes processing

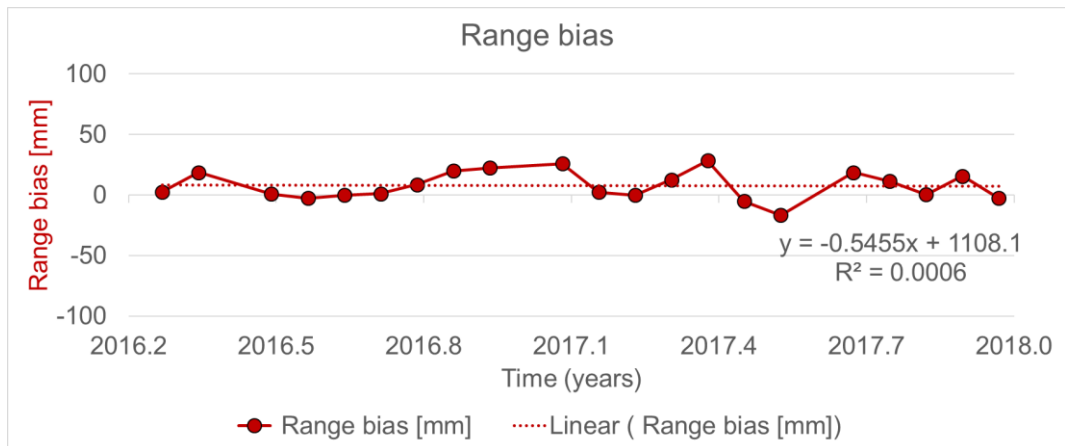
Regarding the geophysical corrections, the ionospheric and wet/dry tropospheric corrections were extracted from the transponder auxiliary files provided by the MPC team.

Then, the solid earth, geocentric tide and ocean loading corrections are selected from the L2 products. A table with the Geophysical corrections used is shown in Table 12. The TRP internal delay is 4.954 meters.

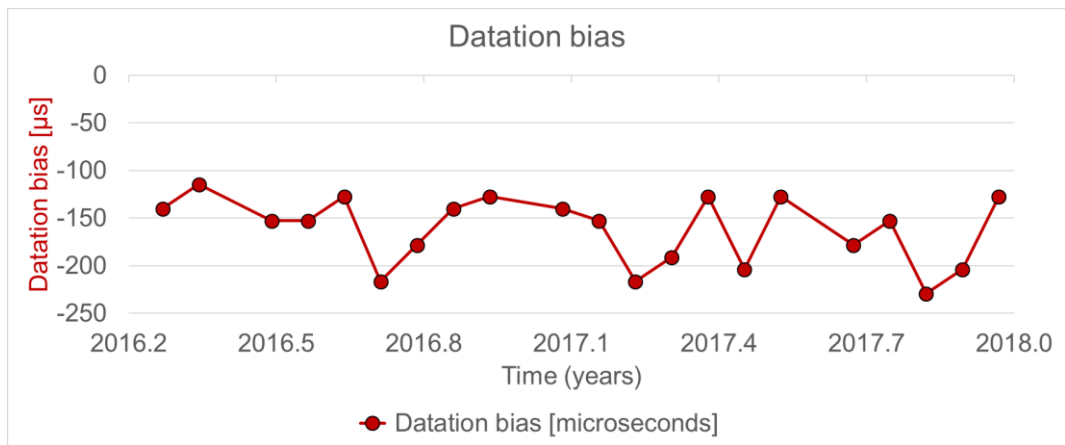
Cycle	Date	Dry Tropo [m]	Wet Tropo [m]	Iono [m]	Solid Earth [m]	Geocentric Tide [m]	Ocean Loading [m]
3	2016/04/09	-2.02600	-0.08710	-0.02418	-0.12970	0.00330	0.00310
4	2016/05/06	-2.04220	-0.07140	-0.03489	-0.04410	0.00280	0.01020
6	2016/06/29	-2.05184	-0.11006	-0.02995	-0.00030	-0.00060	0.00250
7	2016/07/26	-2.04933	-0.07117	-0.02432	-0.08820	-0.00260	-0.00200
8	2016/08/22	-2.05343	-0.07527	-0.02265	-0.12310	-0.00380	-0.00140
9	2016/09/18	-2.05799	-0.12541	-0.02411	-0.03270	-0.00470	0.00360
10	2016/10/15	-2.06529	-0.06351	-0.01800	0.13620	-0.00500	0.00680
11	2016/11/11	-2.06734	-0.07036	-0.01639	0.19500	-0.00380	0.00310
12	2016/12/08	-2.07943	-0.01087	-0.01453	0.09160	-0.00250	-0.00300
14	2017/01/31	-2.06552	-0.01138	-0.01913	-0.08110	0.00020	-0.00220
15	2017/02/27	-2.05001	-0.09089	-0.01818	-0.00790	0.00140	0.00310
16	2017/03/26	-2.05115	-0.06735	-0.01618	0.11520	0.00200	0.00520
17	2017/04/22	-2.04841	-0.04449	-0.02672	0.13670	0.00190	0.00160
18	2017/05/19	-2.05320	-0.03910	-0.03295	0.03340	0.00110	-0.00260
19	2017/06/15	-2.05731	-0.07789	-0.02817	-0.08180	-0.00010	-0.00230
20	2017/07/12	-2.05252	-0.08288	-0.02232	-0.11870	-0.00220	0.00190
22	2017/09/04	-2.05777	-0.00013	-0.02142	0.02520	-0.00470	0.00900
23	2017/10/01	-2.06119	-0.06361	-0.02128	0.05060	-0.00500	0.00510
24	2017/10/28	-2.03975	-0.12175	-0.01537	0.00120	-0.00440	-0.00040
25	2017/11/24	-2.06119	-0.06461	-0.01486	-0.03940	-0.00340	-0.00270
26	21/12/2017	-2.05275	-0.12315	-0.01603	-0.00760	-0.00150	-0.00150

Table 12: Geophysical Corrections of TRP passes processing

Transponder processing results.



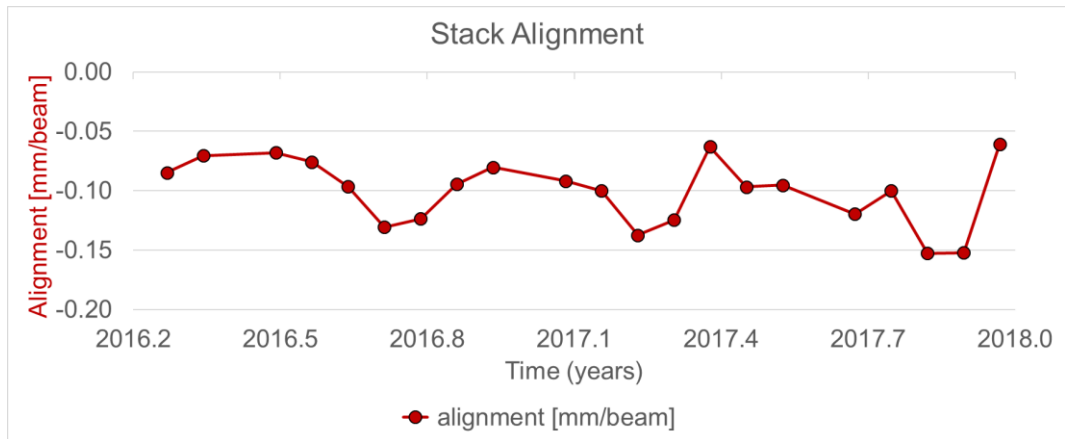
Range Bias Results



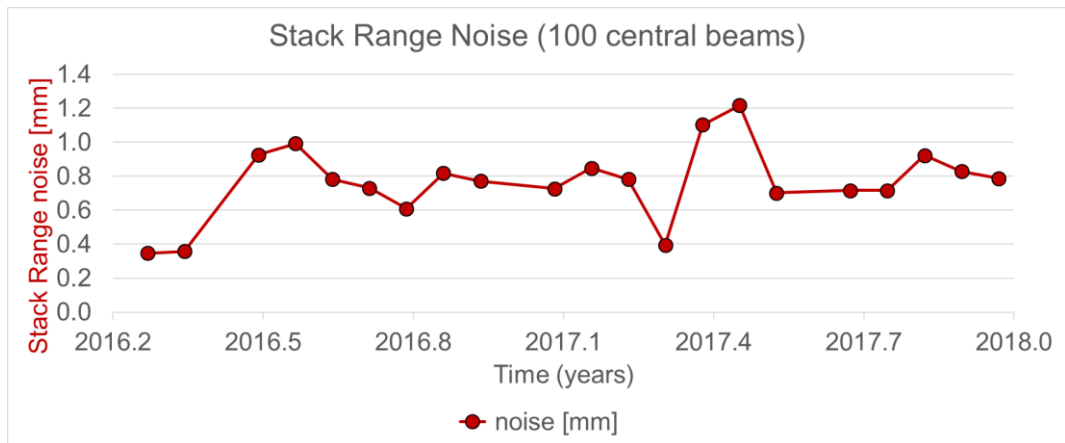
Datation Bias Results.

Figure 114 Range Bias Results and Datation Bias Results

Transponder processing. Stack analysis.



Alignment Results.



Stack Noise Results.

Figure 115 Alignment Results and Stack Noise Results

11.2 Calibration over Corsica sites

Initially developed for monitoring the performance of TOPEX/Poseidon and follow-on Jason legacy satellite altimeters at Senetosa Cape, Corsica, this calibration/validation site, has been extended to include a new location at Ajaccio. This addition enables the site to monitor Envisat and ERS missions, CryoSat 2 and, more recently, the SARAL/AltiKa mission and Sentinel 3A satellites. The maintenance of the facilities is mainly funded by CNES and operations, data retrieval and analysis are performed by the Observatoire de Paris (OBSPM/SYRTE) and the Observatoire de la Côte d’Azur (OCA/Géoazur). Results of the Sentinel-3A SSH absolute calibration have been regularly presented (e.g. OSTST meeting 2017) and recently published in [RD 18].

In situ data, geodetic datum and all necessary information are shared with Noveltis for the extension the absolute calibration through a regional method. In a first step, the absolute bias estimates were computed by Noveltis for the Sentinel-3A altimetry mission at the Corsica calibration sites, in Ajaccio and Senetosa.

As shown in Figure 116, the Sentinel-3A configuration in Corsica is of particular interest, as the same track (741) flies close to both tide gauges in Ajaccio and Senetosa, which gives the opportunity to estimate the absolute bias of the altimeter range at the two sites within a few seconds. This will also help understand some differences that were observed between the two sites for previous satellite altimetry missions.

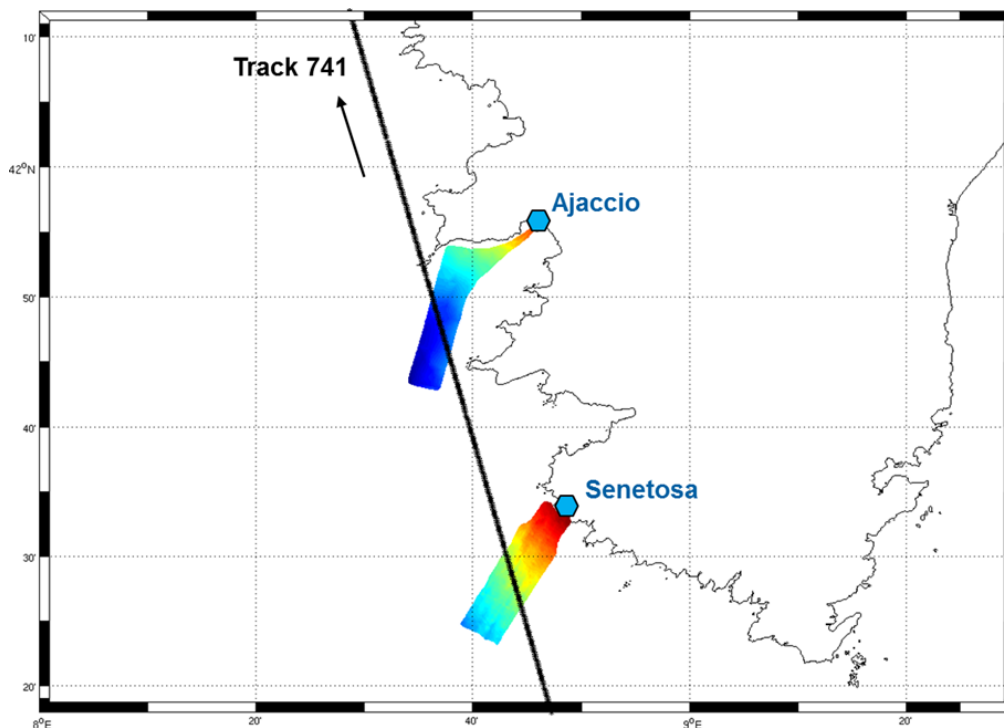


Figure 116: Absolute CALVAL configuration in Corsica. The regions in colours show the two high-resolution mean sea surfaces that were specifically measured to link the calibration sites to the altimetry data



Sentinel-3 MPC
S3MPC STM Annual Performance
Report - Year 1

Ref.: S3MPC.CLS.APR.002
Issue: 1.1
Date: 23/05/2018
Page: 153

The in situ datasets are currently available up to August 2017 for Ajaccio and July 2017 for Senetosa (latest data retrieval, performed every three months in general). The absolute bias estimates were computed in Corsica using the L2 NTC Land products reprocessed with the IPF version 06.07, from cycle 5 to cycle 19. Table 13 summarizes the altimetry products version and the parameters used to compute the bias estimates.

Table 13 : Sentinel-3A products and parameters used to compute the absolute bias estimates

Product version	S-3A NTC Land with IPF version 06.07, from S3 MPC FTP website
Period	Cycles 5 to 19 (06/2016 – 08/2017)
Frequency	20 Hz
Ionosphere correction	GIM
Wet troposphere correction	Model (land contamination in radiometer correction)

The first analyses of the Sentinel-3A bias estimates computed with the regional method have shown that the configuration designed for the Jason-suite and Envisat-suite missions, with tracks oriented in the longitudinal direction of the in-situ high resolution mean sea surfaces, was not well adapted to the Sentinel-3A track 741 that crosses the high resolution mean sea surfaces in the transverse direction. Developments have been made in the calibration method in order to improve the selection of the altimetry points on the in-situ high resolution mean sea surfaces (see Figure 117), which enables to compute more stable absolute bias estimates.

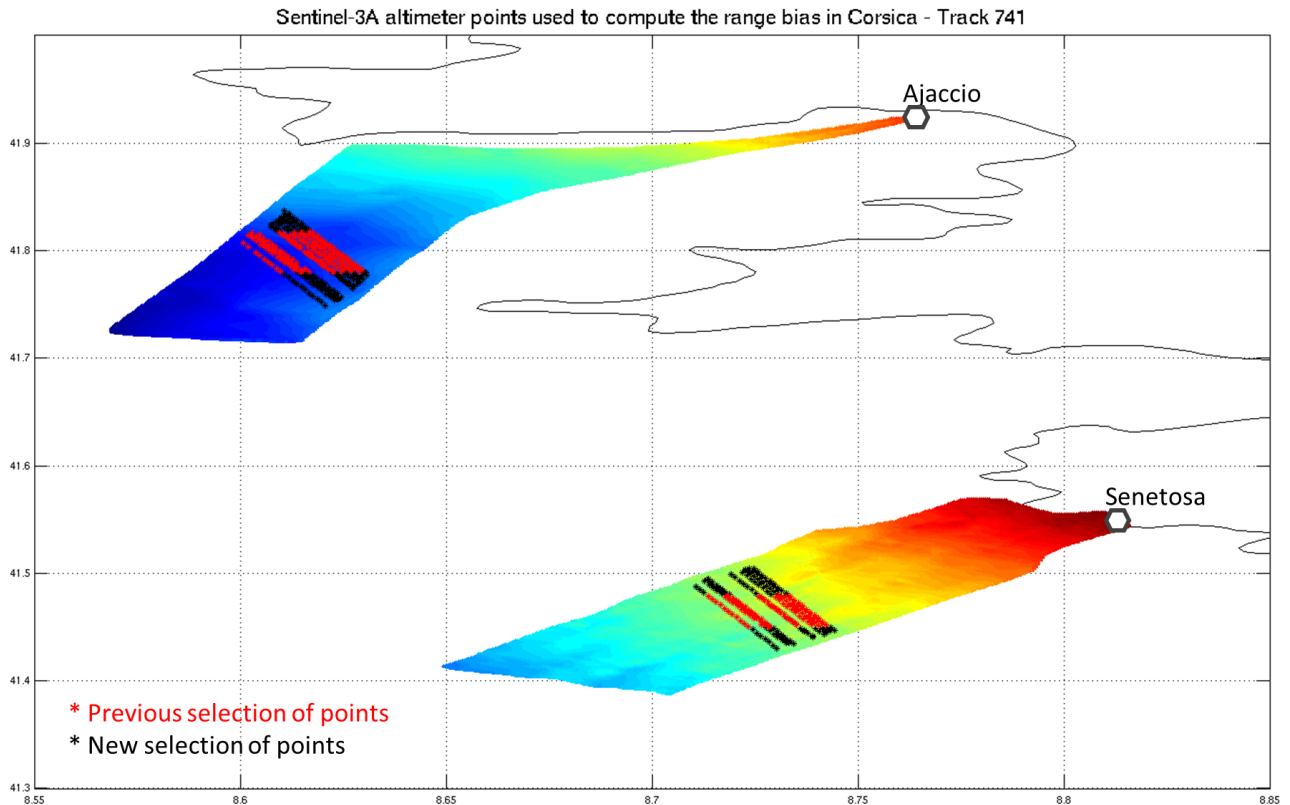


Figure 117: Impact of the change in the method for the selection of the altimetry points on the high-resolution mean sea surfaces at the Corsica calibration sites – Sentinel-3A track 741 – Cycles 5 to 19.

The computation of the bias estimates was performed both for the SAR data and the PLRM data. Table 14 gives the statistics computed over the altimeter range bias for 15 cycles and Figure 118 shows the time series of the bias estimates. The results are given for the bias computation before and after the change in the method mentioned above. The bias estimates presented by Pascal Bonnefond (OBSPM/OCA) at the last OSTST meeting in October 2017 are also given in Table 14 and show in general very good agreement with the bias estimates computed by Noveltis.

Table 14 : Statistics on the Sentinel-3A SAR and PLRM SSH absolute bias estimates in Corsica on track 741, before and after change in the method. The colours refer to the plots on Figure 118.

Calibration site		SAR			PLRM		
		Mean (mm)	Standard deviation (mm)	Number of cycles	Mean (mm)	Standard deviation (mm)	Number of cycles
Senetosa	Previous selection	19	28	15	7	41	15
	New selection	12	26	15	1	36	15
	OCA results (OSTST 2017)	21	29	14	3	47	14



Sentinel-3 MPC
S3MPC STM Annual Performance
Report - Year 1

Ref.: S3MPC.CLS.APR.002
 Issue: 1.1
 Date: 23/05/2018
 Page: 155

Ajaccio	Previous selection	2	43	15	10	63	15
	New selection	28	19	15	35	49	15
	<i>OCA results (OSTST 2017)</i>	25	34	13	14	60	13

The impact of the new developments in the calibration method is particularly strong in the case of the bias estimates computed in Ajaccio, with a reduction of 2 cm in the variability. The mean bias estimates are also closer between the two sites when considering the fact that cycle 15 tends to drag the mean bias down in Senetosa. The bias estimates computed on the PLRM range are in general noisier than the estimates on the SAR range, even if some cycles seem to contribute in a larger manner to the variability of the bias estimates (cycle 15 in Senetosa and cycle 18 in Ajaccio in particular). The investigations performed on these specific cycles have not led to any clear conclusions for now but some complementary analyses are underway.

Now that the method was tuned in Corsica for the absolute bias estimation, the next steps will consist in considering the regional aspect of the technique at this site as well as at the calibration sites in Harvest and Bass Strait. Then, these results will be updated on the fly with the most recent altimetry and in situ data.

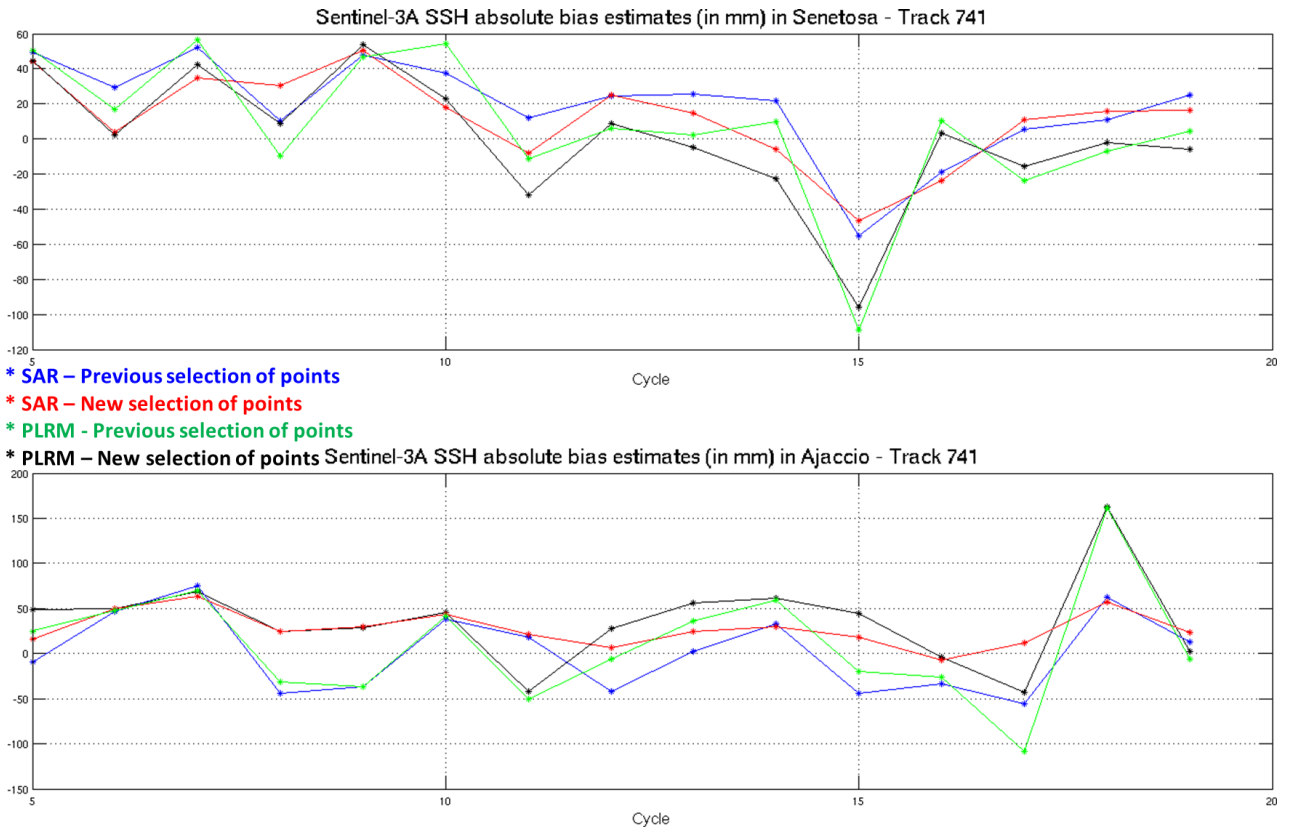


Figure 118: Sentinel-3A absolute bias estimates in Senetosa (upper plot) and Ajaccio (lower plot) on track 741

12 Bias assessment of the different retrackerers

There are several SARM retrackerers provided in the L2 products that are specifically designed to be used for the different surfaces.

- ❖ Ocean retracker derived from SAMOSA model that is meaningful over open ocean and coastal areas.
- ❖ OCOG (ICE 1) retracker which is traditionally used over inland water because it is quite robust. It can also be used over land ice for the same reason but is expected to provide a lower accuracy.
- ❖ Sea ice retracker which is an empirical retracker designed for sea ice
- ❖ Ice margin retracker which is a physical ice sheet model designed for land ice

The aim of this section is to highlight any mean absolute bias that could be identified on all these retrackerers.

12.1 Ocean retracker

There have been several assessments for the range derived over ocean that are detailed in this document. Several figures are found to be below 2 cm for the ocean retracker, which is a small bias, almost negligible.

For the Ku band sigma0 estimated by the ocean retracker, a system bias of 18.9 dB is applied in the L2 ground processor to align it to a mean value of 11 dB over ocean. This means that the Ku-band SARM sigma0 is too strong, but there are some evolutions to be implemented in the future ground processing versions to get a level closer to the ocean mean value without any system bias applied

12.2 OCOG retracker

The estimation of a range bias for this retracker is quite difficult since it is an empirical retracker and, by design, the bias will depend on the waveforms shape and therefore on the surface (ocean, inland waters, sea ice, land ice echoes). Figure 119 shows that the difference between the Ocean and OCOG range varies a lot depending on the considered surface. We can observe a bias of 40-50 cm over ocean because this retracker is not meant to be accurate over this surface, while both retrackerers agree below 20 cm over regions where sea ice dominate (see maps in section 8.3 that were obtained for the previous cycle but that give a good indication of the ocean and sea ice regions during this period). Over Greenland, such a difference is not meaningful since the ocean SAMOSA model is not defined to work over land ice.

Nevertheless, calibration of the OCOG range over the Issykkul Lake found a bias of +28 cm, which is in agreement with the bias observed with this retracker for other altimetry missions. We can therefore conclude that there is no bias identified for the OCOG range.

The backscatter coefficients between both retracker are also compared on Figure 120. It shows a large bias for the OCOG sigma0. Values are close to -35 dB over ocean which means that the mean OCOG sigma0 is close to 46 dB. Despite this strong absolute bias, we also note variations with several dB magnitude depending on the considered surface.

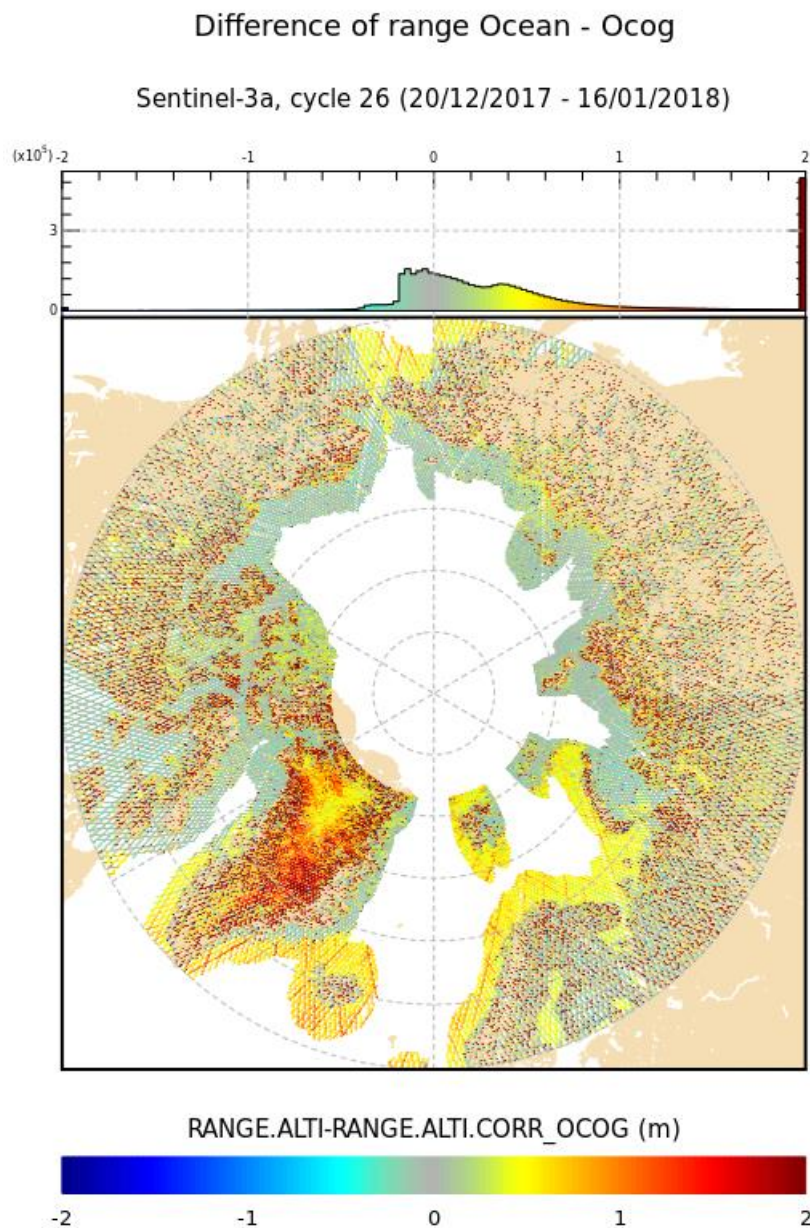


Figure 119 Range difference: OCOG-Ocean over Arctic in L2 Land products STC Cycle 26

Difference of backscatter coefficient Ocean - Ocoq

Sentinel-3a, cycle 26 (20/12/2017 - 16/01/2018)

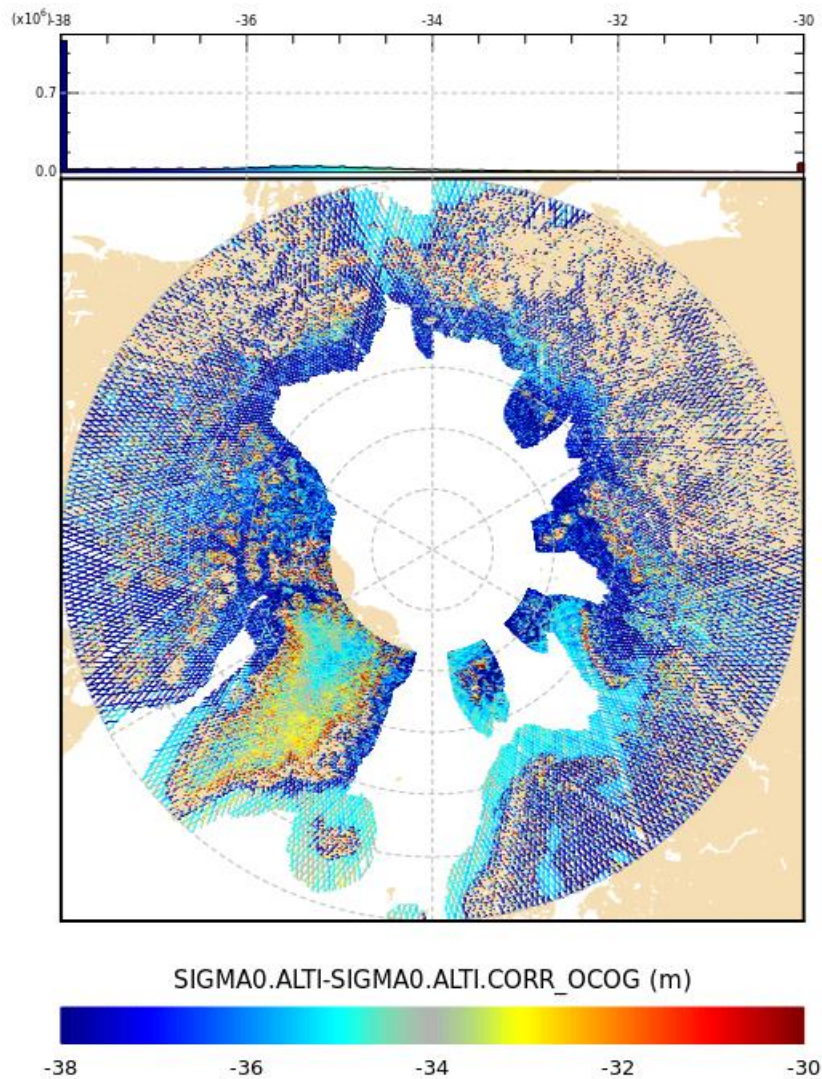


Figure 120 Backscatter coefficient difference: OCOG-Ocean over Arctic in L2 Land products STC Cycle 26

12.3 Sea Ice retracker

The sea ice retracker in the L2 products is not performing well over the sea ice floes. It has been identified that the diffuse echo retracker (used to correct the range measurements of waveforms discriminated as sea ice floes) needs to be upgraded to a TMFRA retracker, as used in the latest Cryosat baseline-D. Then, the lead and floe retracker bias will be calibrated. Replacement of this retracker and calibration is scheduled for the first half of 2018.

	Sentinel-3 MPC S3MPC STM Annual Performance Report - Year 1	Ref.: S3MPC.CLS.APR.002 Issue: 1.1 Date: 23/05/2018 Page: 160
---	--	--

12.4 Ice margin retracker

In order to assess possible residual bias on ice margin range, we compared this retracker output to the ocean range and to the OCOG range over land ice.

Surprisingly, the difference between ice margin range and ocean range is close to zero over almost all surfaces as shown by Figure 121. Over ocean and sea ice, the difference varies between 10 and 20 cm. This could suggest that there is no significant bias on the ice sheet range, given that the ocean range has almost no bias. This must be further confirmed by comparison of elevation data over land ice with external sources, since this is the surface where this retracker is relevant.

Figure 122 also displays the map over Antarctica of the difference between OCOG and ice margin range. This comparison is more meaningful since both retrackerers are supposed to retrieve a good signal over land ice. The difference shows variations between the retrackerers that vary between 50 cm and 2 m, but no clear mean bias can be found between both retrackerers. As explained in section 9.2, values are not defined everywhere, due to the large amount of failure of the ice margin retracker.

The backscatter coefficients between both retrackerers are also compared on Figure 123. It shows a large bias for the OCOG σ_0 . Values are close to -36 dB over ocean which means that the mean OCOG σ_0 is close to 47 dB. Despite this strong absolute bias, we also note variations with several dB magnitude depending on the considered surface.

Figure 124 also displays the map over Antarctica of the difference between OCOG and ice margin backscatter coefficient. In this case values are very close with a bias varying mainly between -1 and -2 dB, OCOG σ_0 being lower than the ice margin one. As for the range, values are not defined everywhere, due to the large amount of failure of the ice margin retracker. The values are different over the sea ice areas where we observe larger and positive differences (+4 dB).

Difference of range Ocean - ice sheet

Sentinel-3a, cycle 26 (20/12/2017 - 16/01/2018)

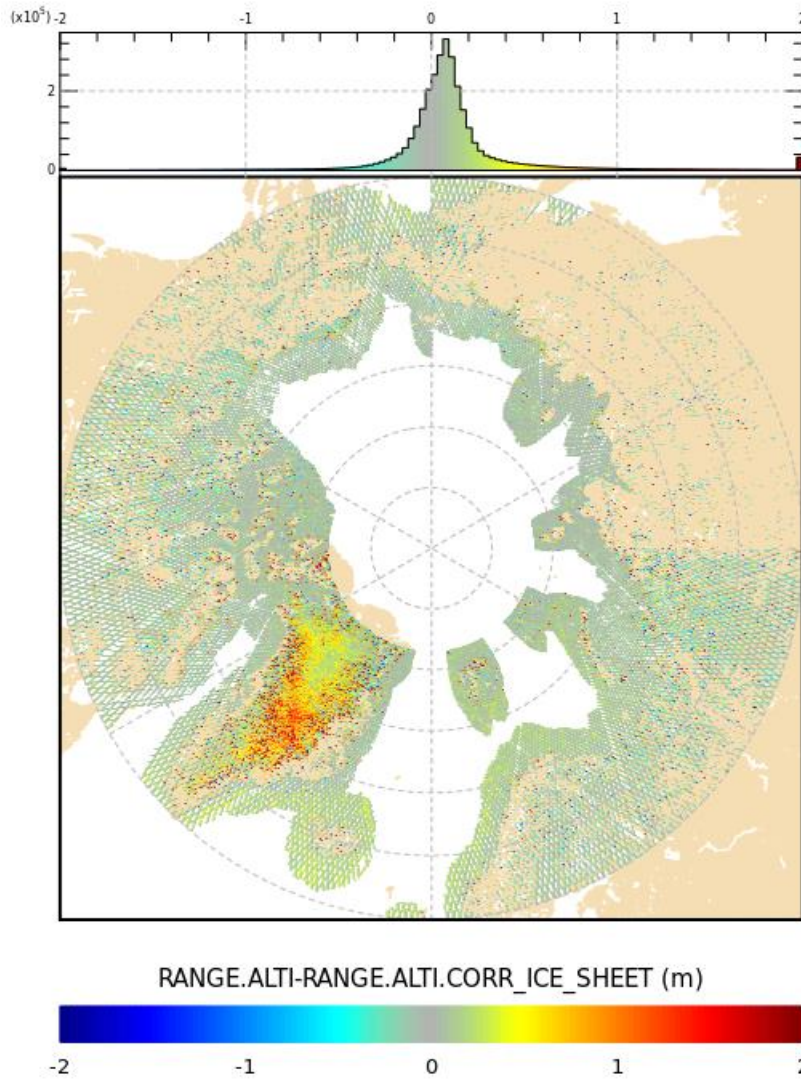


Figure 121 Range difference: Ocean-Ice margin over Arctic in L2 Land products STC Cycle 26

Difference of range Ocog - Ice sheet

Sentinel-3a, cycle 26 (20/12/2017 - 16/01/2018)

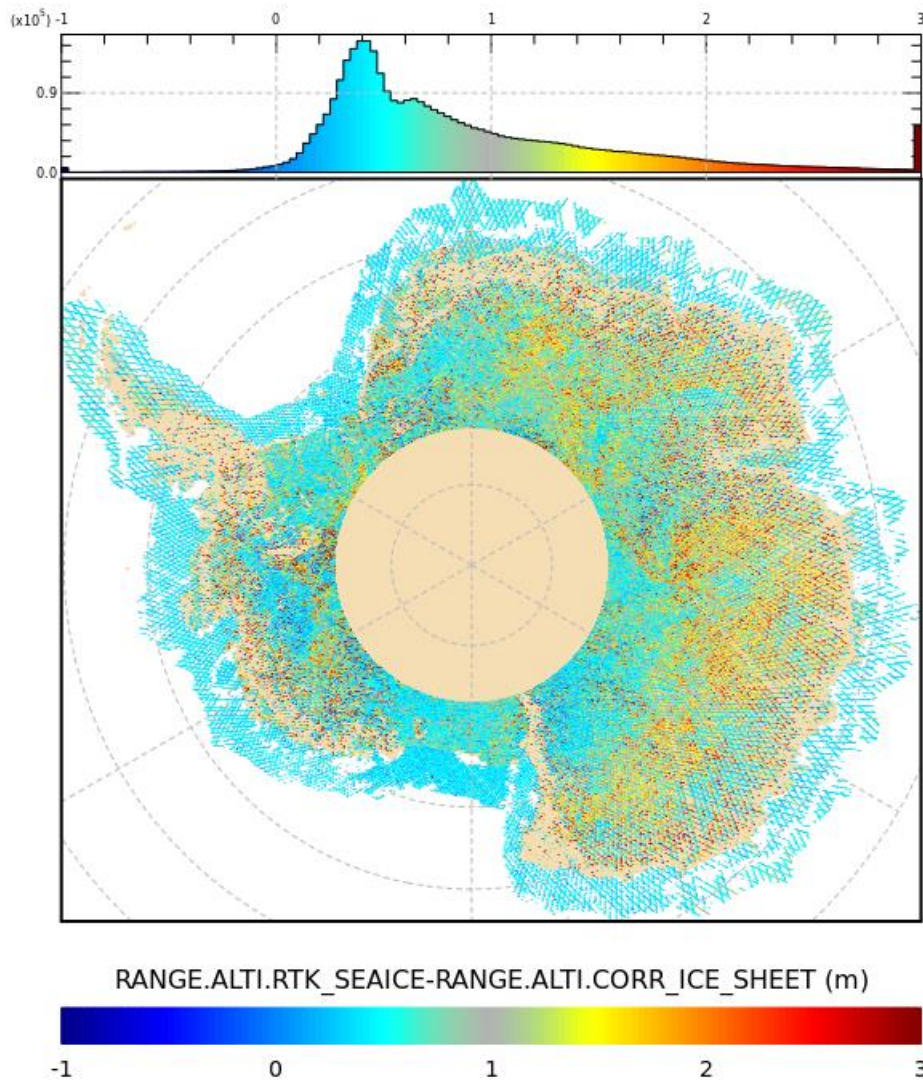


Figure 122 Range difference: OCOG-Ice margin over Antarctica in L2 Land products STC Cycle 26

ifference of backscatter coefficient Ocean - Ice shee

Sentinel-3a, cycle 26 (20/12/2017 - 16/01/2018)

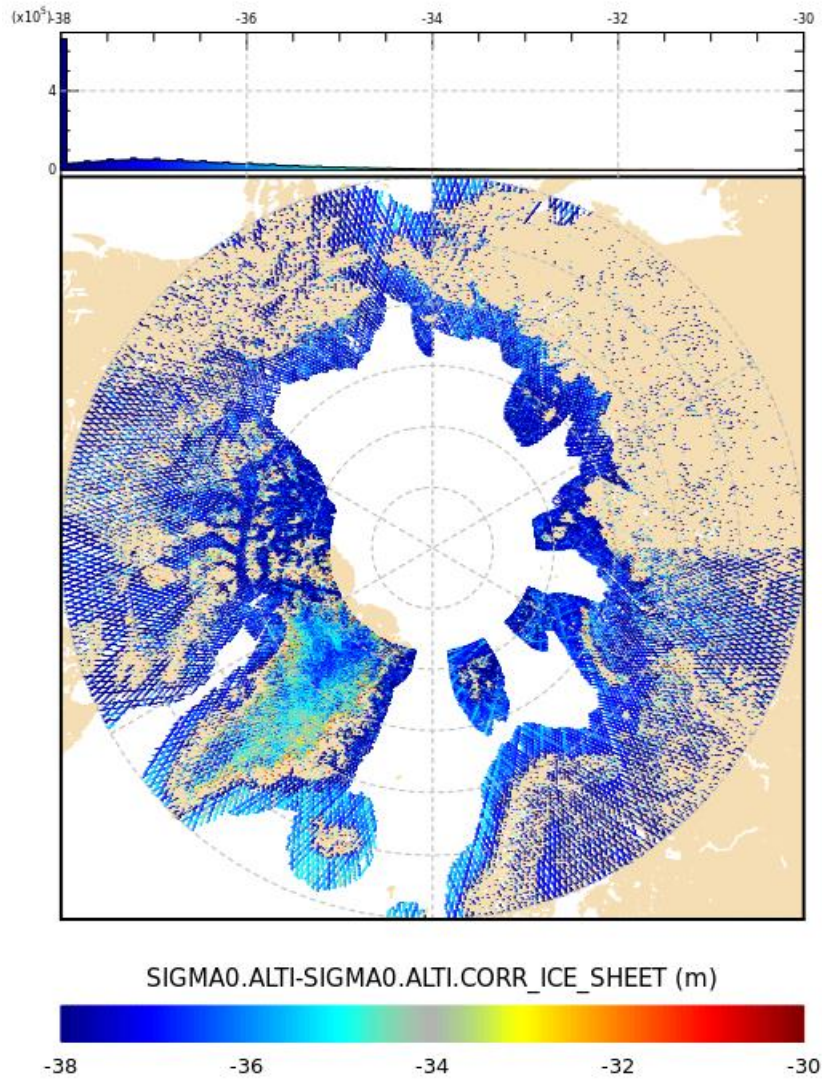


Figure 123 Backscatter coefficient difference: Ocean-Ice margin over Arctic in L2 Land products STC Cycle 26

Difference of backscatter coefficient OcoG - Ice sheet

Sentinel-3a, cycle 26 (20/12/2017 - 16/01/2018)

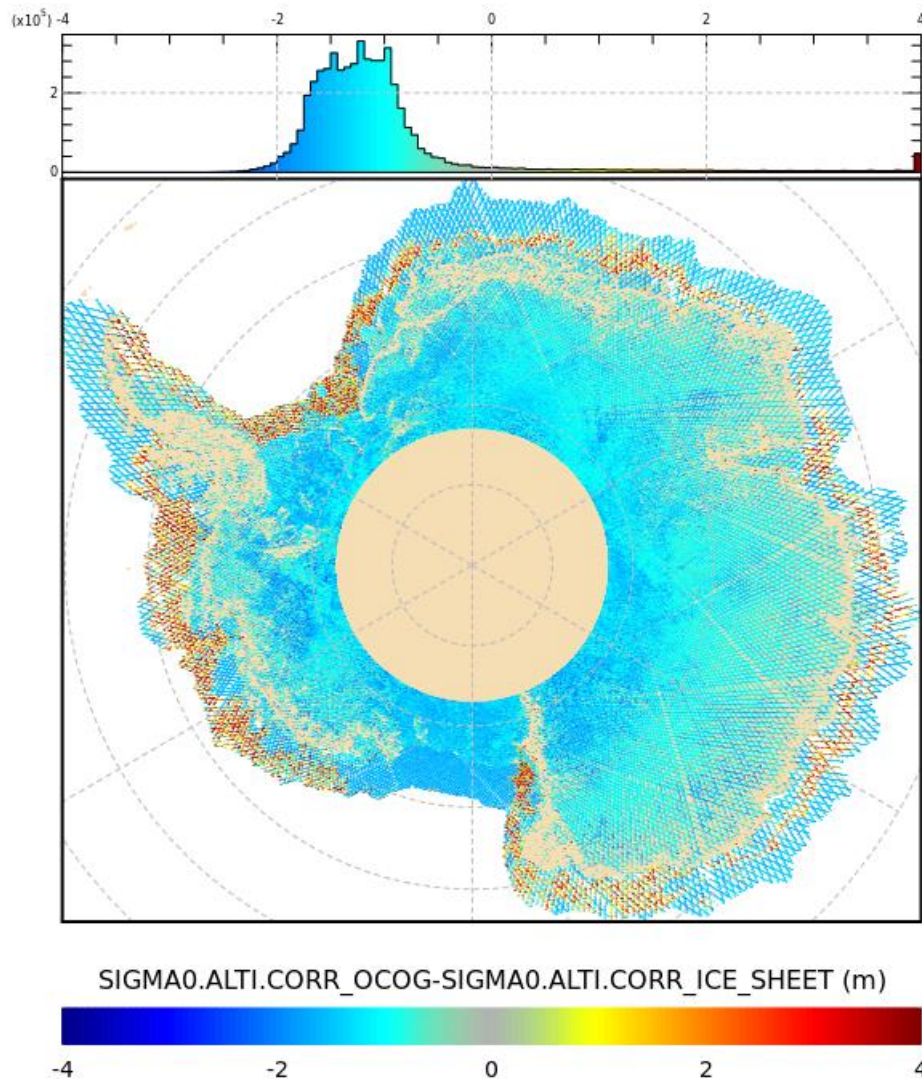


Figure 124 Backscatter coefficient difference: OCOG-Ice margin over Antarctica in L2 Land products STC Cycle 26

12.5 Summary

There is no absolute bias identified on the range parameters estimated by the different retracers. Nevertheless, there are strong absolute biases present on the backscatter coefficients. Values are very close between OCOG and Ice margin retracker (35 and 35 dB wrt a mean value of 11 dB over ocean) while the Ocean retracker has a smaller bias (19 dB). There will be some evolutions to be implemented in the future ground processing versions to get a level closer to the ocean mean value without any system bias applied.

13 Annex - Processing Baseline Details

13.1 Processing Baseline 2.12

13.1.1 Ground processors versions (Instrument Processor Facility)

- ❖ SR_1 IPF version: 06.11
- ❖ MW_1 IPF version: 06.03
- ❖ SM_2 IPF version: 06.07

13.1.2 Evolutions

There is no evolution of algorithm nor model coming from Processing Baseline 2.12. The content is completely described by the list of the anomaly fixes detailed in the following sections.

13.1.3 Fix of anomalies

Anomaly #4 : Error in bathymetry parameter (S3MPC-1078)

- ❖ The bathymetry parameter has some error at the crossing of the Greenwich meridian. The bathymetry is set to zero between 0° and 20°E for some specific latitudes.
- ❖ All versions up to and including 06.06 are impacted
- ❖ Fixed in version 06.07

Anomaly #12 : High level of retracker failure over in-land waters (S3MPC-1064)

- ❖ The OCOG ice retracker shows higher percentage of failure than the ocean retracker over rivers and lakes. Further tuning of the S3 retracker or waveform rejection algorithms is required. Note that only a few targets have been assessed so far by the validation team so the percentage of failure can be different for the different water bodies.
- ❖ All versions up to and including 06.06 are impacted
- ❖ Fixed in version 06.07



Anomaly #13 : Error in the OCOG retracker (S3MPC-1478)

- ❖ The threshold value used in the OCOG retracker is not adapted to Ku band. The effect is an error on the range values which varies depending on the waveform shape. For waveforms close to ocean waveforms, a bias of 80 cm is observed (calibration done over the Lake Issykkul).
- ❖ All versions up to and including 06.06 are impacted
- ❖ Fixed in version 06.07

Anomaly #14 : GIM ionospheric correction not calculated for STC products (S3MPC-1468)

- ❖ The model GIM ionospheric correction is not calculated for STC products, therefore the field is set to default value. Note that the correction is available in NRT and NTC products.
- ❖ All versions up to and including 06.06 are impacted
- ❖ Fixed in version 06.07

13.2 Processing Baseline 2.24

13.2.1 Ground processors versions (Instrument Processor Facility)

- ❖ SR_1 IPF version: 06.12
- ❖ MW_1 IPF version: 06.04
- ❖ SM_2 IPF version: 06.10

13.2.2 Evolutions

In addition to the resolution of the anomalies listed in the following section, Processing Baseline 2.24 brings major evolutions of product quality over ocean, coastal sea ice and land ice surfaces. These improvements are detailed in : <https://earth.esa.int/documents/247904/3147059/Sentinel-3-STM-Product-Evolution-Processing-Baseline-2.24>

13.2.3 Fix of anomalies

Anomaly #1 : Duplicated measurements at 10 minutes granule transition in L2 NRT products (S3MPC-926)

- ❖ There are duplicates of 1 Hz measurements (same 1 Hz time tag) between consecutive granules. At granules transition, the last 1 Hz measurement and the first 1 Hz measurement of the following granule may have the same datation. In some cases, 1 Hz range values might be set to default values because there are not enough 20 Hz observations within the granule to



compute the 1 Hz range. Note that the 20 Hz parameters (range, SWH and Sigma0) are not affected.

- ❖ Fixed in version 06.10

Anomaly #2 : Overflow of the Ku band atmospheric attenuation in the L2 products (S3MPC-1076)

- ❖ The atmospheric attenuation in Ku band is set to default values in the products when value exceeds 1.27 dB. Note that for these measurements the wind speed is well calculated.
- ❖ Fixed in version 06.10

Anomaly #3 : Atmospheric attenuation to default values over edges of MWR calibration (S3MPC-1077)

- ❖ The atmospheric attenuation on Ku band and C band is set to defaults values for sporadic points located in the fringe of the MWR calibration sequences. These isolated 1 Hz values can be found over open-ocean. As a consequence, wind speed, sea state bias, dual frequency ionospheric correction and SSHA parameters are set to default value.
- ❖ Fixed in version 06.10

Anomaly #4 : SAR backscatter coefficient has an error correlated with radial velocity (S3MPC-1251)

- ❖ The SAR Ku band sigma0 from ocean/coastal retracker (sig0_ocean_01_ku) shows an error correlated with radial velocities above 20 m/s. The maximum magnitude of the error is estimated to 0.2 dB for the stronger velocities (25m/s).
- ❖ Fixed in version 06.10

Anomaly #5 : Error in the manoeuvre flag (EUM/Sen3/AR/2268)

- ❖ There is an inconsistency between the product specifications (S3IPF PDS 003 -i1r7- Product Data Format Specification - SRAL-MWR) and the effective values in the products of the manoeuvre presence flag (values set to 4 or 5 instead of 0 and 1 as specified in the documentation).
- ❖ Fixed in version 06.10



Anomaly #6 : Error in Inverse Barometer correction (S3MPC-1253)

- ❖ There is a bias of 1 cm over open-ocean on the inverse barometer correction. Note that this error has no impact in STC and NTC products on the sum of the 2 fields used in the SSHA calculation (inverted barometer height correction (inv_bar_cor) + high frequency fluctuations of the sea surface topography (hf_fluct_cor)).
- ❖ Fixed in version 06.10

Anomaly #7 : High level of retracker failure in continental ice sheets (S3MPC-1014)

- ❖ Over the inland ice sheets of Antarctica and Greenland there are much higher levels of the ice sheet retracker failure than found in previous missions (ie CryoSat LRM or Envisat RA2) over sloping surfaces. The anomaly on the SAR ice margin retracker also impacts the slope correction which is set to FillValue in a high number of occurrences.
- ❖ Improvement is observed with version 06.10 reducing the loss to 20% of the data set over Antarctica. Further tuning of the SRAL L1 processing is required to insure full consistency between L1 processing and L2 ice sheet retracker, so that the expected level of ice sheet retracker coverage is finally met. Meanwhile, users are advised to use the OCOG retracker to exploit a data set with the expected coverage over land ice.
- ❖ All versions up to and including 06.10 are impacted

Anomaly #8 : Sea Ice discrimination identifying too many floes (S3MPC-1013)

- ❖ A comparison of Arctic sea ice discrimination statistics during October 2016 between Sentinel-3A and CryoSat shows that S3 processing is identifying four times more floes to leads than CryoSat's discriminator than would be expected during this period. Sentinel-3A discrimination requires further tuning.
- ❖ Fixed in version 06.10

Anomaly #9 : Large negative values in elevation over ice sheet (S3MPC-1020)

- ❖ Elevation values over ice sheet (elevation_ice_sheet_20_ku) are occasionally set to large negative values (in the order of -214680m). It varies and is not the FillValue of the field. This happens particularly in the areas of ice shelves just off the coast and appears to be isolated points along the track. It does not seem to occur in the interior ice sheets or in the ocean.
- ❖ Fixed in version 06.10

	Sentinel-3 MPC S3MPC STM Annual Performance Report - Year 1	Ref.: S3MPC.CLS.APR.002 Issue: 1.1 Date: 23/05/2018 Page: 169
---	--	--

13.3 Processing Baseline 2.27

13.3.1 Ground processors versions (Instrument Processor Facility)

- ❖ SR_1 IPF version: 06.13
- ❖ MW_1 IPF version: 06.04
- ❖ SM_2 IPF version: 06.12

13.3.2 Evolutions

In addition to the resolution of the anomalies listed in the following section, Processing Baseline 2.27 improves product quality over the land ice with the inclusion of a new parameter in the L2 products, as recommended by the S3VT meeting in March 2017: elevation field derived from the OCOG retracker that provides a better coverage compared to the elevation derived from the ice sheet retracker that was already provided in the products.

13.3.3 Fix of anomalies

Anomaly #15 : Wrong values of ssha over sea ice (S3MPC-2067 and S3MPC-2271)

- ❖ The ssha parameter over sea ice (sea_ice_ssha, int_sea_ice_ssha) exhibits large values of 3.27 m when the GIM ionospheric correction is set to default value. The anomaly on the ssha field is due to bad handling of the default value into the ssha calculation.
- ❖ Fixed in version 06.12

Anomaly #16 : SAR mode slope correction relocates echo position incorrectly (S3MPC-2074)

- ❖ SAR mode slope correction relocates echo position incorrectly down slope and not across track. Note that for LRM slope correction relocates echo in correct direction.
- ❖ Fixed in version 06.12

Anomaly #18 : Numerical Overflow for the Waveform MQE Parameter (S3MPC-2027)

- ❖ There is an overflow for the waveform Mean Quadratic Error between the waveform and the model used for the ocean retracker (mqe_ocean_20_ku) in the products. This results in field padded to default value over sea ice in Antarctica and Arctic and sporadically over open ocean.
- ❖ Fixed in version 06.12

Anomaly #19 : Numerical Overflow for the peakiness parameter (S3MPC-2028)

- ❖ There is an overflow for the peakiness parameters (peakiness_2_20_ku, peakiness_2_20_c, peakiness_1_20_plrm_ku) in the products. This results in fields padded to default value over sea ice in Antarctica and Arctic where peaky waveforms can happen.
- ❖ Fixed in version 06.12

13.3.4 Anomalies not solved

The following list summarizes the anomalies that still affect the products with the Processing Baseline 2.27:

Anomaly #7 : High level of retracker failure in continental ice sheets (S3MPC-1014)

- ❖ Over the inland ice sheets of Antarctica and Greenland there are much higher levels of the ice sheet retracker failure than found in previous missions (ie CryoSat LRM or Envisat RA2) over sloping surfaces. The anomaly on the SAR ice margin retracker also impacts the slope correction which is set to FillValue in a high number of occurrences.
- ❖ Improvement is observed since version 06.10 reducing the loss to 20% of the data set over Antarctica. Further tuning of the SRAL L1 processing is required to insure full consistency between L1 processing and L2 ice sheet retracker, so that the expected level of ice sheet retracker coverage is finally met. Meanwhile, users are advised to use the OCOG retracker to exploit a data set with the expected coverage over land ice (loss of only 2% of data).
- ❖ All versions up to and including 06.12 are impacted

Anomaly #10 : Dry tropospheric correction residual error over land (S3MPC-1518)

- ❖ The dry tropospheric correction at the measurement altitude (mod_dry_tropo_cor_meas_altitude_01) exhibits some residual error correlated to the topography. The error has a magnitude of a few millimetres.
- ❖ All versions up to and including 06.12 are impacted

Anomaly #11 : Quantization of the distance to coast (S3MPC-1519)

- ❖ The distance to coast at 1 Hz and at 20 Hz exhibits some quantization. The effect is larger at 20 Hz for which the value is constant over several 20 Hz measurements.
- ❖ All versions up to and including 06.12 are impacted



Anomaly #12 : Degraded quality of atmospheric attenuation over coastal areas (S3MPC-1934)

- ❖ The MWR atmospheric attenuation was improved over coastal zone except for some specific cases over coastal areas, for which the attenuation is negative (-0.3 dB). This anomaly affects only 0.25% of the ocean measurements and occurs when backscatter coefficient exceeds 18 dB.
- ❖ This anomaly was introduced in version 06.10 and all versions up to and including 06.12 are impacted

Anomaly #13 : GIM ionospheric to default value (S3MPC-2030)

- ❖ The GIM ionospheric correction is systematically set to default values for portions of tracks that are closed to midnight. Therefore, parameters related to the topography observations are impacted (sea_ice_ssha, int_sea_ice_ssha).
- ❖ Fixed in version 06.10 for STC products.
- ❖ All versions up to and including 06.12 are impacted for NTC products. The impact is that ssha, sea_ice_ssha and int_sea_ice_ssha parameters exhibit too large values.
- ❖ All versions up to and including 06.12 are impacted for NTC products. Since IPF version 06.12, the impact is that sea_ice_ssha and int_sea_ice_ssha parameters are calculated without the GIM ionospheric correction.
- ❖ The reprocessed products with IPF 06.10 are not affected by this anomaly.

Anomaly #14 : L2 sea ice freeboard (freeboard 20 ku) is predominantly negative (S3MPC-2244)

- ❖ The freeboard parameter exhibits a mean value centred around -30 cm which is not expected. It is mainly due to the retracker used for the diffuse echoes which is not optimal to properly retrack the double peak waveforms that are characteristics over floes.
- ❖ All versions up to and including 06.12 are impacted



Anomaly #20 : Sea ice lead echoes incorrectly filtered by waveform quality check (S3MPC-2409, S3MPC-2411)

- ❖ The sea ice retracker exhibits a much higher level of failure compared to the other retracker (ocean, OCOG and ice sheet retracker), due to the use of a quality check applied on the waveforms. This results in the sea ice retracking not being applied to waveforms for observations that are associated to leads and sea ice, leads being the dominant population where the retracker is not activated. This anomaly will be corrected in future STM Processing Baseline.
- ❖ All versions up to and including 06.12 are impacted.

Anomaly #21 : 5 millimeter bias between zero-altitude dry tropo correction and measured dry tropo correction (S3MPC-2338)

- ❖ The dry tropospheric correction (mod_dry_tropo_meas_altitude_01) exhibits a bias over all surfaces (ocean and land). It is close to 5 millimeters over ocean (including coastal areas) and less than 5 millimeters over land. This anomaly will be corrected in future STM Processing Baseline.
- ❖ All versions up to and including 06.12 are impacted.

Anomaly #22 : Discrimination flag set to ocean over land (S3MPC-2412)

- ❖ The discrimination flag (surf_type_class_20_ku) which is designed for sea ice is set to ocean over land surfaces.
- ❖ All versions up to and including 06.12 are impacted.

Anomaly #23 : Wrong values of interpolated sea ice ssha over ocean (S3MPC-2413)

- ❖ Values of interpolated ssha for sea ice (int_sea_ice_ssha) show stronger magnitude than the original sea_ice_ssha parameter, over transition zones between ocean and land areas.
- ❖ All versions up to and including 06.12 are impacted.

Anomaly #24 : Ice concentration set to zero over land (S3MPC-2417)

- ❖ Sea_ice_concentration_20_ku is set to zero percent over land but it does not affect the quality of the sea ice parameters using this parameter.
- ❖ All versions up to and including 06.12 are impacted



Sentinel-3 MPC
S3MPC STM Annual Performance
Report - Year 1

Ref.: S3MPC.CLS.APR.002
Issue: 1.1
Date: 23/05/2018
Page: 173

Anomaly #25 : Ice2 PLRM retracker not defined over the ice shelves (S3MPC-2415)

- ❖ The parameters estimated by the Ice2 retracker on PLRM waveforms (range_ice_20_plrm_ku and sig0_ice_20_plrm_ku) are not defined over the ice shelves.
- ❖ All versions up to and including 06.12 are impacted.

Anomaly #26 : SRAL L2 NRT products with zero duration (S3MPC-2340)

- ❖ There are some products generated with a duration less than 1 second, with only a few 20 Hz records inside the product. Note that this anomaly only affects the NRT products.
- ❖ All versions up to and including 06.12 are impacted.

Anomaly #27 : Partial coverage for OCOG retracker in C-band (S3MPC-2365)

- ❖ The output of the OCOG retracker in C-band (range_ocog_20_c and sig0_ocog_20_c parameters) are very frequently set to fill values, whatever the surface.
- ❖ All versions up to and including 06.12 are impacted.

13.4 Processing Baseline 2.33

13.4.1 Ground processors versions (Instrument Processor Facility)

- ❖ SR_1 IPF version: 06.14
- ❖ MW_1 IPF version: 06.07
- ❖ SM_2 IPF version: 06.14

13.4.2 Evolutions

In addition to the resolution of the anomalies listed in the following section, the evolution in Processing Baseline 2.33 deals with the inclusion of the SRAL acquisitions measurements in the SRAL Level 1 products and the evolution needed in the Level 2 ground processor to manage the new MWR calibration timeline.

13.4.3 Fix of anomalies

Anomaly #8 : 5 millimeter bias between zero-altitude dry tropo correction and measured dry tropo correction (S3MPC-2338)

- ❖ The dry tropospheric correction (mod_dry_tropo_meas_altitude_01) exhibits a bias over all surfaces (ocean and land). It is close to 5 millimeters over ocean (including coastal areas) and less than 5 millimeters over land. This anomaly will be corrected in future STM Processing Baseline.
- ❖ Fixed in version 06.14

Anomaly #13 : SRAL L2 NRT products with zero duration (S3MPC-2340)

- ❖ There are some products generated with a duration less than 1 second, with only a few 20 Hz records inside the product. Note that this anomaly only affects the NRT products.
- ❖ Fixed in version 06.14

Anomaly #16 : the field "ssha 20 ku" is always set to Fill Value in LRM mode (S3MPC-2469)

- ❖ The field ssha_20_ku is set to Fill Value when the SRAL altimeter operates in LRM mode.
- ❖ Fixed in version 06.14

**Anomaly #17 : the field "elevation ice sheet 20 ku" is set very often to Fill Value in LRM mode (S3MPC-2477)**

- ❖ The field elevation_ice_sheet_20_ku is set to Fill Value for some measurements over Greenland and Antarctica when the SRAL altimeter operates in LRM mode (before 12 April 2016).
- ❖ Fixed in version 06.14

Anomaly #18 : the field "elevation ocog 20 ku" is set to Fill Value in LRM mode (S3MPC-2478)

- ❖ The field elevation_ocog_20_ku is set to Fill Value for some measurements over Greenland and Antarctica when the SRAL altimeter operates in LRM mode (before 12 April 2016).
- ❖ Fixed in version 06.14

13.4.4 Anomalies not solved

The following list summarizes the anomalies that still affect the products with the Processing Baseline 2.33:

Anomaly #1 : High level of retracker failure in continental ice sheets (S3MPC-1014)

- ❖ Over the inland ice sheets of Antarctica and Greenland there are much higher levels of the ice sheet retracker failure than found in previous missions (ie CryoSat LRM or Envisat RA2) over sloping surfaces. The anomaly on the SAR ice margin retracker also impacts the slope correction which is set to FillValue in a high number of occurrences.
- ❖ Improvement is observed since version 06.10 reducing the loss to 20% of the data set over Antarctica. Further tuning of the SRAL L1 processing is required to insure full consistency between L1 processing and L2 ice sheet retracker, so that the expected level of ice sheet retracker coverage is finally met. Meanwhile, users are advised to use the OCOG retracker to exploit a data set with the expected coverage over land ice (loss of only 2% of data).
- ❖ All versions up to and including 06.14 are impacted

Anomaly #2 : Dry tropospheric correction residual error over land (S3MPC-1518)

- ❖ The dry tropospheric correction at the measurement altitude (mod_dry_tropo_cor_meas_altitude_01) exhibits some residual error correlated to the topography. The error has a magnitude of a few millimetres.
- ❖ All versions up to and including 06.14 are impacted



Anomaly #3 : Quantization of the distance to coast (S3MPC-1519)

- ❖ The distance to coast at 1 Hz and at 20 Hz exhibits some quantization. The effect is larger at 20 Hz for which the value is constant over several 20 Hz measurements.
- ❖ All versions up to and including 06.14 are impacted

Anomaly #4 : Degraded quality of atmospheric attenuation over coastal areas (S3MPC-1934)

- ❖ The MWR atmospheric attenuation was improved over coastal zone except for some specific cases over coastal areas, for which the attenuation is negative (-0.3 dB). This anomaly affects only 0.25% of the ocean measurements and occurs when backscatter coefficient exceeds 18 dB.
- ❖ This anomaly was introduced in version 06.10 and all versions up to and including 06.14 are impacted

Anomaly #5 : GIM ionospheric to default value (S3MPC-2030)

- ❖ The GIM ionospheric correction is sometimes set to default values for portions of tracks that are closed to midnight. Therefore, parameters related to the topography observations are impacted (sea_ice_ssha, int_sea_ice_ssha).
- ❖ All versions up to and including 06.14 are impacted for STC and NTC products.
- ❖ Since IPF version 06.12, the impact is that sea_ice_ssha and int_sea_ice_ssha parameters are calculated without the GIM ionospheric correction.
- ❖ The reprocessed products with IPF 06.12 are not affected by this anomaly.

Anomaly #6 : L2 sea ice freeboard (freeboard 20 ku) is predominantly negative (S3MPC-2244)

- ❖ The freeboard parameter exhibits a mean value centred around -30 cm which is not expected. It is mainly due to the retracker used for the diffuse echoes which is not optimal to properly retrack the double peak waveforms that are characteristics over floes.
- ❖ All versions up to and including 06.14 are impacted

Anomaly #7 : Sea ice lead echoes incorrectly filtered by waveform quality check (S3MPC-2409, S3MPC-2411)

- ❖ The sea ice retracker exhibits a much higher level of failure compared to the other retrackers (ocean, OCOG and ice sheet retrackers), due to the use of a quality check applied on the waveforms. This results in the sea ice retracking not being applied to waveforms for observations that are associated to leads and sea ice, leads being the dominant population

where the retracker is not activated. This anomaly will be corrected in future STM Processing Baseline.

- ❖ All versions up to and including 06.14 are impacted.

Anomaly #9 : Discrimination flag set to ocean over land (S3MPC-2412)

- ❖ The discrimination flag (surf_type_class_20_ku) which is designed for sea ice is set to ocean over land surfaces.
- ❖ All versions up to and including 06.14 are impacted.

Anomaly #10 : Wrong values of interpolated sea ice ssha over ocean (S3MPC-2413)

- ❖ Values of interpolated ssha for sea ice (int_sea_ice_ssh) show stronger magnitude than the original sea_ice_ssh parameter, over transition zones between ocean and land areas.
- ❖ All versions up to and including 06.14 are impacted.

Anomaly #11 : Ice concentration set to zero over land (S3MPC-2417)

- ❖ Sea_ice_concentration_20_ku is set to zero percent over land but it does not affect the quality of the sea ice parameters using this parameter.
- ❖ All versions up to and including 06.42 are impacted

Anomaly #12 : Ice2 PLRM retracker not defined over the ice shelves (S3MPC-2415)

- ❖ The parameters estimated by the Ice2 retracker on PLRM waveforms (range_ice_20_plrm_ku and sig0_ice_20_plrm_ku) are not defined over the ice shelves.
- ❖ All versions up to and including 06.14 are impacted.

Anomaly #14 : Partial coverage for OCOG retracker in C-band (S3MPC-2365)

- ❖ The output of the OCOG retracker in C-band (range_ocog_20_c and sig0_ocog_20_c parameters) are very frequently set to fill values, whatever the surface.
- ❖ All versions up to and including 06.14 are impacted.

Anomaly #15 : Partial coverage for OCOG retracker in LRM mode (S3MPC-2564)

- ❖ The output of the OCOG retracker in Ku-band in LRM mode (range_ocog_20_ku and sig0_ocog_20_ku parameters) are very frequently set to fill values, whatever the surface.
- ❖ All versions up to and including 06.14 are impacted.



14 Annex References

- RD 1** C. Ruf, 2000: Detection of Calibration Drifts in spaceborne Microwave Radiometers using a Vicarious cold reference, **IEEE Trans. Geosci. Remote Sens.**, **38**, 44-52, <https://doi.org/10.1109/36.823900>
- RD 2** S. Brown, C. Ruf, 2005: Determination of an Amazon Hot Reference Target for the on-orbit calibration of Microwave radiometers, **Journal of Atmos. Ocean. Techno.**, **22**, 1340-1352, <https://doi.org/10.1175/JTECH1769.1>
- RD 3** L. Eymard, E. Obligis, N. Tran, F. Karbou, M. Dedieu, 2005: Long term stability of ERS-2 and TOPEX microwave radiometer in-flight calibration, **IEEE Trans. Geosci. Remote Sens.**, **43**, 1144-1158, <https://doi.org/10.1109/TGRS.2005.846129>
- RD 4** C. Ruf, 2002: Characterization and correction of a drift in calibration of the TOPEX microwave radiometer, **IEEE Trans. Geosci. Remote Sens.**, **40**, 509-511, <https://doi.org/10.1109/36.992824>
- RD 5** R. Scharoo, J. Lillibridge, W. Smith, 2004: Cross-calibration and long-term monitoring of the microwave radiometers of ERS, TOPEX, GFO, Jason and Envisat, **Marine Geodesy**, **27**, 279-297, <https://doi.org/10.1080/01490410490465265>
- RD 6** R. Kroodsma, D. McKague, C. Ruf, 2012: Cross-calibration and long-term monitoring of the microwave radiometers of ERS, TOPEX, GFO, Jason and Envisat, **Applied Earth Obs. and Remote Sensing**, **5**, 1939-1404, <https://doi.org/10.1109/JSTARS.2012.2195773>
- RD 7** Estimation des dérives et des incertitudes associées pour les radiomètres micro-ondes. Revue des méthodes existantes, **SALP-NT-MM-EE-22288**
- RD 8** Brown, S., C. Ruf, S. Keihm, and A. Kitiyakara, "Jason Microwave Radiometer Performance and On-Orbit Calibration," *Mar. Geod.*, vol. 27, no. 1-2, pp. 199-220, 2004.
- RD 9** Jee, G., H.-B. Lee, Y. H. Kim, J.-K. Chung, and J. Cho (2010), Assessment of GPS global ionosphere maps (GIM) by comparison between CODE GIM and TOPEX/Jason TEC data: Ionospheric perspective, *J. Geophys. Res.*, 115, A10319,
- RD 10** N. Tran, F. Girard-Ardhuin, R. Ezraty, H. Feng and P. Femenias, "Defining a Sea Ice Flag for Envisat Altimetry Mission," in *IEEE Geoscience and Remote Sensing Letters*, vol. 6, no. 1, pp. 77-81, Jan. 2009. doi: 10.1109/LGRS.2008.2005275
- RD 11** Ablain, M., J. F. Legeais, P. Prandi, M. Marcos, L. Fenoglio-Marc, H. B. Dieng, J. Benveniste, and A. Cazenave (2017), Altimetry-based sea level at global and regional scales, *Surv. Geophys.*, 38, 7-31, doi:10.1007/s10712-016-9389-8.
- RD 12** Pujol, M.-I., Schaeffer, P., Faugère, Y., Raynal, M., Dibarboue, G., Picot, N., 2018, Gauging the improvement of recent mean sea surface models: a new approach for identifying and quantifying their errors. Under review, *Journal of Geophysical Research*.
- RD 13** Tran, N., Labroue, S., Philipps, S., Bronner, E., & Picot, N. (2010). Overview and Update of the Sea State Bias Corrections for the Jason-2, Jason-1 and TOPEX Missions. *Marine Geodesy*, 33(sup1), 348-362. <https://doi.org/10.1080/01490419.2010.487788>



- RD 14** Lauret, O., 2016, Jason-3 validation and cross calibration activities (Annual report 2016) SALP-RP-MA-EA-3060-CLS available from
https://www.aviso.altimetry.fr/fileadmin/documents/calval/validation_report/J3/annual_report_j3_2016.pdf
- RD 15** Roinard, H., 2017, Jason-2 validation and cross calibration activities (Annual report 2017) SALP-RP-MA-EA-23186-CLS available from
http://www.aviso.altimetry.fr/fileadmin/documents/calval/annual_report_****.pdf
- RD 16** Moreau T., Tran N., Aublanc J., Tison C., Le Gac S., Boy F., “Impact of long ocean waves on wave height retrieval from SAR altimetry data”, submitted in Adv. Space Res., 2018.
- RD 17** Abdalla S., 2017. “Wind and Wave Assessment”, Expert Support Laboratories Council Meeting, September 2017, Toulouse.
- RD 18** Bonnefond, P.; Laurain, O.; Exertier, P.; Boy, F.; Guinle, T.; Picot, N.; Labroue, S.; Raynal, M.; Donlon, C.; Féménias, P.; Parrinello, T.; Dinardo, S. Calibrating the SAR SSH of Sentinel-3A and CryoSat-2 over the Corsica Facilities. *Remote Sens.* **2018**, *10*, 92. DOI : 10.3390/rs10010092.

End of document